Hybrid and Multi-Component Hydrogels

Daniel Cornwell

Doctor of Philosophy

University of York

Chemistry

July 2016

Abstract

Low-molecular-weight gelators (LMWGs) form a network via non-covalent interactions to immobilise the surrounding bulk solvent and form a gel. Whilst such gels are highly responsive and dynamic, they are often mechanically weak. In order to enhance the mechanical strength of such networks, the LMWG network can be supplemented with a second network formed from stronger polymer gelators (PGs) to yield a multi-component, multi-functional material – a hybrid gel.

By using this multi-functionality, hybrid gels were made that could demonstrate the following: a) robustness yet responsiveness, b) spatial control over the formation of one network in the presence of another, and c) temporal control over the formation of one network in the presence of another.

For the first aim, a pH-responsive LMWG (1,3:2,4-dibenzylidene-D-sorbitol dicarboxylic acid, DBS-CO$_2$H) was combined with the robust PG agarose. The assembly of DBS-CO$_2$H in the presence and absence of agarose was investigated by NMR and CD spectroscopies, whilst materials properties were examined by rheology. DBS-CO$_2$H was found to retain its pH-responsive character, as was demonstrated by cycling the pH within the gel – whilst the DBS-CO$_2$H network could be switched "on" or "off", the robust agarose network remained intact.

Following this, DBS-CO$_2$H was combined with the photo-inducible PG poly(ethylene glycol) dimethacrylate (PEGDM). Spectroscopic methods and electron microscopy showed that the kinetics and morphology of DBS-CO$_2$H assembly were impacted by the presence of PEGDM. The application of a mask during photoirradiation allowed patterning of the PEGDM network to form a material with two distinct, spatially-resolved regions, defined as a "multidomain gel", achieving the second aim. The different domains had different properties with regards to the diffusion and release of dyes.

DBS-CO$_2$H was then combined with another pH-responsive LMWG (1,3:2,4-dibenzylidene-D-sorbitol-dicarbonyl-glycine, DBS-Gly). The two gelators showed a good degree of kinetic self-sorting, their self-assembly being triggered at different pHs. It was possible to use two proton sources – the slow hydrolysis of glucono-δ-lactone, and the more rapid photoacid generator diphenyliodonium nitrate – to achieve a two-step process of network formation. As the second step was UV-initiated, photopatterned multi-component gels were produced; these materials were both spatially and temporally resolved, achieving the third aim. Finally, the combination of DBS-CO$_2$H, DBS-Gly and PEGDM into a three-gelator, multi-component hybrid hydrogel was investigated.

2

Table of Contents

List of Figures

12

13

14

18

23

List of Schemes

List of Tables

Acknowledgements

To begin with, a big thank you to my parents for all their support over the years of my studies, whether it was financial, logistical, or just being a phone call away when times were hard. I may have thoroughly confused you sometimes when talking about my work (and lots of other things, to be honest), but you were always willing to listen and be encouraging, and for that I am very grateful. My thanks to the rest of my family too for all their interest shown in my research – particularly my grandad for always being excited to receive the latest paper.

I am of course hugely thankful for the support and guidance from my supervisor Professor David Smith – for all his ideas, encouragement and help throughout the project and in my other academic activities, and when things really weren't going so well for me. I am also appreciative of the input from my IPM, Dr Isabel Saez, particularly her useful comments and questions in TAP meetings. I must also thank the University of York and the Department of Chemistry for my funding through a Teaching Studentship.

On the technical side of things, my thanks to Heather Fish (NMR), Karl Heaton (mass spectrometry) and Abi Storey (glassblowing); and also, over in Biology, Meg Stark (SEM/TEM) and Dr Andrew Leech (circular dichroism).

Thanks to all members of the DKS group, past and present, for making the lab and offices a great place to work. Particular acknowledgements must go to Dr Will Edwards and Dr Babatunde Okesola for their help during the early stages of my project, Dr Ching Wan Chan (Rex) for his help with NMR, and especially to Dr Stephen Bromfield and Lizzie Wheeldon for being available whenever a good old moan about research or teaching was needed. I am also indebted to my MChem project student Oliver Daubney for his work on photoacid generators. Best of luck to everyone else still researching or writing-up – Buthaina Albanyan, Nicole Whitelaw, Jorge Ruiz Olles, Vânia Vieira and Phill Chivers.

My life in York has not all been work, and I would not have got through the last few years without some great friends, practically all of whom I met through the Douglas Adams Society (DougSoc). There are far too many of you to list here, but really big special thanks must go to Elise Groves, Chris Reynolds, and Dave Cooper. Thanks for keeping me just the right kind of crazy, and for making me an Eternal Dougling! I'll be back to check in on you from time to time – I expect I'll find you all in 'Spoons…

Declaration

I declare that the work presented within this thesis is entirely my own, except where otherwise acknowledge. This work has not been submitted in part or fully for examination towards any degrees or qualifications. Aspects of this work have been published in the following journal articles: *Soft Matter*, 2013, **9**, 8730–8736; *Angew. Chem. Int. Ed.*, 2014, **53**, 12461–12465; *Mater. Horiz.*, 2015, **2**, 279–293; *J. Am. Chem. Soc.*, 2015, **137**, 15486–15492.

1. Chapter 1: Introduction

1.1. Low-molecular-weight-gelators

Gels are a colloidal form of soft material brought about by the co-existence of two different phases: a liquid-like phase containing a sample-spanning solid-like network, which prevents bulk flow of the liquid through physical effects such as capillary forces and surface tension.[1] This solid-like phase typically makes up less than 1% of the material, with the molecules that form these solid-like networks being known as gelators.

It is possible, in broad terms, to separate gelators into two main categories based on the size of the molecule. The first is that of the more traditional polymer gelators (PGs):[2] long-chain polymer molecules with appropriate crosslinking, be it covalent or supramolecular,[3,4] are able to form the sample-spanning network required for gel formation. Both natural (e.g., gelatin, agarose) and synthetic (e.g., poly(acrylic acid), poly(ethylene glycol)) PGs are known, and have been used in a wide variety of applications, from gelling agents in food to tissue engineering.[5–7] PGs often form relatively robust networks (particularly those with covalent crosslinking), but as a result they are sometimes quite unresponsive to stimuli, and it can be difficult to program-in desired properties.

The second category of gelator is that of the low-molecular-weight gelators (LMWGs); these are small molecules that through non-covalent interactions and a hierarchical self-assembly process are also able to form a sample-spanning solid-like network, and hence a 'supramolecular' gel (alternatively known as molecular or physical gel).[8–12] The non-covalent interactions may take the form of hydrogen-bonding, van der Waals forces, hydrophobic interactions, π-π interactions, metal-ligand bonding, etc., whilst the hierarchical process of self-assembly usually sees these non-covalent interactions driving the formation of fibrils, which then aggregate into (nano)fibres (though ribbons, sheets and spheres are also known).[13] The fibres then entangle to form the sample-spanning network, immobilising the surrounding bulk solvent Figure 1.1).
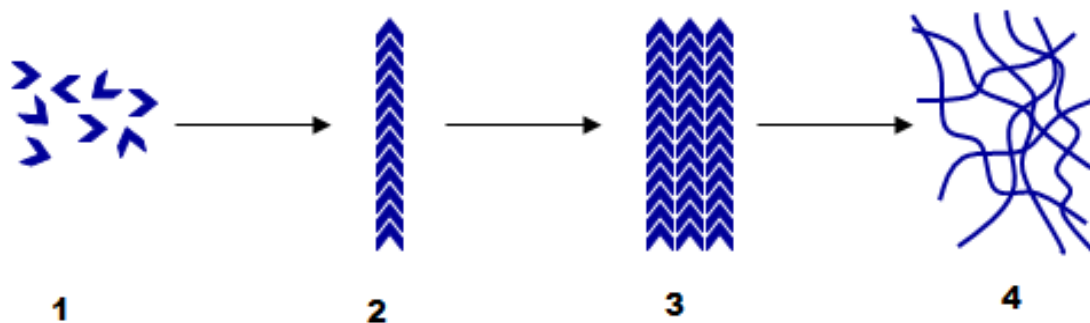
Figure 1.1: A typical hierarchical process of self-assembly for a supramolecular gel; individual LMWG molecules (1) assemble into fibrils (2), which assemble into fibres (3), which then entangle to form the sample-spanning solid-like network (4).

The weak, reversible non-covalent interactions that hold the gelator network together can be particularly responsive to certain external stimuli, such as temperature or pH. The macroscopic properties of the final gel can also be tuned by modification of the gelators at the molecular level: for example, changing the functional groups can, via the hierarchical self-assembly process, lead to a change in the materials properties or functionality of the gel. This responsive and tuneable nature of supramolecular gels means that they have the potential to be used in a variety of high-tech applications.[14–16]

Modification of the materials properties of the final gel can also be achieved by other methods, two of which are of particular interest here: i) the use of more than one molecular component to form the supramolecular gel (i.e., a multi-component gel), or ii) combining the LMWGs with polymer science in some way.

1.2.   Multi-component gels of low-molecular-weight gelators

There are three principal types of multi-component gels of LMWGs, as defined by Buerkle and Rowan[13] (see Figure 1.2 for illustrations):

 i) A two-component gel in which neither molecular component can form a gel by itself, but through non-covalent interaction with the other molecular component can self-assemble to form a sample-spanning network.

 ii) A two component gel where both molecular components are gelators in their own right. In these systems, the gelator molecules can interact to form co-fibres, or self-sort into their individual networks.

 iii) A gelator plus a non-gelling component, which serves to alter the function or performance of the gel in some way.
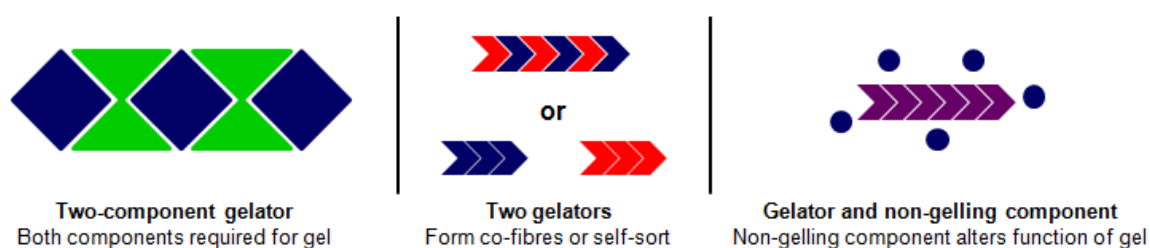
Figure 1.2: Representation of the three main types of multi-component gels of LMWGs. Image adapted from reference 13.

Here, the multi-component gels of specific interest are of the second type; in particular, those systems which exhibit self-sorting. Again, this class of multi-component gel can be broadly divided into two types: i) self-sorting gels where the gelator molecules are structurally very similar, and ii) self-sorting gels where the gelator molecules are structurally very different.

1.2.1. Structurally similar self-sorting multi-component gels of two LMWGs

Fuhrhop and Boettcher provided an early example of self-sorting between structurally similar gelators when investigating mixtures of different alkyl aldonamides.[17] These hydrogelators had different lengths of alkyl tails (8 or 12 carbons) and different chiralities of the sugar head groups (D or L glucose, galactose or mannose) (Figure 1.3). They summarized their findings with three rules regarding self-sorting in these systems: i) for two alkyl aldonamides where the chain length is the only difference, self-sorting does not occur; ii) racemic mixtures crystallise to give platelet- or tube-like crystals, and iii) self-sorting readily occurs for diastereoisomers if there is the opposite chirality at C3 and C5.

D-Glu 12

L-Glu 8
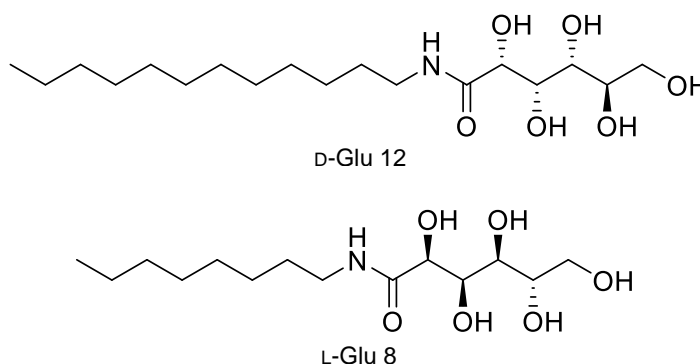
Figure 1.3: Example structures of alkyl aldonamide gelators with glucose head groups of differing chirality and alkyl chains of different lengths, as investigated by Fuhrhop and Boettcher.[17] These two gelators are able to self-sort.

Smith and co-workers investigated self-sorting in mixtures of structurally related peptide-based, bola-amphiphile-like dendritic gelators, examining the effects of size (generation of dendron), shape (length of central carbon chain) and chirality (D or L-lysine as dendron building blocks).[18] It was found that whilst differences in size and chirality led to self-sorting, differences in shape did not (similar to the lack of self-sorting observed by Fuhrhop and Boettcher when only chain length differed);[17] it was therefore proposed that interactions between the dendritic groups drove the self-assembly of the gelator fibres, and that self-sorting is dependent on the nature and location of the molecular information used in the molecular recognition pathway, which is responsible for gel formation. In related work, Moffat and Smith expanded on this idea by investigating mixtures of lysine-based dendritic gelators with different peripheral groups (either carbamate- or amide-based) (Figure 1.4).[19] Whilst a mixture of two gelators with carbamate and amide peripheral groups was able to self-sort (Figure 4**a**/4**b**, 4**a**/4**c**), a mixture of two gelators with two different amide groups (Figure 4**b**/4**c**) showed equal interaction with each other; this contrast was likely due to amide-amide hydrogen bonding being preferable over amide-carbamate hydrogen bonding, again suggesting that self-sorting is dependent on the nature of the molecular information used in the molecular recognition pathway.

Figure 1.4: Structures of lysine-based dendritic gelator and different periphery groups investigated by Moffat and Smith.[19]

Steed and co-workers have similarly examined blends of a series of structurally-related gelators, all with a common bis(urea) motif and amino-acid derived end groups, as well as differing spacer chain lengths (Figure 1.5).[20] They observed that whether self-sorting or co-assembly occurred was dependent on the degree of similarity between the gelators. A blend of gelators with differing spacer chain lengths but identical head groups readily self-sorted due to structural mismatch. Blends with the same chain length but differing head groups would either self-sort or co-assemble – for example, glycine/alanine and alanine/phenyl derived gelator blends co-assembled (due to sufficient structural similarities between gelators), but a glycine/phenylalanine derived gelator blend self-sorted (due to sufficient structural differences between gelators).

R = H or Me

R = H, Me or CH2Ph

Figure 1.5: Structurally similar peptide-derived bis(urea) gelators with differing spacer chain length and head groups, as investigated by Steed and co-workers.[20]

The effects of chirality on self-sorting were investigated by Cicchi and co-workers, who used enantiomers of a carbamate-based LMWG (Figure 1.6).[21] They observed that in a mixture, the enantiomers assembled into distinct fibres with opposite helicity, with the macroscopic gelation capacity of the mix being only slightly different from a gel of each individual LMWG (e.g., the T_{gel} of the racemic mixture was suppressed by only 6-7 °C). The authors noted that the ease with which

the LMWG building blocks could be functionalised would potentially allow for the easy production of functionalised chiral supramolecular structures.
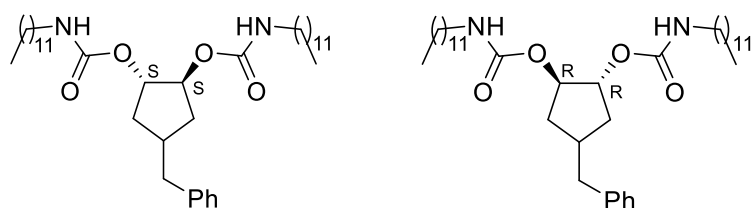
Figure 1.6: Enantiomeric LMWGs capable of self-sorting as used by Cicchi and co-workers.[21]

Ghosh and co-workers have carried out significant investigations into the molecular design of self-sorting, structurally similar aromatic donor or acceptor chromophores,[22] some of which formed supramolecular gels. The strategy they employed involved 1,5-dialkoxynaphthalene (DAN) donors and naphthalene tetracarboxylic acid diimide (NDI) acceptors, both symmetrically functionalised with amide groups (Figure 1.7a and b). The two chromophores chosen could usually undergo charge-transfer interactions between their aromatic groups to stack alternately; however, in the systems investigated, varying the distance between the amide groups in the donor and acceptor to cause a length mis-match between the two chromophores could lead to their self-sorting, as the stronger hydrogen bonding interactions between amide groups was favourable over the weaker charge-transfer interactions. However, in systems where the length of the DAN and NDI compounds were very similar, both charge-transfer interactions and hydrogen bonding were observed, with cooperative self-assembly of the LMWGs occurring.[23] Ghosh and co-workers also investigated asymmetrical NDI LMWGs (Figure 1.7c), both in combination with symmetrical NDI LMWGs[24] and with DAN LMWGs.[23] In both systems self-sorting was observed, due again to the mis-match in the placement of the hydrogen-bonding amide groups. Ghosh and co-workers used similar systems to these to show that chiral NDI LMWGs forming helical fibres can induce helicity in achiral DAN LMWGs which usually form non-helical fibres;[25] macroscopic hydrophobic interactions between the two-self sorted networks were found to be the cause of this. Additionally, Ghosh and co-workers have also used these systems to show that the nature of the solvent can also affect whether self-sorting via hydrogen bonding or donor-acceptor interactions was preferred;[26] even if the structure of the LMWGs initially allowed for charge-transfer interactions to drive formation of the gel network, if a sufficiently polar solvent was used, then over time nanoscale rearrangement into self-sorted networks would occur.

a)

DAN donor, n = 1-3

b)

NDI acceptor, n = 0-2

c)

Asymmetrical NDI acceptor
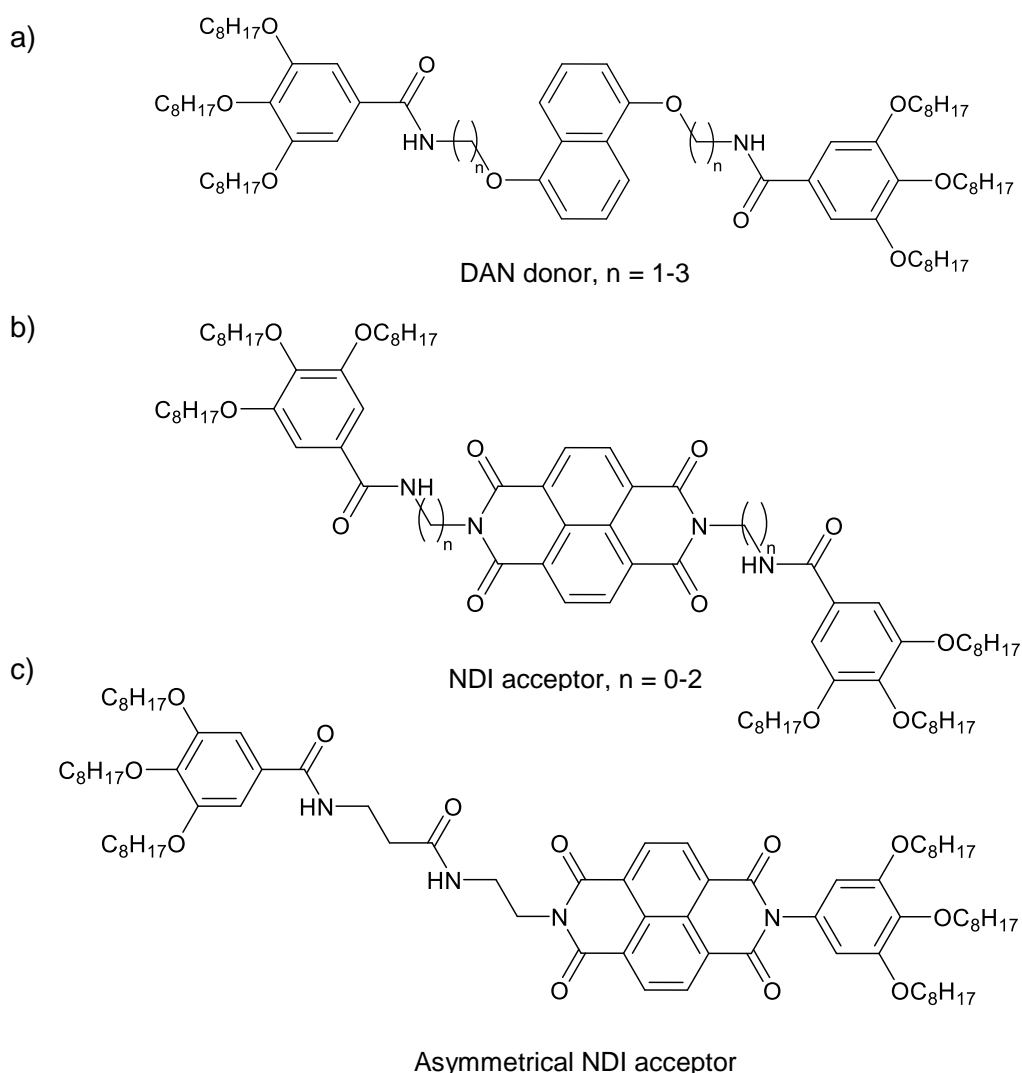
Figure 1.7: Examples of DAN donors and NDI acceptors used as LWMGs by Ghosh and co-workers.[22–26]

Other groups have also utilised strategically designed pairs of LMWGs incorporating donor-acceptor chromophore systems but with differing molecular lengths to cause self-sorting. In what was one of the earliest examples of self-sorting between LMWGs, Shinkai and co-workers utilised this self-sorting to create gels in which the entanglement of the two types of LMWG fibre created heterojunctions, with films of the gels capable of photoelectrical conversion under visible light.[27] Afrasiabi and Kraatz similarly investigated the potential to use peptide-based LMWGs in photoelectrical conversion devices; the donor and acceptor molecules could have one of two "parent" peptide structures, allowing for co-assembly or self-sorting, determining the efficiency of quenching and exciplex-like emission.[28]

In addition to the structural effects as described in all the above examples, kinetic effects can also be used to drive the self-sorting of structurally similar LMWGs. Adams and co-workers

described an example of two structurally similar dipeptide-based gelators where the self-sorting was pH-controlled;[29] the gelator molecules had different pK_a values (Figure 1.8), so that in a mixture one would assemble before the other as the pH was gradually lowered. This could be visualised by ^{1}H NMR spectroscopy, with one gelator becoming NMR invisible before the other as the networks assembled; the disappearance of the NMR signals occurred at a pH slightly below the pK_a of each gelator. By using pH change as the assembly trigger, the self-assembly process could be controlled by the pH of the system – for example, at a final pH in-between the two pK_a values, one gelator had formed a network, whilst the other remained in solution. Adams and co-workers later expanded on this study using additional dipeptides, again observing self-sorting due to their different pK_a values, but also noted that two very structurally similar dipeptide LMWGs with slightly different pK_a values co-assembled (the authors suggested the structural similarity as the cause).[30] It was also observed that a naphthalene dipeptide which assembled into aggregates rather than a sample-spanning network was able to disrupt the gelation of another LMWG.
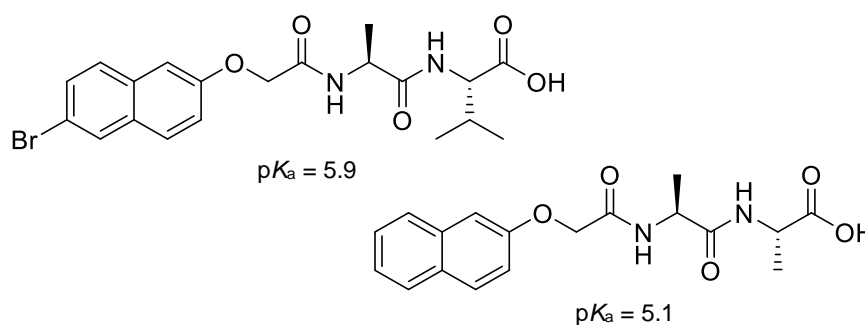
Figure 1.8: The structures of the pH-controlled self-sorting LMWGs used by Adams and co-workers; p*K*a values are given underneath each structure.[29]

1.2.2.   Structurally different self-sorting multi-component gels of two LMWGs

There are fewer examples of gels formed from structurally different self-sorting LMWGs – this is possibly due to the disruptive effects of one fibre network on the other, or disruption of one LMWG's molecular recognition pathway by the other LMWG in the system.

Smith and Smith examined self-sorting in a mixture of two very different gelators – one derived from dibenzylidene-D-sorbitol, and the other derived from cholesterol (Figure 1.9) – each reliant on completely different intermolecular forces for gel fibre formation, so there was no competition in molecular recognition pathways.[31] It was shown that each gelator formed an individual network, with each network maintaining its own characteristics – for example, the differential scanning calorimetry (DSC) signatures of the gel-sol transition temperature for both individual gel networks were still observed within the mixture. Additionally, the presence of one gelator had little effect on the other – variable temperature NMR showed the sol-gel transition of one gelator occurred in the same temperature range whether it was by itself or in a mixture.
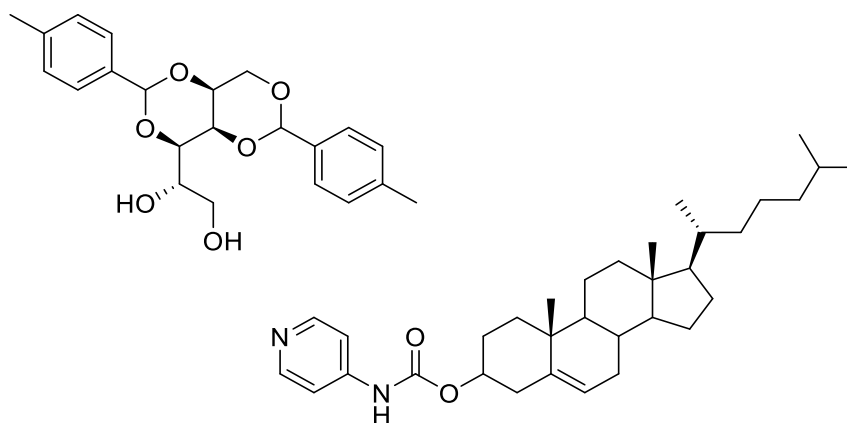
Figure 1.9: Structures of dibenzylidene-D-sorbitol derived gelator (left) and cholesterol-based gelator (right), used by Smith and Smith and a self-sorting system.[31]

Velázquez and Luque reported an example where a diaminocyclohexane/tartaric acid multi-component gelating system self-sorted in the presence of an oligoamide gelator.[32] Remarkably, the multi-component gel showed improved mechanical and thermal stability when compared to the individual gels; it was proposed that this was due to beneficial interactions between the two self-sorted gelator networks.

Hao and co-workers have described an interesting example where a system could be switched between a precipitate and self-sorting gelators through addition of NaCl.[33] The system was comprised of the gelators β-cyclodextran (β-CD) and sodium laurate (SL) in a water/DMF mixture. In a 1:1 mixture, inclusion complexes of SL in β-CD were formed, giving precipitates (or solutions at low concentration). However, adding more of one gelator induced gelation for that component – for example adding more SL caused a SL gel network to form. On adding NaCl to a precipitate of the 1:1 β-CD/SL inclusion complex also induced gelation – firstly of SL, which was then followed by the orthogonal gelation of β-CD.

1.3.   Combinations of low-molecular-weight gelators and polymers

There has been significant recent interest in the broad idea of combining polymers with supramolecular chemistry in order to affect gel properties.[3,4,34] As previously mentioned, one specific approach in this area is to combine LMWGs with polymers. This is a powerful means to extend the scope of both classes of material and provide access to new properties and applications. There are four key categories that are considered here (Figure 1.10):

1. Direct polymerisation of the self-assembled LMWG fibres, facilitated by polymerisable groups in the gelator molecules.
2. Capture of the LMWG network in a polymerisable solvent; in some cases, the LMWG fibres can then be washed out to yield nano-imprinted porous materials.

3. Addition of a non-gelling polymer in solution to the supramolecular gel.
4. Addition of a polymer in solution which is capable of directed and controlled interactions with the LMWG.

Polymerisation of LMWG fibres
Via polymerisable groups in gelator molecule

Capture of LMWG fibres in polymer matrix
Fluid monomer phase polymerised around self-assembled network

Addition of non-gelling polymer to LMWG gel
Can directly or indirectly influence LMWG network

Directed interactions between LMWG and polymer
Via a recognition motif of controlled supramolecular interactions

Key: ⌒‿--- = LMWG fibre   ⌒‿ = Polymer

Figure 1.10: Illustrations of four of the main types of LMWG-polymer combinations.

1.3.1. Polymerisation of LMWG fibres

Feringa and co-workers were the first to achieve polymerisation of self-assembled LMWG fibres.[35] They synthesised a methacrylate derivative of *trans*-1,2-bis(3-methylureido)cyclohexane (Figure 1.11), which could act as a LMWG in a variety of organic solvents, self-assembling via hydrogen-bond formation. The self-assembly of the gelator into fibres provided an ideal spatial arrangement of the methacrylate groups, which were then readily polymerisable through addition of a photoinitiator and subsequent photoirradiation. The resulting gels showed an increase in both thermal and long-term stability compared to the unpolymerised gel. Electron microscopy showed that whilst the unpolymerised gel consisted of mainly straight, occasionally intertwined fibres, the polymerised gel consisted of a highly cross-linked network, explaining the observed changes in materials properties.
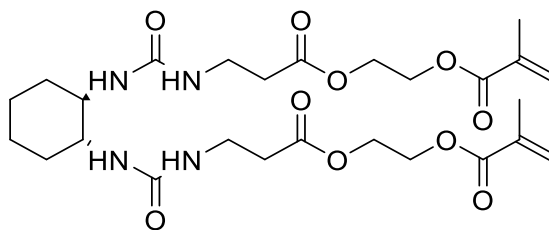
Figure 1.11: Photopolymerisable methacrylate derivative of *trans*-1,2-bis(3-methylureido)cyclohexane LMWG.[35]

Acrylate-functionalised LMWG polymerisation has also been exploited by Hanabusa and co-workers within liquid crystal gels, where the polymerisation of the gel fibres led to lower driving voltages for the electrooptic switching between light-scattering and transparent states of the liquid crystals.[36] Such a system shows how covalently captured gel fibres can have a beneficial effect in high-tech materials.

George and Weiss studied a series of LMWGs with conjugated diacetylene units[37] - diacetylenes are able to undergo solid-state polymerisation by 1,4-addition reactions if the monomers are suitably aligned. 10,12-Pentacosadiynoic acid and derivatives (Figure 1.12a) were able to gelate a variety of organic solvents; upon photoirradiation many of the gel networks were polymerised. For most of the polymerised gels, microscopic phase-separation between the solvent and the gelator network was observed (i.e., the polymer was insoluble in the gelation solvent), but overall gel integrity was maintained. Somewhat surprisingly, the polymerised gels were no more thermally or temporally stable than the unpolymerised gels – it was suggested (from X-ray diffraction) that the polymerised fibres maintained their morphology, with no additional crosslinking between fibres to reinforce the network. This suggests very precise translation of the self-assembled structural information in the polymerisation step.
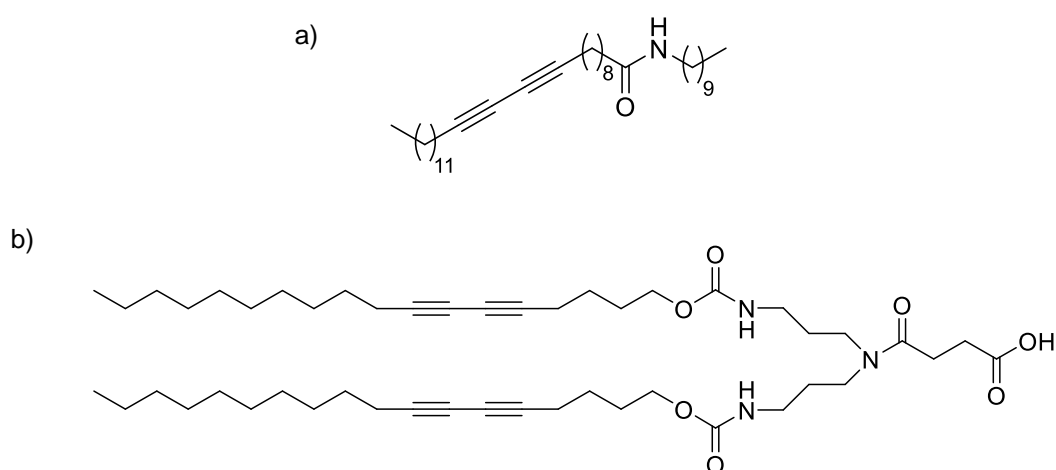
Figure 1.12: Exemplar structures of diacetylene containing LMWGs: a) 10,12-pentacosadiyonic acid derived gelator,[37] and b) dendritic gelator.[38]

Kim and co-workers similarly examined the self-assembly and subsequent photopolymerisation of dendritic LMWGs containing diacetylene units (Figure 1.12b); the polymerisation occurred at the periphery of the self-assembled structures.[38] During polymerisation the nanostructures became insoluble, and capture of the gel fibres was confirmed by solid-state X-ray diffraction. Shinkai and co-workers photopolymerised diacetylene units in a copper-porphyrin LMWG; the resulting polymer was insoluble but did retain the fibrous nanostructure of the self-assembled network.[39] Many other groups have also used diacetylene for the photopolymerisation of LMWG fibres,[40–46] making it one of the most used methods for capturing gel fibre nanostructures.

Smith and co-workers have used Grubbs' metathesis, a reversible approach capable of 'error checking' to polymerise self-assembled networks of dendritic gelators with peripheral alkene groups (see Figure 1.4).[47,48] A solution of Grubbs' second generation catalyst was diffused into a pre-formed gel, whereupon alkene metathesis occurred, and the network was covalently captured as a robust, thermally stable material. This material was shown by electron microscopy to consist of nanoscale fibres (Figure 1.13), and could be dried to a solid and then re-swollen in compatible solvents. When a non-polymerisable gelator was added, self-sorting of the networks occurred; following addition of Grubb's catalyst, the non-polymerisable network could then be washed out of the polymerised material to leave a more porous and highly swellable xerogel.
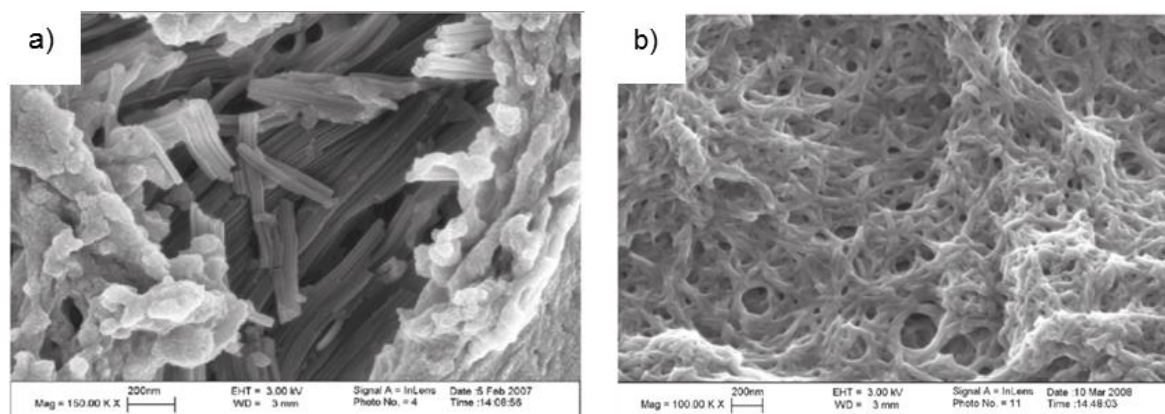
Figure 1.13: SEM images of the insoluble material produced by metathesis of dendritic LMWG; a) shows the nanofibres visible through a crack in the polymerised material surface; b) shows the nanofibre network after re-swelling of the dried material. Images reproduced from reference 48.

Díaz and co-workers used copper-catalysed 1,3-dipolar cycloaddition of alkynes and azides ('click' chemistry) to cross-link and polymerise LMWGs based on the alkyne and azide derivatives of the undecylamide of *trans*-1,2-diaminocyclohexane (Figure 1.14), using a variety of azide or alkyne cross-linkers, plus direct triazole crosslinking of the gelators.[49] They observed increases in both thermal and mechanical stability when compared to non-cross-linked gels, though it is unclear if these increases were mainly due to inter-fibre cross-linking, intra-fibre polymerisation, or a combination of both. Díaz and co-workers have also used click chemistry to stabilise gels

containing phthalocyanine, improving the thermal stability of the gels and incorporating a photoactive unit into the captured nanostructure.[50] The same research group also used the photochemical thiol-ene click chemistry to tune the rate of drug release from a gel, with crosslinking in the nanostructure reducing the release rate.[51]
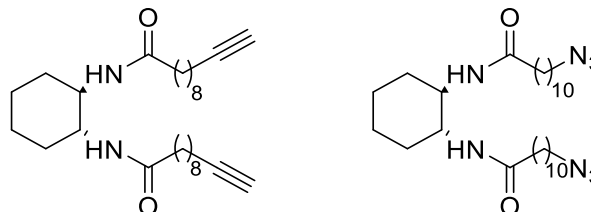
Figure 1.14: Alkyne and azide derivatives of the undecylamide of *trans*-1,2-diaminocyclohexane LMWGs.[49]

Another method for covalent capture of self-assembled LMWG fibres was investigated by Steed and co-workers, where hydrolysis of triethoxysilane end groups of a triethoxysilane bis(urea) gelator (Figure 1.15) was used.[52] Diffusion of (or immersion in) HCl caused hydrolysis and subsequent polymerisation of the $Si(OEt)_3$ groups, with a transparent gel becoming a white polymer block after several hours; analysis by SEM showed that the polymerised network had a very similar structure to the unpolymerised network. The polymerised material also had enhanced mechanical strength, presumably as a result of the embedded nanostructures.
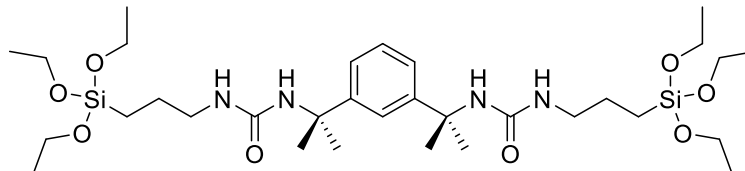
Figure 1.15: Triethoxysilane bis(urea) LMWG; hydrolysis and subsequent polymerisation occurs at the SiOEt₃ and groups.[52]

Adams and co-workers used electrochemical oxidation of carbazole-protected amino acid LMWGs (Figure 1.16) as a means of polymerising the gel nanostructure.[53] The polymerised gels had a different structure (open and porous) compared to the polymers produced from dissolved carbazole-protected amino acids, and were electrochromic (cycling clear to green depending on applied charge). It was suggested that other such protected peptides could be fully or partially polymerised to make materials with distinctive and useful microstructures, and that electro-patterning of the gels could also be possible with patterned electrodes, potentially making the materials of use for sensing and bioelectronics applications.
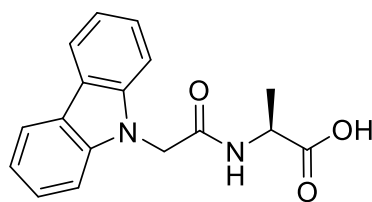
Figure 1.16: Structure of carbazole-protected amino acid LMWG, as used by Adams and co-workers.[53]

To summarise this method, it can enable molecular-scale information to be translated into nanoscale architectures by self-assembly and for those to then be captured in a more permanent form by polymerisation; it is possible to either crosslink a three-dimensional gel network, or individual gel nanofibres. In the first case, this yields crosslinked polymer gels, but there is potential to tune the molecular-scale composition much more precisely. In the second case, well-defined nanostructures are formed, the properties of which often reflect the molecular-scale programming. The approach could ultimately yield versatile, discrete nanomaterials to rival others – for example, carbon nanotubes.

1.3.2. Capture of LMWG fibres in a polymer matrix

Möller and co-workers were the first to propose and utilize the technique of capturing a LMWG network inside a polymer matrix by polymerisation of a fluid monomer around the LMWG fibres.[54] They used two different LMWGs to gelate a methacrylate liquid phase, which was then polymerised to a resin. The LMWG fibres could then be washed out of the polymer to yield nanoporous membranes – the pore sizes depended on the LMWG used and the temperature at which gelation occurred (a lower temperature led to smaller pore size, as the gelators aggregated more rapidly and into smaller fibres). The resulting membrane could be functionalised by charging the pore walls with anionic sites – the methacrylate ester groups reacted with taurine, which added a sulfonate anion. Möller and co-workers later used the polymer matrix technique to capture and study the aggregation of benzamide derived LMWGs.[55,56] These examples show that embedding then removing a LMWG network can extend the function of standard polymeric materials.

The production of porous membranes by this method has been studied by several other research groups. Weiss and co-workers reported similar results when using the gelator tetraoctadecylammonium bromide with methylmethacrylate or styrene as the polymerisable solvent, removing the LMWG network by simply washing the polymer with water.[57] Nolte and co-workers described gluconamide gelators that could gelate a mixture of methacrylates; again, the LMWG network could be removed by water to leave well-defined pores, as could be seen by transmission electron microscopy (TEM) (Figure 1.17) – though the helical character of the gelator fibres was not reflected in the pores, most likely due to shrinking of the methacrylate during

polymerisation.[58] The groups of John, Pina and Steed have similarly investigated the formation of nanoporous membranes of polymerised divinylbenzene and methacrylates respectively.[59–61]
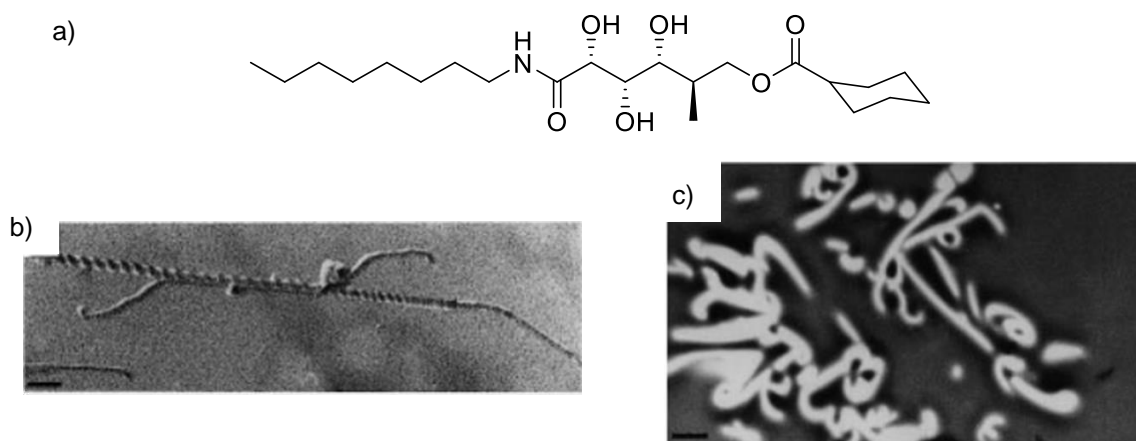
Figure 1.17: a) Structure of a gluconamide gelator used by Nolte and co-workers; b) TEM image of helical fibre of gluconamide gelators (scale bar = 110 nm); c) pores left in methacrylate polymer after gelator removed by washing (scale bar = 1.35 μm). Images reproduced from reference 58.

Mésini and co-workers were able to produce polymer resins with helical pores by using 3,5-bis(5-hexylcarbamoylpentyloxy)benzoic acid decyl ester (BHPB), which formed helical tape-like nanostructures in polymerisable ethylene glycol diacrylate.[62] Washing the polymer resin with DCM dissociated BHPB, and subsequent TEM analysis showed the presence of helical pores patterned by the LMWG nanostructure(Figure 1.18). The extent to which such porous polymerised materials retain the structural features of the LMWG assemblies used to pattern them is clearly dependent on several factors, including the polymerisation event, the rigidity of the LMWG fibres, and the washing conditions.
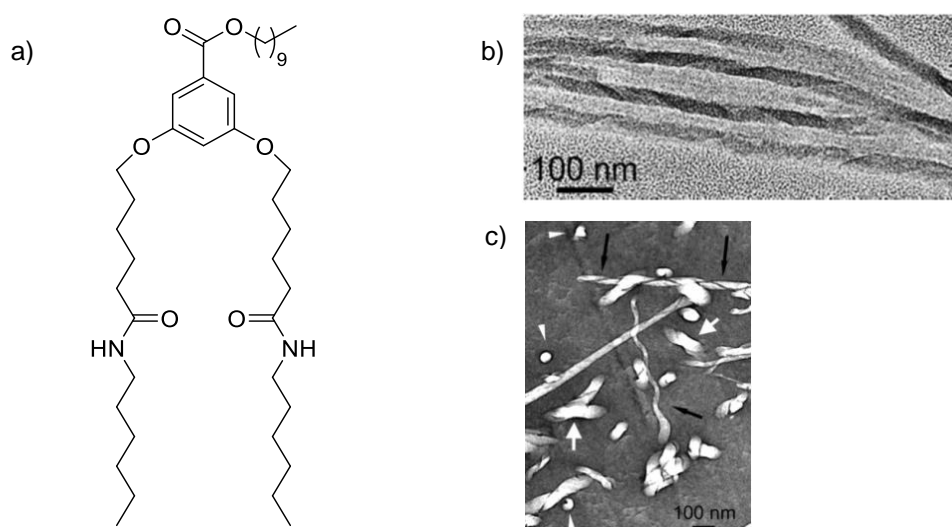
Figure 1.18: a) BHPB gelator used by Mésini and co-workers; b) TEM image of helical tapes of BHPB gelators; c) helical pores in polymer matrix after removal of BHPB – black arrows = pore viewed perpendicular to axis, white arrows = pore viewed along axis. Images reproduced from reference 62.

42

In addition to producing nanoporous membranes, there has been interest in enhancing the materials properties of polymeric materials by embedding LMWG networks within them. Stupp and co-workers examined the scaffolding/toughening of polystyrene through incorporation of dendron rod-coil (DRC) LMWGs (the incorporation of LMWGs into other polymeric materials was also examined to a lesser extent).[63–65] The presence of the LMWG nanoribbons directed polymer orientation into a more aligned state, which in turn modified the materials properties of the polymer – for example, impact strength was significantly increased (Figure 1.19). This was in part due to the increased alignment of the polymer, which limited crack propagation in the material, and also due to the LMWG network acting as a nano-skeleton to dissipate impact energy. It was also noted that the presence of the LMWG could add a degree of self-healing to the material, as the non-covalent interactions could reform after breaking by mechanical stress. Such self-healing materials are useful in extending the working life of materials and provide ability to recover after stress.

Figure 1.19: Left: pure polystyrene polymer cylinder; middle: hard polymer material containing both polystyrene and a LMWG network; right rubbery polymer containing both poly(2-ethyl hexyl methacrylate) and a LMWG network. Image reproduced from reference 64.

Smith and co-workers investigated the gelation of a styrene-divinylbenzene mix by a dendritic gelator with terminal alkene groups (see Figure 1.4c), and the polymerisation of the solvents.[66] Though the gelator could have polymerised under the conditions used to polymerise the styrene-divinylbenzene mix, this was not found to be the case – instead, the gelator network remained unpolymerised and reactive within the material. This was evidenced by addition of the reactive stain osmium tetroxide (OsO_4), which reacted selectively with the terminal alkene groups of the gelator, allowing the network to be visualised by TEM (Figure 1.20). The presence of the self-assembled network also acted as a "nano-skeleton", enhancing the materials properties of the polymerised material – for example, the glass transition temperature of the polymer was significantly increased. The LMWG could be washed out of the polymer to give a nano-imprinted material. Moffat and Smith have also examined pyrene-functionalised dendritic LMWGs embedded in polymerised styrene-divinylbenzene. When made as a polymer wafer, the material had two distinct "faces" with different properties (fluorescence, and nano-texture), as the gelator

concentrates at the more hydrophilic surface (glass base of the mould) during polymerisation.[67] Such bi-face materials with embedded photoactive nanostructures at one face have potential applications in device fabrication.

Figure 1.20: TEM image of poly(styrene-divinylbenzene) with embedded dendritic LMWG (dark fibres and spots); the gelator network is visualised through the use of the reactive stain OsO4. Image reproduced from reference 66.

Kim and Chang also combined fluorescent LMWGs with the cross-linkable monomer solvent ethylene glycol dimethacrylate.[68] The organogel showed a thermochromic gel-sol transition, which was maintained after polymerisation of the solvent. Under 365 nm irradiation, the colour change accompanying the gel-sol transition within a film of the polymer matrix was observed to be from orange to green (Figure 1.21). The supramolecular self-assembly of the LMWG was shown to be key to the thermochromic properties of the polymeric material, as a polymer film with non-assembled LMWGs dispersed within did not exhibit thermochromism.
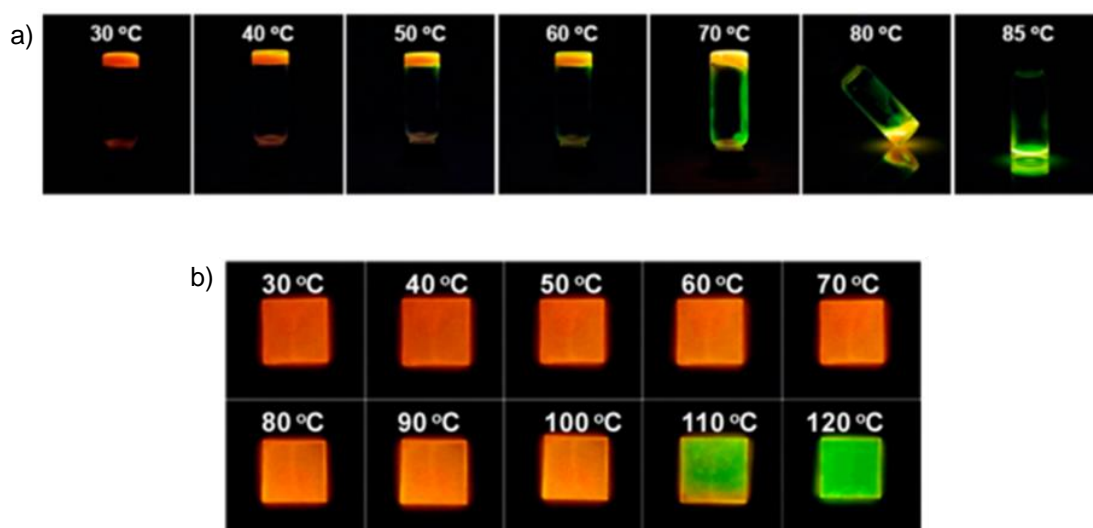
Figure 1.21: Photographs (under 365 nm irradiation) of fluorescent thermochromic LMWG systems prepared by Kim and Chang, a) gelling unpolymerised solvent at increasing temperature and undergoing gel-sol transition with accompanying thermochromic colour change; b) LMWG network in polymer film, with thermochromic colour change observed with increasing temperature.

Wilder and co-workers examined the effect of adding the LMWG dibenzylidene-D-sorbitol (DBS) to a dental composite consisting of photopolymerisable ethoxylated bisphenol A dimethacrylate (EBPADMA) with zirconia-modified amorphous calcium phosphate (Zr-ACP) to aid remineralisation.[69] The polymers used in dental applications have problems, including shrinkage of the material and biocompatibility issues with incomplete monomer to polymer conversion. It was found that by introducing DBS a slightly higher rate of conversion occurred, due to a reduction in the mobility of polymerising chain ends through increased viscosity, which favours free radical propagation. The polymerised material also was stronger and suffered less shrinkage than in the absence of DBS. It should be noted, however, that the addition of DBS also reduced the release of calcium and phosphate ions from the ACP, limiting the extent to which this material could promote remineralisation.

1.3.3. Polymerised LMWG fibres within a polymer matrix

There are some examples where the above two approaches for combining LMWGs and polymers have been mixed to form materials where a network of polymerised LMWG fibres are captured within a polymer matrix.

Chang and co-workers produced such materials using a hetero-bifunctional gelator with both acryl and diacetylene polymerisable groups (Figure 1.22a) to gelate hexyl methacrylate (HMA).[70] When cured under UV light, polymerisation of both the gelator and the monomer took place; the presence of polydiacetylene caused the polymeric material to exhibit strong fluorescence when irradiated with 365 nm UV light (Figure 1.22b). Selective polymerisation and fluorescence could also be achieved by photo-patterning – the acryl groups of HMA and the LMWG could be polymerised significantly faster than the diacetylene groups (10 minutes vs. 24 hours), so by application of a mask only in those areas exposed to UV light did polydiacetylene form; the resulting fluorescent pattern could be observed by confocal laser scanning microscopy (Figure 1.22c). Chang and co-workers have since investigated a series of related hetero-bifunctional gelators combined with HMA, and observed that in general there is an increase in both thermal and mechanical stability of poly(HMA) with the inclusion of the polymerised hetero-bifunctional gelator fibres.[71]
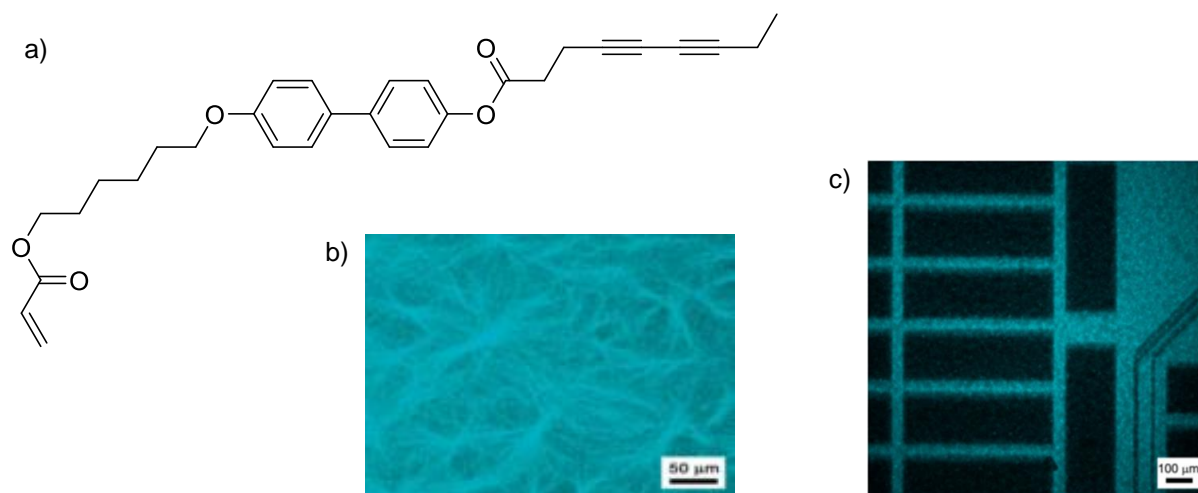
Figure 1.22: a) Hetero-bifunctional LMWG with both acryl and diacetylene polymerisable groups used by Chang and co-workers; b) fluorescent polymerised gel fibres within poly(HMA) matrix; c) photo-patterned polymer film – fluorescing areas contain polydiacetylene. Images reproduced from reference 70.

Yang and co-workers used the gelator *N*-octadecyl maleamic acid (ODMA) to gelate a mixture of polymerisable 2-hydroxyethyl methacrylate (HEMA), methacrylic acid (MAA) and poly(ethylene glycol) dimethacrylate (PEG200DM).[72] The LMWG nanostructures and solvent monomers were then polymerised by UV curing, with the inclusion of L-phenylalanine ethyl ester and BOC-L-phenylalanine as templates. The templates were removed to give molecularly imprinted materials, which showed a high affinity for adsorption of L-phenylalanine over D-phenylalanine (Figure 1.23). The ODMA fibres were also found to reinforce the rigidity of the polymer matrix. It was suggested that materials prepared in such a way may have applications as a stationary phase in chromatography; in this way they are related to molecularly imprinted polymer technology.[73]
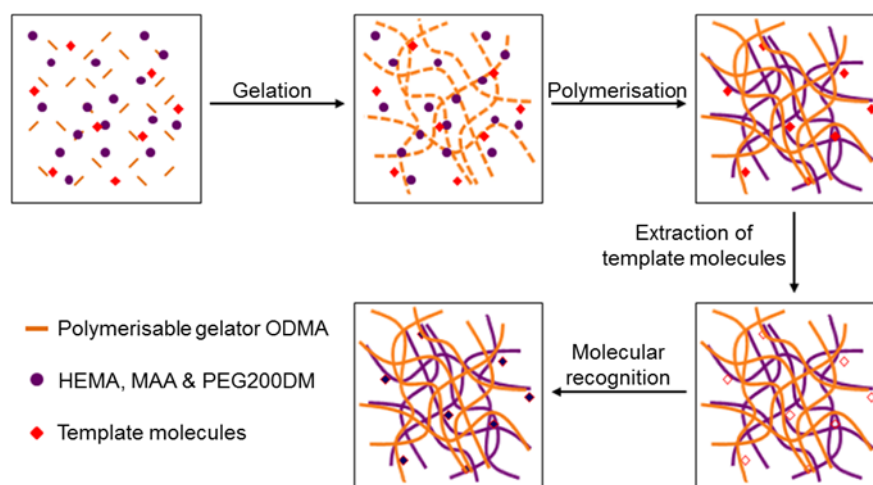
Figure 1.23: Illustration of the preparation of molecularly imprinted polymer/polymerised LMWG materials by Yang and co-workers, and the process of molecular recognition. Image adapted from reference 72.

Korley and co-workers prepared a polymer nanocomposite by gelation of ethylene oxide-epichlorohydrin copolymer (EO-EPI) polymer solution by polymerisable diacetylene- and cholesterol-based LMWGs.[74] The gel was compression-moulded to form a film, and curing under UV light was used to polymerise the diacetylene groups. The resulting material had a significantly improved tensile storage modulus (elasticity) compared to both a polymer film without the polymerised LMWG, or one containing cholesterol as a filler, demonstrating again how incorporation of nanofibres can modify and improve materials properties.

Xu and co-workers created gels in which a reaction could be controlled by the polymerised gel network;[75] to achieve this, they polymerised a self-assembled network of naphthalene tripeptide LMWGs with peripheral acrylamide units in the presence of acrylamide monomers and crosslinkers. This produced a polymer hydrogel with embedded fibrillar nanostructure. Incorporation of a small amount of acrylamide-functionalised ruthenium bipyridine catalyst allowed the gels to be used to catalyse the oscillating Belousov-Zhabotinsky reaction. The self-assembled fibres played a key role in controlling the periodicity of this oscillating reaction, as the concentration of LMWG used controlled the pore size formed in the final polymer gel, and hence the rate of diffusion of the reagents.

1.3.4. Addition of a non-gelling polymer in solution to supramolecular gels of LMWGs

In recent years there has been increasing interest in the effects on adding a non-gelling polymer to a supramolecular LMWG gel – these effects may be caused by direct interaction with the polymer (e.g., adsorption), or indirect processes, (e.g., the polymer changing the solution viscosity). Hanabusa and co-workers were, in 1999, the first to investigate the addition of non-gelling polymers to a LMWG organogel.[76] They found that adding either poly(*N*-vinylpyrrolidone) or poly(ethylene glycol) to a 1-propanol gel of a L-valine-containing benzenedicarbonyl derivative significantly enhanced the strength of the gel; adding poly(styrene) to a similar gel made in cyclohexane, however, caused little increase in the gel strength. The authors did not comment in this study as to the reasons for this difference, or to how the addition of polymers increased the strength of the gel.

There were surprisingly few developments in this area over the next ten years; in fact, all the notable work comes from Liu and co-workers. They initially investigated a novel method for forming gels from self-assembling nanostructures of the molecule lanosta-8,24-dien-3β-ol:24,25-dihydrolanosterol (L/DHL) with diisooctylphthalate (DIOP).[77,78] When L/DHL (10% wt) was dissolved in DIOP by heating, then allowed to cool to room temperature, a viscous, opaque paste was formed, which was shown by SEM to consist of separate, needle-like fibres (Figure 1.24a). However, on addition of a very small amount (0.0006% wt) of ethylene/vinyl acetate copolymer

(EVACP) to the system, a transparent gel was obtained, with interconnecting, branched fibres observed by SEM (Figure 1.24b). The change is nanostructure was reasoned to be caused by adsorption of the polymer onto the growing tip of the fibre, which then caused what the authors termed "crystallographic mismatch branching" – the EVACP disrupted structural match between the growing tip of the fibre and the new layers adding to it, causing branching of the fibre (Figure 1.24c) – this is quite a remarkable effect for such a small amount of additive.
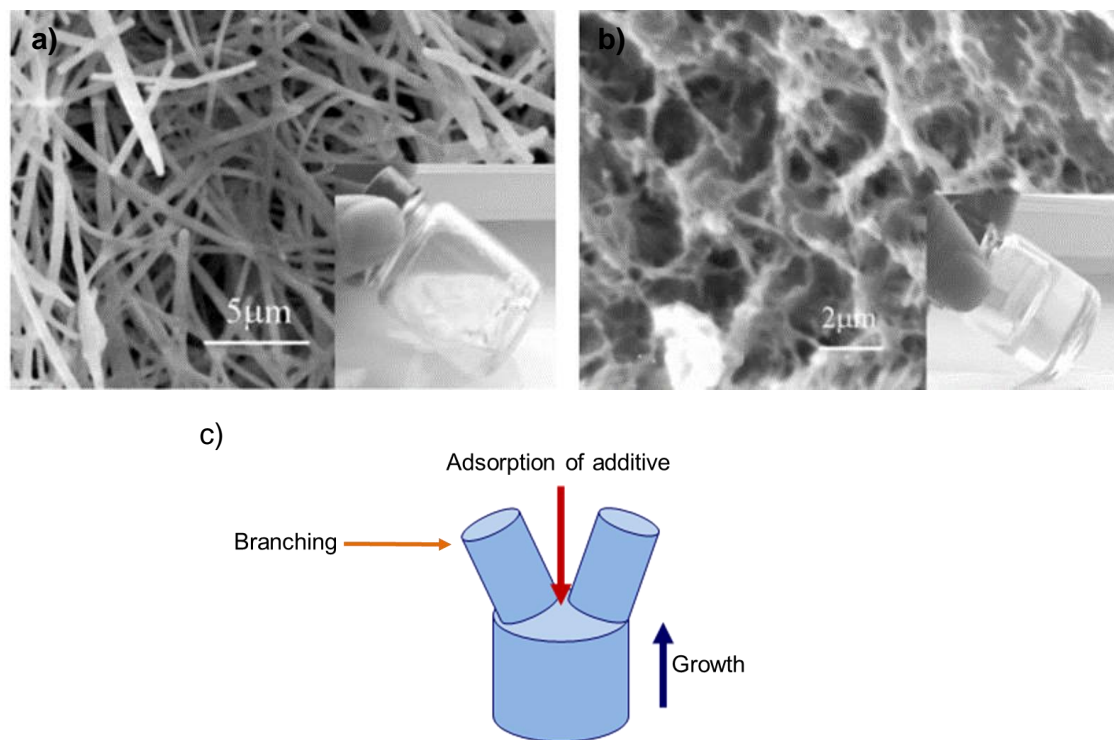
Figure 1.24: SEM images of L/DHL/DIOP systems studied by Liu and co-workers: a) Separate needle-like fibres of L/DHL in DIOP; b) addition of EVACP caused a network of interconnected branched fibres to form; c) illustration of crystallographic mismatch branching. Images reproduced from reference 77.

Liu and co-workers later used the adsorption of polymers onto growing fibres to influence the mechanical and nanoscale properties of gels formed from *N*-lauroyl-L-glutamic acid di-*n*-butylamide, which form spherulite fibre networks in propylene glycol,[79] or mixed fibre/spherulite fibre networks in benzyl benzoate.[80] They found that the addition of poly(methyl methacrylate co-methacrylic acid) (PMMMA) and EVACP slowed nucleation of the gelator molecules in addition to causing a higher level of branching in the gelator fibres; addition of EVACP also inhibited formation of fibres of *N*-lauroyl-L-glutamic acid di-*n*-butylamide in propylene glycol, with only spherulite nanostructures being formed.

Cui, Shen and Wan studied the behaviour of the gelator 4-(4'-ethoxyphenyl)phenyl-*β-O*-D-glucoside in a water-1,4-dioxane mix; they observed that the gel network gradually collapsed to form crystals due to fibril aggregation.[81] With the addition of poly(2-hydroxyethyl methacrylate)

(PHEMA), however, the gel was stabilised; it was proposed that PHEMA was adsorbed onto the growing gel fibres, causing branching, which prevented aggregation of the fibrils, and therefore the collapse of the gel.

Nandi and co-workers examined the addition of the biopolymer chitosan to a folic acid gel.[82] They observed that the gels with chitosan added had fibres that were both thinner and more branched – suggestive that the polymer was adsorbed onto the growing tip of the gelator fibre to cause crystallographic mismatch branching, and adsorbed onto the side of the fibre to hinder lateral growth; in both cases, chitosan interacts with folic acid via hydrogen bonding. The increased branching led, as in the above examples, to increased mechanical strength when compared to a folic acid gel without chitosan. The gels were also tested for their abilities to adsorb dyes and heavy metal ions from water, suggesting that such biomaterial-derived gels may have applications in water purification. Nandi and co-workers have also studied the addition of poly(4-vinylpyridine-co-styrene) to folic acid gels, again observing crystallographic mismatch branching, and improvements in mechanical and thermal stability.[83] The gels with poly(4-vinylpyridine-co-styrene) were also shown to have semi-conductivity, from extended π-conjugation between the LMWG and polymer.

Adams and co-workers demonstrated how the addition of polymers can have viscosity-induced effects on the properties of LMWG gels. They added dextran biopolymers to hydrogels of a pH-dependant naphthalene-dipeptide LMWG;[84] They found that by changing the molecular weight or wt% of the dextrans added, the viscosity of the solution before gelation could be altered. Increased viscosity lengthened gelation time, whilst decreasing the mechanical strength. When observed by TEM, the gels with dextran were seen to have thinner fibres in a less well-defined network when compared to gels without dextran (Figure 1.25). The change in morphology and gelation time with addition of dextran was attributed to a reduction in diffusion of the LMWG due to increased viscosity of the solution; this meant that the LMWG self-assembly occurred more slowly and with less lateral assembly.
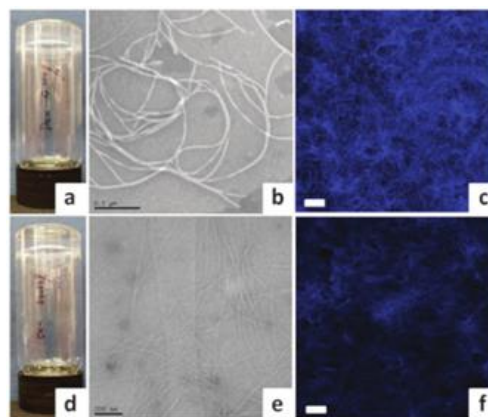
Figure 1.25: a) Image of hydrogel of naphthalene-dipeptide; b) TEM and c) confocal micrograph of gel (with Nile Blue stain); d) hydrogel of naphthalene-dipeptide with added dextran; e) TEM and f) confocal microscopy showing that the gel fibres are significantly thinner. Image reproduced from reference 84.

Adams and co-workers later studied the effects of dextrans and other polymers – poly(ethylene glycol), poly(vinylpyrrolidone), poly(ethylene oxide), poly(acrylic acid) – on the rheological properties of gels of naphthalene- or Fmoc-dipeptide LMWGs.[85] Again, in contrast to Liu and co-workers, they found that the mechanical strength of the gels decreased with the addition of polymers – here, the LMWGs formed spherulites, which upon addition of the polymers became smaller and less interconnected – hence the weakening in mechanical strength. They also found that the identity of the polymer additive also significantly affected the final rheological properties of the gels. They suggested that for some of the polymers added there might also be adsorption onto the gel fibres occurring as well as changes in the solution viscosity.

Yang and co-workers reported the addition of hyaluronic acid (HA) polymer to a LMWG hydrogel based on succinated Taxol.[86] They found that in the presence of the polymer the hydrogel fibres were more likely to bundle, slightly enhancing the mechanical strength of the gel. They also noted that the addition of more than 30% HA appeared to boost the anticancer activity of the nanofibres – they suggested this was a result of HA assisting in tumour targeting because it is a ligand for a protein overexpressed in the cancer cells. This showed how polymeric additives have the capacity to not only affect gel rheology and nanostructure, but may also introduce their own functionality to the material.

Ulijn and co-workers observed that peptide-based LMWGs could self-assemble in the presence of clusters of proteins (i.e., biological polymers) – specifically clusters of bovine serum albumin or β-lactoglobulin.[87] The proteins clustered at much lower concentrations than usual when in the presence of the LMWGs, whilst the presence of protein clusters also affected the self-assembly of the LMWGs. The resulting gels had different morphological and rheological properties compared

to gels made without the proteins. These effects were attributed to cooperative interactions between the LMWG and biopolymer.

Thordarson and co-workers have suggested that order in which the LMWG, solvent and polymer are mixed can play an important role in the properties of the resulting gels. They found that dissolving an Fmoc-dipeptide LMWG in liquid PEG before the addition of water (to give a 50:50 ratio of water to polymer volume), to trigger gelation by solvent-switching, yielded gels with greater rheological strength than if the LWMG was first dissolved in water before the addition of PEG. They suggested that by first dissolving the LMWG in PEG, hydrophobic effects caused it to self-assemble into a different nanostructure *via* stabilised intermolecular hydrogen bonding (usually disrupted in the presence of water). The presence of PEG also caused molecular crowding effects, further stabilising the LMWG hydrogen bonding interactions during the hierarchical assembly into nanofibres. The use of the large amount of liquid PEG in these gels also enabled solvation and incorporation into the gel of poorly-water soluble anti-cancer drugs such as Temozolomide and Taxol, and their subsequent controlled release.

Overall, it is clear that the presence of polymers in the solution phase can impact on LMWG assembly either by interactions with the gel fibres or through viscosity effects. Importantly, this is a cheap and simple method of modifying LMWG nanoscale morphology and rheology, with small amounts of polymeric additive often having relatively large effects.

1.3.5. Directed interactions between LMWGs and polymers

It is possible to design systems in which directed and controlled supramolecular interactions between LMWGs and polymers can occur in order to modify the overall gelation event in a more precise manner. These systems differ from the previous category, as interactions between LMWGs and polymers in those cases were of a non-specific and non-directed nature; here the interactions have more complementarity.

Exemplifying how a degree of specificity can be introduced to polymer-LMWG interactions, McNeil and co-workers studied the adsorption of poly(acrylic acid) (PAA) onto fibres of pyridine-based gelators (Figure 1.26).[88] It was found that the adsorption of the polymer, through acid-base interactions between the basic pyridine of the gelator and the carboxylic acid of PAA, reduced fibre growth rate - thinner fibres were observed by TEM due to this degree of control. It was proposed that this would lead to longer fibres, more fibres, or both, increasing entanglement in the gel and enhancing gel strength.
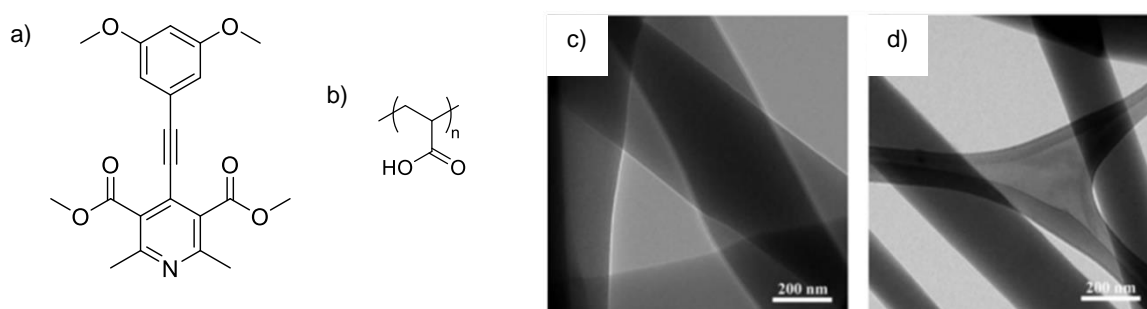
Figure 1.26: Structures of a) pyridine-based LMWG and b) poly(acrylic acid), as used by McNeil and co-workers, and TEM images of gel c) without and d) with PAA, resulting in thinner fibres. Image reproduced from reference 88.

Reinhoudt and co-workers studied a cholesterol-saccharide LMWG (Figure 1.27a) which could form a gel with many organic solvents, but was unable to gelate a water/DMSO mix, instead formed colloidal particles/vesicles.[89] With the addition of a suitable amount of the boronic acid-appended poly(L-lysine) (Figure 1.27b), however, a gel was formed, which was observed by TEM to consist of an extended network of vesicles. The authors determined that the polymer partially coated the vesicles through boronic acid-glucopyranosyl interactions – this then caused aggregation of the vesicles to occur to form the gel network. The physical properties of the gel (e.g. T_{gel}) could be controlled by varying the amount of polymer, and hence the level of crosslinking of the vesicles (Figure 1.27c). This system is related to vesicle-derived gels, a class of gels in their own right.[90]
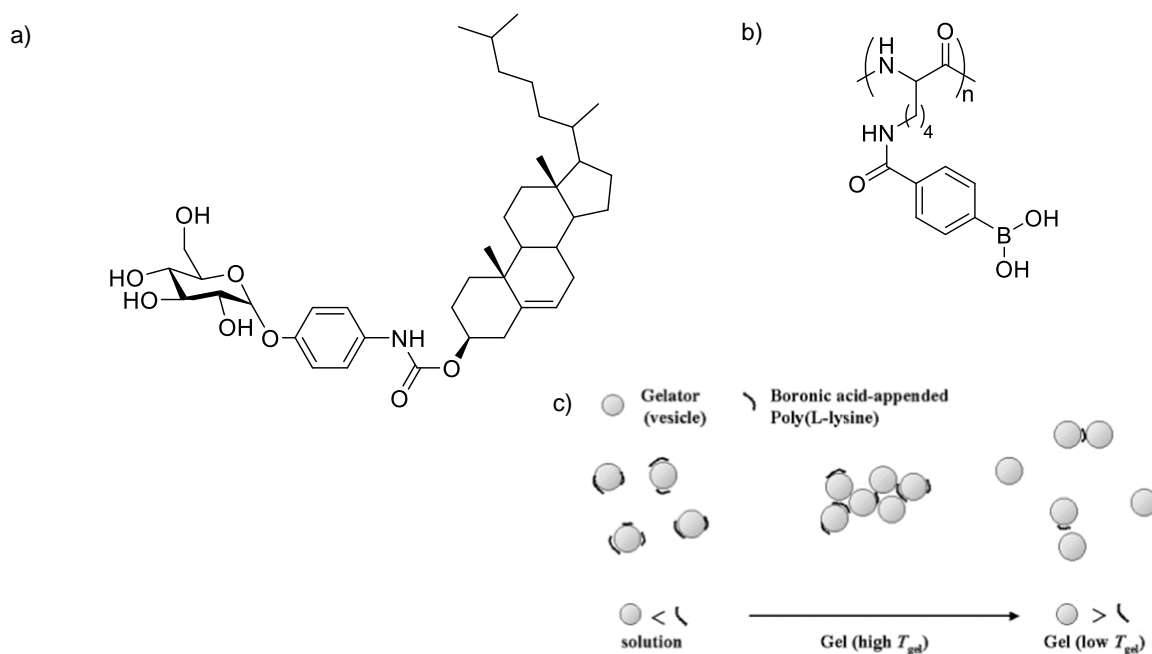
Figure 1.27: a) Cholesterol-saccharide LMWG and b) boronic-acid appended poly(L-lysine), as used by Reinhoudt and co-workers, produce a gel consisting of polymer crosslinked vesicles; c) varying the concentration of polymer controls crosslinking and the physical properties of the gel. Image reproduced from reference 89.

Polymers can also be used as templates for the formation of highly-ordered one-dimensional nanostructures from complexes of the polymer with LWMGs. Shinkai and co-workers combined nucleobase-appended gelators with thymine as the nucleotide with complimentary polynucleotides (Figure 1.28a), to form gels.[91] For example, they found that a cholesterol-based nucleobase gelator (Figure 1.28b), which could gelate polar solvents such as *n*-butanol, could be combined with the polynucleotide in a water/*n*-butanol mix to form a non-gelling complex of the two; the solvent mix was removed and replaced with just *n*-butanol, and after heating, a gel was formed – a gel was not formed when using just the gelator and following the same procedure. This lead the authors to the conclusion that the polynucleotide templates the LMWG molecules into a helical nanostructure through hydrogen bonding interactions with the polynucleotide – essentially, the polymer acts as a helical "pillar", with the gelator forming a spiral around it (Figure 1.28c).
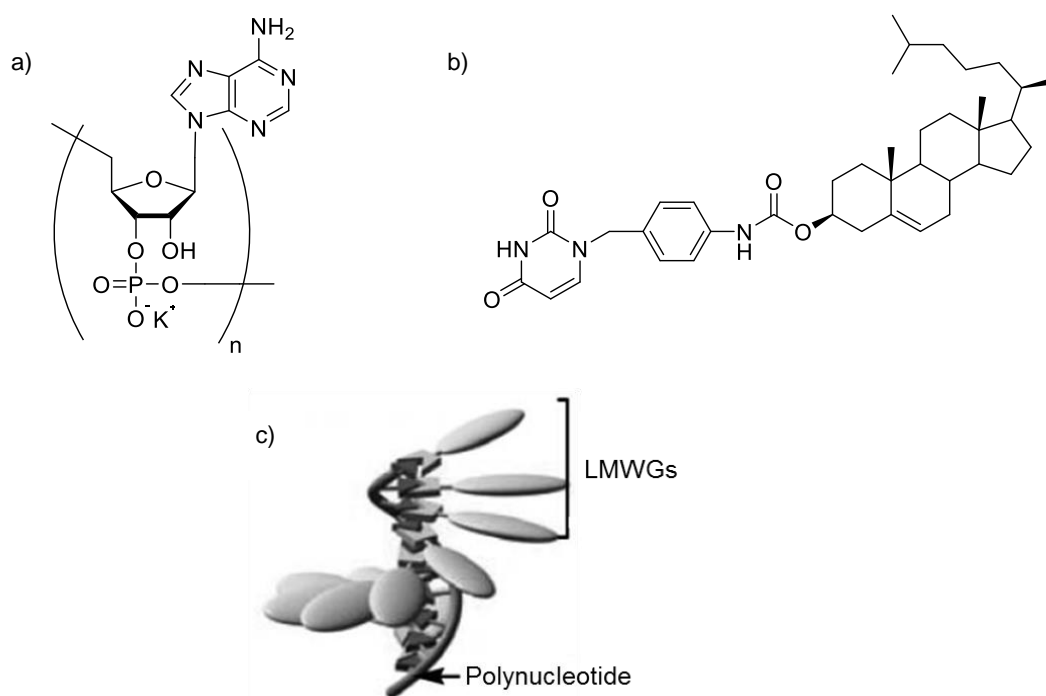
Figure 1.28: Exemplar a) polynucleotide and b) nucleobase-appended gelator, used by Shinkai and co-workers to form c) templated polymer-LMWG complexes. Image reproduced from reference 91.

Wang and co-workers have explored a similar concept, using dendritic gelators complexed with polyelectrolytes; Addition of the polymer template led to a lower minimum gelator concentration and faster gelation time, thought to be due to improved molecular recognition brought about by pre-organisation "fixing" the LMWG molecules in place on the polymer.[92,93]

Polymers can also be used to directly interact with the LMWG fibres to create crosslinking and improve the mechanical properties of the resulting gels. Rowan and co-workers studied a supramolecular hydrogel produced through helical assembly of guanosine-derived gelators around sodium ions.[94] Non-gelling copolymers containing guanosine-derived moieties were added and

found to be incorporated into the helical assemblies, forming supramolecular crosslinks in the system. At suitable concentrations of polymer, the mechanical strength of the gels could be dramatically improved (up to 40 times stronger) due to the additional crosslinking.

Nandi and co-workers examined a system consisting of the LMWG Fmoc-tryptophan (FT) and PEG;[95] FT formed hydrogels which exhibited thixotropy (regeneration of the gel after mechanical disruption of the gelator network) due to the strong hydrogen-bonding interactions between individual gelator molecules and the self-assembled fibres. The addition of PEG increased the rate of gel regeneration, with the polymer proposed to act as a sort of "molecular adhesive", forming hydrogen bonds with the active ends of the fibres after mechanical disruption. After assembly, PEG continued to act as an additional connecter between the LMWG fibres, reinforcing the overall gel structure.

1.3.6. Other combinations of LMWGs and polymers

There are some examples of LMWG-polymer combinations which do not fit into any of the categories described above. For instance, it has been shown that LMWGs can be used to gel liquid polymers to form novel electrolytes – this is a case of using a LMWG to improve a polymer system (similar to the those discussed in 1.3.2).[96] An interesting example from Nandi and co-workers involved a folic acid gel in which aniline was bound *via* non-covalent interactions to the surface of the self-assembled LMWG fibres;[97] the aniline could then be polymerised to form "shells" around the fibres, resulting in an increase in the mechanical stability and conductivity of the gel. Another example from Yang and co-workers saw the incorporation of a polymer nanogel into a hydrogel of LMWGs in order to improve thermal stability and controlled release.[98]

1.4. Hybrid gels of low-molecular-weight gelators and polymer gelators

Another approach to combining LMWGs with polymers is to mix them with polymer gelators (PGs); this approach sits between the two general methods discussed above in sections 1.2 and 1.3, in that the final material is composed of two independent gel networks (a self-sorting multi-component gel) which combines LMWGs with polymer science. LMWGs and PGs each have their own different advantages and disadvantages; quite often the weak, reversible interactions that drive formation of gels from LMWGs mean the final material is mechanically weak, whilst gels formed from PGs are often much stronger. On the other hand, it is often much easier to introduce responsiveness into LWMG systems due to the easily tuneable nature of the individual building blocks and revisable nature of the assembly process.

Here, this combination of LMWGs and PGs is referred to as *hybrid gels* – note that some authors use this term to refer to combinations of LMWGs with non-gelling polymers, but here it

will be used exclusively to refer to LMWG and PG combinations. There are also examples of PG/PG combinations, which have recently seen intense interest – these combinations are often referred to as interpenetrating polymer network (IPN) gels,[99,100] or double-network gels;[101] they are however beyond the scope of consideration here.

Hybrid gels of LMWGs and PGs have great potential to display the best characteristics of each of their component gel networks – e.g., responsiveness from the LMWG, and robustness from the PG. Such multi-functional materials have great appeal for biomedical applications such as tissue engineering or drug delivery. Given the great potential, it is surprising that hybrid gels were rarely reported in literature until recent years. Hybrid gels can be broadly divided into three categories: *semi-hybrid gels*, *hybrid organogels and hybrid hydrogels*.

1.4.1. Semi-hybrid gels

There are some examples in the literature where LMWGs have been combined with polymers that have the capacity to be used as PGs, but are not actually being used as such in these cases. Instead, the polymers are used to form non-gelling support networks to improve the materials properties of the gel formed by the LMWGs. These materials are therefore strongly related to those discussed in sections 1.3.4 and 1.3.5.

Feng and co-workers demonstrated that the polysaccharide sodium alginate (which hydrogelates through crosslinking on addition of divalent cations or on protonation) could be added to hydrogels of 1,4-bi(phenylalanine-diglycol)-benzene (PDB) (Figure 1.29a) to form a semi-interpenetrating network by partially disrupting the LMWG interactions; the amide NHs of PDB interact with the carboxylates of the sodium alginate.[102] The gels with sodium alginate added had better mechanical and water retention properties; it was also possible to achieve controlled release of certain dyes (acting as drug models) from the semi-hybrid gel, as the sodium alginate introduced electrostatic forces, either attractive or repulsive depending on the dye, allowing the gel to retain or release dyes respectively.

Feng and co-workers also experimented with combining the PDB LMWG with a non-gelling polymer network of sodium hyaluronate (HA);[103] this glycosaminoglycan can also potentially form gels through covalent crosslinking. The addition of HA gave the dried PDB xerogels significantly better swelling properties than in the absence of HA; the swollen PDB/HA gels had much bigger pores than a swollen PDB gel, which provided enough room for cell migration and proliferation, allowing for easy 3D growth of cells (Figure 1.29b) – this is potentially useful for tissue engineering, disease model and drug release applications.
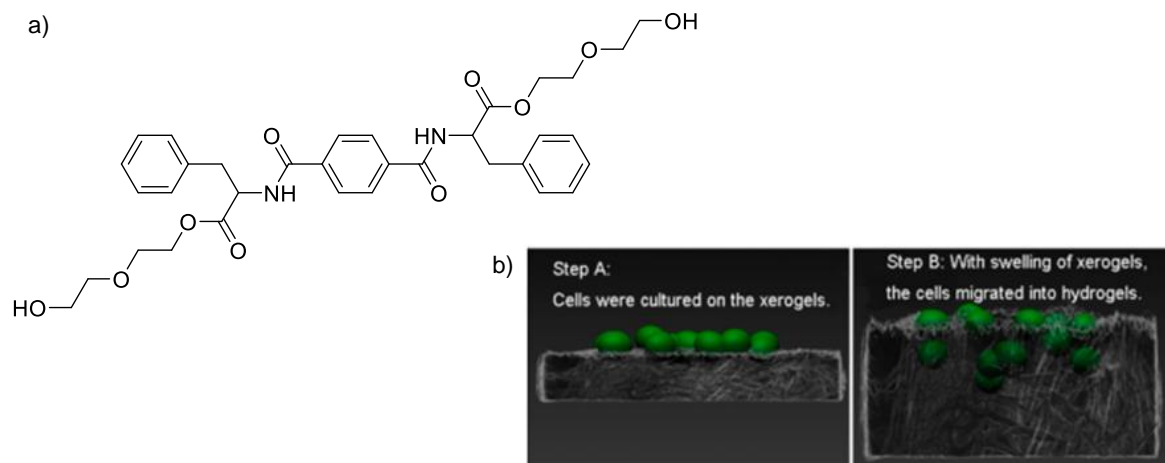
Figure 1.29: a) Structure of 1,4-bis(phenylalanine-diglycol)-benzene (PDB) LMWG as used by Feng and co-workers; b) schematic illustration of 3D cell culturing strategy using PDB/HA semi-hybrid hydrogels: cells are cultured onto a xerogel (step A); swelling of the gel, facilitated by HA then allows the cells to migrate into the bulk of the gel to form a 3D culture (step B). Image reproduced from reference 103.

Yu and co-workers also studied the assembly of a gelator within a pre-formed, non-gelling fibrous network – in this case, a two-component oligopeptide hydrogelator assembling within a chitosan, alginate and chondroitin network, designed to somewhat mimic the protein/polysaccharide composition of soft tissue.[104] The authors found that there were peptide-polysaccharide interactions within the resulting polymer/LMWG combination, which caused a change in the oligopeptide gel morphology – most notably a larger pore size.

1.4.2. Hybrid organogels

Hybrid organogels are defined as systems that combine LMWGs and PGs in an organic solvent. Guenet and co-workers studied the combination of an oligo(*p*-phenylenevinylene) LMWG (known as OPV16) (Figure 1.30a) with isotactic, syndiotactic and atactic polystyrene in *cis*- or *trans*-decalin or benzene.[105] OPV16 was highly compatible with the non-gelling atactic polystyrene with its self-assembled fibre morphology remaining unaffected; with the stereoregular isotactic or syndiotactic polystyrenes, which were capable of forming PG networks, hybrid organogels were formed – the individual gelator networks could be imaged by atomic force microscopy (AFM) (Figure 1.30b). The authors postulated (but did not investigate) that the morphology of the LMWG network could be affected by changing the concentration of the PGs – the higher the PG concentration, the smaller the PG network pore size, which influences the growth of the LMWG network, as the PG network was formed first in these materials.
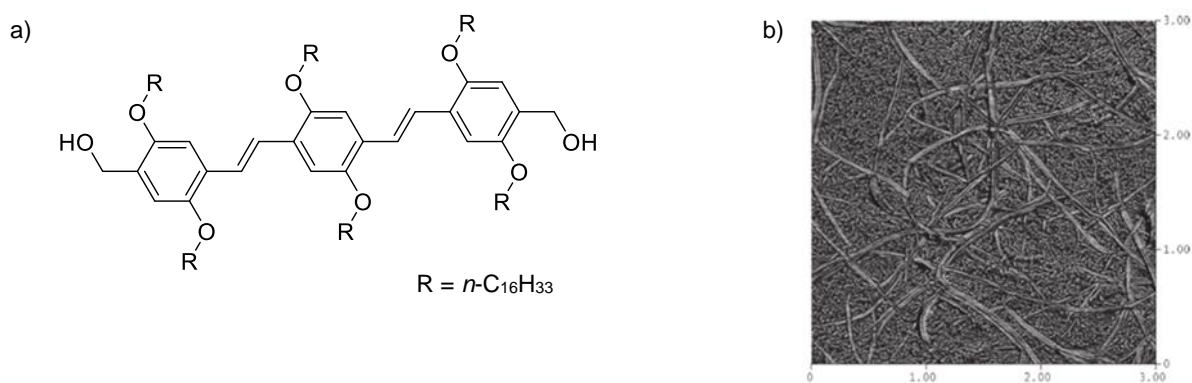
Figure 1.30: a) Structure of oligo(p-phenylenevinylene) LMWG OPV16 as used by Guenet and co-workers; b) AFM image of the hybrid organogel of OPV16 and isotactic polystyrene – two distinct sizes of fibres can be seen, with the larger fibres being of the LMWG and the smaller of the PG. Image reproduced from reference 105.

1.4.3. Hybrid hydrogels

At the start of this project, examples of hybrid hydrogels, in which a LMWG was combined with a PG in water, were relatively rare.

Yang and co-workers were the first to report hybrid hydrogels; they used a two-component supramolecular gel of H-Lysine(Fmoc)-OH with one of three other Fmoc-peptides (Figure 1.31) mixed with the PG agarose; the hybrid hydrogel was formed from a dispersion of the two gelator systems by a heat-cool cycle.[106] The agarose gel provided the materials with enhanced strength when compared to either the individual supramolecular or agarose gels. It was demonstrated that the hybrid hydrogels could incorporate additional components - Congo red was used as a model drug, with emission spectroscopy showing the presence of interactions between the dye and the LMWG nanofibres. The rate of release of Congo red could also be varied depending on the two-component LMWG system used – Fmoc-leucine and Fmoc-phenylalanine had stronger supramolecular interactions with the dye, hence a slower rate of release. In follow-up work, Yang and co-workers demonstrated that a similar hybrid hydrogel of Fmoc-3-(2- naphthyl)-D-alanine and agarose could be used to extract the dye methyl violet from aqueous solutions more efficiently that either of its individual constituent gels.
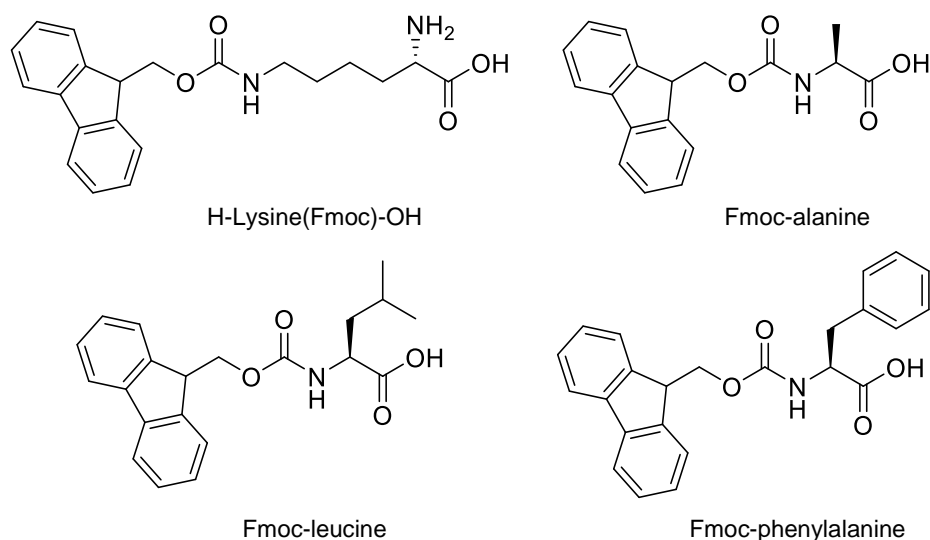
Figure 1.31: The multi-component peptide-based LMWG system used by Yang and co-workers, consisting of H-lysine(Fmoc)-OH in combination with one of three Fmoc-amino acids; this multi-component gel system was combined with the PG agarose to produce hybrid hydrogels.

Qi and co-workers also investigated drug release from hybrid hydrogels. Their hybrid gel was composed of the LMWG Fmoc-diphenylalanine (Fmoc-FF) and the polysaccharide PG konjac glucomannan (KGM).[107] In this material, a solvent-switch approach was needed to trigger gelation of the LMWG, by first dissolving it in a small amount of DMSO before addition of the aqueous PG solution; the PG network was then formed by slow gelation over several days. Again, the hybrid hydrogel was found to have a higher mechanical strength than compared to a gel of just Fmoc-FF; this increase in strength was found to be due to the nanostructure of the hybrid gel, in which the Fmoc-FF fibres were interpenetrated and interwoven with KGM chains – the authors made an analogy to the structure of reinforced concrete. The Fmoc-FF fibres in the hybrid hydrogel were also observed (by electron microscopy) to be thinner than in the Fmoc-FF gel; this was reasoned to be due to the presence of the KGM, which increased the viscosity of the solution, decreasing the rate of diffusion of Fmoc-FF, as well as causing more crowded assembly sites. Docetaxel was used as a drug model for *in vitro* release studies; it was found that an increase in KGM concentration lead to a decrease in docetaxel release rate (attributed to a more stable gel structure), though the rate could be increased by introducing β-mannanase – an enzyme able to degrade KGM – to the diffusion medium. This demonstrates how responsivity can be built into hybrid gels.

There are further examples of hybrid hydrogels; however, as these were published concurrent with the research presented in this thesis, they will be discussed at the relevant point.

1.5.   Project aims

The main theme of this project is the combination of low-molecular-weight and polymer gelators, especially to expand the fundamental understanding of this as yet very little-explored class of gels. There was a particular focus on how to control the formation of one network within the presence of another, and how to install some functionality into the gels produced from these combinations so they act as proof-of-principle demonstrations to the potential of hybrid gels. There are three main areas to be examined: (i) the combination of a LMWG with a PG to yield a material that can be described as responsive yet also robust, to clearly demonstrate the advantages of combining the two distinct classes of gelators; (ii) controlling the formation of one gel network in space in the presence of another gel network to yield a material with two or more spatially-resolved regions; and (iii) controlling the formation of one gel network in time in the presence of another, i.e., to determine when it forms, with scope to combine the final two aims into one material which is both spatially and temporally resolved.

1.5.1.   Responsive yet robust hybrid hydrogels

The production of responsive yet robust hydrogels rested on the possibility of combining a LMWG and PG with orthogonal methods of network production to best demonstrate the responsive of the LMWG component. Previous research in the area had largely focused on combinations of gels with the same methods of network production, meaning in those cases each network was responsive to the same stimuli; through using orthogonally assembled networks it was hoped that each network would respond to a different stimulus. There was a particular aim here to show that the LMWG network could be repeatedly switched "on" or "off" within the PG matrix through application of a stimulus, whilst the polymer network would remain intact and unaffected.

It is worth noting that such a responsive yet robust hybrid hydrogel had not been demonstrated before – the closest example involved the irreversible breakdown of the PG network, which of course severely affected the robustness of the gel.[107]

1.5.2.   Spatial resolution in hybrid hydrogels

This part of the project aimed to utilise a gelator for which the formation of gel network could be spatially controlled. To achieve this, it was thought that the best method for spatial control would be to use a photo-activated gel, potentially one activated by UV light. It was hoped that these different regions would show distinct diffusion properties, giving such materials potential for controlled release applications.

1.5.3. Temporal resolution in hybrid hydrogels

The control of when a gel network is formed in time could be said to be dependent on one of two factors, either (i) through careful control of the rate of network formation from a stimulus already present in the gel (e.g., a slow-releasing proton source to form a pH-responsive network), or (ii) from application of an external stimulus (e.g., UV light) to activate a gelator to form its network it the presence of another, pre-formed gel network. It was hoped that temporal control could be achieved using a variety of methods, including photoacid generation, and also to combine this approach with spatial control to yield materials with both spatial and temporal resolution.

2. Chapter 2: Responsive Yet Robust Hybrid Hydrogels

Results from this chapter were published in D. J. Cornwell, B. O. Okesola and D. K. Smith, *Soft Matter*, 2013, **9**, 8730–8736.

2.1. Introduction

In order to create hybrid hydrogels which can harness the advantages of the two independent networks, the first consideration is the selection of appropriate and compatible LMWGs and PGs; a large factor in this compatibility derives from the methods used to create each gelator network. Previous studies had chosen to use gelators that were both formed by heat/cool methodology,[106,108] or simple mixing of both gelators;[107] whilst this enabled quick and/or simple production of robust hybrid gels, it could be thought to limit the responsiveness of the final material, as both networks respond to the same stimulus (in those cases, change in temperature). Additionally, the relatively rapid and simultaneous formation of both networks prevented any detailed study of the kinetics of formation of one network in the presence of the other.

For the first hybrid hydrogels to be made here, a LMWG and a PG with orthogonal methods of gel production were chosen: the LMWG component was a pH-responsive 1,3:2,4-dibenzylidene-D-sorbitol derivative, and the PG component was the thermally responsive agarose. Each of these gelators will be considered and characterised individually first, before the hybrid hydrogels are discussed.

2.2. DBS and derivatives

1,3:2,4-Dibenzylidene-D-sorbitol (also known as dibenzylidene-D-sorbitol or DBS) (Scheme 2.1) is a well-known low-molecular-weight gelator. It was first identified as early as 1891 by Meunier, who obtained a mixture of two compounds, which he stated to be isomeric diacetals, from acid catalysed condensation of two equivalents of benzaldehyde with D-sorbitol;[109] one of these compounds formed a gel in certain organic solvents, while the other did not.
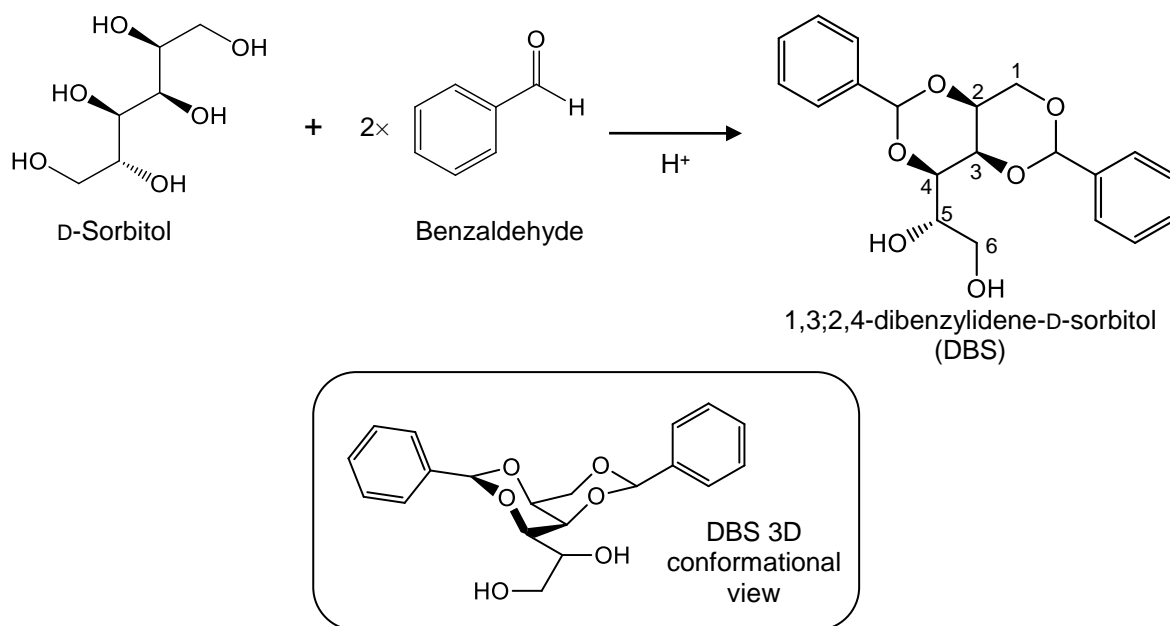
Scheme 2.1: Synthesis of 1,3;2,4-dibenzylidene-D-sorbitol from D-sorbitol and benzaldehyde, and 3D conformational view.

It would not be until 1942 and the work of Wolfe and co-workers that it was revealed that DBS was not in fact a mixture of isomers, but actually a single species.[110] They determined that the synthesis also yielded mono- and tri-substituted derivatives – it was likely one of these derivatives that Meunier had erroneously identified as an isomer of DBS. Wolfe and co-workers were also able to identify that DBS had the acetal functionalisation pattern of 1,2,3,4. The precise 1,3:2,4 pattern was then determined in 1944 by Angyal and Lawler, who carefully hydrolysed DBS to yield 2,4-monobenzylidene sorbitol (MBS).[111] It should be noted, as emphasised by Brecknell and co-workers in 1976,[112] that DBS should be most fully described as 1,3(*R*):2,4(*S*)-dibenzylidene-D-sorbitol. The acetal carbons formed during synthesis are new chiral centres, and as they are formed under thermodynamic control, it can be assumed that the phenyl groups occupy equatorial positions on the resulting six-membered rings.

Derivatives of DBS are synthesised by either modification of the free alcohol groups at the 5 or 6 positions (before or after acetal formation),[113–116] or by using a substituted benzaldehyde with functional groups on the aromatic wings.[114,117–127]

DBS and its derivatives have a long history of use in a variety of commercial applications, including personal care products (such as solid antiperspirants),[128–136] adhesives,[137–139] and as nucleating and clarifying agents in plastic or thermoplastic materials.[140–145] All these applications rely upon the formation of DBS (or DBS derivative) nanofibres in an organic phase or medium.

DBS and derivatives self-assemble into nanofibrils and nanofibres *via* either hydrogen-bonding or π-π stacking interactions – the dominant non-covalent interactions depend on the polarity of the solvent.[146] In non-polar solvents, H-bonding between the 6-OH and the acetal oxygens drives self-assembly, whilst in more polar solvents it is primarily π-π stacking between the aromatic groups.

Prior to the beginning of this project, there were surprisingly no reports of DBS or any DBS derivative forming a gel in pure water – only organogels had been observed in over 100 years of this class of gelators' existence. All previously reported DBS gelators were too hydrophobic to fully dissolve in water and allow for self-assembly to take place.

2.3. Synthesis of 1,3:2,4-dibenzylidene-D-sorbitol-*p,p*'-dicarboxylic acid (DBS-CO$_2$H)

In order to overcome the problems of solubility in water, it was reasoned that the modification of DBS with pendant carboxylic acid groups would yield a hydrogelator; these added groups would increase polarity (and therefore hydrophilicity) on the periphery of the self-assembled nanostructure (there is also precedent for carboxylic acid functionalised LMWGs[9,147]). Synthesis was achieved by drawing on literature methods for synthesising DBS derivatives;[114,120] this is summarised in Scheme 2.2. In the first step, D-sorbitol was condensed with two equivalents of 4-carboxybenzaldehyde methyl ester in the presence of *p*-toluene sulfonic acid (*p*-TsOH) to yield a mixture of mono-, di- and tri-substituted derivatives; the unwanted mono- and tri-substituted derivatives were removed by washing with boiling water and boiling DCM respectively, to yield DBS-CO$_2$Me in 77% yield. This was followed by saponification of the methyl ester groups with NaOH, and subsequent acidification with NaHSO$_4$ to give DBS-CO$_2$H in 69% yield, with no further purification required. The product identity was confirmed by ^{1}H and ^{13}C NMR, and ESI-MS with a *m/z* value of 445.1143 (100% [M–H]$^-$).
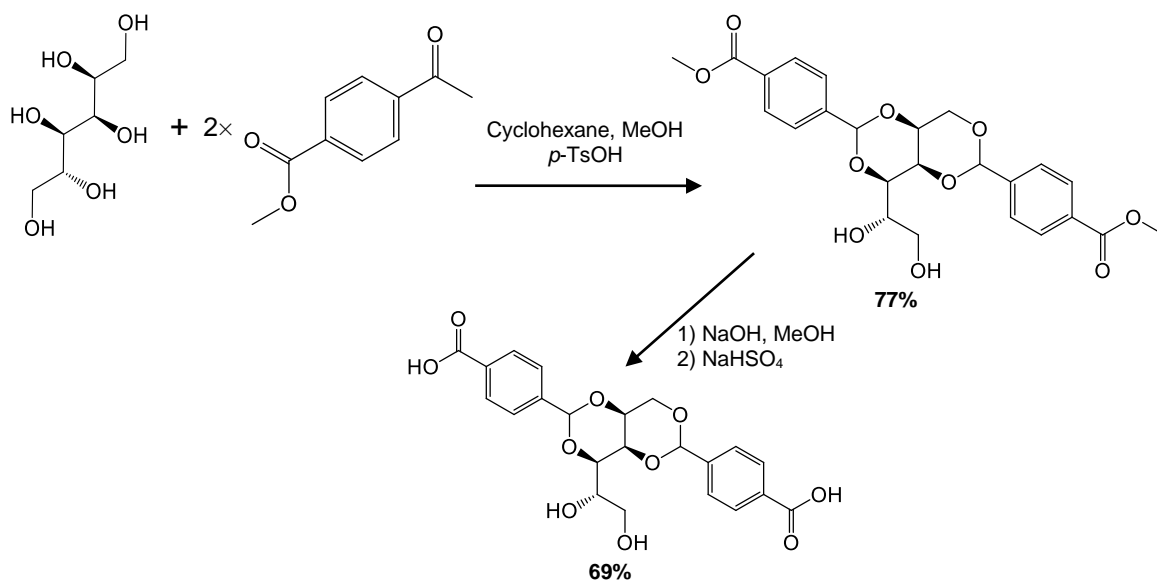
Scheme 2.2: Synthesis of DBS-CO₂H

2.4. Gelation studies of DBS-CO₂H

During the synthesis of DBS-CO$_2$H, upon acidification by addition of NaHSO$_4$, a white, stable gel was observed to form. This strongly suggested that DBS-CO$_2$H was able to act as a hydrogelator; incorporating the carboxylic acid groups had increased the hydrophilicity. Like many other CO$_2$H-modified LMWGs,[148–152] it was clear that DBS-CO$_2$H would only form hydrogels at pH values below the pK_a of the carboxylic acid groups, with protonation being a pre-requisite of gelation. This is a result of the solubility of the deprotonated carboxylate which causes it to dissolve, with protonation lowering the solubility just enough to trigger self-assembly and gelation.

In order to form a homogenous gel, slow acidification of a basic solution of the LMWG is preferable to addition of a dilute aqueous acid (such as HCl), which can result in inhomogeneous and weak gels.[150] The addition of glucono-δ-lactone (GdL) was a method first pioneered by Adams and co-workers;[150] GdL hydrolyses slowly in water to the free D-gluconic acid (Scheme 2.3),[153] which gradually lowers the pH and hence allows slow and controlled formation of homogeneous gels.
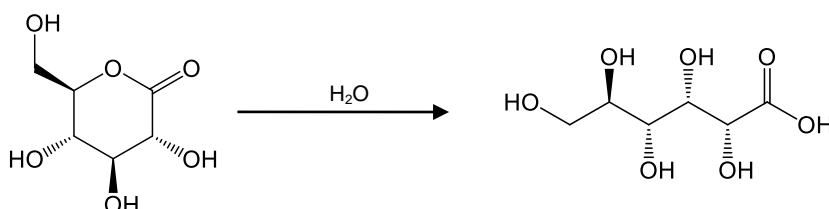
Scheme 2.3: The hydrolysis of glucono-δ-lactone to gluconic acid; this reaction is accompanied by a decrease in solution pH.

2.4.1. Preparation and T_{gel} studies of DBS-CO$_2$H hydrogels

To prepare gels of DBS-CO$_2$H, a known amount of gelator was weighed into standard sample vials and deionised water (1 ml) was added. Aliquots of NaOH (10 μl, 0.5 M) were then added until the gelator was fully dissolved. The solutions were then transferred to a sample vial containing GdL (6-8 mg, 33.7-44.9 mM) and left overnight to allow acidification and hence gelation to occur – with the formation of translucent gels being observed; Figure 2.1 shows the formation of a DBS-CO$_2$H hydrogel. The samples were deemed to be gels if they survived for longer than 1 minute using the tube inversion method. By this method, the minimum gelator concentration (MGC) was determined to be 0.15% wt/vol, regardless of the amount of GdL used.
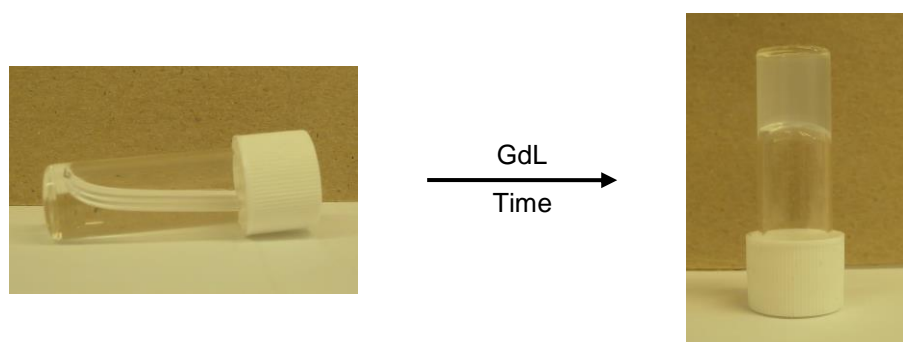
Figure 2.1: Formation of DBS-CO₂H hydrogel; clear, basic solution (left) changes to translucent gel (right) with decrease in pH over time, brought about by hydrolysis of GdL.

The thermal stability of the gels was assessed by determining their T_{gel} values by tube inversion methodology. T_{gel} is the temperature at which a gel-sol transition occurs, which in simple table-top rheology is usually defined as the temperature at which a gel collapses upon tube inversion.[154] The gel samples were placed in a thermoregulated oil bath, which was then heated from 20°C at a rate of 1°C min^{-1}. T_{gel} values were recorded for gels made with 6 mg and 8 mg of GdL, and are presented in Table 2.1.

Table 2.1: T_{gel} data for DBS-CO$_2$H and hybrid gels. ">100" signifies that the gel remained stable over the boiling point of the solvent; the collapse of the gel after this point can be attributed to the boiling of the solvent rather than a breakdown of the gel network.

% wt/vol DBS-CO$_2$H		T_{gel} / °C	
		6 mg (33.7 mM) GdL	8 mg (44.9 mM) GdL
0.15		**39**	**>100**
0.20		**47**	**>100**
0.25		**54**	**>100**
0.30		**>100**	**>100**

Those gels with 6 mg GdL showed gradually increasing T_{gel} values with increasing % wt/vol of the LMWG; those with 8 mg GdL all had T_{gel} values of >100°C. This indicates using a greater amount of the acidifying agent gives a more complete network formation, due to the faster rate of acidification increasing the total number of gel fibres, which in turn increases the thermal stability. However, as the gels were formed by a change in pH, they were not thermo-reversible; when the gels collapsed, they formed a precipitate, and remained in this state upon cooling. Thus it must be noted that what is observed it not a true reversible gel-sol transition, but rather a disruption of the gelator network.

2.4.2. ^{1}H NMR studies of DBS-CO$_2$H hydrogels

When studied by NMR spectroscopy, free, mobile LMWGs have a suitable relaxation time, which means they can be considered "NMR visible"; conversely, an aggregate such as a solid-like gel network has a much slower relaxation time, causing the NMR signals to be broadened, and often hidden in the baseline.[155] Hence, solid-like gel networks can be considered "NMR invisible". By using a probe molecule that does not aggregate or interact with the gelator molecules, peak integration can then allow quantification of the amount of mobile gelator, meaning it is possible to quantify gelator molecules in rapid equilibrium with the solid-like fibres, or the gradual formation of a gelator network over time.[156–159] For ^{1}H NMR studies, samples of the gels were prepared by adding D$_2$O (0.7 ml) to DBS–CO$_2$H (1.4 mg), followed by sonication to disperse the solid. NaOH$_{(aq)}$ (21 µl, 0.5 M) was added to dissolve all the solid, and DMSO (1.4 µl) was then added to act as an internal standard. The solution was then transferred to a vial containing GdL (5.6 mg, to give 44.9 mM), followed by shaking. The sample was then immediately transferred to a NMR tube and placed in the spectrometer for spectra to be recorded.

DMSO was chosen as the reference molecule, as it has a single, sharp peak at $\delta \approx 2.6$ppm that does not overlap with any peaks from either DBS-CO$_2$H or GdL. There is significant overlap in the ^{1}H NMR spectra for DBS-CO$_2$H and GdL in the region of $\delta = 4.5$-3.5 ppm. However, there is no overlap with the Ar-H at $\delta \approx 8.0$-7.5 peaks for DBS-CO$_2$H, meaning the integral values from these peaks can be compared to the integral values of the probe molecule; although there is no overlap with the DBS-CO$_2$H Ar-CH peak at $\delta \approx 5.8$, this peak can become affected by the nearby solvent peak, making the integral values measured inaccurate.

Using the internal standard of DMSO as the means of quantifying the concentration of the mobile gelator also means that the relative error of the measurements is relatively small. Any possible error in quantification is firstly due to the concentration of DMSO, which can only vary by no more than $\pm$ 2.5%, given that all measurements were made using accurate μL pipettes. The second source of error is in the integration of the DBS-CO$_2$H and DMSO signals in the NMR spectra; this integration was carried out using the automated integration function in the NMR processing software, and is assumed to be accurate to $\pm$ 0.005. With both these factors taken into consideration, the maximum error present cannot be more than $\pm$ 3%.

Initially, ^{1}H NMR spectra were taken at the "start" (within one hour of preparation) and "end" (usually $\geq$ 16 hours after preparation) of gelation. Using this "snapshot" method of recording, and by comparing integral values of selected DBS-CO$_2$H peaks to the DMSO peak, it was observed that at the "start" of gelation, most of the gelator was still free in solution, as hydrolysis of GdL (and hence decrease of pH) had only just begun, whereas at the "end" of gelation (where pH is *ca*. 3) most, if not all, of the molecule had been incorporated into a gelator network (Figure 2.2).
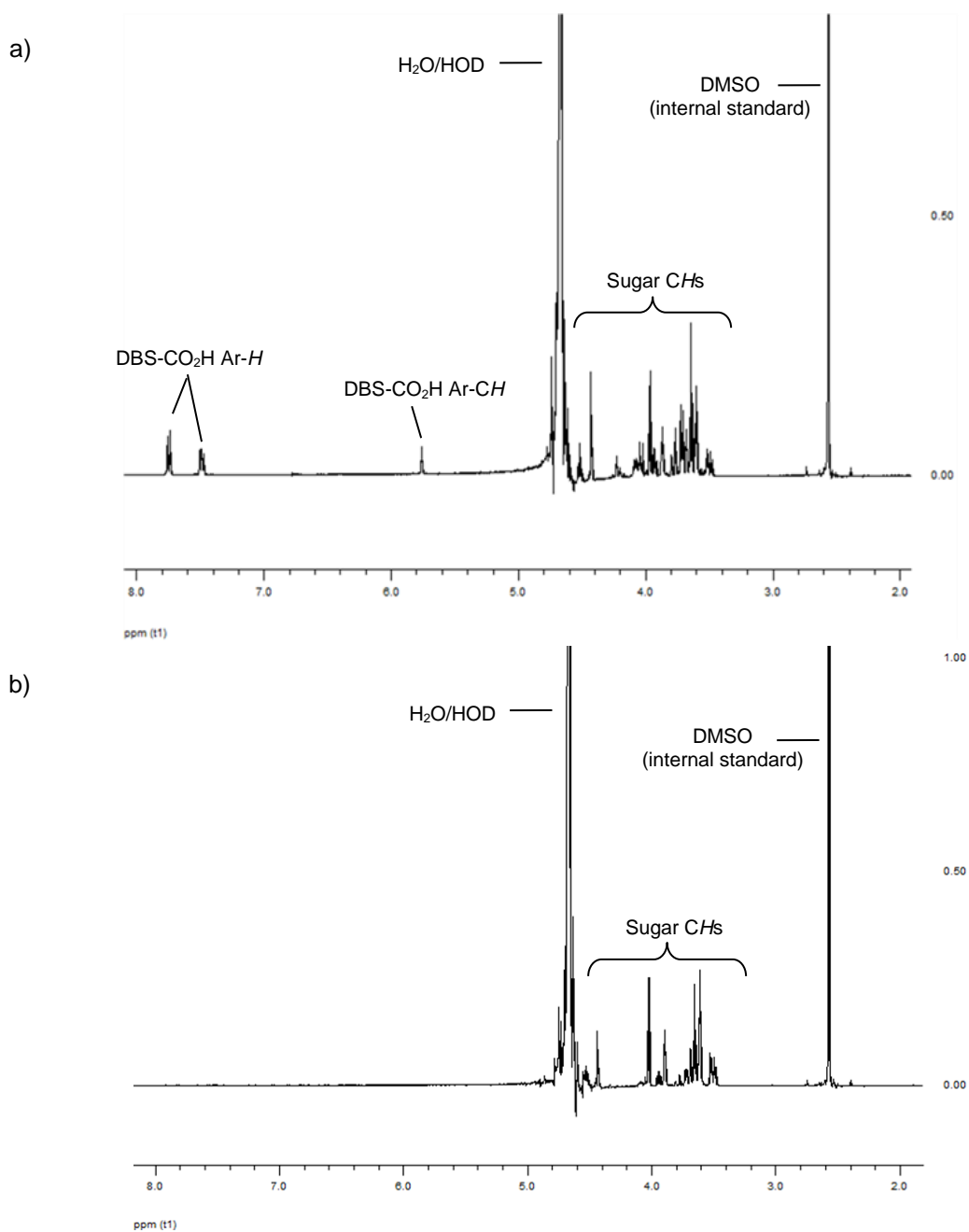
Figure 2.2: ^{1}H NMR spectra (400 MHz, D$_2$O) of DBS-CO$_2$H gel (0.2% wt/vol) at (a) start of gelation and (b) end of gelation; the absence of signals related to DBS-CO$_2$H in (b) indicates that all of the LMWG has been incorporated into a sample-spanning solid-like network.

More detailed information on the kinetics of gelation was obtained by monitoring the evolution of the NMR spectrum over time after the addition of GdL. This was achieved by preparing a sample of DBS-CO$_2$H by the method describe above, and recording NMR spectra every 30 minutes for 14 hours. By determining the concentration of mobile DBS-CO$_2$H from the spectra, the rate of formation of the gelator network could be plotted (Figure 2.3).
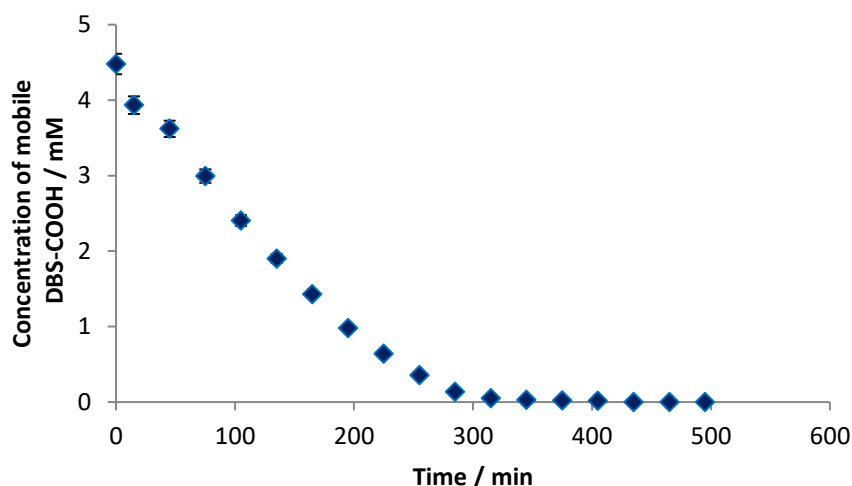
Figure 2.3: Plot of average rate of formation of the DBS-CO₂H network, as monitored by ¹H NMR.

Avrami's kinetic model (Eq. 1) was originally developed to help understand crystallisation processes,[160–162] but can also be applied to supramolecular gelation, as the growth of gel fibres can be likened to a form of crystallisation, in which a 'solid-like' phase forms from a solution phase. Furthermore, in gelation there are clear dimensional restrictions to the growth of the fibres. The Avrami model, in which X(t) represents the volume fraction of the gel phase, K is the effective "time constant" for gelation and as such varies with temperature and concentration, n is the Avrami exponent (which reflects the dimensionality of 'crystal' growth, with 1 being 1D growth, 2 being 2D, etc.) and t is time, can be rearranged into Eq. 2. It is assumed that the nucleation in the system occurs instantaneously, and that the growth of the fibres in the gel phase are independent of each other.[155]

$$1 - X(t) = \exp(-Kt^n) \qquad \text{(Eq. 1)}$$

$$\ln(\ln(1/1\text{-}X(t))) = \ln K + n\ln(t) \qquad \text{(Eq. 2)}$$

$$X(t) = ([\text{LMWG}](\infty) - [\text{LMWG}](t))/([\text{LMWG}](\infty)\text{-}[\text{LMWG}](0)) \qquad \text{(Eq. 3)}$$

The volume fraction of the gel phase X(t) can be expressed in terms of LMWG concentration (extrapolated from NMR signal intensity or other spectroscopic methods) at equilibrium ([LMWG](∞)), at time t ([LMWG](t)) and at the start of the experiment ([LMWG](0)) using Eq. 3. This relationship enables linear fitting of Eq.2 to determine the Avrami exponent n, which is the gradient of the line of best fit.[163] It should be noted that when using NMR methods to determine

the extent of assembly, an assumption is made that the disappearance of NMR signal represents the incorporation of the gelator into the nanoscale fibres – however, immobilisation of the gelator into other kinds of solid-like phase would also cause the same effect.

The Avrami model for measuring kinetics of LMWG fibre growth has previously only been applied to systems where the gel forms from a supersaturated solution of the LMWG. The LMWG was dissolved in hot solvent, then held at a set temperature to gelate whilst an analytical method (such as rheology, CD or fluorescence spectroscopy) was applied to gain data to be used in the Avrami model.[163,164] For these system, the rate of gelation was dependent on the temperature the solution was held at (cooler temperature = faster gelation), though the Avrami coefficient n was found to be the same, independent of temperature or analytical method applied.

For pH-initiated gelation, in order to apply the Avrami model, the following assumptions must be made: 1) the basic solution of the LMWG is equivalent to a supersaturated solution and 2) the rate of pH change (which is dependent on temperature and concentration of GdL present) is in effect equivalent to holding a supersaturated solution at different temperatures causing different rates of gelation to occur. Therefore it is also assumed that n will be independent of the rate of pH change (which can also change during the experiment itself).

However, it could be considered that what is observed in the NMR study of concentration vs time (as seen in Figure 2.3) is as much a measure of the rate of pH change, as the reduction in the concentration of the mobile gelator – in which case n would be dependent on the rate of pH change and any conclusions drawn from its value would have to be treated with caution. Clearly, pH-dependent gelation processes have a number of variable which change during the gelation event. As such, the results and conclusions from applying the Avrami model to the pH-dependent LMWG systems should be treated with a degree of caution. However, in spite of these limitations it is suggested that differences in observed Avrami coefficients between structurally similar gelators or systems where the same LMWG is used in the presence or absence of a polymer gelator, which have been treated under identical conditions of pH change, should represent fundamental differences in their assembly modes and gelation kinetics, even if their absolute meaning is difficult to precisely quantify and interpret.

Applying Avrami's kinetic model to the concentration vs. time data acquired by NMR (Figure 2.4), an Avrami exponent of n = 1.61 was calculated, indicating there may be a degree of branching or two-dimensional growth of the gel fibres.
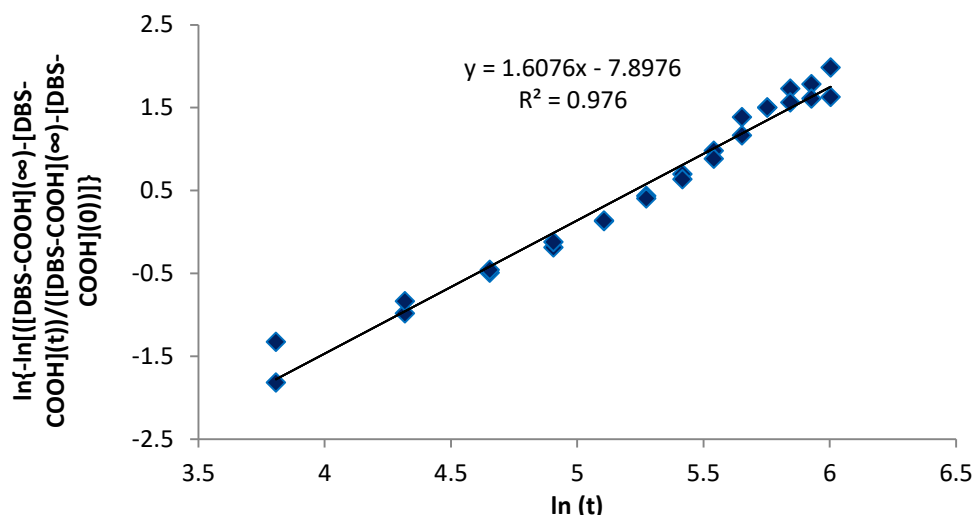
Figure 2.4: Avrami plot for formation of DBS-CO$_2$H network, using data from two runs; n = gradient of line = 1.61.

2.4.3. Circular dichroism studies of DBS-CO$_2$H hydrogels

Circular dichroism spectroscopy can be considered as "chiral spectroscopy"; it is essentially UV-Vis spectroscopy using circularly polarised light. The spectrum measures the difference in absorbance between left-handed and right-handed circularly polarised light, which is then reported as an ellipticity.[155,165,166] Achiral molecules exhibit no bands in the CD spectrum, whereas chiral molecules can exhibit a signal in the same region where they would have UV-Vis absorption. However, on their own, small chiral molecules often display little or no CD signal; it is only when assembled into a chiral nanostructure that the interactions with the polarised light are enhanced enough to generate a CD signal. As such, CD spectroscopy is a useful technique for probing the chiral nanoscale organisation of self-assembled gel-phase materials.

For DBS-CO$_2$H, the presence of the aromatic rings provided a useful chromophoric 'handle', which was found to be distinct against the background of GdL/gluconic acid and solvent (Figure 2.5a). As such, CD was used to probe the assembly of DBS-CO$_2$H, though it should be noted that this experiment was performed below the gelation threshold of DBS-CO$_2$H (0.02% wt/vol), and therefore what was observed was the assembly of organised nanofibres within the sample but not the formation of a full sample-spanning network; sample preparation was the same as for gels in all other respects.

Samples were prepared as described above; the only alteration was to decrease the amount of DBS-CO$_2$H to 0.02 % wt/vol. On standing a sample for five hours after the addition of GdL, the CD spectrum recorded showed the aromatic rings of DBS-CO$_2$H experiencing a chiral microenvironment, as confirmed by the observation of a CD band with a maximum at 260 nm with

an intensity of *ca*. -41 mdeg (Figure 2.5b). The major peak at ca. 220 nm can be assigned to the presence of GdL/gluconic acid.
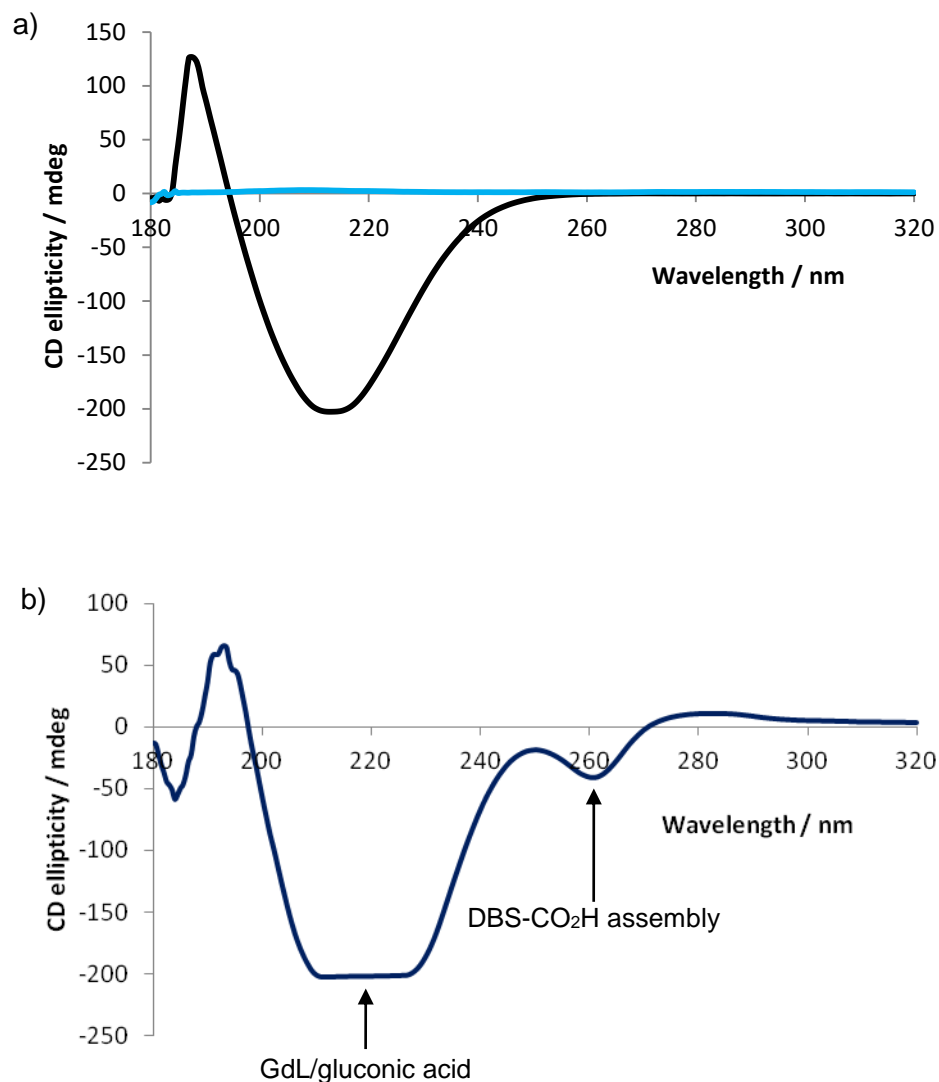
Figure 2.5: a) CD spectra of GdL/gluconic acid (black) (44.9 mM) and H$_2$O (light blue); b) DBS-CO$_2$H (0.02% wt/vol, 44.9 mM GdL).

When recording CD spectra, the level of absorbance can cause variations in the maximum ellipticity observed; when the absorbance is particularly high, too little light will reach the detector and reliable spectra cannot be recorded – this is referred to as saturation. It is possible to know if saturation is occurring by observing the high tension (HT) voltage, which is approximately proportional to the level of absorbance. If the value of HT goes above *ca.* 600 V, then the detector is considered saturated; this leads to the considerable oscillation in the resulting CD spectrum. For the above sample of DBS-CO$_2$H the HT data recorded (Figure 2.6) only goes above 600 V below 200 nm – corresponding to the region in the CD spectra of DBS-CO$_2$H where greater oscillation is

observed (Figure 2.5b). Comparing HT values between CD experiments can therefore be used to determine if the differences in ellipticity reported are due to variation in HT.
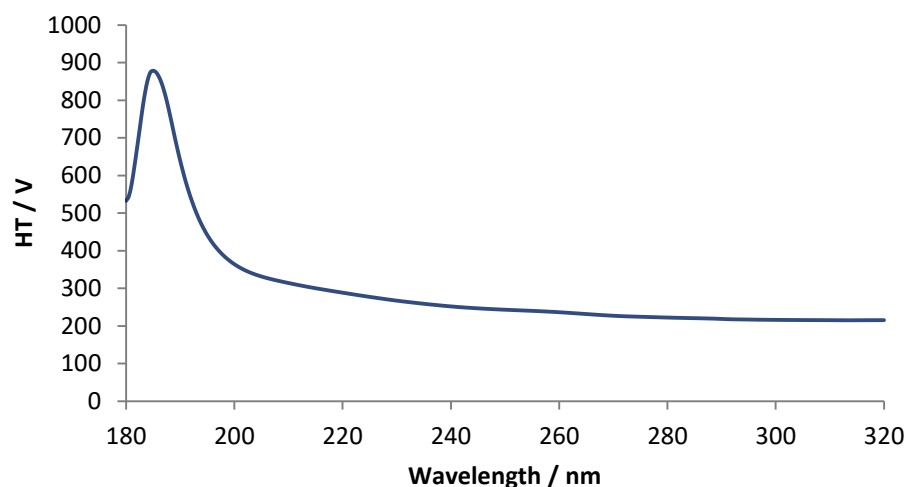
Figure 2.6: HT data for CD spectra of DBS-CO₂H (0.02% wt/vol, 44.9 mM GdL).

A CD experiment that directly probed the initial stages of fibre growth was also possible; by recording CD spectra every 5 minutes for two hours after the addition of GdL, the bands associated with DBS-CO$_2$H could be seen to slowly emerge (Figure 2.7). This additional kinetic information could be used to provide further insight into the dynamics of assembly of the LMWG fibres. By plotting time (after addition of GdL) against the CD ellipticity at 260 nm, it was seen that there was an induction phase, followed by a slight increase in CD ellipticity, only after which the emergence of the CD band associated with the DBS–CO$_2$H nanofibres was observed (Figure 2.8). These observations fit well with a model in which the initial step is where the pH is lowering before nucleation of the LWMG takes place, and that only once this has occurred can fibre growth take place.
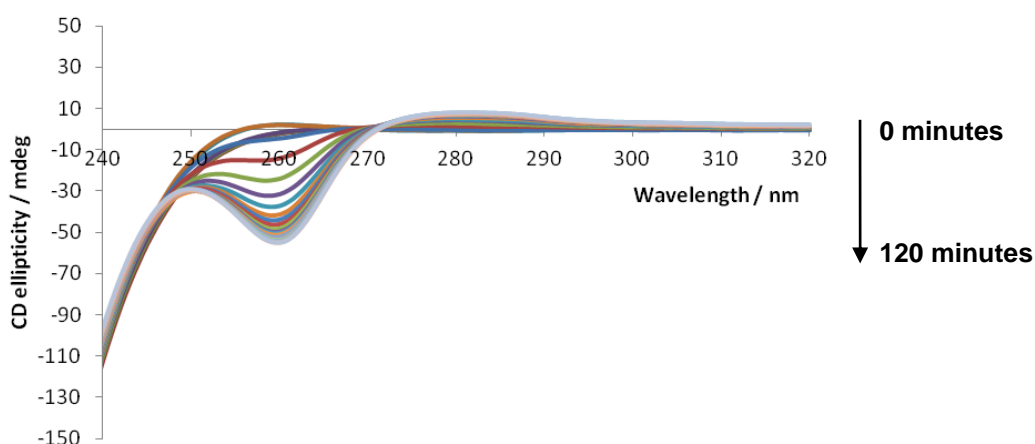
Figure 2.7: Evolution of CD spectrum of DBS-CO₂H (0.02% wt/vol) over a 2-hour period, after addition of GdL (44.9 mM).

73
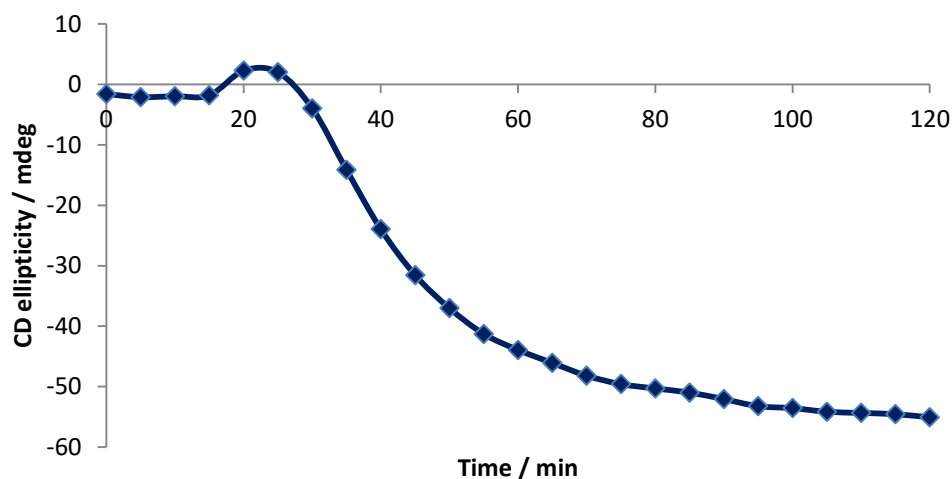
Figure 2.8: Evolution of CD spectrum of DBS-CO₂H (0.02% wt/vol) over a 2-hour period, monitoring the ellipticity at 260 nm, after addition of GdL (44.9 mM).

It is interesting to note that the DBS-CO$_2$H nanofibres had a higher ellipticity after 2 hours than they did at 5 hours (see Figure 2.5b for comparison); this would indicate further slow evolution of the nanofibres over time, and suggests that DBS-CO$_2$H may first assemble into a metastable state,[31,167–169] which then evolves into a more stable form with a lower ellipticity value over time. It should also be noted thought that this higher ellipticity could be due to a higher value of HT – *ca.* 240 V for the 5 hour sample vs. *ca.* 270 V for the 2 hour sample (Figure 2.9).
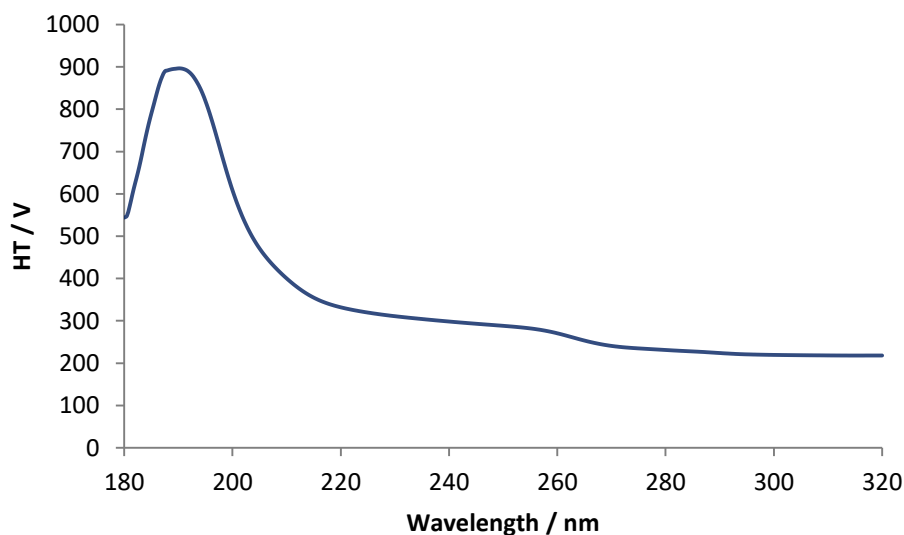
Figure 2.9: HT data recorded after 2 hours for the CD spectra of DBS-CO₂H (0.02% wt/vol) as ellipticity was monitored over a 2-hour period (see Figure 2.8).

2.4.4.   SEM imaging of DBS-CO₂H hydrogels

SEM images of a 0.2% wt/vol, 8 mg GdL hydrogel of DBS-CO$_2$H were obtained by taking a small portion of the gel, and placing it on a copper support, then freeze-drying by immersing in liquid nitrogen, followed by lyophilising overnight. Excess solid material was broken off with a spatula and then the sample was sputter coated with a thin layer (about 12 nm) of gold/palladium to prevent sample charging, before placing the sample on a metal SEM stub and imaging with a field emission gun scanning electron microscope (FEG-SEM).

The freeze-drying of samples for SEM can cause some significant change to the overall structure of the gel network. During freeze-drying, water is crystallised into ice crystals, which are then sublimated to leave the dried product. However, the growth of the ice crystals – which is in effect an expansion of the solvent – push the non-aqueous components of the sample (in this case the gel fibres) to the edges of the crystals; after sublimation the solid components remain in these positions. When observed by SEM then, the voids left by the ice crystals (sometimes referred to as ice crystal "ghosts") are present, meaning that the nanostructure seen in the SEM images is not fully representative of what exists in the hydrated sample.[170] Additionally, the length of time taken to freeze the sample affects the size of the ice crystals and their subsequent voids – the slower the rate of cooling, the larger the ice crystals. However, for the purposes of observing whether or not gelators are forming fibrous networks, this freeze-drying method is acceptable, though no data on pore size or approximate fibre diameter can be reliably obtained due to the changes in the nanostructure caused by the ice crystal formation.

The SEM images of the xerogel of DBS-CO$_2$H (Figure 2.10) showed the presence of well-defined fibres, with noticeable branching – supportive of an Avrami co-efficient significantly >1.
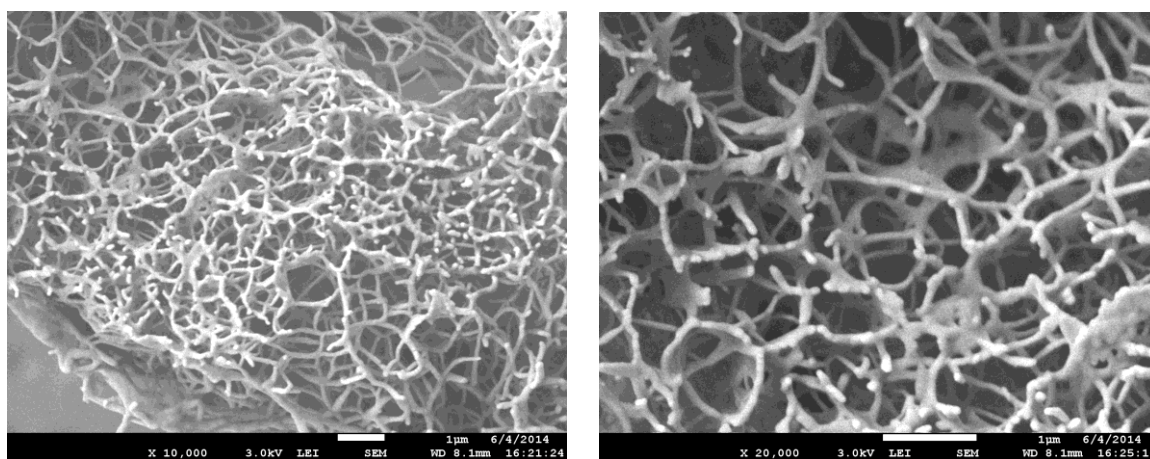
Figure 2.10: SEM images of freeze-dried DBS-CO₂H xerogel. Scale bars = 1 µm

2.5.   Agarose Hydrogels

2.5.1.   Background

Agarose is a polysaccharide consisting of alternating units of 1,3-linked β-D-galactose and 1,4-linked 3,6-anhydro-α-L-galactose,[171] and is able to form robust polymer hydrogels. Agarose gel networks are made by the formation of double helices via non-covalent interactions between two polysaccharide chains; there are deviations in the polysaccharide chains causing "kinks", which terminate the double helix structures so that each has "free" chains at both ends.[172] Following the formation of bundles of double helices, these free chains then contribute to aggregation and network formation by creating "junction zones" (Figure 2.11);[173] the trigger for this network formation is a heat-cool cycle. Agarose gels are widely used in biomolecule purification,[174] as well as in tissue engineering applications.[5]
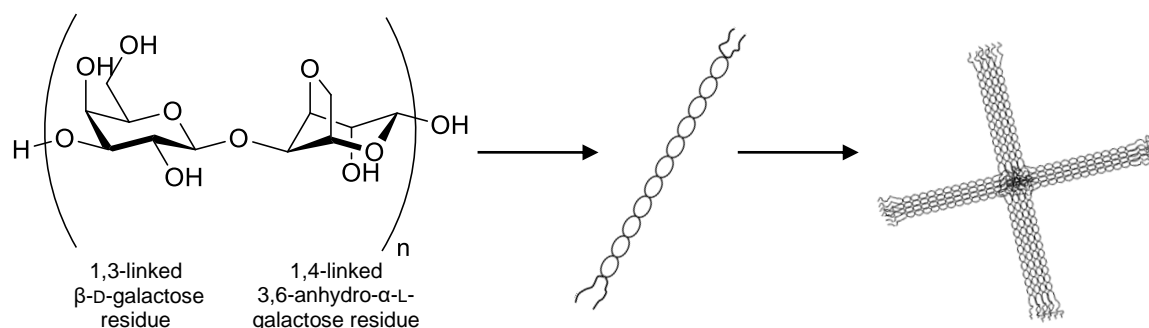
Figure 2.11: Formation of double helix structure with terminal "kinks" from agarose polysaccharide; the double helices then aggregate into bundles, which are held together physically by the formation of "junction zones" between the free terminal polysaccharide chains.

2.5.2.   Preparation and T_{gel} studies of agarose hydrogels

Gels of agarose were formed by adding 1 ml of deionised water to a known mass of agarose in a 2 ml sample vial. The vial was then heated to 90°C in an oil bath, and held at this temperature for 5 minutes, with shaking every minute to dissolve the agarose. The solutions were removed from the oil bath and allowed to cool to room temperature, upon which a clear gel was formed after *ca.* 20 minutes (Figure 2.12). The useable MGC was established to be 0.5% wt/vol at neutral pH (although it was possible to form gels with less than this, they tended to be very weak, and not suitable for use in hybrid gel studies). Addition of NaOH and GdL made no difference to the MGC for agarose. The thermal properties of agarose gels with concentrations 0.4-1.0% wt/vol were tested, with T_{gel} values in the range of 95-98°C being recorded – gel collapse in this case is associated with the solvent nearing boiling point.
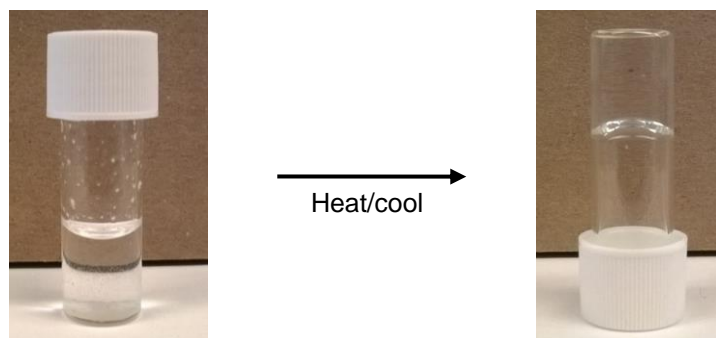
Figure 2.12: Formation of agarose hydrogel from cold suspension of solid agarose(left); heating to 90°C followed by cooling to room temperature results in a robust, transparent gel(right).

As the agarose hydrogel formed relatively quickly, NMR kinetic studies were not possible; likewise, CD kinetic studies were not possible due to the agarose aggregates generating no CD signal.

2.5.3. SEM imaging of agarose hydrogels

Samples for SEM were prepared in the same way as described for gels of DBS-CO$_2$H (see 2.4.4 for a discussion on the limitations on the information that can be obtained from freeze-drying samples for SEM). The agarose xerogel was seen to consist of a network of flexible, narrow fibres (Figure 2.13) – the thinness of the fibres would appear be consistent with the optically transparent nature of the gel.
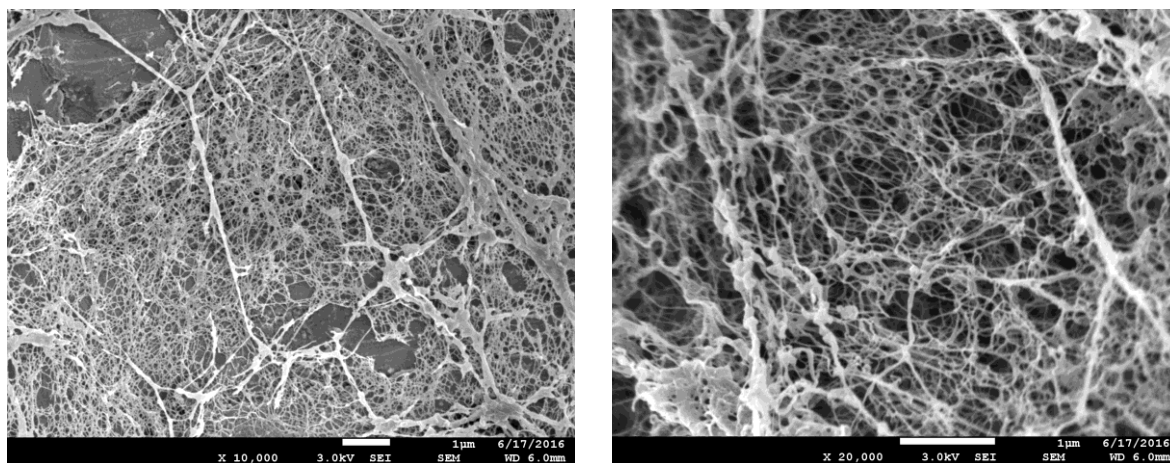
Figure 2.13: SEM images of xerogels of agarose (0.5 % wt/vol); scale bars = 1 µm

2.6. Hybrid hydrogels of DBS-CO₂H and agarose

2.6.1. Preparation and T_{gel} studies of hybrid hydrogels of DBS-CO₂H and agarose

Hybrid gels were made by dissolving DBS-CO₂H in water through addition of $NaOH_{(aq)}$ (0.5 M), following the method as described previously. Agarose (5 mg, 0.5% wt/vol) was then added to the vial, which was heated at 90°C for 5 minutes and then cooled to 50°C at which temperature GdL (6-8 mg) was added; this cooling step was included to prevent an increased rate of GdL hydrolysis if it had been added at a higher temperature. On cooling the vial to room temperature a clear agarose gel was then formed after *ca*. 20 minutes. This gel became translucent after standing overnight (Figure 2.14) – this translucency was considered to be visually indicative of the formation of the DBS-CO₂H gelator network, as a pure agarose gel left for the same length of time remained optically transparent.
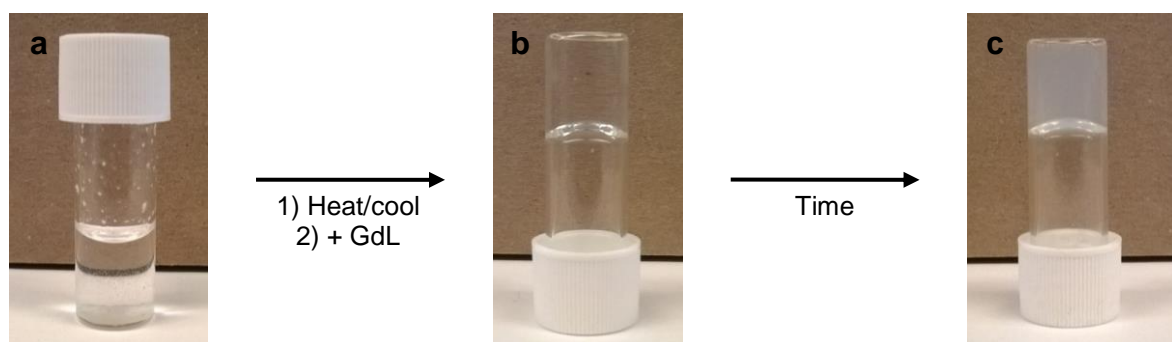
Figure 2.14: Formation of hybrid hydrogel of DBS-CO₂H and agarose; GdL is added after heating of basic solution of DBS-CO2H with agarose suspension(a); clear agarose gel then forms (b), changing to translucent over time as LMWG network forms (c).

Interestingly, the T_{gel} values of all of the hybrid gels were higher than 100°C (i.e., above the boiling point of the solvent) – higher than that of either agarose alone or DBS-CO₂H with 6 mg of GdL, and equivalent to the stability of the DBS-CO₂H gel when 8 mg of GdL was used. This may indicate that the hybrid material is thermally stabilised compared to the two individual gel networks, suggestive of some degree of positive interaction between gel networks.

2.6.2. Rheological studies of hybrid hydrogels of DBS-CO₂H and agarose

2.6.2.1. Introduction to Rheology

Rheology is the science of deformation and flow of materials in response to an applied stress or strain.[175] Given the nature of gels as soft materials, rheology is an ideal method for characterising their macroscopic materials properties,[176] and offers significant advantages over simple table-top methods, such as tube inversion.

Typical rheological testing is divided into the two categories of flow and elasticity.[177] Flow quantifies the viscosity of a material (i.e., resistance to flow) and is an irreversible deformation –

the material will not return to its prior form once the applied stress/strain is removed. Elasticity quantifies how a material recovers after stress/strain is applied – it is a reversible deformation. Materials that exhibit both flow and elastic properties (such as gels) are termed *viscoelastic*. Whilst in an ordered solid, the elasticity is brought about by bond stretching along crystallographic planes, in the case of viscoelastic materials, the elastic component is a result of diffusion of the molecules within the amorphous material.[178]

The rheological properties of a material are usually measured by sandwiching the material between two parallel surfaces (geometries)[155] – typically a two-plate or a cone-and-plate setup, depending on the nature of the testing. The material is sheared between the two surfaces, and by using variable parameters such as strain or frequency, materials properties can be determined.

For viscoelastic materials such as gels, a back and forth oscillatory stress/strain is applied.[155] In a purely elastic material, this sinusoidal stress/strain would produce a strain/stress exactly in phase with it – there is no lag between the applied and measured signals, and the material is said to have a phase angle (δ) of 0°. For a purely viscous material, the stress/strain would produce a strain/stress a quarter of a cycle out of phase with it – so the phase angle would be 90°. For viscoelastic materials, the phase angle is somewhere between 0° and 90°. From the input stress/strain and the measured strain/stress, a complex modulus, G^*, can be derived.

This complex modulus can then be broken down into its elastic and viscous components, known as the storage modulus, G', and the loss modulus, G'', respectively, such that:

$$G^* = G' + iG'' \qquad \text{(Eq. 4)}$$

These moduli are related to the amplitudes of stress (σ_0) and strain (ε_0), as well as the phase angle, δ, and are obtained from Eq. 5 and 6:

$$G' = G^*\cos\delta \qquad \text{(Eq. 5)}$$

$$G'' = G^*\sin\delta \qquad \text{(Eq. 6)}$$

The ratio of G' to G'' is the ratio of stored energy to lost energy; for a gel, $G' > G''$, meaning more energy is stored than lost. At the point when $G' = G''$, the gel loses its viscoelastic properties and is converted into a sol.

For gels, a variety of properties can be tested through the measurement of G' and G''. However, optimisation of the experimental parameters and sample preparation are key.[155] Useful measurements can only be made within the linear viscoelastic region (LVR), where both moduli remain independent of the frequency of oscillation and the applied stress/strain; therefore the LVR is often determined first.

2.6.2.2. Preparation of hydrogels of DBS-CO$_2$H and agarose, and hybrid hydrogels of DBS-CO$_2$H and agarose for rheology

For the preparation of agarose-containing gels for rheology, special vials were made. These consisted of an 8 mL sample vial where the base had been cleanly removed, and could be reattached with heat-shrink tape (Figure 2.15). After preparation of gel within the vial, the base could be removed to give a disc of gel *ca*. 20 mm in diameter – the same diameter as the selected upper plate geometry of the rheometer.

Figure 2.15: Vials used in the preparation of some hydrogel samples for rheological analysis; left: disassembled vial; right: reassemble vial, where removable base is held in place with the heat-shrink seal.

Gels of only agarose were first prepared by dissolving 0.5% wt/vol worth of agarose in H$_2$O at 95°C; 500 µL volumes of this hot solution were then transferred to preparation vials and allowed to cool – discs *ca*. 1.5 mm thick were formed.

Gels of DBS-CO$_2$H were prepared by making the solution to the standard method; gelation was carried out directly on the lower plate of the rheometer, using a sealed bottomless glass vial as a mould to hold 500 µL of the solution. The solution was left overnight, after which gels of *ca.* 1.5 mm thick had formed. This method was necessary because the DBS-CO$_2$H gels could not be transferred by hand to the plate, owing to their fragile structures.

To prepare DBS-CO$_2$H/agarose hybrid gels, a chosen % wt/vol of DBS- CO$_2$H was first suspended in H$_2$O by sonication, followed by addition of NaOH$_{(aq)}$ (0.5 M) in 10 µL aliquots to dissolve the solid. To this solution, 0.5% wt/vol of agarose was added, followed by heating to 95°C to dissolve. The solution was cooled to 60°C, at which point GdL (8 mg mL^{-1}) was added; 500 µL volumes of the solution were then transferred to preparation vials and allowed to cool. This method also produced discs of gels *ca*. 1.5 mm thick.

2.6.2.3. Rheological measurements

Rheological measurements were carried out using a Malvern Instruments Kinexus Pro Plus rheometer. A parallel plate geometry was used, with an upper plate of 20 mm in diameter, and a gap between the geometries of 1 mm.

After sample loading, the first tests to be performed were strain-controlled amplitude sweeps in order to determine the LVR for the various hydrogels. These were performed at a frequency of 1 Hz, with shear strain amplitude increasing from 0.01% to 100%. It should be noted that many of the runs were manually halted well before both 100% shear strain was reached, and before the crossover point for the values of *G'* and *G''*, as it was considered that once the value of *G'* had decreased by more than 5% of its initial value that the limit of the LVR had been reached. If, however, the runs had been carried on past the points of manual stopping then more information about the nature of the gels could have been gained. Notably, the values of G', G'' and the yield strain/stress (value of strain/stress at the crossover point of G' ad G''), when treated as a function of the oscillatory frequency or applied strain/stress and concentration of gelator, can be used in mathematical models to gain insight into the structure of the gel[178] – for example, whether they are coilloidal systems, cellular system or soft glassy solids.[179,180]

Typical results (the "middle values" from three or more runs) are shown in Figure 2.16; results from other runs were considered valid if they were within ± 10% of the values presented here.

Figure 2.16: Comparison of typical results from amplitude sweep rheological analysis of DBS-CO$_2$H, agarose, and DBS-CO$_2$H and agarose hybrid hydrogels.

From Figure 2.16, it can clearly be seen that the values of the storage modulus *G'* are significantly larger than those of the loss modulus *G''*, confirming that the materials are indeed gels

in nature. Clearly agarose has a greater G' than DBS-CO$_2$H, and further, it maintains its gel properties to a higher shear strain (*ca*. 8% vs. *ca*. 3%) Further, both *G'* and *G''* are greater for the hybrid gel than either gel alone, and in addition the limit of the LVR is at a higher shear strain (>10%).

Further mechanical analysis was conducted through a frequency sweep, at which the shear strain was kept constant at 0.3% – this value was chosen as it was within the limit of the LVR for all the gels analysed. The frequency itself was varied between 0.1 and 10 Hz; typical results are compared in Figure 2.17; results from other runs were within ± 10% of the values presented here.

Figure 2.17: Comparison of typical results from frequency sweep rheological analysis of DBS-CO$_2$H, agarose, and DBS-CO$_2$H and agarose hybrid hydrogels.

These results confirm that the hybrid gel has a higher stiffness (highest values of *G'*, 1812 Pa versus 1259 Pa for agarose and 691 Pa for DBS-CO$_2$H at a frequency of 1 Hz) than either individual component; the increase in the limit of the LVR (Figure 2.16) shows that the hybrid gels are also mechanically tougher than either individual gel, in agreement with the results from T$_{gel}$ analysis which suggested a higher thermal stability. The increase in stiffness is most likely attributed to the rigid, aligned nanostructure that DBS-CO$_2$H is known to form; it is possible that this property also increases the limit of the LVR – the rigid structure acts to "reinforce" the overall gel structure. DBS-CO$_2$H on its own has both the lowest values of *G'*, and the shortest LVR; the latter of these observations is predictable from table-top studies, where DBS-CO$_2$H gels were seen to be reasonably fragile. The improved performance of the hybrid gel suggests that there may be a synergistic relationship between the gel networks in the hybrid gel.

2.6.3. ^{1}H NMR studies of hybrid hydrogels of DBS-CO$_2$H and agarose

For ^{1}H NMR studies, samples of the gels were prepared by adding D$_2$O (0.7 ml) to DBS–CO$_2$H (1.4 mg), followed by sonication to disperse the solid. NaOH$_{(aq)}$ (21 µl, 0.5 M) was added to dissolve all solid, and DMSO (1.4 µl) to act as an internal standard. Agarose (0.35 mg) was then added, followed by heating to 90°C to dissolve. The solution was cooled to 50°C, at which point GdL (5.6 mg, to give 44.9 mM) was added, followed by shaking to dissolve. The solution was then quickly transferred to a NMR tube and placed in the spectrometer for spectra to be recorded.
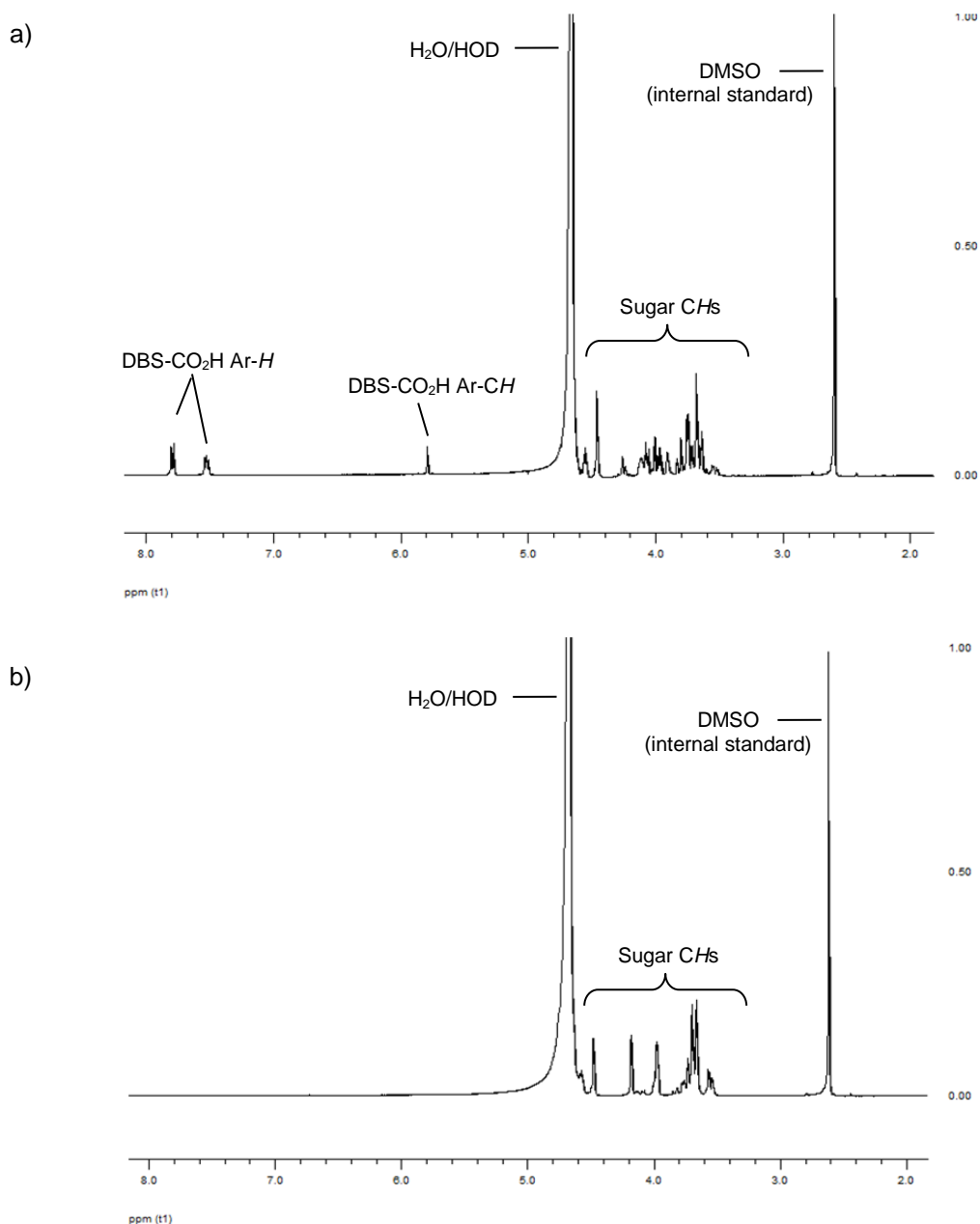
Figure 2.18: ^{1}**H NMR spectra (400 MHz, D$_2$O) of hybrid hydrogel of DBS-CO$_2$H (0.2% wt/vol) and agarose (0.5% wt/vol) at a) start of gelation and b) end of gelation; the absence of signals related to DBS-CO$_2$H in (b) indicates that all of the LMWG has been incorporated into a sample-spanning solid-like network.**

83

The "snapshot" method of monitoring the LMWG network formation gave the same results as for pure DBS-CO$_2$H gels – gelation of the LMWG was completed overnight, with none remaining in solution (Figure 2.18).

More detailed kinetic information was again obtained by recording ^{1}H NMR spectra every 30 minutes after the addition of GdL, and plotting the rate of formation of the LMWG network (Figure 2.19). When compared to the rate of formation of the LMWG network in the absence of agarose (previously shown in Figure 2.3) the presence of the agarose gel network appeared to have very little impact on the kinetics of DBS-CO$_2$H assembly into supramolecular gel fibres.
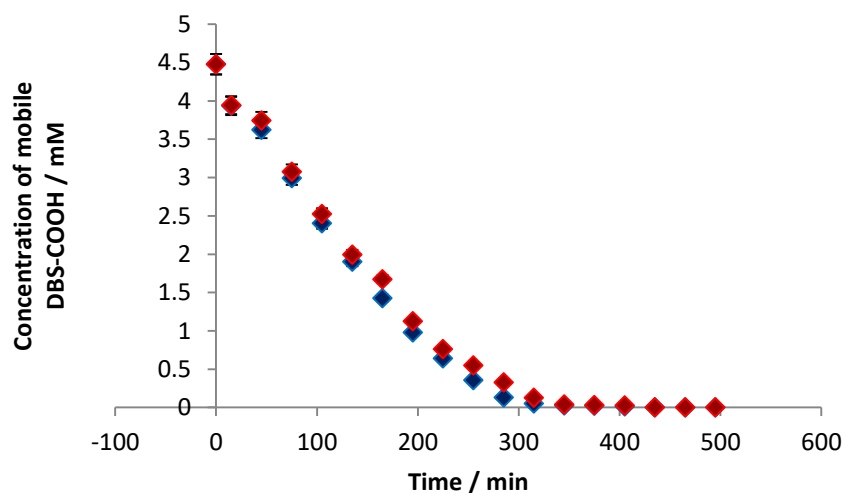
Figure 2.19: Plot of average rate of formation of the DBS-CO$_2$H network in presence (red) and absence (blue) of agarose.

The kinetic data were then fitted to Avrami's kinetic model (Figure 2.19); for the DBS-CO$_2$H/agarose hybrid gel, the value of the Avrami exponent, n, was found to be 1.52. This value is slightly less than that for the DBS-CO$_2$H gel (n = 1.61), and may indicate there is slightly less branching or 2D growth in the self-assembly of DBS-CO$_2$H in the presence of agarose – although the difference is only just outside the margin of experimental error.
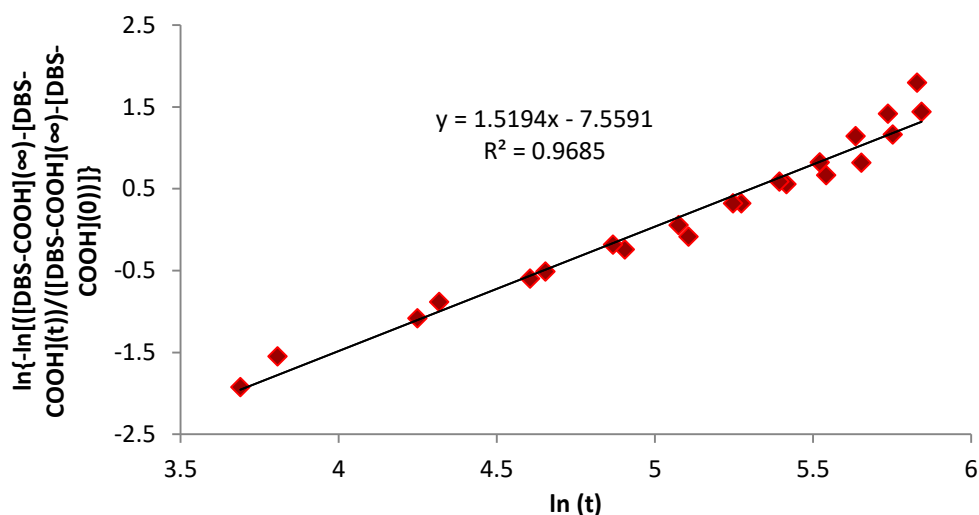
Figure 2.20: Avrami plot for formation of DBS-CO₂H network in presence of agarose; gradient of line = n = 1.52.

2.6.4. CD studies of hybrid hydrogels of DBS-CO₂H and agarose

As with the CD studies of DBS-CO₂H, the samples of the hybrid system prepared for CD were prepared with sub-gelation amounts of the gelators (0.02% wt/vol DBS-CO₂H and 0.05% wt/vol agarose), so again what was observed by CD was not the formation of a sample-spanning network, but the assembly of the chiral nanofibres.

In the presence of agarose (which does not have a distinctive CD signal), and after standing for 5 hours following the addition of GdL, DBS-CO₂H had a CD band at *ca*. 259 nm, with an intensity of *ca*. -34 mdeg (Figure 2.21a) and HT value of *ca*. 270 V (Figure 2.21b); this is comparable to the CD spectra of DBS-CO₂H in the absence of agarose (260 nm and maximum of ca. -41 mdeg, Figure 2.5b, HT value of *ca*. 230 V, Figure 2.6), and suggests that nanofibres can assemble in a similar way either in the absence or presence of agarose, and would seem to indicate that variations in HT of at least ± 40 V between experiments are not overly significant to the maximum ellipticity reported.
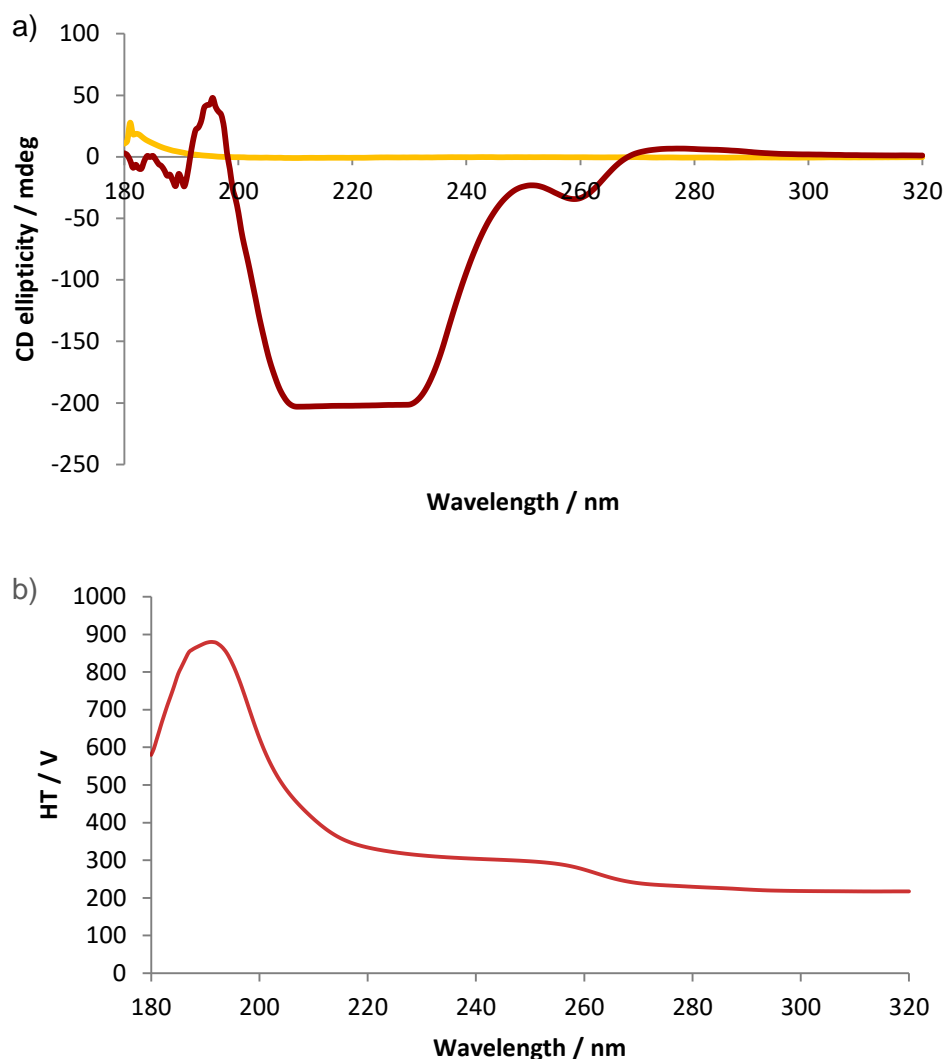
Figure 2.21: a) CD spectra of agarose (yellow) and DBS-CO₂H/agarose (0.02% and 0.05% wt/vol) (red) after standing for 5 hours; b) HT data for DBS-CO₂H/agarose.

A CD experiment that directly probed the initial stages of fibre growth by recording CD spectra every 5 minutes for 80 minutes after the addition of GdL was also carried out; again, the bands associated with DBS-CO$_2$H slowly emerged (Figure 2.22). By plotting time (after addition of GdL) against the CD ellipticity at 260 nm, the evolution of the CD spectra for the hybrid gel could be compared to those of the DBS-CO$_2$H gel (Figure 2.23). It is evident that in the presence of agarose, the initial nucleation phase takes longer (40 min rather than 25 min) and that the subsequent fibre growth is somewhat slower. It also appears from the plot that the DBS-CO$_2$H alone forms a nanostructure with higher ellipticity. However, as already mentioned, on further standing (for up to 5 hours) the ellipticity of DBS-CO$_2$H decreased to *ca*. -40 mdeg, whilst this kind of change in CD spectrum was not observed in the presence of an agarose network. This may indicate that the slower fibre growth which takes place in the presence of agarose actually yields a more thermodynamically stable fibre form – a possible advantage of assembling LMWGs within an

agarose network, whereas in the absence of agarose a metastable fibre network[31,167–169] is initially formed. This would be in-line with the earlier discussion in which it was suggested that the presence of both networks indicated some synergistic rheological effects. A comparison of HT data (Figure 2.24) for these experiments showed no significant difference in values, indicating the maximum values of ellipticity recorded were not due to HT differences.
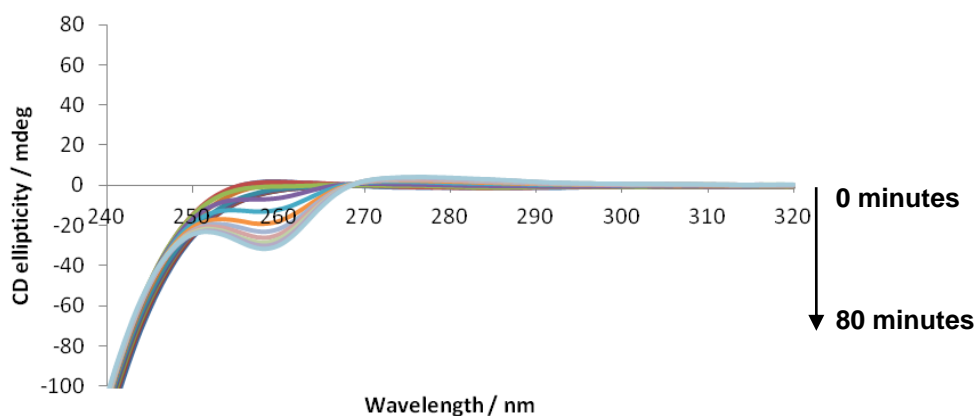
Figure 2.22: Evolution of CD spectrum of hybrid system of DBS-CO$_2$H (0.02% wt/vol) and agarose (0.05% wt/vol) over an 80 minute period, after addition of GdL (44.9 mM).
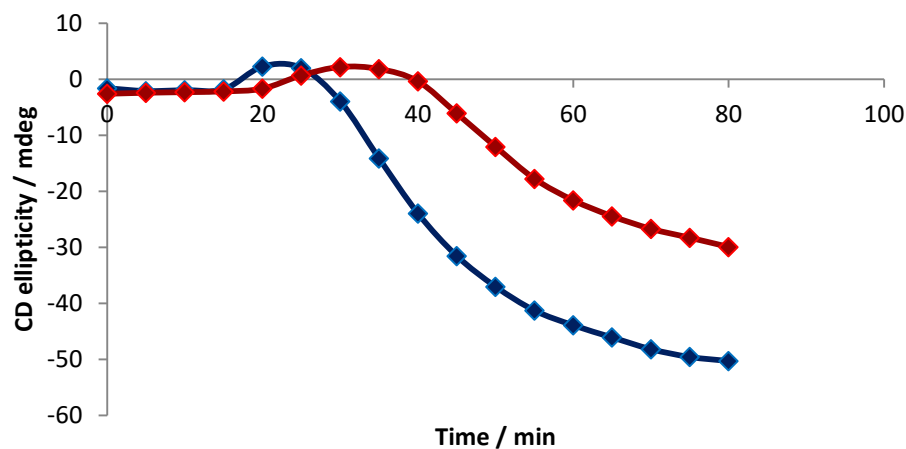
Figure 2.23: Comparison of evolution of CD spectra over time, monitoring ellipticity at 260 nm, after addition of GdL (44.9 mM); DBS-CO$_2$H (blue); hybrid system of DBS-CO$_2$H and agarose (red).
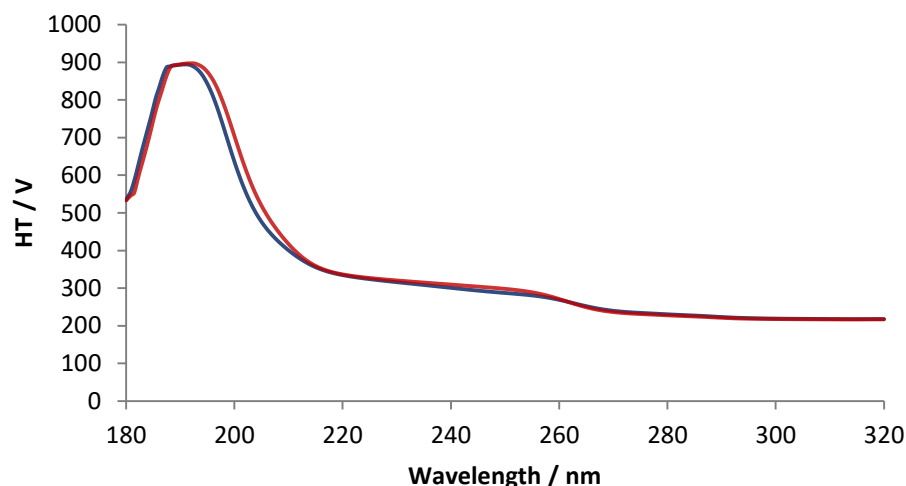
Figure 2.24: HT data recorded after 80 minutes for the CD spectra of DBS-CO$_2$H (0.02% wt/vol) (blue) and DBS-CO$_2$H/agarose (0.02% and 0.05% wt/vol) (red) as ellipticity was monitored over a 2-hour period (see Figure 2.23).

The presence of two regions within this time-resolved experiment made it difficult to fit these data to Avrami type kinetics. However, this experiment clearly showed that DBS-CO$_2$H could assemble into chiral nanostructures in the presence of an agarose network. It should also be noted that at the low concentrations used the presence of the agarose partially inhibits the assembly, and also prevents the nanofibres from re-organising over longer timescales. This demonstrates that CD is a more effective method than NMR to probe the initial fibre assembly process, as it provides more information on nanoscale dynamics and organisation, whilst NMR simply reports the overall immobilisation of the LMWG into a solid-like network.

2.6.5. SEM imaging of hybrid hydrogels of DBS-CO$_2$H and agarose

SEM was used to explore any differences in the assembly mode of the DBS-CO$_2$H fibres in the hybrid gel, compared to the DBS-CO$_2$H gel, and to be certain that the LMWG was not simply crystallising or precipitating within the agarose gel network. Samples for SEM were prepared in the same way as described for gels of DBS-CO$_2$H (see 2.4.4 for a discussion on the limitations on the information that can be obtained from freeze-drying samples for SEM).

The xerogel of the hybrid material (Figure 2.25) appeared to have some characteristics of both the agarose gel and the DBS-CO$_2$H gel (Figure 2.13 and Figure 2.10 respectively) – there appear to be two different thicknesses of fibres present, with the thicker fibres being presumably DBS-CO$_2$H (consistent with gels of DBS-CO$_2$H being optically translucent), and the thinner fibres being agarose. This suggests that there is some level of self-sorting occurring between the two.

88
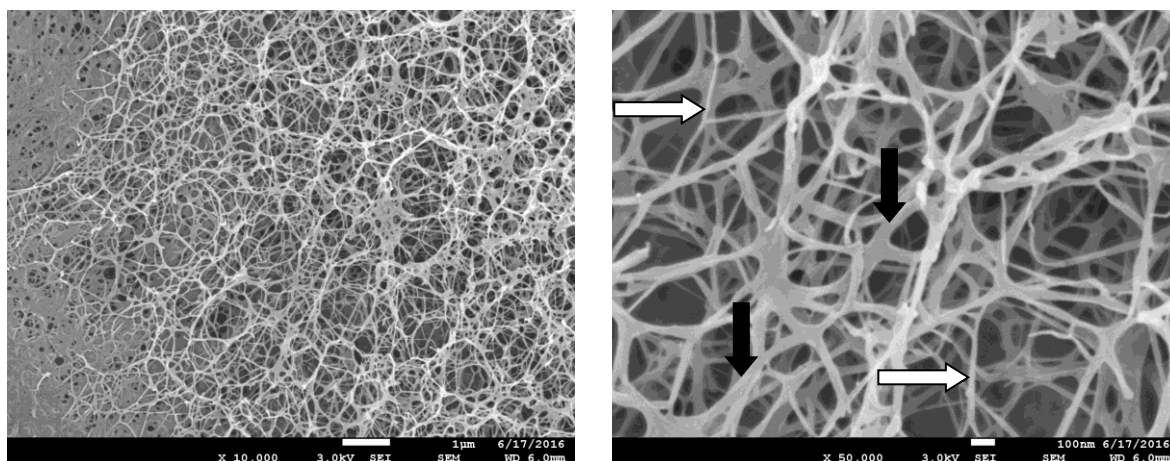
Figure 2.25: SEM images of xerogels of hybrid hydrogels of DBS-CO$_2$H (0.2% wt/vol) and agarose (0.5 % wt/vol); scale bars = 1 μm (left) and 100 nm (right). In the image on the right the two different thicknesses of fibres can clearly be seen; the thinner agarose fibres are indicated with white arrows, the thicker DBS-CO$_2$H fibres with black arrows.

2.7. Responsive, pH "switchable" hybrid hydrogels of DBS-CO$_2$H and agarose

The gel of DBS-CO$_2$H and agarose was then used to demonstrate that hybrid gels can have network-specific responsive behaviour. The aim was to use pH changes to assemble or disassemble the DBS-CO$_2$H network, whilst leaving the more robust agarose network, and therefore the whole macroscopic gel, intact.

A hybrid hydrogel of DBS-CO$_2$H and agarose was prepared by the standard method, as given above. NaOH$_{(aq)}$ (0.054 M, 1 ml) was then applied to the top of the gel, and allowed to diffuse in. The diffusion progress was quite visible, with the translucence of the hybrid gel turning clear with the progress of the diffusion front. When the gel was clear (after *ca.* 24 hours), the basic solution was removed, and a solution of GdL (14 mg dissolved in 0.5 ml) was applied. The diffusion was again quite visible, with translucence indicating the slow re-formation of the LMWG network appearing with the progress of the diffusion front, with the gel becoming fully translucent again after *ca.* 24 hours. Importantly, the gel remained intact as the pH was cycled between acidic and basic conditions, which is a consequence of the robust and unresponsive nature of the agarose polymer gel network; on its own, DBS-CO$_2$H gel is destroyed by the addition of base. Addition of a small amount of universal indicator (20 μL) could be used to visualise the diffusion processes with greater ease (Figure 2.26).
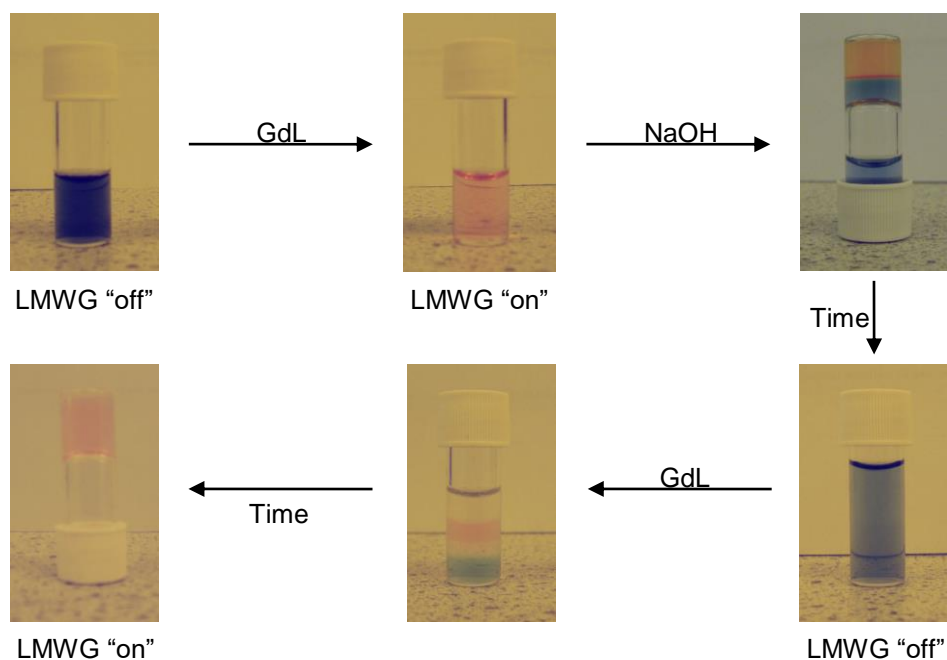
Figure 2.26: Progression of pH "switchable" gel; addition of NaOH increases pH and "switches off" the LMWG network as DBS-CO₂H is deprotonated and mobilised; addition of GdL returns the system to acidic pH and the LMWG network is "switched on" again, as DBS-CO₂H becomes re-protonated and immobilised.

^{1}H NMR spectroscopy was used to determine what was occurring on the molecular scale during an equivalent experiment, although some alteration to accommodate differences in diffusion rates between sample vials and NMR tubes was required – associated with the diameter/depth ratio. A DBS–CO₂H/agarose gel was prepared as described above, and immediately placed in the spectrometer to record the initial concentration of mobile DBS–CO₂H. After leaving the tube overnight for DBS–CO₂H to fully gelate, a spectrum was again recorded. Subsequently, NaOH (20.8 mg) was dissolved in D₂O (1 ml, to give 0.54 M), and 100 µl of this solution was added onto the top of the gel sample in the NMR tube and allowed to diffuse into the gel. Spectra were recorded periodically, until it was deemed that all the DBS–CO₂H was mobile again (ca. 36 hours). The NaOH solution was then removed by pipette. GdL (8 mg) was dissolved in D₂O (100 µl, to give 0.45 M), then added onto the top of the gel sample in the NMR tube, and allowed to diffuse, with spectra being recorded periodically until it was deemed that all the DBS–CO₂H was again immobilised in a gelator network (ca. 4 days). A selection of the spectra are presented in Figure 2.27. At all points in this experiment the sample remained as a gel.
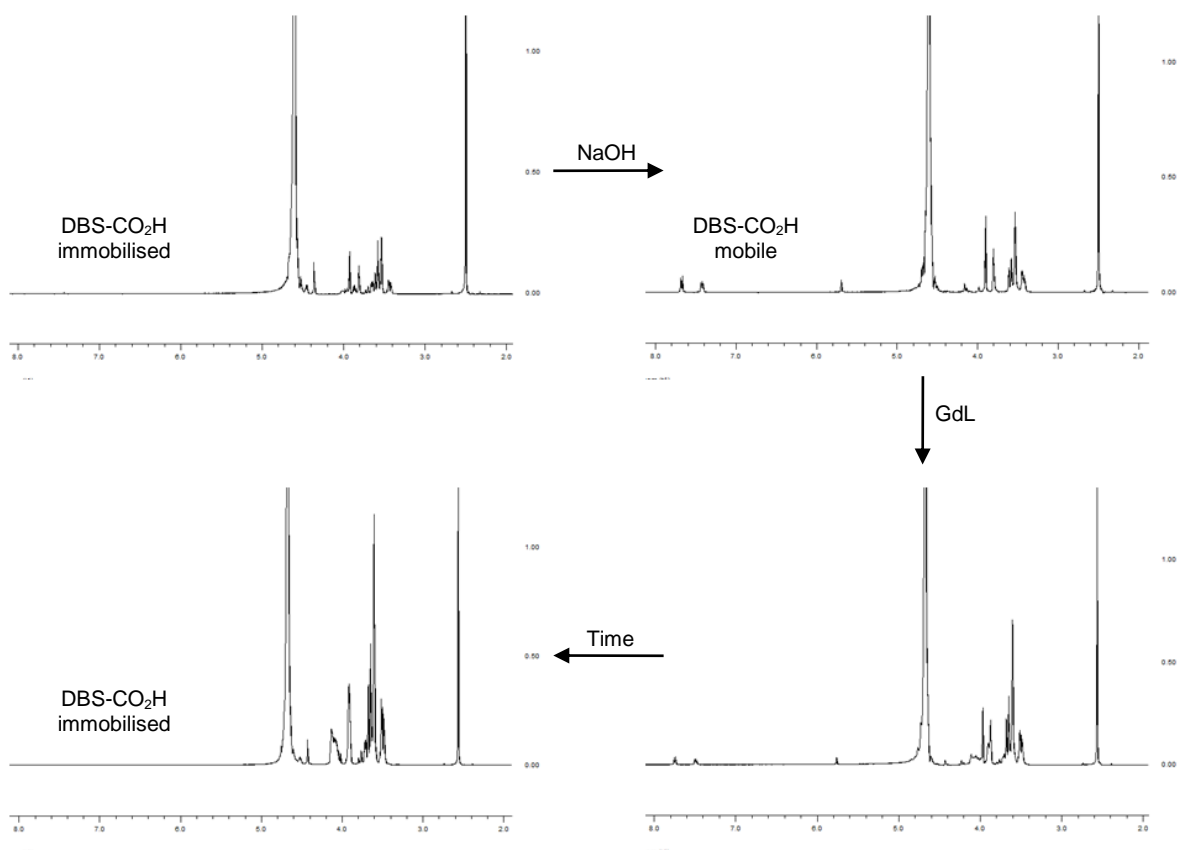
Figure 2.27: Progression of "switchable" gel as visualised by ^{1}H NMR spectroscopy; signals associated with DBS-CO$_2$H become visible or invisible upon addition of base or acid respectively.

This experiment therefore demonstrates that the agarose gel is able to maintain a robust material whilst allowing effective diffusion of acid or base stimuli through the system, and that the hybrid hydrogel has both responsive yet robust characteristics, as the LMWG network is capable of pH-triggered breakdown and re-assembly in the presence of a PG network.

2.8. Conclusions and Outlook

What has been demonstrated in this chapter is that the LMWG DBS-CO$_2$H retained its ability to self-assemble in the presence of the PG agarose, and through combing the two a hybrid hydrogel was obtained. From SEM, the hybrid gel was seen to consist of a mixture of DBS-CO$_2$H and agarose nanostructures. NMR studies showed that the presence of agarose appeared to have little effect on the kinetics of DBS-CO$_2$H immobilisation, though in CD studies the presence of agarose did appear to somewhat limit the initial kinetics of nanofibre nucleation and their reorganisation over time. Importantly, this system demonstrated orthogonal assembly of two gelator networks into a hybrid system, which through rheological studies was shown to be mechanically stronger than either individual constituent component gel.

Concurrent with the publication of this research, two further publications exploring hybrid hydrogels were released. The first came from Feng and co-workers, who combined the PDB gelator (previously discussed in Introduction) with a calcium-alginate gelling system.[181] This was achieved by first using PDB to gel (by heat/cool method) a solution of sodium alginate, followed by diffusion of a $CaCl_2$ solution into the gel, which caused a PG network to form via ionic interactions between Ca^{2+} and carboxylate groups of alginate. The addition of the PG network enhanced the mechanical stability of the supramolecular hydrogel; increasing the concentration of calcium ions further improved the mechanical stability due to greater crosslinking of the polymer gelator. Cells seeded onto the hybrid hydrogel showed better viability, adhesion and spreading than compared to the supramolecular gel. There was potential that changing the concentrations of PDB, sodium alginate or $CaCl_2$ could be used to tune these hybrid hydrogels to particular cell types. The main obstacle for using this hybrid hydrogel in biomedical applications is the use of the heat/cool cycle to form the LMWG network (as seen with previous hybrid hydrogel examples)[106,108] – this is not particularly suitable for encapsulating cells for 3D tissue growth, or indeed for encapsulating most biomacromolecules, such as enzymes.

To overcome this issue, Yang and co-workers investigated the use of a mild hydrogelation process (enzyme or reducing agent triggered) on a mixture of naphthalene-peptide LMWGs and sodium alginate, followed by soaking in a $CaCl_2$ solution to form a calcium alginate network, and hence a hybrid hydrogel.[182] These hybrid hydrogels had significantly increased stabilities and mechanical strengths. Emission spectroscopy suggested that interactions between the LMWG and alginate networks contributed towards this, with the authors identifying extensive hydrogen bonding between the networks. Phosphatase enzymes could be immobilized in some of the hybrid gels, and used at least 20 times without significant decrease in activity; by comparison phosphatases immobilized in calcium alginate alone showed a very marked decrease in activity after just the first use, most likely due to leaching of the enzyme. Whilst these systems allow production of a hybrid hydrogel at ambient temperature and for the encapsulation of biomacromolecules (and even potentially 3D cell cultures), their overall complexity may create limits for their practical applications.

Whilst the use of the heat/cool cycle to produce the DBS-CO_2H and agarose hybrid gels would limit their use for biomedical applications, the unique ability they had over the above[181,182] and previous examples[106–108] is the responsiveness of the LMWG network to a stimulus. This made this system the first example of a responsive yet robust hybrid hydrogel, one which both demonstrated and utilised to an advantage the better properties of each of its constituent components in the final hybrid material. Although the combination of DBS-CO_2H and agarose might best be described as a model system for these types of hybrid hydrogels, similar combinations of orthogonally assembling

LMWGs and PGs could have great potential in applications such as controlled release or switchable self-healing systems.

3. Chapter 3: Photopatterned Multidomain Hybrid Hydrogels

Results from this chapter were published in D. J. Cornwell, B. O. Okesola and D. K. Smith, *Angew. Chem.,* 2014, **126**, 12669-12673; D. J. Cornwell, B. O. Okesola and D. K. Smith, *Angew. Chem. Int. Ed.*, 2014, **53**, 12461–12465.

3.1 Introduction

Whilst the hybrid hydrogel system of DBS-CO$_2$H and agarose demonstrated the concept of a responsive yet robust gel, and showed how orthogonally assembling gel networks could be combined into one material, the main disadvantage of the material was the need for a heat/cool cycle to form the agarose network. As discussed, the use of heat would be problematic for 3D cell culturing or encapsulation of biomacromolecules. It therefore seemed that the next logical step in investigating hybrid hydrogels would be to replace agarose with an alternative PG, one which did not require a heat/cool cycle to assemble, but would still be formed by an orthogonal method to DBS-CO$_2$H.

Additionally, prior to this research there existed no examples of any hybrid hydrogel combining a LMWG with a synthetic, covalently crosslinked PG. This was also taken into consideration in the choice of PG.

3.2 Poly(ethylene glycol) and derivatives

Poly(ethylene glycol) (PEG) is a water soluble polymer, and commercially available in both linear and branched structures in a wide range of molecular weights. The polymer consists of repeat units of the ethylene glycol diol with two hydroxyl end groups, which can be easily converted to other functional groups.[183] PEG is also known as poly(ethylene oxide), PEO, particularly if the chain length is above 150 repeat monomers.[184] PEG and its derivatives are some of the most widely-used hydrogels in biomedical applications, including drug delivery and tissue engineering[5–7,183] – it is particularly useful for the latter of these as it has good biocompatibility, is non-immunogenic and has resistance to protein adsorption.[185,186]

PEG can be covalently crosslinked in order to form a gelator network; crosslinked PEG is not readily available, but crosslinking can be achieved by several methods, including irradiation,[187,188] free radical polymerisation,[189] and specific reactions such as Click chemistry[190,191] or the use of enzymes.[192–194] UV photopolymerisation is probably the most common method of preparing a crosslinked network for PEG hydrogels – this method also allows for spatial control by photopatterning methods. Generally, a PEG acrylate is chosen for UV photopolymerisation – usually PEG methacrylate (PEGMA), PEG diacrylate (PEGDA) or PEG dimethacrylate (PEGDM),

all of which are relatively easy to synthesise. Whilst crosslinked PEG is not easily biodegradable, additional modifications can be incorporated into the polymer chain to introduce degradable segments.[195–201]

3.3 Synthesis of PEGDM

PEGDM was selected as the PEG derivative to be used to form the polymer gel network in the hybrid hydrogels, and was synthesised according to a method from the literature[202] – summarised in Scheme 3.1. PEG, M_n = 8000 g mol^{-1} (PEG8K), was stirred with 2.2 equivalents of methacrylic anhydride in the presence of triethylamine in dry dichloromethane for 4 days. The solution was then filtered over alumina, and the product precipitated by addition of diethyl ether, to give the product in 60% yield. The product identity as PEG8KDM (hereafter referred to simply as PEGDM) was confirmed by ^{1}H and ^{13}C NMR and MALDI-MS.
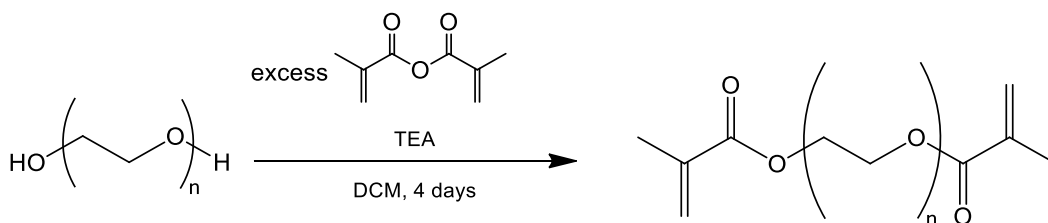
Scheme 3.1: Synthesis of PEGDM from PEG and methacrylic anhydride (n ≈ 180).

3.4 Gelation studies of PEGDM

In order to form a sample-spanning gelator network, PEGDM must be chemically crosslinked. In order for this to occur, the preferable method is to use a photoinitiator to trigger polymerisation of the methacrylate groups. One of the most commonly used photoinitiators for PEGDM is 2-hydroxy-4′-(2-hydroxyethoxy)-2-methylpropiophenone (also known by the trade name Irgacure 2959); henceforth it is referred to as photoinitiator (PI). It has an activation wavelength λ = 365 nm; when exposed to UV light with this wavelength, PI undergoes photolysis to generate two radical species (Scheme 3.2), which can then cause radical photopolymerisation.
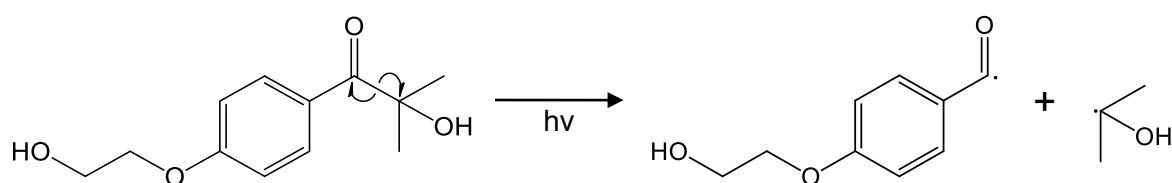
Scheme 3.2: Photolysis of photoinitiator 2-hydroxy-4′-(2-hydroxyethoxy)-2-methylpropiophenone under UV light to generate radical species.

3.4.1 Preparation and T_{gel} studies of PEGDM hydrogels

PEGDM hydrogels were prepared according to an established procedure from the literature;[203] PEGDM was dissolved at varying % wt/vol in a 0.05% wt/vol of PI. The solutions were cured with a long wavelength UV source for 5-10 minutes (dependent on PEGDM concentration) to obtain very robust, transparent hydrogels (Figure 3.1). The MGC was found to be 4% wt/vol (though 5% wt/vol was used in further studies as it was found to have greater long-term stability).
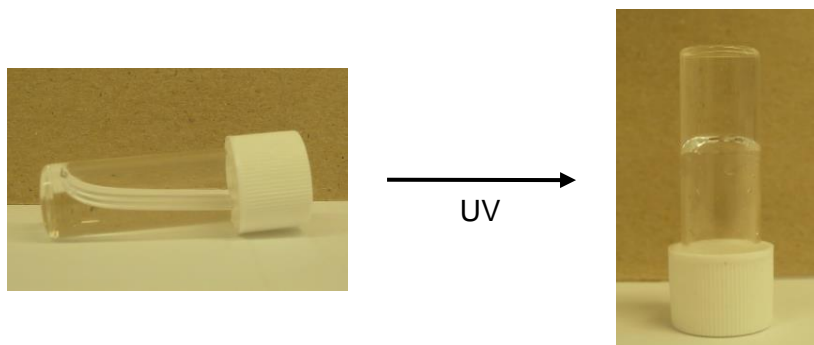
Figure 3.1: Formation of PEGDM hydrogel; solution of PEGDM and PI forms a robust, transparent hydrogel upon exposure to UV light to activate PI.

The PEGDM hydrogels were observed to not have a T_{gel} value, due to their robust, covalently crosslinked structure. Furthermore, kinetic studies of PEGDM by NMR or CD were not possible due to the quick gelation time, and due to PEGDM generating no CD signal owing to its lack of chirality.

3.4.2 NMR of PEGDM hydrogels

The ^{1}H NMR spectra of a PEGDM gel prepared in D$_2$O (with a DMSO probe molecule) revealed that not all the methacrylate alkenes were photopolymerised into crosslinks (Figure 3.2); in reality, for a 5% wt/vol gel, approximately 75% of the alkenes were polymerised, with approximately 25% remaining unpolymerised – probably as some alkenes become isolated within the gel network and cannot find a reactive partner. The percentages of polymerised alkenes remained the same for a 10% wt/vol gel.
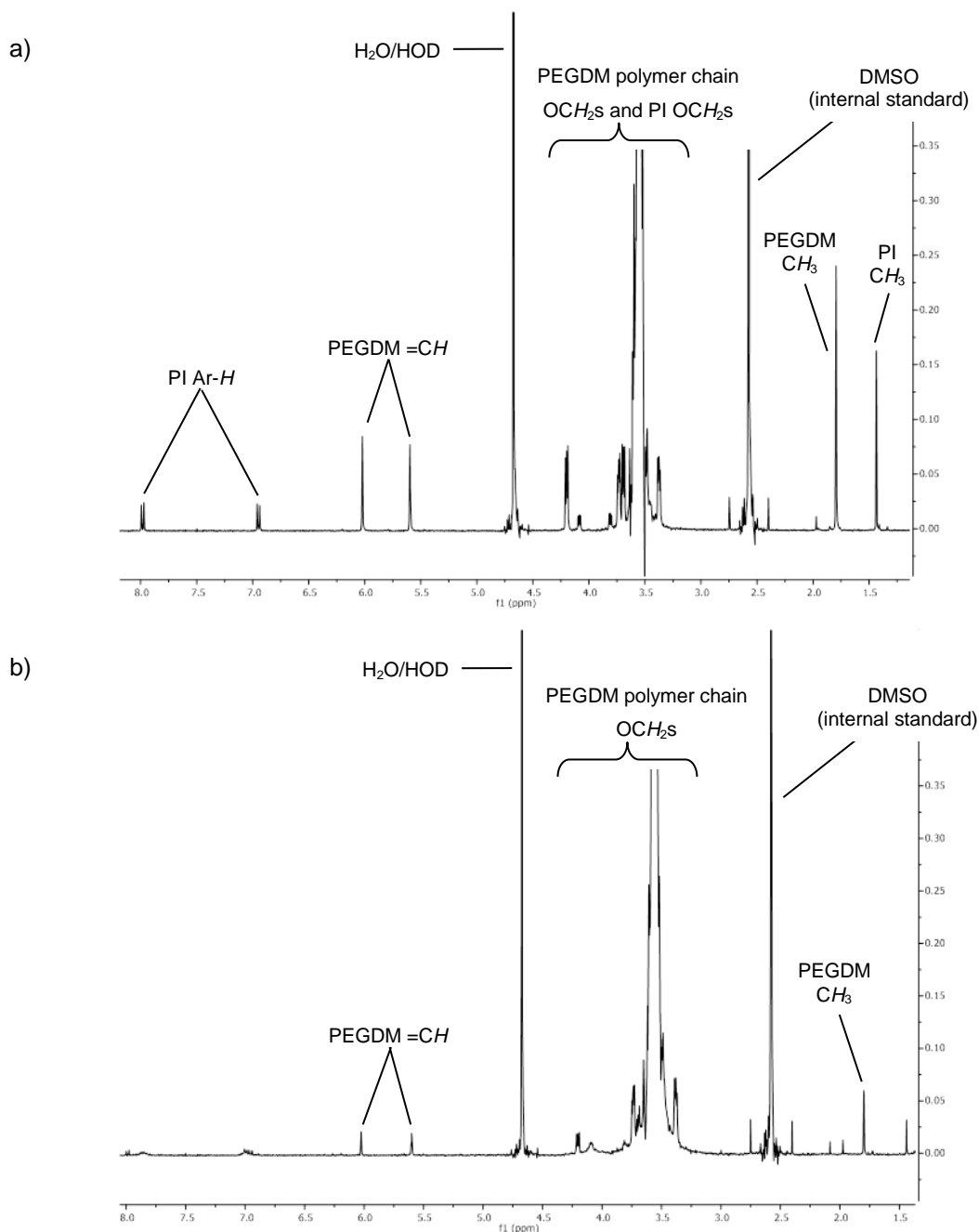
Figure 3.2: ^{1}H NMR spectra (400 MHz, D$_2$O) of PEGDM hydrogel (5% wt/vol) a) before UV curing and b) after UV curing. The PEGDM signals are significantly reduced after photopolymerisation, whilst the PI signals are almost absent after its activation.

3.4.3 SEM imaging of PEGDM hydrogels

Samples for SEM were prepared in the same way as described for gels of DBS-CO$_2$H (see 2.4.4 for a discussion on the limitations on the information that can be obtained from freeze-drying samples for SEM). The PEGDM xerogel was seen to consist of a random mix of films, ribbons and fibres (Figure 3.3). This poorly-defined structure is due to the nature of the PEGDM sample-spanning gel network, where each PEG polymer chain acts as a sort of nanofibril to form a very

97

dense network, and as such no larger fibres are formed. Upon drying, the nanostructure collapses somewhat into the polymer films seen in the SEM images.
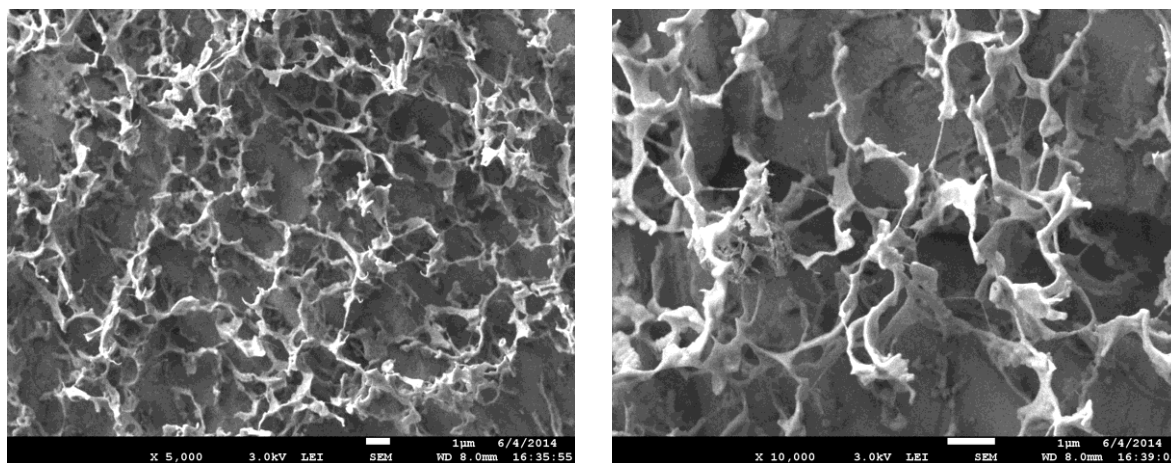
Figure 3.3: SEM images of xerogels of PEGDM (5% wt/vol); scale bars = 1 µm.

3.5 Hybrid hydrogels of DBS-CO₂H and PEGDM

3.5.1 Preparation and T_{gel} studies of hybrid hydrogels of DBS-CO₂H and PEGDM

Hybrid gels were prepared by adding known amounts of DBS-CO₂H to a 1 mL solution of PEGDM (5% wt/vol) and PI (0.05% wt vol) in 2.5 mL sample vials, followed by sonication to disperse the solid. NaOH$_{(aq)}$ (0.5 M) was added in 10 µL aliquots to dissolve DBS-CO₂H, followed by GdL (6-8 mg). The uncapped vials were then cured under UV light for 5-10 minutes to obtain a clear PEGDM hydrogel, which was then left overnight for gelation of DBS-CO₂H to occur; by the next day, the gel had gone from clear to translucent, indicative of the formation of the LMWG network (Figure 3.4).
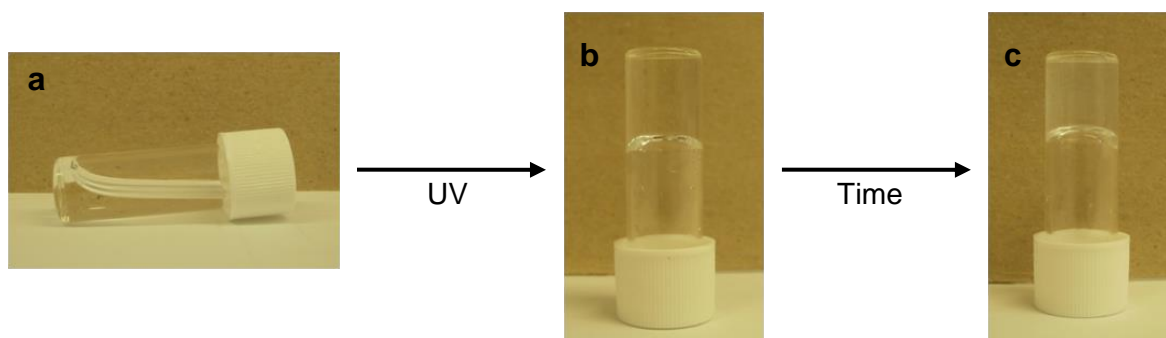
Figure 3.4: Formation of hybrid hydrogels of DBS-CO₂H and PEGDM; photoirradiation of a solution of both gelators with PI and GdL (a) triggers photopolymerisation to form the crosslinked PEGDM network and to yield a clear gel (b); the gel goes from clear to translucent (c) as the LMWG network forms over time with the slow hydrolysis of GdL.

Like the PEGDM hydrogels, all the hybrid gels of DBS-CO₂H and PEGDM, regardless of LMWG, PG or GdL concentration, did not have T_{gel} values, nor showed any visible changes upon

heating, attributable to both the robust nature of the crosslinked PEGDM gel and the thermal stability of the DBS-CO_2H networks.

3.5.2   Rheological studies of hybrid hydrogels of DBS-CO_2H and PEGDM

3.5.2.1   *Preparation of hydrogels of DBS-CO_2H and PEGDM, and hybrid hydrogels of DBS-CO_2H and PEGDM for rheology*

It was initially thought that the specially-made vials used for preparing agarose-containing samples for rheology would be suitable for the preparation of PEGDM-containing hydrogels; however, on exposure to UV light, no full gelation was observed to take place. This may be due to the seal around the base of the vials limiting the exposure of the solution to UV light, or due to some interaction between the photoinitiator and the constituent compounds of the heat-shrink seal (which is partially exposed to the liquid in the vial due to the removable bases not fitting perfectly flush with the other part of the vial). Due to this problem, an alternative preparation method had to be devised.

The best method was found to be to simply add 1 mL of the PEGDM containing solution to a sample vial with a diameter of 20 mm. For gels of just PEGDM, 50 mg (5% wt/vol) PEGDM and 0.5 mg (0.05% wt/vol) PI were dissolved in 1 mL deionised H_2O, transferred to the vial and cured for 10 minutes. The disc of gel (*ca.* 3 mm in thickness) could then be carefully removed from the vial and placed onto the lower plate of the rheometer.

For the hybrid hydrogels of DBS-CO_2H and PEGDM, the solutions were prepared as described in section 3.5.1, using 50 mg (5% wt/vol) PEGDM, 0.5 mg (0.05% wt/vol) PI, 2 mg (0.2% wt/vol) DBS-CO_2H and 8 mg GdL. After UV curing, the gels were left overnight for hydrolysis of GdL to occur, leading to formation of the LMWG network. The disc of prepared gel (*ca.* 3 mm in thickness) was then carefully removed from the vial before being placed on the rheometer.

Samples of DBS-CO_2H alone were again prepared by making the solution to the standard method; gelation was then carried out directly on the lower plate of the rheometer, using a sealed bottomless glass vial as a mould to hold 1 mL of the solution. This method likewise produced gels of *ca.* 3 mm thickness.

3.5.2.2   *Rheological measurements*

After sample loading, the first tests to be performed were amplitude sweeps in order to determine the LVR for the various hydrogels. These were performed at a frequency of 1 Hz, with shear strain amplitude increasing from 0.01% to 100%, though some of the runs were halted well before 100% shear strain as the limit of the LVR had been reached before this point. Typical results are compared in Figure 3.5; results from other runs were within ± 10% of the values presented here.
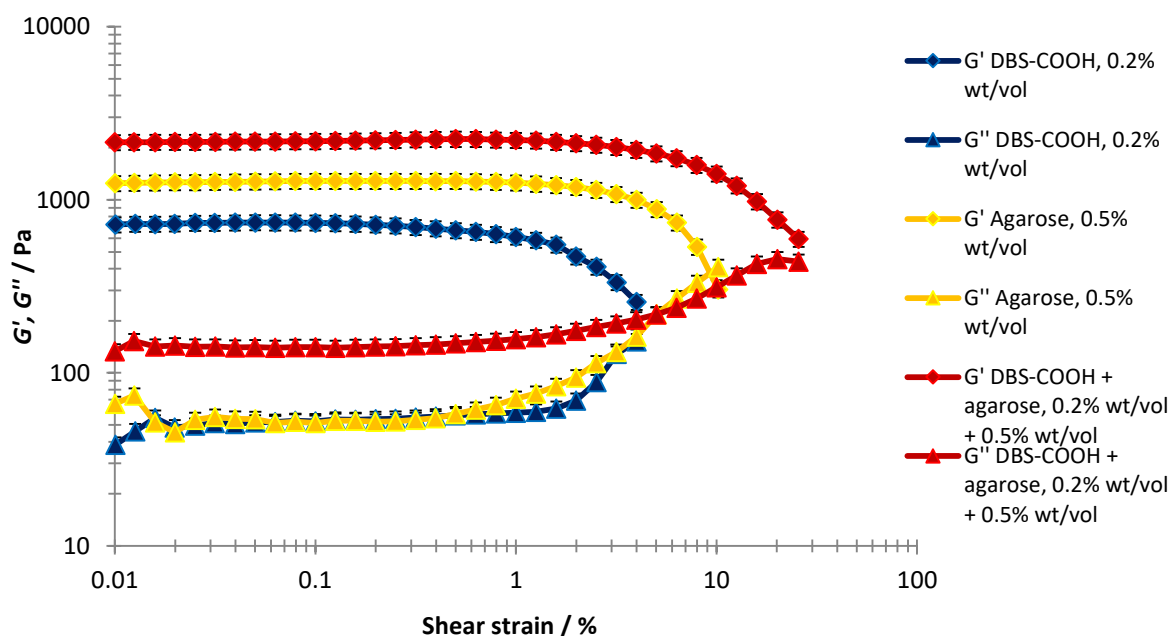
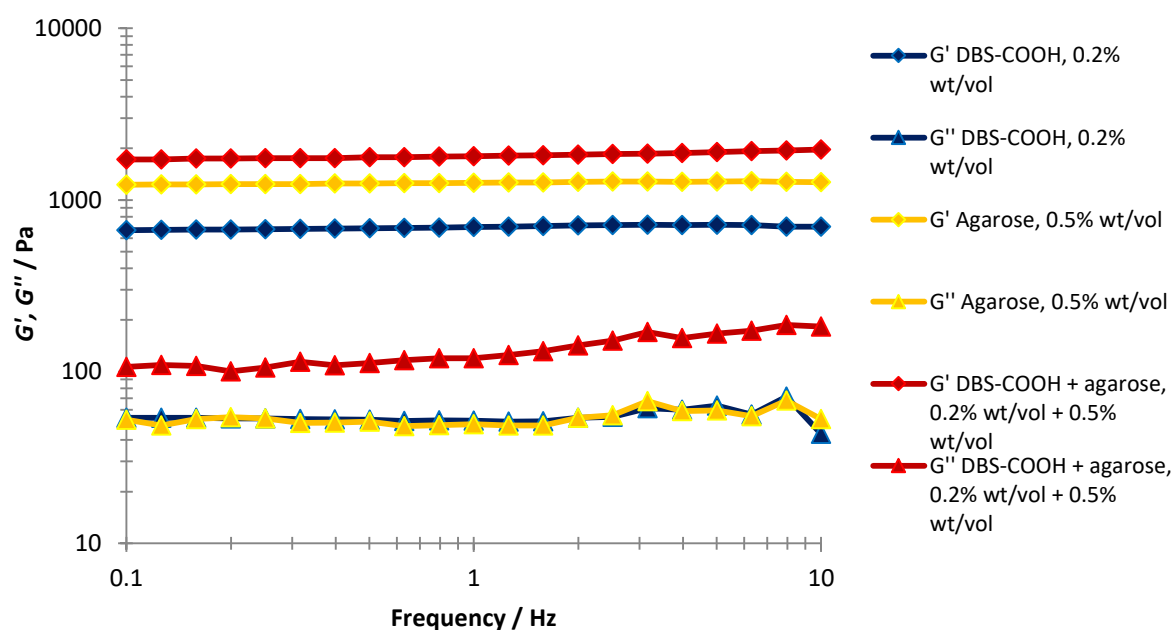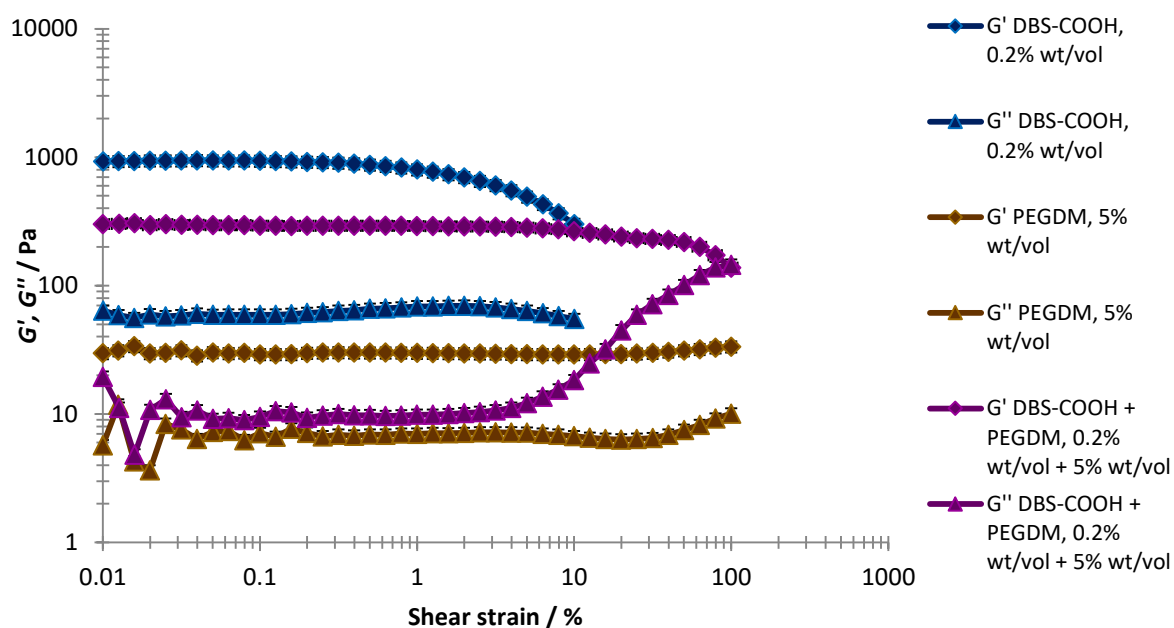**Figure 3.5: Comparison of typical results from amplitude sweep rheological analysis of DBS-CO$_2$H, PEGDM, and DBS-CO$_2$H and PEGDM hybrid hydrogels.**

Figure 3.5 shows that the values of the storage modulus *G'* are significantly larger than those of the loss modulus *G''*, confirming the materials are definitely gels. PEGDM has a very low value of *G'* compared to DBS-CO$_2$H, but a much greater LVR – even at 100% strain the gel did not collapse. Somewhat surprising is that the values of *G'* and *G''* for the hybrid hydrogel sit in between those for the two individual gels, and whilst the LVR is greater than that of DBS-CO$_2$H, there is a notable increase in the values of *G''* and decrease in the values of *G'*, suggesting at least the beginnings of breakdown of the gel. As such it can be suggested that the hybrid gel has intermediate rheological behaviour between its constituent components. However, clearly the PEGDM significantly increases the resistance to shear strain, and mechanical robustness and ability to be handled.

Further mechanical analysis was conducted through a frequency sweep, at which the shear strain was kept constant at 0.3% – this value was chosen primarily as it was within the limit of the DBS-CO$_2$H gels. However, the frequency itself was only varied between 0.1 and 1 Hz in this case, as a higher frequency caused "slipping" of the rheometer geometry with PEGDM samples, producing unreliable results. Typical results are compared in Figure 3.6; results from other runs were within ± 10% of the values presented here.
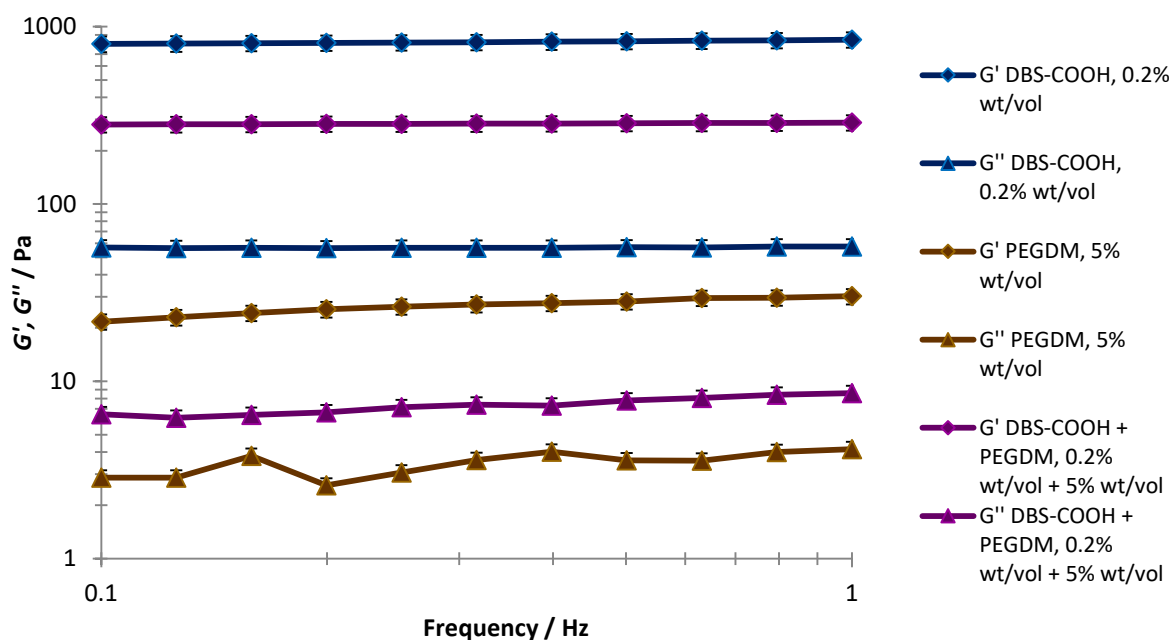
Figure 3.6: Comparison of typical results from frequency sweep rheological analysis of DBS-CO₂H, PEGDM, and DBS-CO₂H and PEGDM hybrid hydrogels.

From the frequency sweep analysis, it can be seen that at 1 Hz, the G' value for the hybrid gel is 288 Pa, whilst the value of G' for DBS-CO$_2$H on its own is significantly higher at 845 Pa. This might seem somewhat unexpected at first, given that when DBS-CO$_2$H was combined with agarose, the value of G' for the hybrid was higher than either individual gel. In the case of the DBS-CO$_2$H and PEGDM hybrid though, the much higher % wt/vol of the PG must be taken into account, as it is expected that the rheological properties of this component, being present in much greater amounts than the LWMG component, will dominate the overall rheological profile of the hybrid gel. The PEGDM gel itself is not particularly rigid, as seen from its value of G' at 1Hz, which is only 30 Pa. Interestingly, from the results of the amplitude sweep (Figure 3.5), PEGDM is clearly very robust - this is likely due to the structure of the polymer gelator network, which is comprised of many flexible, crosslinked polymer chains. In the hybrid gel, it is clear that the presence of DBS-CO$_2$H has a significant strengthening effect - attributed to the rigid, aligned nanostructure of DBS-CO$_2$H somewhat "reinforcing" the overall gel structure. However, from the amplitude sweep, it is seen that the presence of DBS-CO$_2$H in the hybrid gel does reduce the robustness of the material, as evidenced from a shorter LVR – clearly the LMWG network is at least partially broken down inside the hybrid material when subjected to the higher strains. Unlike the hybrid hydrogels of DBS-CO$_2$H and agarose, it is unclear from this rheological analysis whether there is any synergistic relationship between the DBS-CO$_2$H and PEGDM in these hybrid hydrogels.

3.5.3 ^{1}H NMR studies of hybrid hydrogels of DBS-CO$_2$H and PEGDM

Hybrid hydrogels of DBS-CO$_2$H and PEGDM were prepared for ^{1}H NMR studies by adding D$_2$O (0.7 mL) to DBS–CO$_2$H (1.4 mg), followed by sonication to disperse the solid. NaOH$_{(aq)}$ (21 µl, 0.5 M) was added to dissolve all solid and DMSO (1.4 µl) was added to act as an internal standard. GdL (5.6 mg), PEGDM (35 mg) and PI (0.35 mg) were then added, and the solution was transferred to an NMR tube. UV photopolymerisation was then carried out by placing the NMR tube under UV light for 10 minutes.
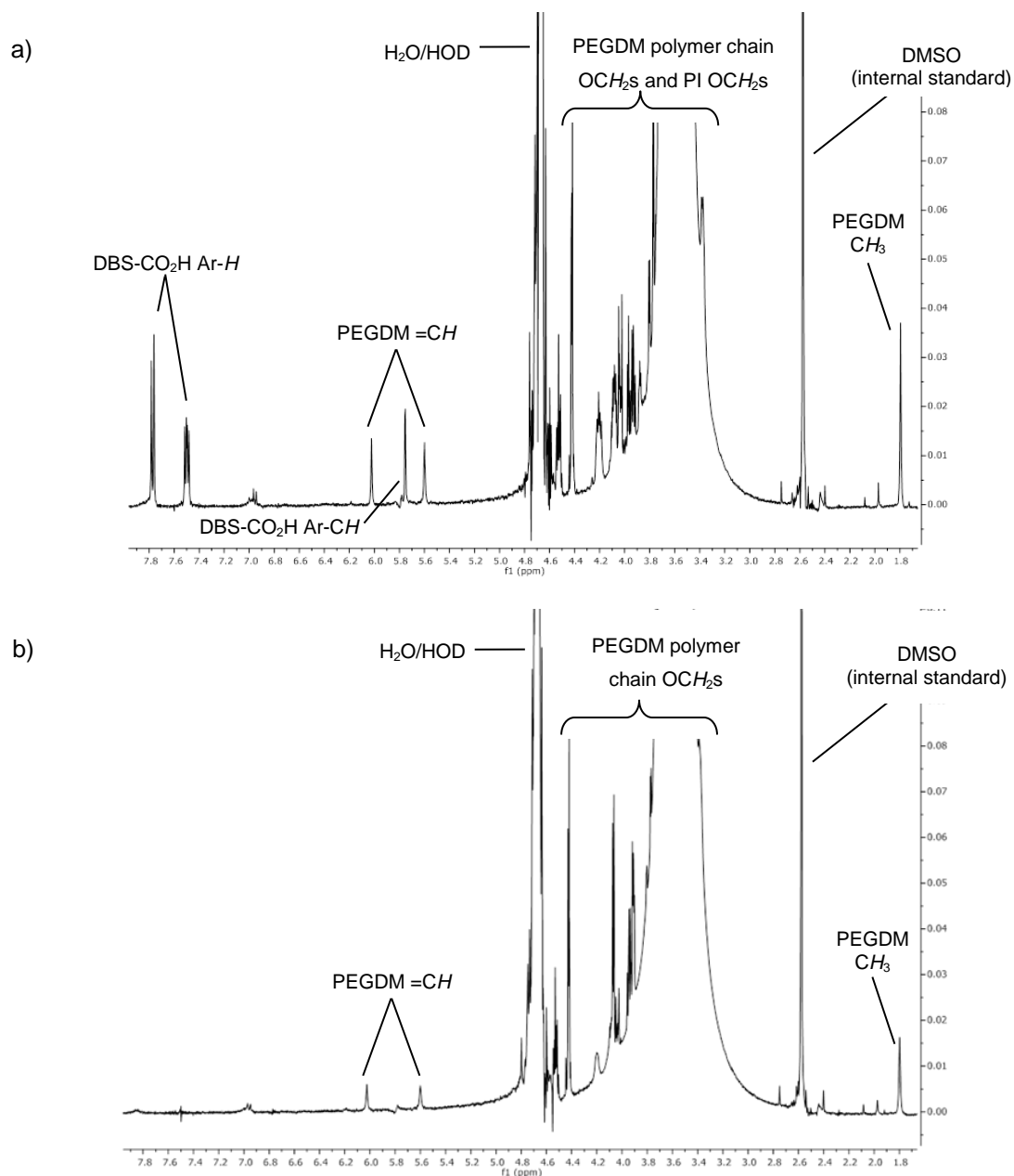
Figure 3.7: ^{1}H NMR spectra (400 MHz, D$_2$O) of hybrid hydrogel of DBS-CO$_2$H (0.2% wt/vol) and PEGDM (5% wt/vol) at a) before UV curing and start of DBS-CO$_2$H gelation and b) after UV curing and end of DBS-CO$_2$H gelation; the absence of signals related to DBS-CO$_2$H in (b) indicates that all of the LMWG has been incorporated into a sample-spanning solid-like network.

Using the "snapshot" method, recording spectra immediately after UV curing and again after GdL hydrolysis, it was seen that, as for with the hybrid gel containing agarose, all of the DBS-CO$_2$H was immobilised and incorporated into a LMWG network (Figure 3.7).

More detailed kinetic information was then obtained by recording ^{1}H NMR spectra every 30 minutes following the addition of GdL and photopolymerisation, and plotting the concentration of mobile LMWG versus time (Figure 3.8). Interestingly, there was a significant decrease in the rate of DBS-CO$_2$H network formation in the presence of PEGDM when compared to DBS-CO$_2$H by itself or in the presence of agarose.
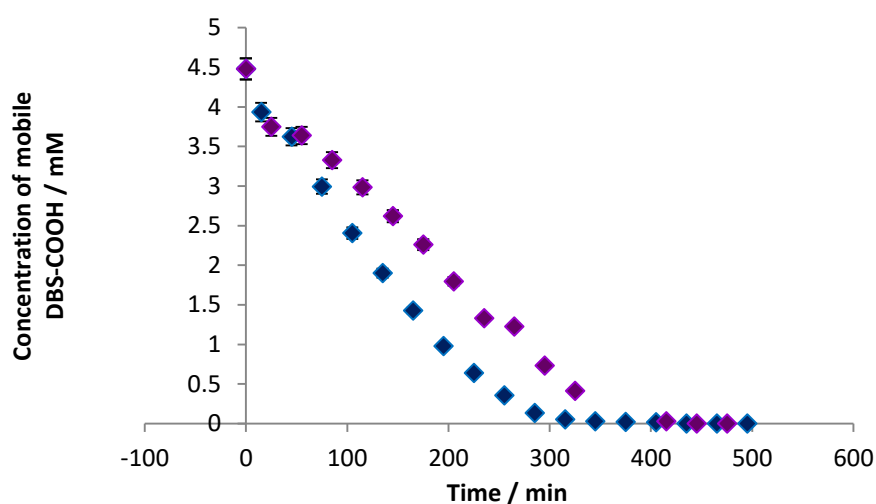
Figure 3.8: Plot of average rate of formation of the DBS-CO$_2$H network in presence (purple) and absence (blue) of PEGDM.

The kinetic data was then fitted to Avrami's kinetic model[160–163] (Figure 3.9); see section 2.4.2 for comments on the use of the Avrami model with pH-responsive LMWGs. For the hybrid hydrogel of DBS-CO$_2$H and PEGDM, the value of the Avrami exponent, n, was found to be 1.45. This value is significantly less than that for the DBS-CO$_2$H gel alone (n = 1.61), and suggests that there may be less branching or 2D growth of DBS-CO$_2$H fibres in the presence of PEGDM. The reason for this, and the observation that DBS-CO$_2$H assembles at a notably slower rate in the presence of PEGDM, is most likely due to the increase in the viscosity of the solution brought about by the presence of the polymerised PG, which limits the rate of diffusion and has been observed in other reports of hybrid hydrogels[107,181] and combinations of polymers and LMWGs.[84,85]

103
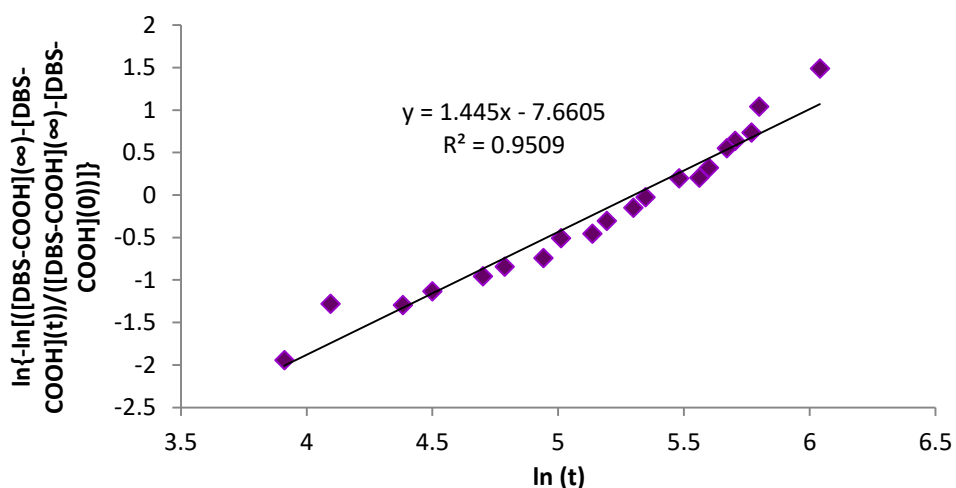
Figure 3.9: Avrami plot for formation of DBS-CO₂H network in presence of PEGDM; gradient of line = n = 1.45.

3.5.4 CD studies of hybrid hydrogels of DBS-CO₂H and PEGDM

The samples of the hybrid system prepared for CD were prepared with sub-gelation amounts of the gelators (0.02% wt/vol DBS-CO$_2$H and 0.5% wt/wt PEGDM), so as in Chapter 2 what was observed by this technique was not the formation of a sample-spanning network, but the assembly of the nanofibres.

In the presence of PEGDM (which does not have a distinctive CD signal), and after standing for 5 hours following the addition of GdL, DBS-CO₂H had a CD band at ca. 261 nm, with an intensity of ca. -62 mdeg (

Figure 3.10a); this is comparable to the CD spectrum of DBS-CO$_2$H in the absence of PEGDM (260 nm and maximum of ca. -41 mdeg, Figure 2.5b), and suggests that nanofibres can assemble in a similar way either in the absence or presence of PEGDM. However, as the intensity is somewhat greater, this also suggests that, as for in the presence of agarose, the DBS-CO$_2$H can access a more thermodynamically stable, somewhat different fibre form. The HT data comparing the DBS-CO$_2$H/PEGDM hybrid system with DBS-CO$_2$H showed some difference in the values of HT at 260 nm between the samples (*ca.* 40 V), though as previously stated this may not have a significant effect on the recorded ellipticity.
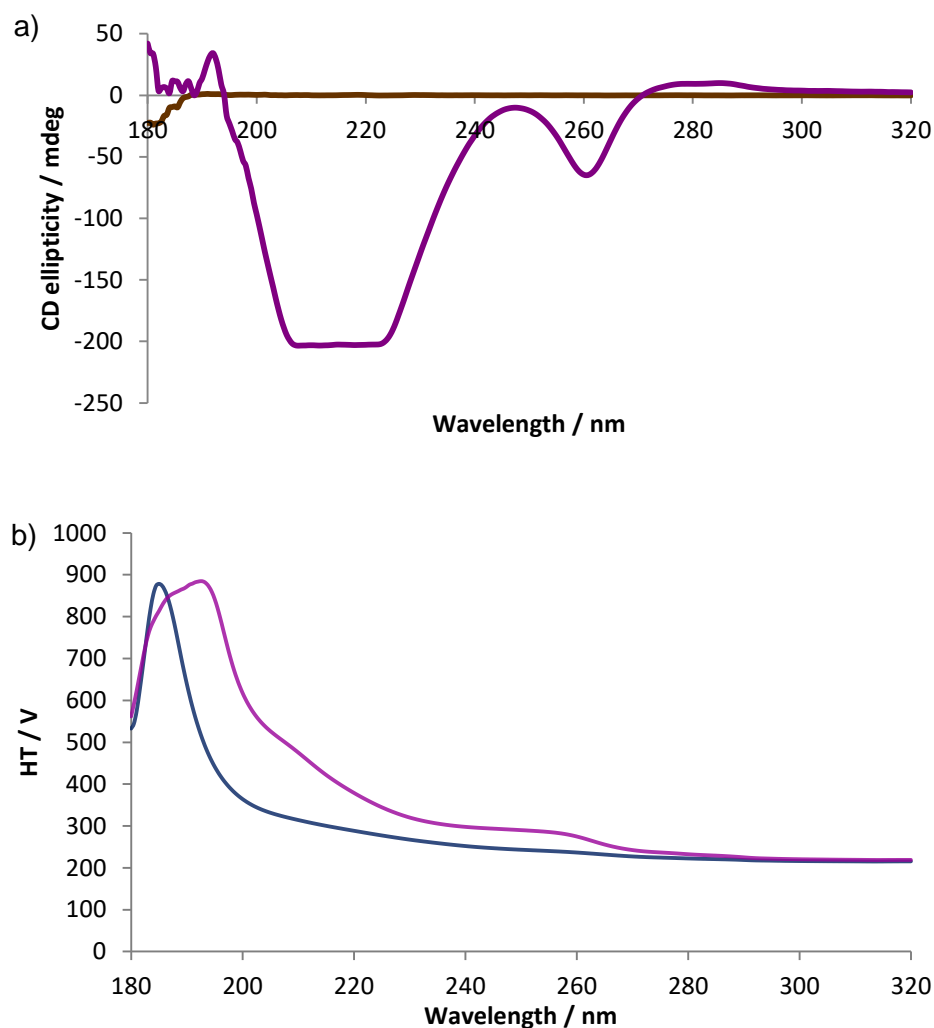
Figure 3.10: a) CD spectrum of PEGDM (brown) and hybrid system of DBS-CO₂H and PEGDM (0.02% wt/vol and 0.5% wt/vol respectively) (purple) after standing for 5 hours; b) HT data for DBS-CO₂H and PEGDM (0.02% wt/vol and 0.5% wt/vol respectively) (purple) compared with HT data for DBS-CO₂H (0/02% wt/vol) (blue, previously presented in Figure 2.6).

A CD experiment that directly probed the initial stages of fibre growth by recording CD spectra every 5 minutes for 2 hours after the addition of GdL was also carried out; again, the bands associated with DBS-CO₂H could be seen to slowly emerge (Figure 3.11). By plotting time (after addition of GdL) against the CD ellipticity at 260 nm, the evolution of the CD spectra for the hybrid gel could be compared to those of the DBS-CO₂H gel (Figure 3.12). The induction phase for DBS-CO₂H in the presence of PEGDM was significantly longer (similar to what was observed in the presence of agarose), again suggestive that the increased viscosity of the solution from addition of the polymer limits diffusion and initial nucleation of the LMWG. The timescale of the rapid increase in ellipticity for both systems is fairly similar (*ca.* 20 minutes), though the hybrid system shows greater ellipticity after 2 hours. However, as previously discussed, on further standing (for up to 5 hours) the ellipticity of DBS-CO₂H decreased to *ca.* -40 mdeg, whilst the ellipticity of the

105

hybrid system decreased to *ca.* -60 mdeg – again, this shows further slow evolution of the nanofibre morphology.[31,167–169] A comparison of HT data (Figure 3.13) for these experiments showed no significant difference in values, indicating the maximum values of ellipticity recorded were not due to HT differences.
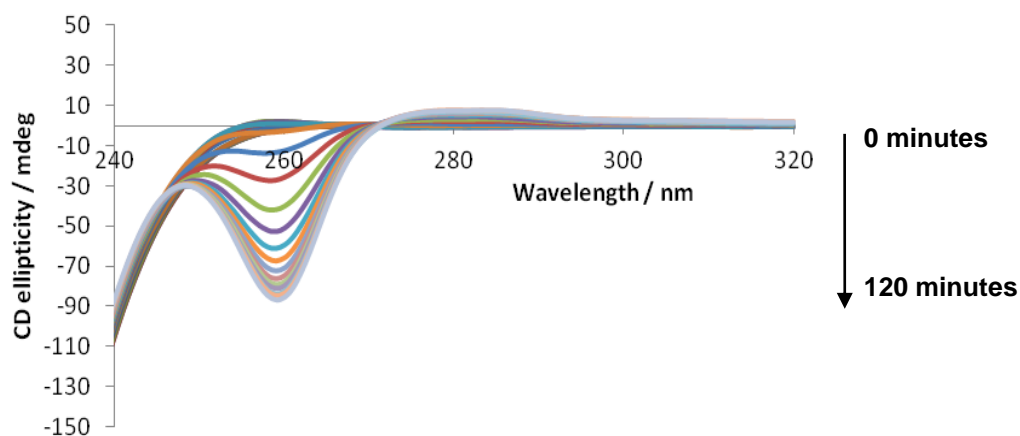
Figure 3.11: Evolution of CD spectrum of hybrid system of DBS-CO$_2$H (0.02% wt/vol) and PEGDM (0.5% wt/vol) over a 2 hour period, after addition of GdL (44.9 mM).
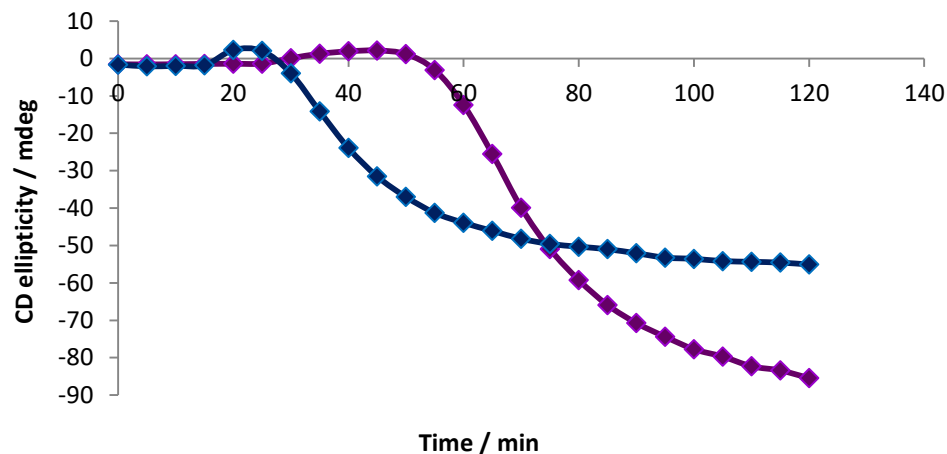
Figure 3.12: Comparison of evolution of CD spectra over time, monitoring ellipticity at 260 nm, after addition of GdL (44.9 mM); DBS-CO$_2$H (blue); hybrid system of DBS-CO$_2$H and PEGDM (purple).
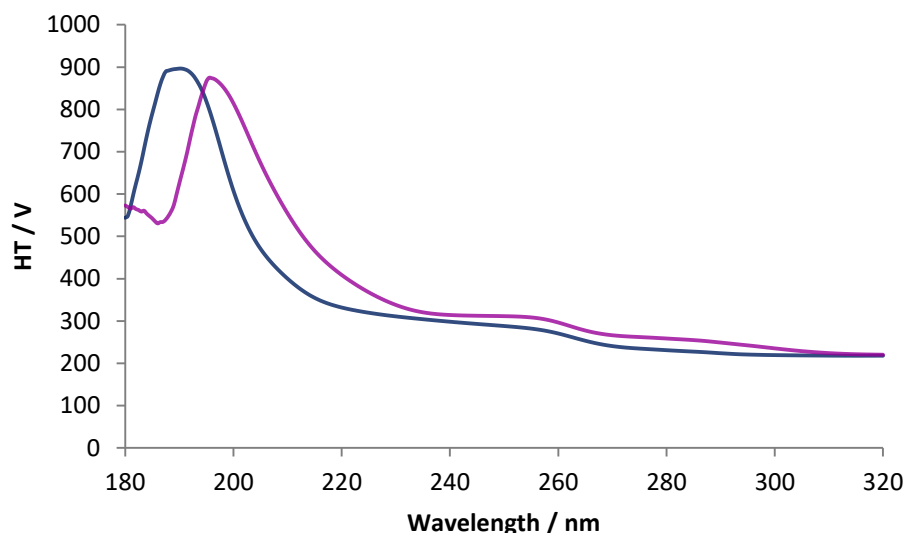
Figure 3.13: HT data recorded after 2 hours for the CD spectra of DBS-CO$_2$H (0.02% wt/vol) (blue) and DBS-CO$_2$H/PEGDM (0.02% and 0.5% wt/vol) (purple) as ellipticity was monitored over a 2-hour period (see Figure 3.12).

3.5.5   SEM imaging of hybrid hydrogels of DBS-CO$_2$H and PEGDM

Samples for SEM were prepared by the previously described freeze-drying method (see 2.4.4 for a discussion on the limitations on the information that can be obtained from freeze-drying samples for SEM). The xerogel of the hybrid hydrogel (Figure 3.14) showed a combination of the characteristics of both DBS-CO$_2$H and PEGDM gels – importantly, it was clear that the DBS-CO$_2$H fibre network could still be observed, with it appearing to be embedded or coated in the PEGDM films.
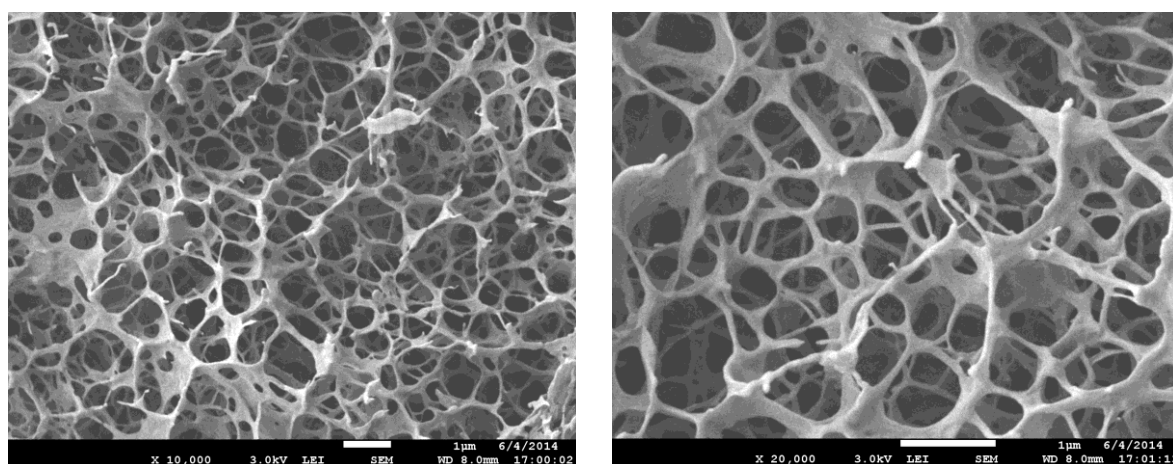
Figure 3.14: SEM images of xerogels of hybrid hydrogels of DBS-CO$_2$H (0.2% wt/vol) and PEGDM (5 % wt/vol); scale bars = 1 μm.

3.6   Functionality of hybrid hydrogels of DBS-CO$_2$H and PEGDM

3.6.1   Photopatterning of hybrid hydrogels of DBS-CO$_2$H and PEGDM

Controlling the internal structure of a gel by photopatterning methods has great potential for developing nano-patterned materials with enhanced properties,[204–226] and is particularly attractive for tissue engineering and drug delivery applications. As one network in the hybrid system described here was formed through photo-irradiation, it became an option to investigate the possibility of obtaining spatial resolution in the hybrid system by photopatterning regions of hybrid gel into a bulk sample. In particular, it was reasoned that the materials properties of the gel could be modified depending on whether one or two gel networks were present in a given region.

To form such spatially resolved gels, a 5% wt/vol solution (10 mL) of PEGDM (with 0.05% wt/vol PI) was prepared, and to this was added DBS-CO$_2$H (20 mg, to give 0.2% wt/vol), followed by sufficient NaOH (0.5 M) to dissolve the LMWG. Finally, 80 mg of GdL was added, and the solution was poured into a square glass mould. A Y-shaped mask (Y for 'York') was then applied over the top and the mix was cured under UV light for 20 minutes; only in those areas exposed to UV light did the PEGDM gel form. The moulds were then left overnight to allow the DBS-CO$_2$H network to assemble throughout the sample as slow acidification progressed (

Scheme 3.3).
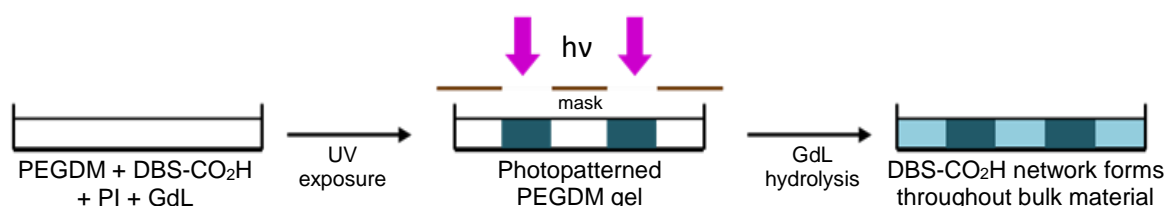
Scheme 3.3: Process of production of a multidomain gel of PEGDM and DBS-CO$_2$H; the patterned PG network is formed first by selective exposure to UV light, followed by formation of the LMWG network throughout the bulk sample as a result of GdL hydrolysis.

After this time, the whole mould was filled with gel, but two regions were clearly distinct, with the 'Y' spatially-patterned gel visible in the centre – the hybrid region was less translucent, which may be due to the LMWG fibres being thinner or less clustered in this region, leading to greater optical transparency (Figure 3.15A). The hybrid region was also noticeably stronger – whilst the non-hybrid region could easily be broken (Figure 3.15B), the hybrid region could be removed intact (Figure 3.15C). This shows that the presence of a PG network can significantly enhance the mechanical stability of LMWG-derived gels. This type of material is defined as a 'multidomain gel'. As such, this builds on the concept of multi-component gels by introducing a degree of spatial and temporal control to the gelation process.
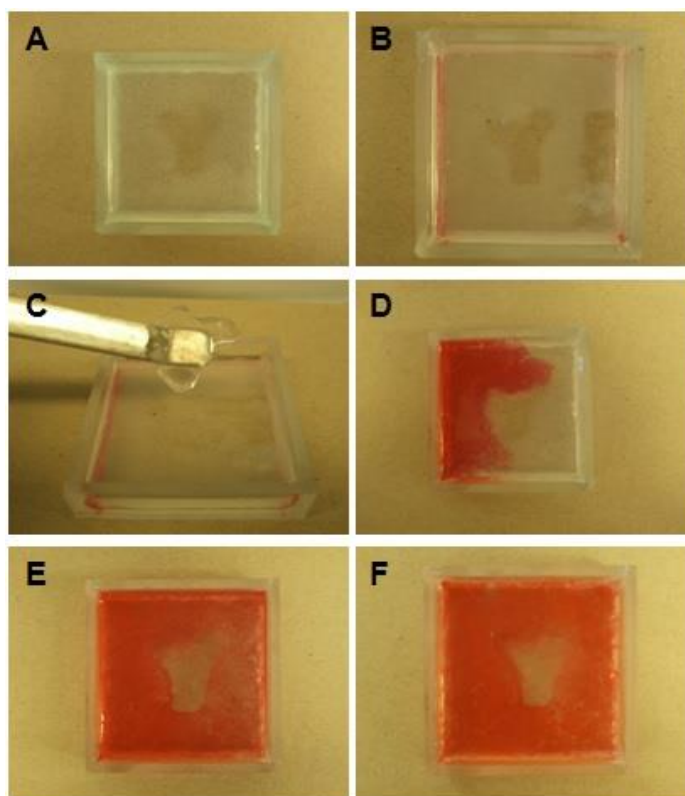
Figure 3.15: (A) Patterned multi-domain gel consisting of non-hybrid single-network region (more translucent) and hybrid dual-network Y-shaped region (less translucent). (B) The non-hybrid domain is easily deformed, whilst (C) the hybrid region can be removed intact. (D) Diffusion of DR80 dye from left edge at ca. 60 s. (E) Diffusion of dye at ca. 3 h. (F) Diffusion of dye at ca. 24 h – non-hybrid region is nearly completely stained, whilst there is only minimal diffusion into hybrid region.

An aqueous solution of Direct Red 80 (DR80) dye (1 mg/mL) was then applied to the edge of the gel (Figure 3.15D). Rapid diffusion of the dye was seen in the non-hybrid region (Figure 3.15E), and after 24 hours the whole single network LMWG gel domain was stained red (Figure 3.15F). In contrast, the dye barely diffused into the hybrid PG/LMWG domain, even after 2 days. This is likely due to the denser network of crosslinked PEGDM in the hybrid domain preventing easy diffusion of the relatively large Direct Red 80 dye molecules.

3.6.2   Controlled release from hybrid hydrogels of DBS-CO$_2$H and PEGDM

3.6.2.1   Controlled release

In order to further elucidate the diffusional properties of dyes within these hybrid gels, several different dyes were then investigated. This allowed the potential of these hybrid systems for controlled release to be evaluated. Direct Red 80 (DR80), malachite green (MG) and methylene blue (MB) (Figure 3.16) – were encapsulated within a gel sample. To achieve this, 0.1 mg of selected dye was dissolved in 1 mL H$_2$O, and then to this solution was added 0.5 mg PI and 50 mg PEGDM; for hybrid gels, after addition of PEGDM and PI, 2 mg of DBS-CO$_2$H was added, followed by sonication to disperse and then addition of NaOH$_{(aq)}$ (0.5 M) to dissolve. The solutions

were then transferred to vials containing 8 mg of GdL, followed by shaking to dissolve. All solutions were cured in uncapped 2.5 mL vials under UV light for 10 minutes to obtain gels.
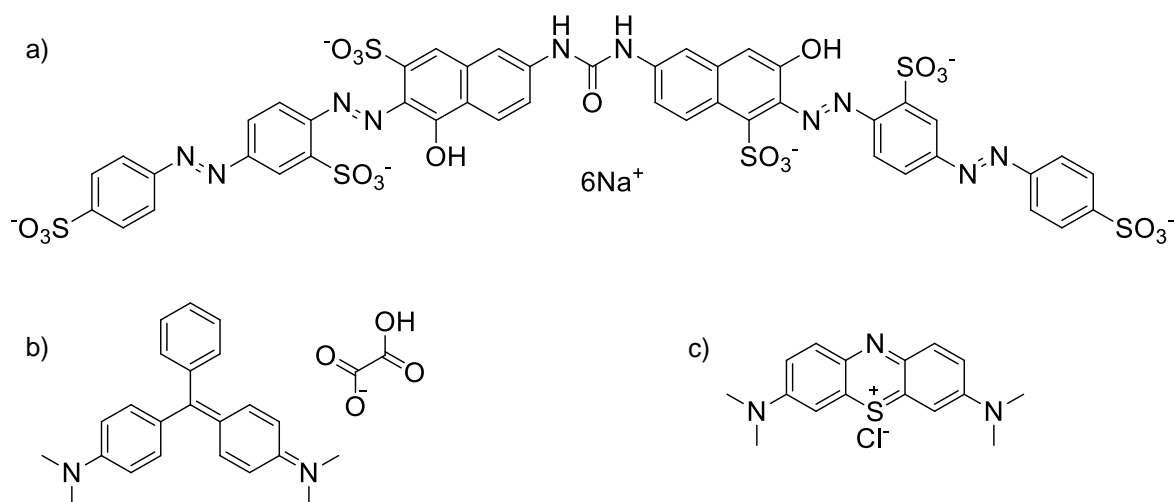
Figure 3.16: Structures of dyes: a) Direct Red 80, b) malachite green oxalate, and c) methylene blue chloride.

The 1 mL cylinders of the gels as prepared were then cut in half horizontally to give two smaller cylinders of 0.5 mL in volume, and these were submerged in 30 mL of pH 7 phosphate buffer solution. The release of the dyes over time was monitored by UV-vis spectroscopy, by taking a 2 mL sample every hour (for 7 hours), then returning it to the bulk solution. A final sample was taken at 24 hours. Absorbance of MB was recorded at 663 nm, absorbance of MG at 617 nm, and absorbance of DR80 at 541 nm. The percentage of dye released was calculated from calibration curves. The results are presented in Figure 3.17, comparing the % dye released from the PEGDM gel alone and for the hybrid hydrogel of PEGDM and DBS-CO₂H.
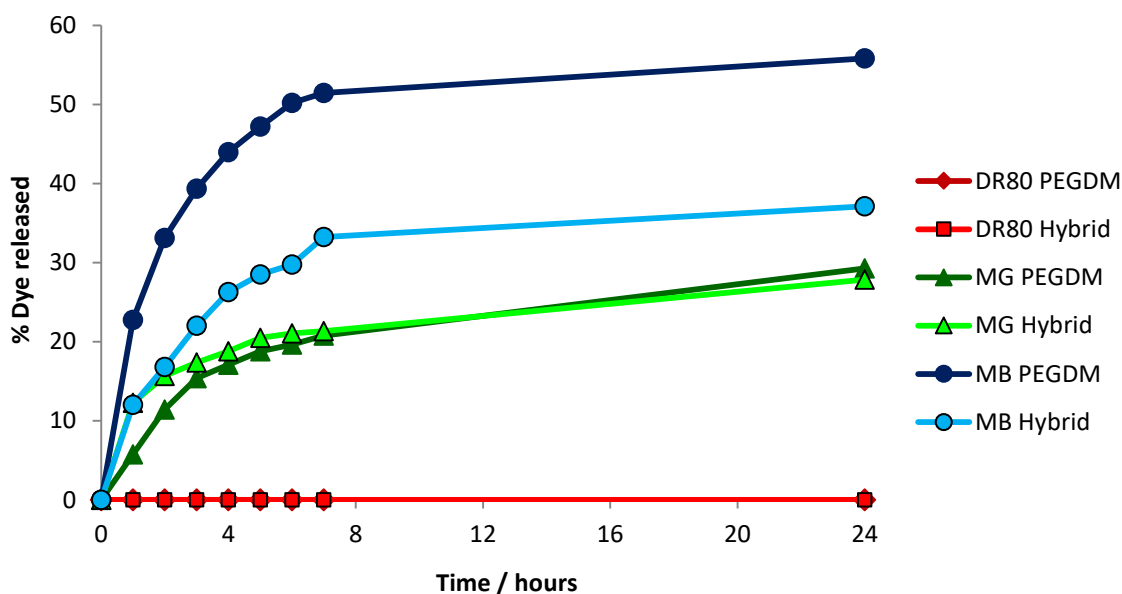
Figure 3.17: Comparison of the percentages of dye released from both PEGDM and hybrid gels in pH 7 phosphate buffer solution.

For DR80, no release of dye either from the PEGDM or the hybrid gels was observed. This is consistent with what was observed in the multidomain gel experiments, where DR80 was not observed to diffuse into the photo-patterned hybrid domain – it is again most likely that the large size of DR80 physically hinders its diffusion out of the PEGDM gel network (i.e., a consequence of sterics).

For MG, the dye was released from the gel network over a 24 hour timescale, with up to *ca.* 25% being released. This suggests that this smaller dye is able to diffuse out of the PEGDM network, although some dye clearly remains entrapped – possibly locked in poorly accessible pores within this relatively dense network. Interestingly, the PEGDM and the hybrid gels both released MG at a very similar rate, indicating that the presence of the LMWG network has no obvious impact on diffusion and that the PEGDM network is dominating the behaviour.

MB, however, showed very different diffusion depending on whether the gel was PEGDM or a hybrid. For the hybrid gel, only 35% was released over 24 hours, whereas for PEGDM alone, as much as 55% was released (more than either of the larger dyes for this system). This indicates that for MB, the presence of DBS-CO$_2$H in the hybrid hydrogel appears to hinder dye diffusion and release. This effect of the LMWG cannot be due to sterics, or a similar effect would have been seen for the release of MG. Therefore, it appeared that there must be some specific interactions between MB and the DBS-CO$_2$H network. It is known from literature that acid and/or hydrazide functionalised LMWGs can form specific interactions with MB, either through intercalation into the LMWG fibres,[227,228] or by acid-base interactions at the fibre periphery.[229]

111

In order to confirm there were specific interactions between DBS-CO$_2$H and MB, a simple adsorption study was carried out. 0.5 mL H$_2$O was added to 3 mg of DBS-CO$_2$H (0.6 % wt/vol) in sample vials. The vials were then sonicated to disperse the solid, and 10 µL aliquots of 0.5 M NaOH$_{(aq)}$ were added to dissolve (pH ≈ 11). The solutions were then transferred to 8 mL sample vials containing 13 mg of GdL, followed by shaking to dissolve. The vials were then left overnight for gelation to occur. The higher % wt/vol of DBS-CO$_2$H was needed in this experiment to prevent the gel collapsing in the subsequent adsorption studies.

The next day, 4 mL of a dye solution (methylene blue chloride, 20 µg/mL, or malachite green oxalate, 20 µg/mL) was added to the top of the gels. The systems were allowed to stand undisturbed at room temperature for a total of 24 hours. At 0, 2, 4, 6 and 24 hours, a 2 mL aliquot of the supernatant solution was taken for UV-vis spectroscopy, then returned to the bulk solution.

Absorbance was measured at maximum absorbance wavelength of 663 nm for MB (Figure 3.18). For MG, the maximum absorbance wavelength was at 617 nm (Figure 3.19). Extrapolating concentrations from the spectra (using calibration plots) showed that after 24 hours, *ca.* 50% MB was adsorbed into the gel, whilst only *ca.* 24% MG from a similar concentration of dye was adsorbed (simple diffusion and dilution effects would lead to *ca.* 11% adsorption of dye).
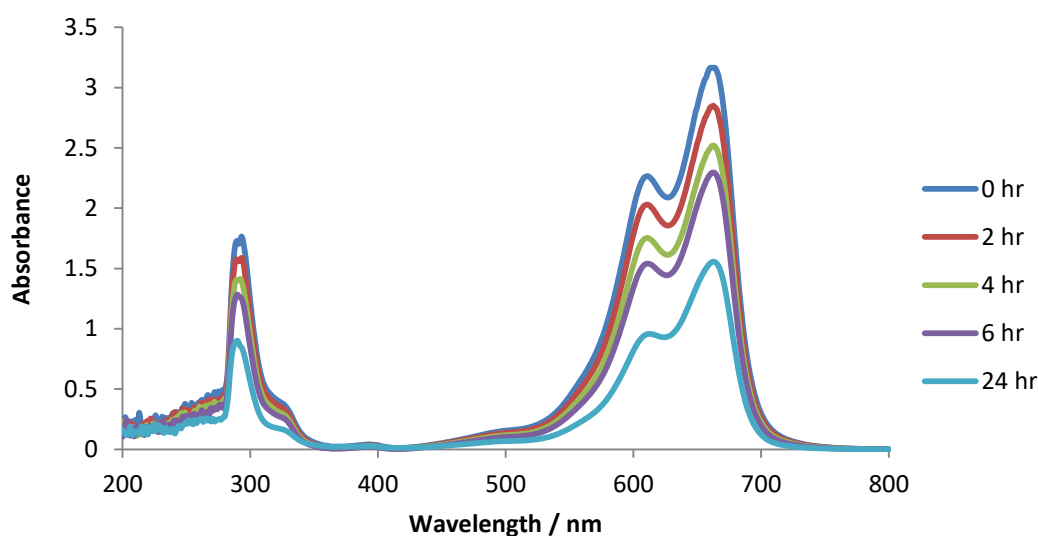
Figure 3.18: UV-vis spectrum for the time-dependent adsorption study of methylene blue (MB) onto DBS-CO₂H.
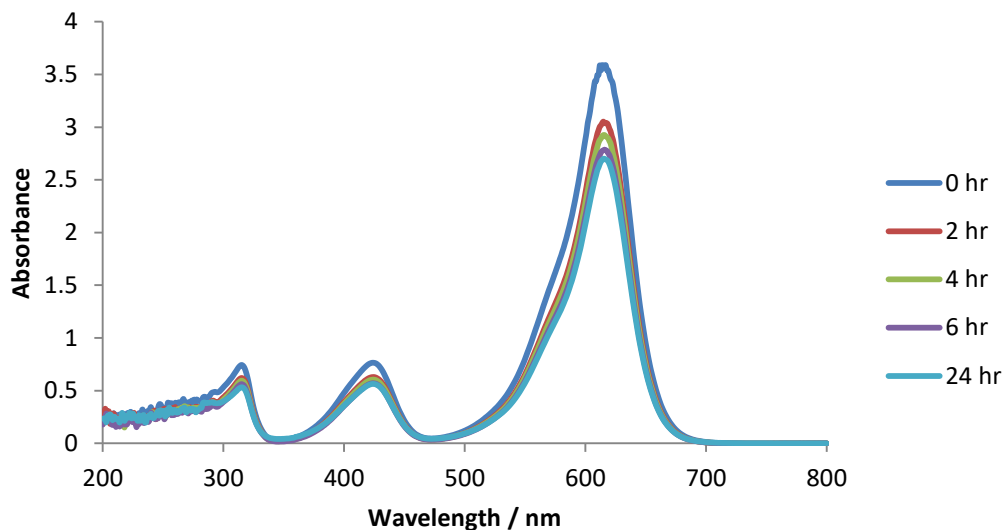
Figure 3.19: UV-vis spectrum for the time-dependent adsorption study of malachite green (MG) onto DBS-CO$_2$H.

This study demonstrated that whilst DBS-CO$_2$H clearly had an affinity for both MB and MG, it was able to adsorb a greater amount of the former, though the exact nature of the interactions that drove this were still unclear.

3.6.2.3 *TEM imaging of DBS-CO$_2$H hydrogels containing MB dye*

In order to better probe the mechanism of DBS-CO$_2$H/MB interactions, transmission electron microscopy (TEM) was used to study the fibre morphology of DBS-CO$_2$H gels containing MB dye, in order to observe any changes in morphology from adsorption of the dye. These gels were prepared at 0.2% wt/vol of DBS-CO$_2$H by the method previously given in Chapter 2, with the addition of 0.1 mg/mL MB dye. To prepare samples for TEM, a small portion of gel was removed with a spatula and 'drop-cast' onto a heat-treated copper TEM grip. Excess material was removed using filter paper and left to dry for 20 minutes prior to imaging, and a uranyl acetate stain was used for contrast. TEM images of DBS-CO$_2$H without and with MB are shown in Figure 3.20.
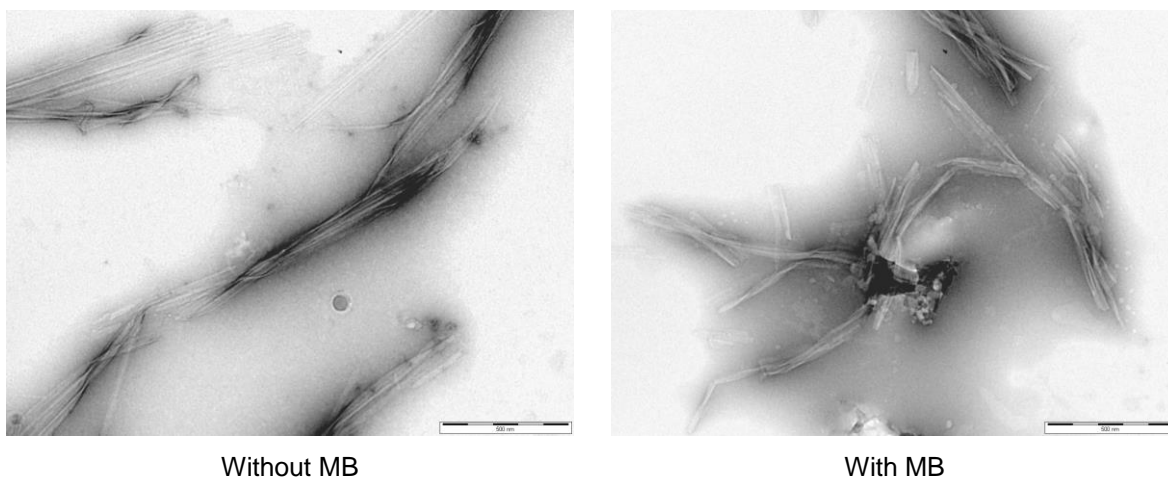
Without MB   With MB

Figure 3.20: TEM images of 0.2% wt/vol DBS-CO$_2$H xerogels; left, without MB dye, right, with MB dye (0.1 mg/mL). Scale bar = 500 nm. The xerogels are negatively stained with uranyl acetate. The fibres in both samples show similar morphologies (rigid fibres).

Both samples appeared to have very similar morphologies. There are two possible mechanisms for dye interactions with DBS-CO$_2$H – intercalation or acid-base interactions. Intercalation would likely cause a change in fibre morphology,[227,228] which was not observed here. Therefore, it seems that acid-base interactions at the fibre periphery are the most likely cause for the stronger interactions between MB and DBS-CO$_2$H – probably between the heterocyclic amine of MB and the carboxylic acid groups in DBS-CO$_2$H (though there may also be interactions between the tertiary amines of MB, as this would also account for the slightly higher than expected adsorption of MG, which also has these tertiary amine groups).

3.7   Conclusions and Outlook

What has been demonstrated in this chapter is the first known example of a hybrid hydrogel combining a LMWG (DBS-CO$_2$H) and a synthetic PG (PEGDM) – the only previous example of a hybrid gel which used a synthetic PG was an organogel.[105] From SEM, the hybrid gel was seen to consist of a mixture of DBS-CO$_2$H and PEGDM nanostructures. NMR studies showed that the presence of PEGDM appeared to have some effect on the kinetics of DBS-CO$_2$H immobilisation, and likewise in the CD studies the presence of PEGDM did appear to slow the initial kinetics of nanofibre nucleation and their reorganisation over time – though CD also confirmed that DBS-CO$_2$H still assembled into its chiral nanostructures. Rheologically, the hybrid hydrogel was shown to have improved stiffness over the individual PG component (though lower than the individual LMWG component), and an improved robustness over the individual LMWG component (though lower than the individual PG component), showing that the combination of the two gelators can improve the less desirable properties of each individual gel.

Most importantly, this hybrid system demonstrated that through controlled exposure to UV photoirradiation, different regions could be spatially patterned into the material, resulting in a multidomain hydrogel. This was the first report of multidomain hydrogels to include a LMWG system. In these multidomain gels, either one or two gelator networks were present in each domain, which led to differences in materials behaviour and diffusion. Additionally, on examining the controlled release of dyes from hybrid gels, it was seen that both networks played active roles, either due to the density of the network (PEGDM) or through specific interactions between the dye molecules and the gelator network (DBS-CO_2H).

Such photopatternable materials with controlled release abilities would have great potential in several fields of application. Firstly, in microfluidics, where patterns to control diffusion could be designed. Secondly, in drug delivery, where writing in the different domains would generate gels with differential kinetics of drug release, depending on the composition of the domain – for example, burst release from a weak LMWG domain, with sustained controlled release from a robust hybrid domain. Thirdly, in tissue engineering, where complex microscale patterns with greater spatial definition (achievable with laser irradiation) could be used to encourage differential cell growth. This latter application would also benefit from the use of two-photon polymerisation (2PP),[230–232] which would allow for patterning in 3D – the main drawback of the simple masking method used here it that it only allows for only 2D photopatterning. For these biomedical applications, whilst PEGDM is reasonably biocompatible (and can be further modified to improve its biocompatibility[195–201]), DBS-CO_2H, being formed at a relatively acidic pH, is likely to not be – hence a LMWG which forms a gel at a more biologically-friendly pH would need to be used.

4. Chapter 4: DBS-Peptide Gelators and Multi-Gelator Self-Sorting

Results from this chapter were published in D. J. Cornwell, O. J. Daubney and D. K. Smith, *J. Am. Chem. Soc.*, 2015, **137**, 15486–15492.

4.1. Introduction

There has been much recent interest in using LMWGs as biomaterials for potential applications in the fields of drug delivery and tissue engineering.[233] Hydrogels are particularly suitable for the latter of these applications, as they have the potential to be able to closely mimic the extracellular matrix if suitable biologically active motifs, such as cell adhesion sequences, are incorporated into the gelator structure.[14,234–236] In particular, LMWGs incorporating short peptide sequences have become a very-well researched area in the development of hydrogels for tissue engineering – they have the advantages of being low-cost and easy to produce, which can enable the investigation of a series of related compounds.[237] Peptide-based LMWG hydrogels have been shown to have possible uses in a variety of tissue growth applications, including regeneration of optic nerves[238–240] or spinal cords,[241,242] cartilage repair,[243] cardiac tissue growth,[244] angiogenesis,[245] and osteointegration of metal prostheses.[246]

To further the investigation of hybrid hydrogels as potential materials for biomedical applications, it was necessary to begin investigating alternative LMWGs to DBS-CO$_2$H, as this gelator forms its gel networks at a relatively acidic – and hence not particularly biologically friendly – pH values. Taking inspiration from dipeptide-based LMWGs,[237] it was decided that the first step in attempting to increase the biocompatibility of DBS-derived LMWGs would be to append amino acids and/or short peptide sequences onto DBS-CO$_2$H through the formation of an amide bond.

4.2. Synthesis of DBS-peptide LMWGs

The synthesis of DBS-peptide compounds was carried out by coupling DBS-CO$_2$H with two equivalents of a methyl ester-protected amino acid using coupling agent *O*-(benzotriazol-1-yl)-*N,N,N′,N′*-tetramethyluronium tetrafluoroborate (TBTU) in the presence of diisopropylethylamine (DIPEA) in DMF, in a method adapted from the work of Ulijn and co-workers.[247] This was followed by saponification of the methyl ester groups with two equivalents of NaOH$_{(aq)}$ (1 M) (Scheme 4.1).
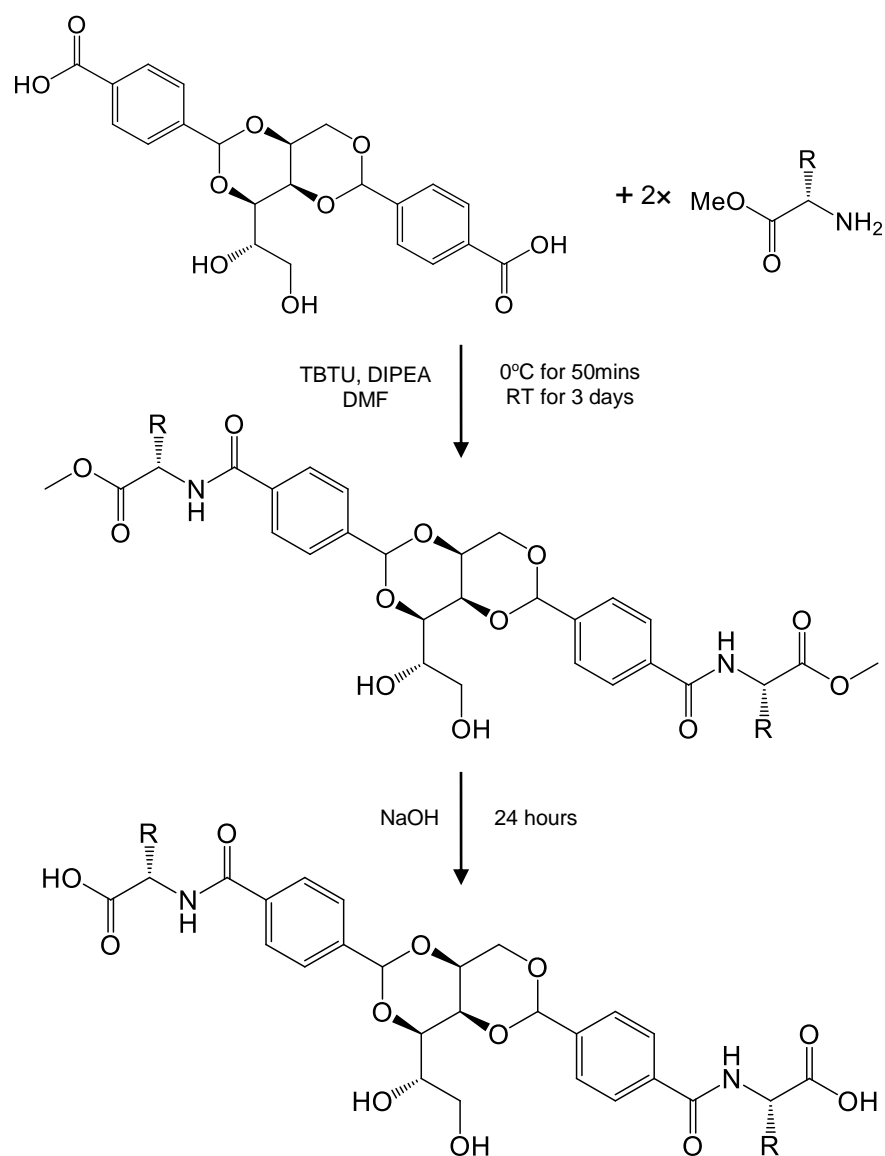
Scheme 4.1: Synthesis of a DBS-peptide from DBS-CO₂H and a methyl ester-protected L-amino acid through TBTU coupling followed by NaOH saponification.

For example, synthesis of 1,3:2,4-dibenzylidene-D-sorbitol-dicarbonyl-glycine (DBS-Gly) was achieved by first coupling DBS-CO$_2$H with two equivalents of H$_2$N-Gly-OMe using TBTU, to give 1,3:2,4-dibenzylidene-D-sorbitol-dicarbonyl-glycine methyl ester (DBS-GlyOMe) in 61% yield. ^{1}H NMR identified a triplet at 8.99 ppm corresponding to the newly formed amide group and a singlet at 3.65 ppm corresponding to the methyl protecting group, and ESI-MS gave product peaks at m/z values of 589.2035 (5%, [M+H]$^+$) and 611.1839 (100%, [M+Na]$^+$).

The methyl ester protecting groups were then cleaved by saponification using two equivalents of NaOH$_{(aq)}$ (1 M) in a water-methanol mix. This was followed by addition of NaHSO$_4$ to acidify and produce a white, stable gel. The gel was dried to give DBS-Gly (Figure 4.1) as a brown solid in

59% yield. ^{1}H NMR showed an absence of the methyl ester protecting group, and ESI-MS gave a product peak at a *m/z* value of 559.1592 (100%, [M-H]⁻).

The syntheses of 1,3:2,4-dibenzylidene-D-sorbitol-dicarbonyl-phenylalanine (DBS-Phe, Figure 4.1) and 1,3:2,4-dibenzylidene-D-sorbitol-dicarbonyl-tryptophan (DBS-Trp, Figure 4.1) were similarly carried out, with yields of 68% (DBS-PheOMe) and 69% (DBS-Phe), and 97% (DBS-TrpOMe) and 52% (DBS-Trp). Attempts were also made to synthesise both 1,3:2,4-dibenzylidene-D-sorbitol-dicarbonyl-alanine (DBS-Ala) and 1,3:2,4-dibenzylidene-D-sorbitol-dicarbonyl-aspartic acid (DBS-Asp), but these were unsuccessful due to the high solubility of the intermediate in DMF.

DBS-Gly
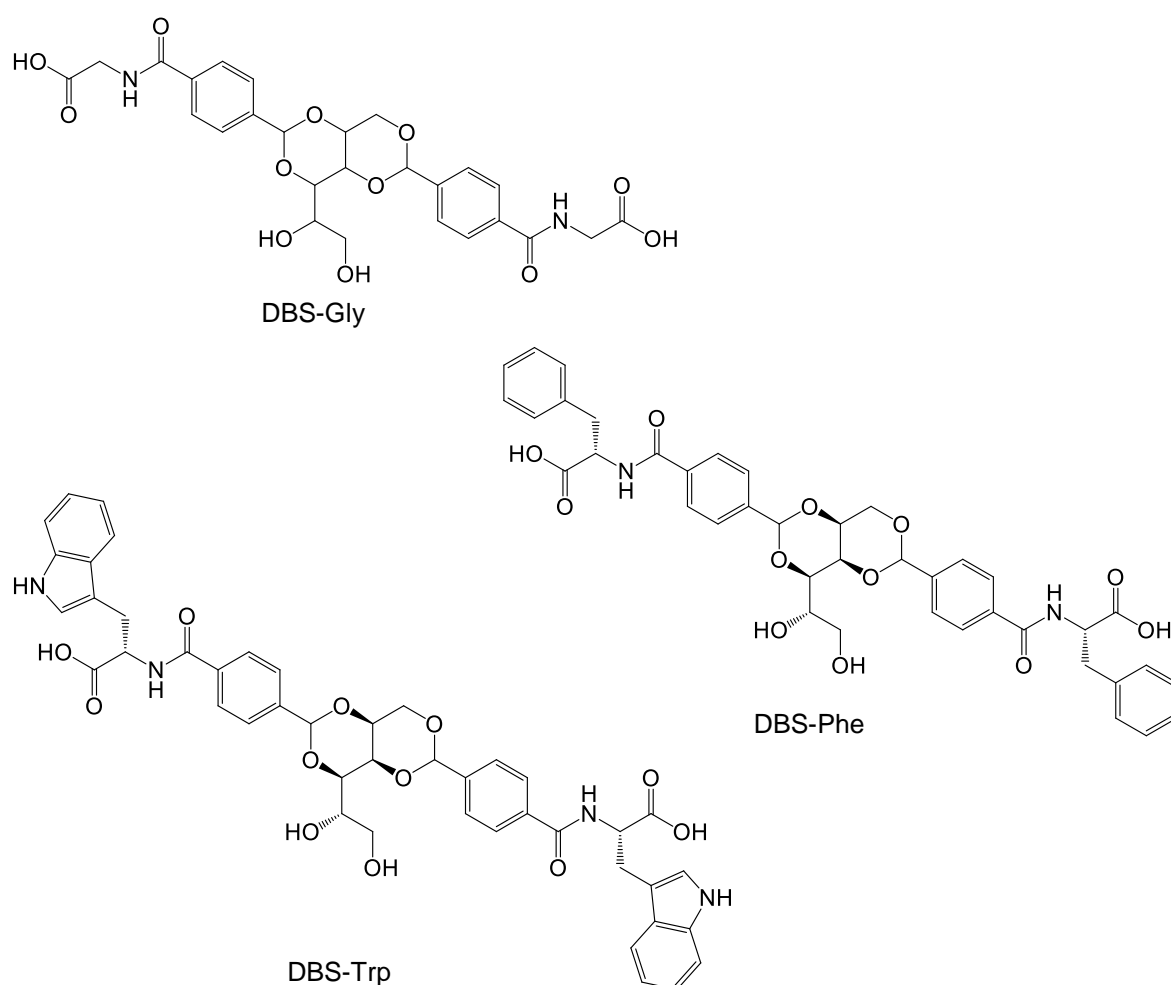
DBS-Phe

DBS-Trp

Figure 4.1: Successfully synthesised DBS-peptide potential LMWGs DBS-Gly, DBS-Phe, and DBS-Trp.

4.3.   Gelation studies of DBS-peptide LMWGs

4.3.1.   Reproducibility of certain results

The initial three batches of DBS-Gly successfully synthesised showed great promise as a gelator that produced a gel by either heat-cool or pH change methods, and as such both approaches are

discussed below. However, after the initial batches of DBS-Gly were almost exhausted, it became apparent that there were issues regarding the solubility of subsequent batches of the gelator. Whilst these batches of DBS Gly were all able to form gels by applying the pH change methodology, only certain batches functioned as heat-cool LMWGs, and even then with varying levels of success. When heated to dissolve the solid, some batches remained insoluble and instead of gelation, only precipitation, or partial inhomogeneous gelation were observed.

The synthesis was closely examined but no obvious problems were found. The different batches of DBS-Gly (including the original, fully-functional batches) were compared by ^{1}H NMR to check for impurities that could either disrupt or promote gelation, but none were observed. The different batches of DBS-Gly were washed with a variety of hot and cold solvents (to attempt to remove any impurities not visible by NMR), but these made little difference to the solubility of the compound. The pK_a values of the different batches were determined, and whilst there was some variation, with values ranging from *ca.* 4.1 to 4.4, there was no clear divide between those batches that functioned as heat-cool LMWGs and those that did not, and this variation was within the range of error for the pH meter used.

It was concluded that the issue of solubility is likely to be due to the packing structure that DBS-Gly adopts in the solid form produced during the final stages of synthesis. Similar issues were encountered by Escuder and co-workers, who found that relatively slight changes in environmental parameters during gel preparation affected the polymorph structure.[248] By extension, it can be assumed that as a gel is formed as part of the synthesis for DBS-Gly, small, and not easily controllable, changes in the surrounding environment could affect the packing structure for the LMWG, and hence its solubility when it comes to producing gels by the heat/cool method. The pH change method remains unaffected as it involves deprotonation to solubilise the gelator, and the protonated version is formed in the same way each time. As such, the pH change approach is fully reproducible, while the heat-cool method remains irreproducible until a means of reliably forming the compound in the desired sold polymorph is found.

4.3.2. Preparation and T_{gel} studies of hydrogels of DBS-peptide LMWGs

4.3.2.1. DBS-Gly

Gels of DBS-Gly were prepared by first weighing a known amount of the gelator into a 2.5 ml glass sample vial; 1 ml of H_2O was then added and the tube was sealed. One of two methods could then be used to induce gelation. The first was a heat-cool method, in which the sample was heated to 95°C in a thermoregulated oil bath to fully dissolve the LMWG, then cooled to room temperature to induce self-assembly, after which an optically transparent gel was formed (Figure 4.2a).

The second method used a pH change, where the LMWG was dissolved by addition of 10 µl aliquots of NaOH$_{(aq)}$ (0.5 M), followed by addition of GdL ($\geq$ 10 mg); the sample was then left overnight to allow for GdL hydrolysis to slowly acidify the solution, leading to homogeneous gel formation. For those gels made by the pH change method, a translucent gel was produced (Figure 4.2b) – this difference in gel transparency indicates that there may be some difference in the resultant fibre morphology from each method. The samples were deemed to be gels if they survived for longer than 1 minute upon tube inversion.
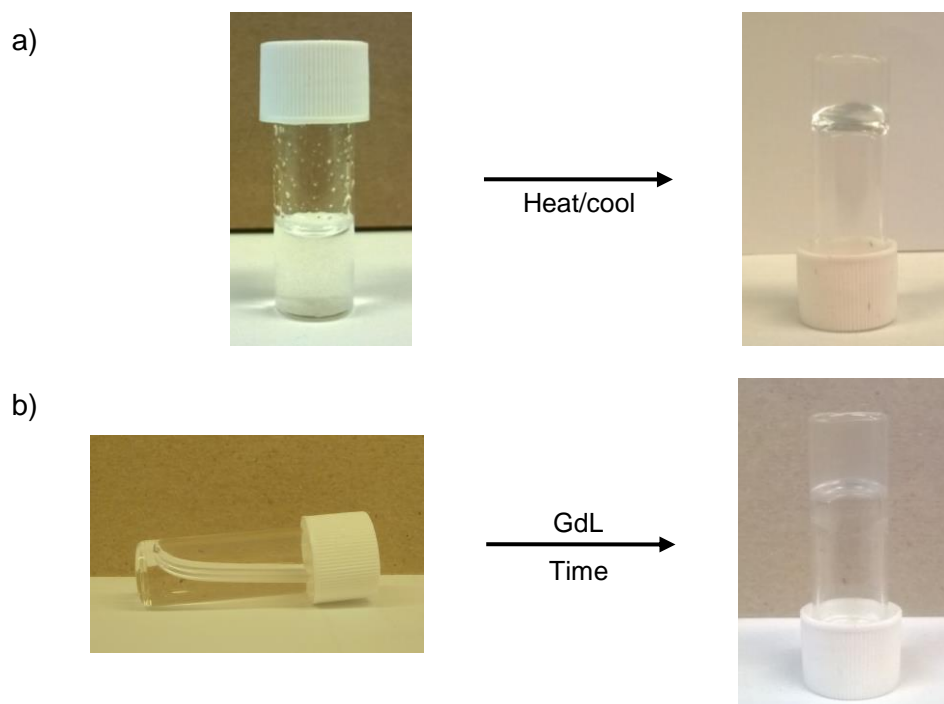
Figure 4.2: a) Formation of DBS-Gly hydrogel by heat-cool method from cold suspension of the solid LMWG; heating to 95°C followed by cooling to room temperature results in a transparent gel; b) formation of DBS-Gly hydrogel by pH change; clear, basic solution changes to translucent gel with decrease in pH over time, brought about by hydrolysis of GdL.

For the heat-cool method of preparation, the minimum gelator concentration (MGC) was found to be 0.07% wt/vol, whilst for the pH change method of preparation, the MGC was found to be 0.45% wt/vol. It was unclear at this point why there is such a significant difference, though it should be noted that for the pH change method, lower gelator concentrations did produce a gel, albeit one which was very inhomogeneous and unable to fully gelate all the solvent. It is possible that the presence of the by-product of GdL hydrolysis may slightly inhibit gelation.

For the gel produced by the pH change method, the decrease in pH over time after the addition of GdL was monitored. To achieve this, 1 mL H$_2$O was added to 4.5 mg of DBS-Gly in a 2.5 mL sample vial. The vial was then sonicated to disperse the solid, and 10 µL aliquots of 0.5 M NaOH$_{(aq)}$ were added to dissolve. The pH was then recorded with a pH meter, with the recorded value being referred to as pH at 0 minutes. 10 mg of GdL was then added, followed by shaking to

dissolve, and the pH was recorded again (pH at 1 min). Further pH readings were then taken at 30 minute intervals, up to 6 hours, with a final reading taken after 24 hours. The results in Figure 4.3 show a rapid drop in pH from *ca*. 10.5 to *ca*. 6.8 immediately after addition of GdL, suggesting rapid conversion of GdL to gluconic acid by excess NaOH present. The change in pH is then slower as the GdL is slowly hydrolysed to gluconic acid, which then protonates the DBS-Gly.
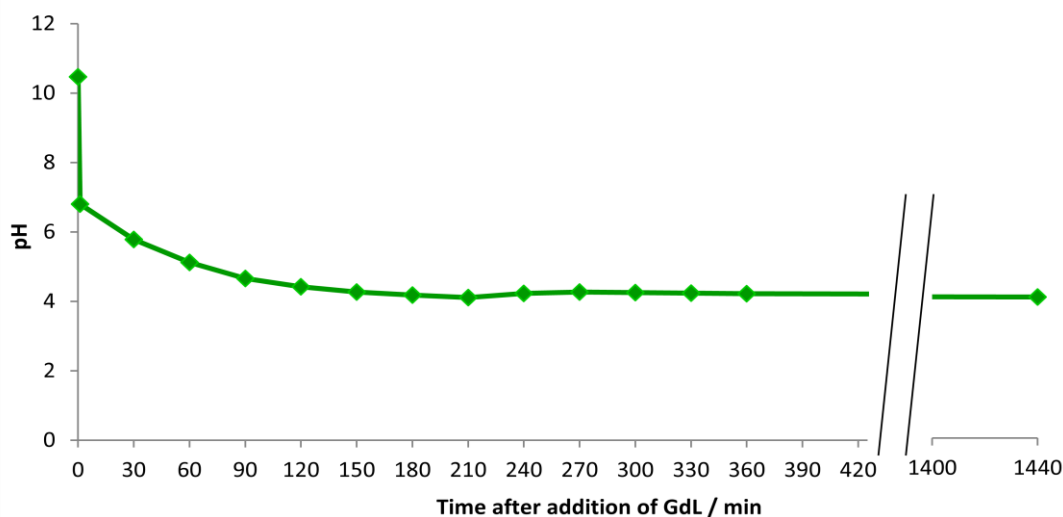
Figure 4.3: pH change over time after addition of GdL (10 mg mL^{-1}) for a DBS-Gly (0.45% wt/vol) gel system.

The thermal stability of the gels prepared by the heat-cool method was assessed by determining their T_{gel} values by tube inversion methodology.[154] The gel samples were placed in a thermoregulated oil bath, which was heated from 20°C at a rate of 1°C min^{-1}. A phase diagram was plotted showing the T_{gel} values as a function of concentration of DBS-Gly (Figure 4.4). The T_{gel} value increased with concentration, up to 0.12% wt/vol, where it plateaued at *ca*. 86°C. This means that at concentrations above 0.12% wt/vol network formation was complete, and adding more gelator did not increase the thermal stability of the gel.

The thermal stability of the gels prepared by the pH change method was also investigated; in these cases, varying the concentration of LMWG from 0.45% wt/vol to 0.7% wt/vol with 10 mg mL^{-1} GdL; in all the cases, the T_{gel} values were >100°C, indicating complete network formation.

121
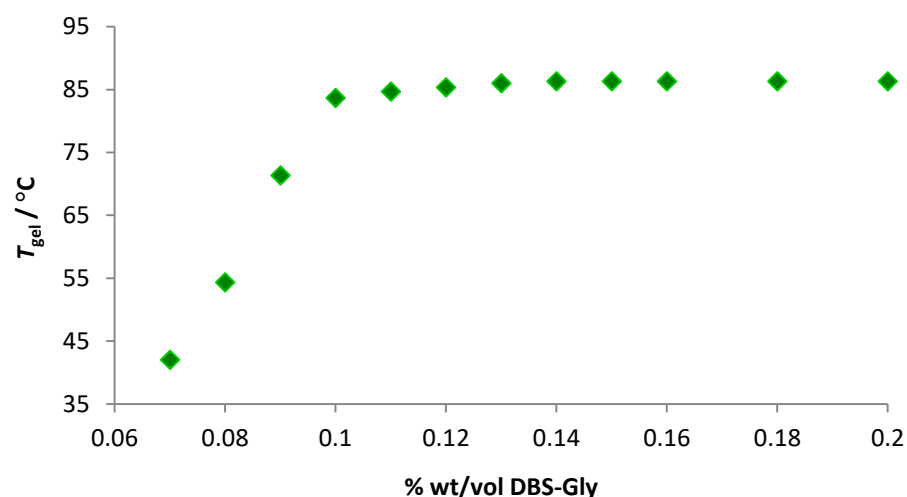
Figure 4.4: Plot of T_{gel} values for DBS-Gly gels made by heat-cool method as a function of % wt/vol of the LMWG.

4.3.2.2. DBS-Phe and DBS-Trp

The same procedures (heat-cool and pH change) used for forming gels of DBS-Gly were also applied to both DBS-Phe and DBS-Trp, with amounts of the compounds ranging from 0.05 to 1.0% wt/vol. However, no gels were produced by either method for either compound – instead, precipitates were observed.

To explain this, it is necessary to consider the interactions that drive the LMWG network formation for DBS-Gly: in addition to the π-π stacking, H-bonding and general hydrophobicity[146] that drives the formation of DBS-CO$_2$H networks, the addition of the peptide groups introduces the possibility of additional hydrogen bonding between amide groups or solvent (hydrophilic peripheries). For DBS-Phe and DBS-Trp, the presence of phenyl and indole groups respectively may mean that the peripheries become just a little too hydrophobic, counteracting the effects of the amide or carboxylic acid groups, and hence the solubility of these compounds is just too low for the possibility of self-assembly and gelation to occur.

4.3.3. ^{1}H NMR studies of hydrogels of DBS-Gly

4.3.3.1. Heat-cool method

Hydrogel samples of 0.1 % wt/vol DBS-Gly (1.78 mM) in D$_2$O, containing 0.2% wt/vol DMSO as a reference, were prepared by the heat-cool method; *ca.* 0.7 ml of the hot solution was transferred to NMR tubes and allowed to cool to a gel. A ^{1}H NMR of the gel after cooling revealed that *ca.* 92 % (1.64 mM) of the gelator was incorporated into the solid-like gelator network; the remaining 8% was mobile and therefore visible by NMR. It cannot be ruled out that this 8% is in fast equilibrium with the gel fibres and hence observable by NMR.

VT-NMR studies of DBS-Gly, where the sample was heated from 25 to 75°C, revealed an exponential increase in peak intensity, and therefore an exponential increase in the concentration of mobile DBS-Gly (Figure 4.5). This again shows that hydrogels of DBS-Gly are a highly temperature responsive system. Interestingly, if the T_{gel} value for a 0.1% wt/vol gel, ~86°C, is inserted into the equation of the exponential curve (concentration of mobile DBS-Gly = $0.0806e^{0.022T}$), the concentration of mobile DBS-Gly is ~0.53 mM – meaning that ~1.25 mM is still immobilised in the gel network, which interestingly is equivalent to 0.07% wt/vol – the MGC for DBS-Gly gels when prepared by the heat-cool method. This equation can also be used to calculate the theoretical temperature at which the gelator becomes completely solvated again ($T_{100\%}$); for a DBS-Gly gel of 0.1% wt/vol, this is calculated to be *ca.* 140°C – though obviously this is above the boiling point of the solvent.
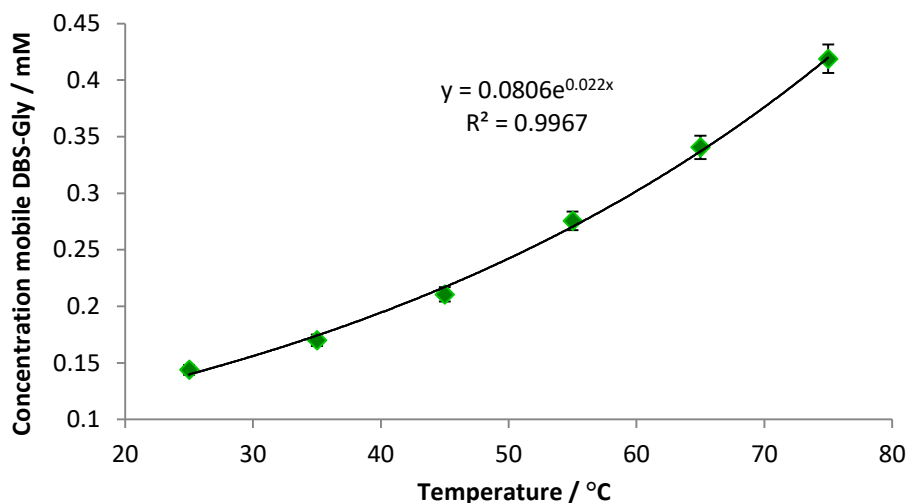
Figure 4.5: Plot of concentration of mobile DBS-Gly vs. Temperature, as determined by VT NMR for a gel produced by heat-cool method.

The thermodynamic parameters associated with the gel−sol transition, ΔH_{diss}, and ΔS_{diss} values could also be found using the van't Hoff method, which treats the dissolution of gel fibres in the same way as the dissolution of a crystalline solid, according to Eq. 7:[158]

$$\ln[sol] = -\frac{\Delta H_{diss}}{RT} + \frac{\Delta S_{diss}}{R} \qquad \text{Eq. 7}$$

When ln[sol] is plotted against 1/T, the gradient of the plot is equal to $-\Delta H_{diss}/R$ and the intercept equal to $\Delta S_{diss}/R$. For a DBS-Gly gel of 0.1% wt/vol, ΔH_{diss} = 18.9 kJ mol^{-1}, and ΔS_{diss} = 10.5 J K^{-1} mol^{-1}.

4.3.3.2. pH change method

Hydrogel samples of 0.45 % wt/vol DBS-Gly (8.03 mM) in D_2O, containing 0.2% wt/vol DMSO as a reference, were prepared by the pH change method, with 10 mg mL^{-1} GdL; *ca.* 0.7 ml of the solution was transferred to an NMR tube. ^1H NMR spectra of the gel were recorded immediately after addition of the solution to the NMR tube, then again after *ca.* 16 hours of gelation (Figure 4.6). The spectra revealed that *ca.* 95% of DBS-Gly was incorporated into a solid-like network.
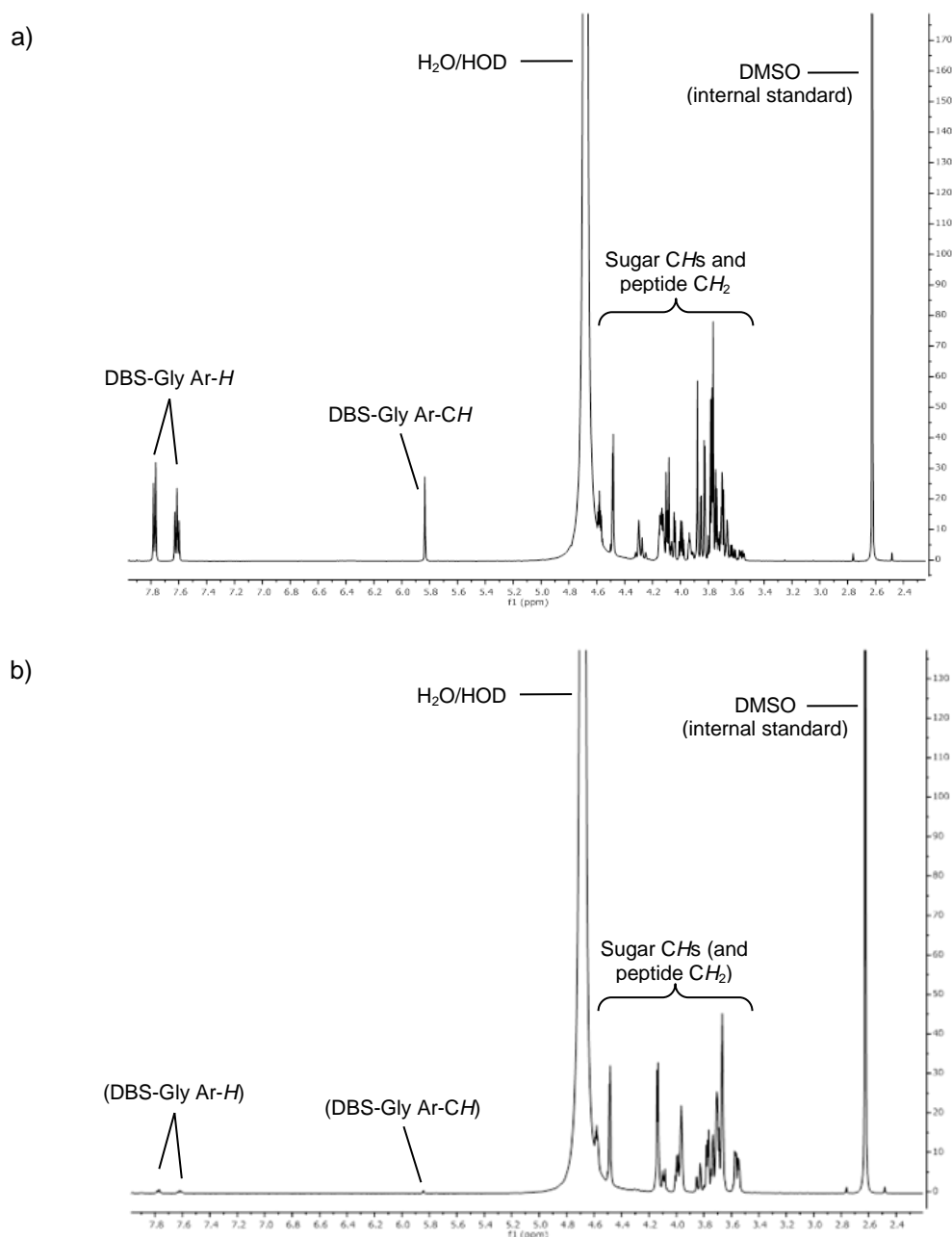
Figure 4.6: ^1H **NMR spectra (500 MHz, D_2O) of DBS-Gly gel (0.45% wt/vol) made by pH change method at (a) start of gelation and (b) end of gelation; the near absence of signals related to DBS-Gly in (b) indicates that most of the LMWG has been incorporated into a sample-spanning solid-like network.**

124

More detailed information on the kinetics of gelation was obtained by monitoring the evolution of the NMR spectrum over time after the addition of GdL. This was achieved by preparing a sample of DBS-Gly by the method describe above, and recording NMR spectra every 30 minutes for 14 hours. By determining the concentration of mobile DBS-Gly from the spectra, the rate of formation of the gelator network could be plotted (Figure 4.7). It is clear that there is some initial rapid assembly, as the concentration of mobile gelator drops from *ca*. 8 mM to *ca*. 7 mM in the first 30 minutes – this may be attributed to a "burst" release of protons as GdL is quickly converted to gluconic acid by residual NaOH (as seen with the pH monitoring study in Figure 4.3). There is then a period of buffering as the pH gradually lowers towards the pK_a value of DBS-Gly; once this value is reached, there is then gradual assembly of the LMWG network over the course of several hours.
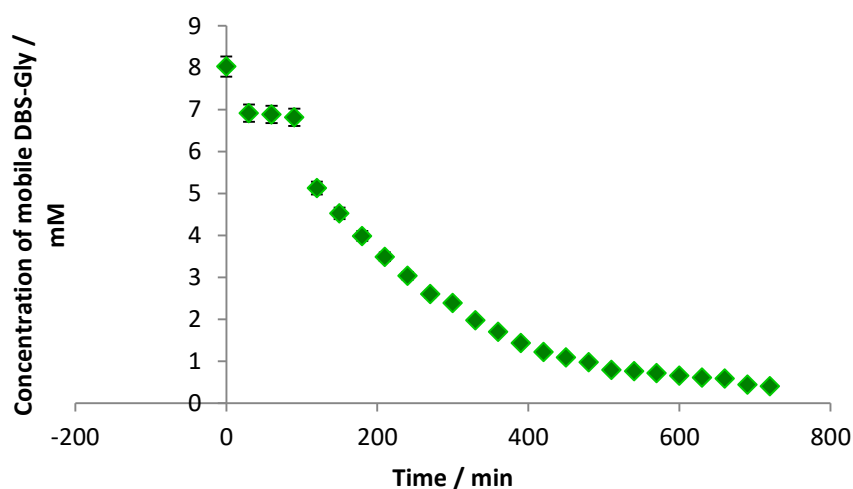
Figure 4.7: Plot of average rate of formation of a DBS-Gly network by pH change method.

The kinetic data were then fitted to Avrami's kinetic model[160–163] (Figure 4.8); see section 2.4.2 for comments on the use of the Avrami model with pH-responsive LMWGs. For DBS-Gly, the value of the Avrami exponent, n, was found to be 1.06. This value is significantly less than for that of DBS-CO$_2$H (n=1.61), and indicates that DBS-Gly forms more 1D, unbranched fibres by this gelation method, compared to the more 2D, branched fibres of DBS-CO$_2$H. This might reflect a greater solubility of DBS-Gly and hence less tendency of the fibrils formed to aggregate laterally.

The chart shows data points with a linear fit:

$$y = 1.0648x - 5.8632$$
$$R^2 = 0.991$$

X-axis: ln (t)

Y-axis: ln{-ln[([DBS-Gly][∞]-[DBS-Gly](t))/([DBS-Gly][∞]-[DBS-Gly](0))]}
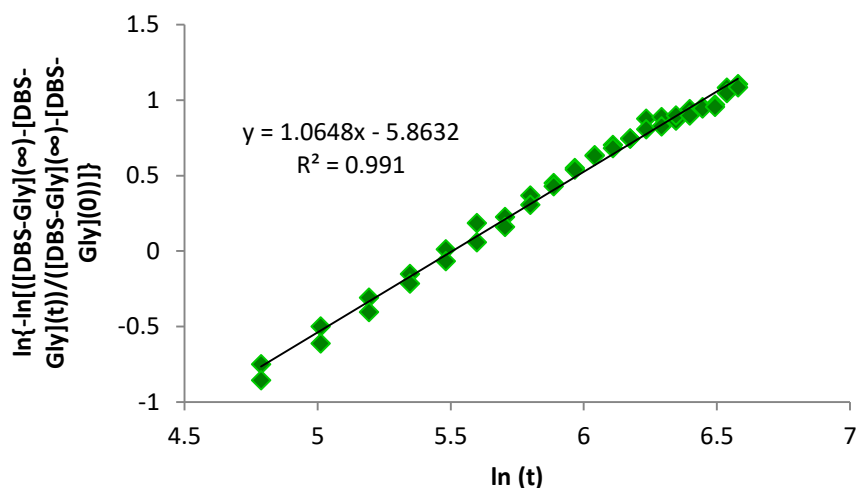
Figure 4.8: Avrami plot for formation of DBS-Gly network; n = gradient of line = 1.06.

4.3.4. CD and VT CD studies of hydrogels of DBS-Gly

4.3.4.1. Heat-cool method

CD spectroscopy was used to probe the nanoscale organisation of DBS-Gly gels prepared by the heat-cool method. CD spectra were collected for 0.01% wt/vol and 0.05% wt/vol samples (Figure 4.9a); the experiment was performed below the gelation threshold, where the formation of nanoscale fibres but not a full sample network can be observed. Preparation of the samples was the same as for gels in all other respects. Spectra could only be recorded above 210 nm, as below this wavelength the detector became saturated.

Interestingly, the two samples had different CD spectra; 0.01% wt/vol showed a positive signal, whilst 0.05% wt/vol showed a negative signal. The likely explanation for this difference is that at the lower concentration, there is simply not enough gelator present for fibre formation to take place, and what is being observed in the spectra is the signal for individual molecules of DBS-Gly. With an increase in concentration, fibre formation takes place and brings about the change in CD signal. Whilst the HT data (Figure 4.9b) shows some significant difference between the samples (values of HT are greater for 0.05% wt/vol), this is likely due to there being more absorbance with more LMWG present in the sample.
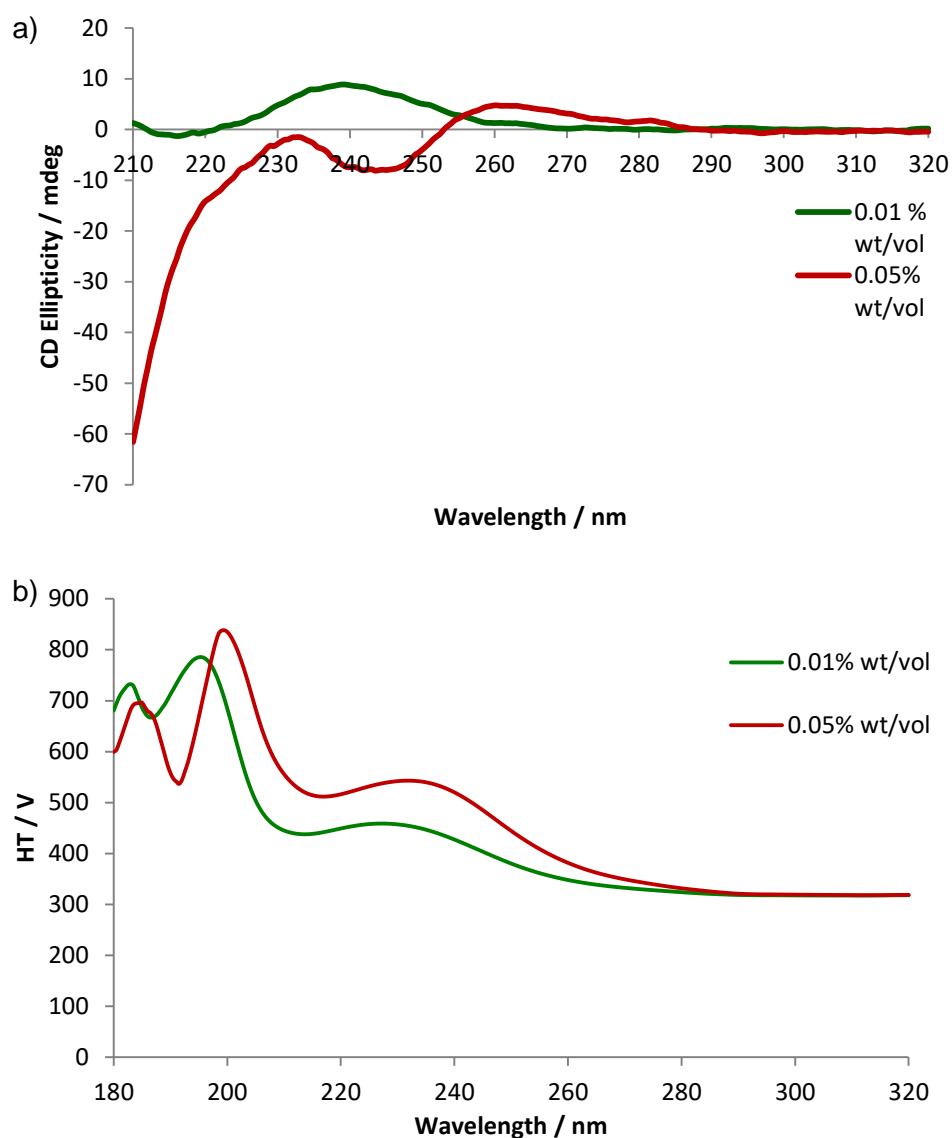
Figure 4.9: a) CD spectra of DBS-Gly (heat-cool method) at 0.01% wt/vol (green) and 0.05% wt/vol (red); b) HT data.

Importantly, VT-CD agrees with this hypothesis. When the 0.05% wt/vol sample was heated, the intensity of CD band decreased in negativity with increasing temperature (Figure 4.10), gradually changing from a negative signal to a positive signal, indicating the CD signal does correspond to a temperature-responsive self-assembled system. The signal continues to increase even up to 90°C, indicating that the nanoscale fibres are still disassembling, increasing the ratio of individual gelator molecules to gelator molecules in fibres.
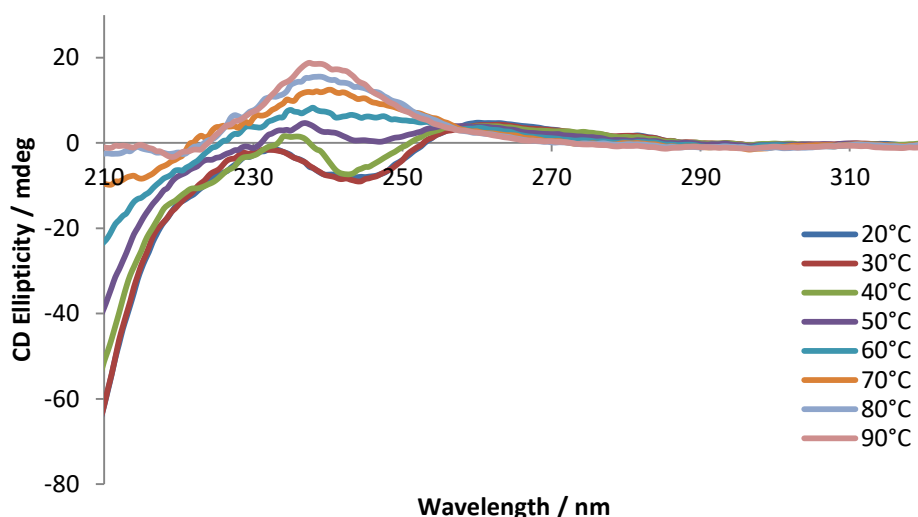
Figure 4.10: VT CD spectra for DBS-Gly (heat-cool method, 0.05% wt/vol) over temperature range 20-90°C.

4.3.4.2. pH change method

For pH change gels, the presence of GdL masked any other CD signals present – hence for these samples CD studies were not possible.

4.3.5. SEM imaging of hydrogels of DBS-Gly

Samples of DBS-Gly gels were prepared for SEM by removing a small portion of the prepared gel with a spatula and placing it on a copper support, followed by freeze-drying by immersion in liquid nitrogen and then lyophilising overnight. Excess solid material was broken off with a spatula and then the sample was sputter coated with a thin layer (about 12 nm) of gold/palladium to prevent sample charging, before placing the sample on a metal SEM stub and imaging (see 2.4.4 for a discussion on the limitations on the information that can be obtained from freeze-drying samples for SEM).

4.3.5.1. Heat-cool method

For xerogels of DBS-Gly prepared by the heat-cool method, reasonably flexible, thin fibres were observed (Figure 4.11) – presumably the thinness of the fibres being linked to the optically transparent nature of the gel.
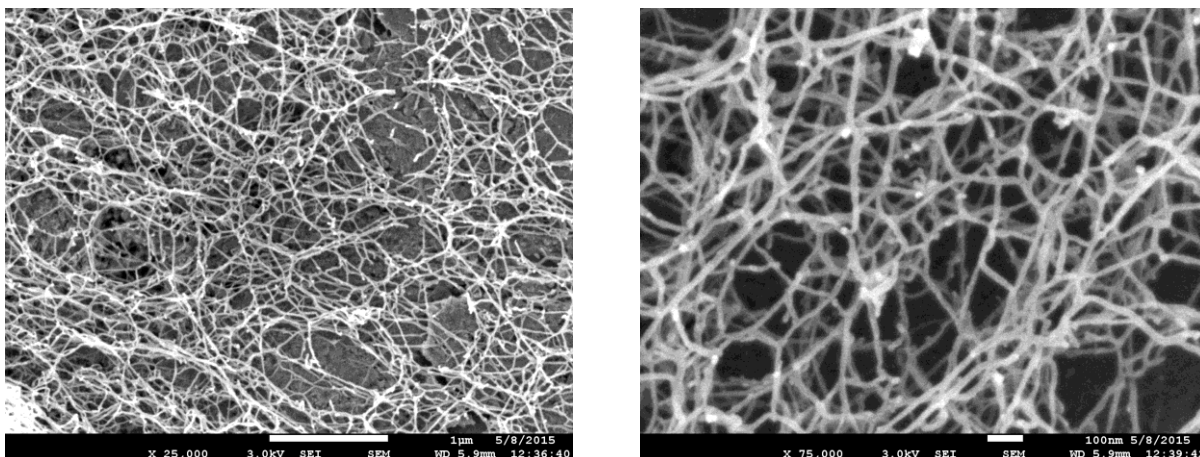
Figure 4.11: SEM images of DBS-Gly hydrogels, 0.1% wt/vol, prepared by heat/cool method. Left: 25000× magnification, scale bar = 1 µm; right: 75000× magnification, scale bar = 100 nm.

4.3.5.2. 3.6.2. pH switch

For xerogels of DBS-Gly prepared by the pH-switch method, the fibres observed by SEM appear to be thicker than those prepared by the heat-cool method – though this may be due to a higher % wt/vol being required (Figure 4.12) (and again the limitations of the freeze drying method make direct comparisons of fibre diameter difficult). There also seems to be less branching in the fibres themselves (compared to DBS-CO$_2$H, Figure 2.10 in Chapter 2), in keeping with the Avrami constant of n = 1.06.
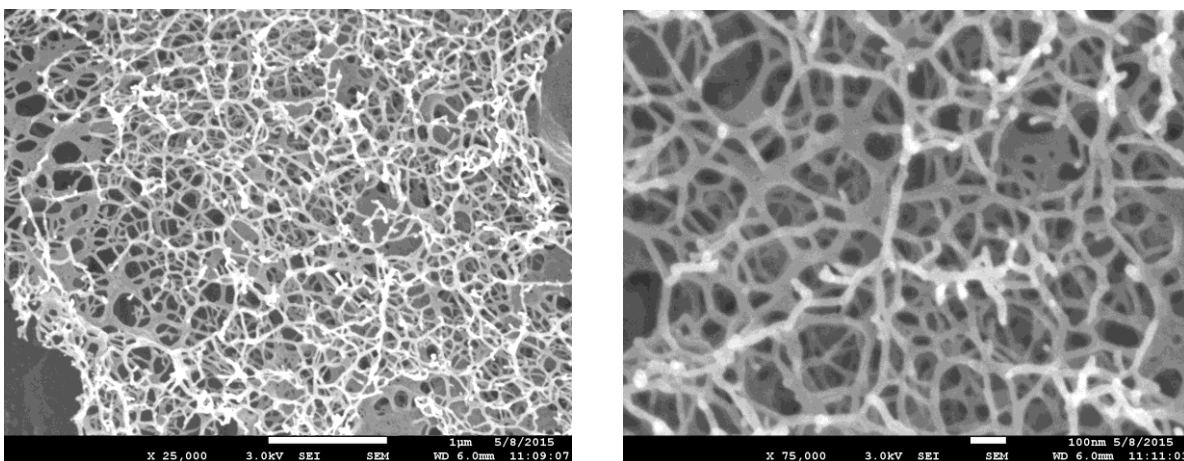
Figure 4.12: SEM images of DBS-Gly hydrogels, 0.45% wt/vol, prepared by pH change method. Left: 25000× magnification, scale bar = 1 µm; right: 75000× magnification, scale bar = 100 nm.

4.4. Multi-component self-assembly and self-sorting

As DBS-Gly functioned well as a pH-change activated LMWG, this opened up the possibility of combing DBS-Gly with DBS-CO$_2$H to produce a multi-component gel.[13,249] As both LMWGs required acidification to form their networks, instead of orthogonal stimuli, this meant that a combination of the two would either lead to self-sorting, or co-assembly. The work of Adams and

co-workers had shown that with two pH-responsive LMWGs, if the difference in pK_a values was significant enough, then self-sorting could occur.[29]

4.4.1. Determination of pK_a values for DBS-Gly and DBS-CO$_2$H

The pK_a values for both gelators were determined by titration against HCl. To achieve this, a stock solution of each gelator at 0.2% wt/vol was prepared, using the minimum amount of NaOH$_{(aq)}$ (0.5 M) to dissolve the solid. 5 mL of these solutions were used for each titration. To these solutions, aliquots of HCl (0.1 M) were added, in 15 µL volumes for DBS-Gly and 20 µL volumes for DBS-CO$_2$H – the different volumes were used due to the different concentrations of LMWGs. The pH values were recorded from a pH meter once the readings had stabilised after *ca.* 10 minutes. By plotting titration curves (Figure 4.13), the pK_a values could be extrapolated. It should be noted that the self-assembly of the LWMGs into gel nanofibres around their pK_a values mean those values could only be estimated.[250]
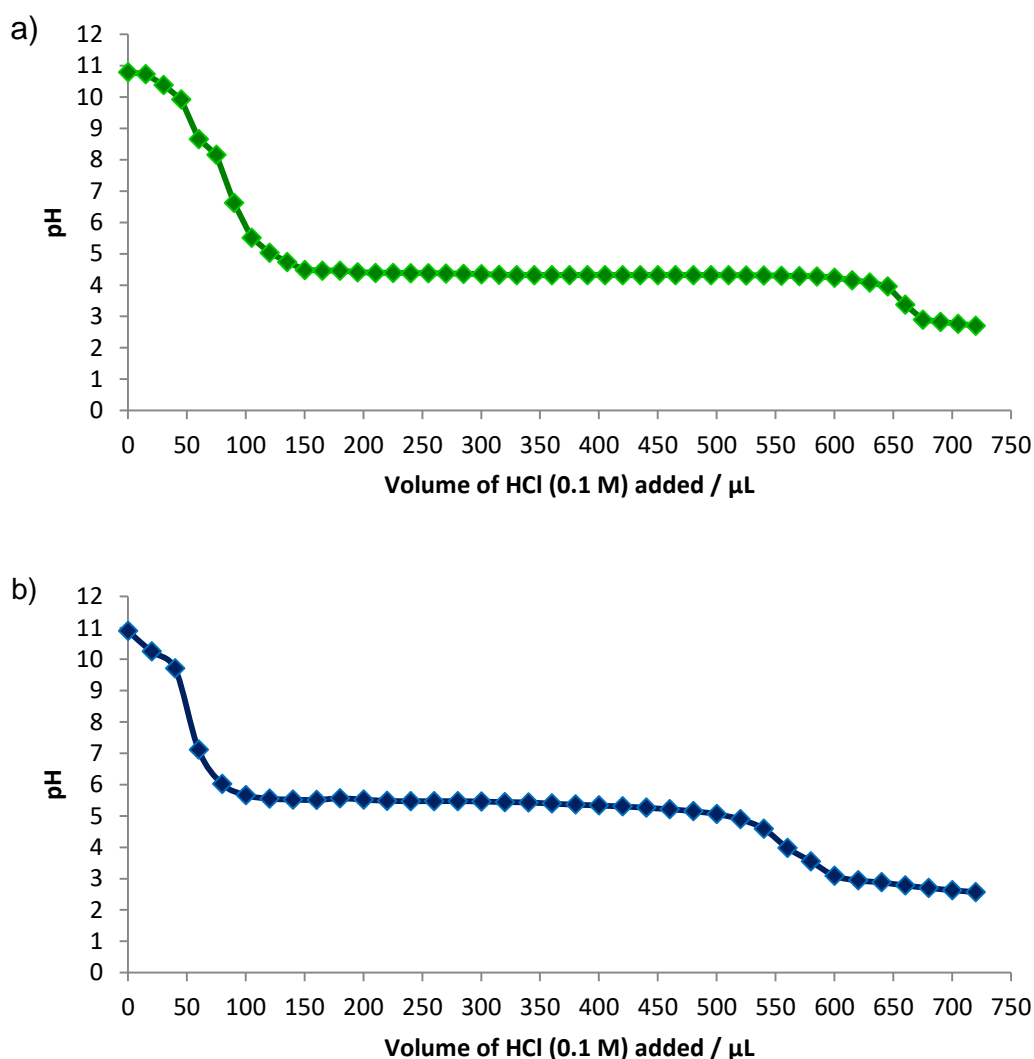
Figure 4.13: Titration curves for a) DBS-Gly, and b) DBS-CO$_2$H

From the titration curves, the pK_a for DBS-Gly was estimated to be *ca.* 4.3, whilst for DBS-CO$_2$H, the pK_a was estimated to be *ca.* 5.4. Explaining this significant difference in terms of the structural difference between the two gelators is challenging, especially as the apparent pK_a values of LMWGs can be affected by the self-assembly step, which perturbs the proton equilibrium, causing the pK_a to differ from what would be expected from small molecule analogues.[251–255] Additionally, it might be expected that each LMWG would have two distinct pK_a values, given that they both have two acids; however, as the acids are relatively distant from each other, and the ten-membered ring structure at the core of the gelator is relatively rigid, there is no conjugation between the acid groups, and as such only one apparent pK_a is observed.

4.4.2. Table-top studies of multi-component hydrogels of DBS-Gly and DBS-CO$_2$H

Because of the significant difference in pK_a values, it was reasoned that kinetically controlled self-sorting[29] of DBS-Gly and DBS-CO$_2$H may occur. To investigate this further, a gel containing both gelators was prepared by adding 1 mL H$_2$O to DBS-Gly (4.5 mg, 0.45% wt/vol) and DBS-CO$_2$H (4.5 mg, 0.45% wt/vol) in a 2.5 ml sample vial. The vial was then sonicated to disperse the solid, and 10 µL aliquots of NaOH$_{(aq)}$ (0.5 M) were added to dissolve, bringing the pH to *ca.* 11. The solution was then transferred to a vial containing GdL (18 mg), and then left overnight for gelation to occur; the resulting gel was translucent in appearance (Figure 4.14), and had a T_{gel} value of >100°C, consistent with the appearance and T_{gel} values of its constituent components. Whilst this indicated that a combination of the two LWMGs could form a gel, it did not, however, give any indication as to whether self-sorting or co-assembly was occurring.
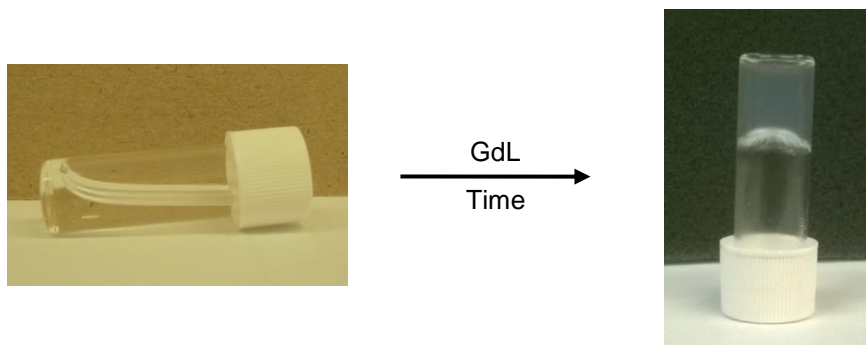
Figure 4.14: Formation of a multi-component hydrogel of DBS-Gly (0.45% wt/vol) and DBS-CO$_2$H (0.45% wt/vol); clear, basic solution (left) changes to translucent gel (right) with decrease in pH over time, brought about by hydrolysis of GdL.

4.4.3. NMR studies of multi-component hydrogels of DBS-Gly and DBS-CO$_2$H

To further investigate these multi-component gels, a series of NMR studies were carried out. These involved preparing solutions with 0.45% wt/vol of both gelators, in D$_2$O with 2 µL DMSO per mL as an internal reference, and using the minimum amount of NaOH$_{(aq)}$ (0.5 M) to dissolve all components. To these solutions, GdL was added in varying amounts: a) 4 mg mL^{-1} (22.5 mM), b)

5.7 mg mL^{-1} (32.0 mM), and c) 14.3 mg mL^{-1} (80.3 mM). Each concentration of GdL was chosen to give a different ratio of GdL to gelator – it was theorised that at low concentrations of GdL, the protons released from hydrolysis to gluconic acid would favourably reprotonate DBS-CO$_2$H first, as it has the higher pK_a value. The solutions were transferred to NMR tubes, and spectra were recorded every 30 minutes for 14 hours. The concentration of the mobile gelators could then be determined from the spectra, and from this the % of gelator assembled into a network could be inferred (Figure 4.15).
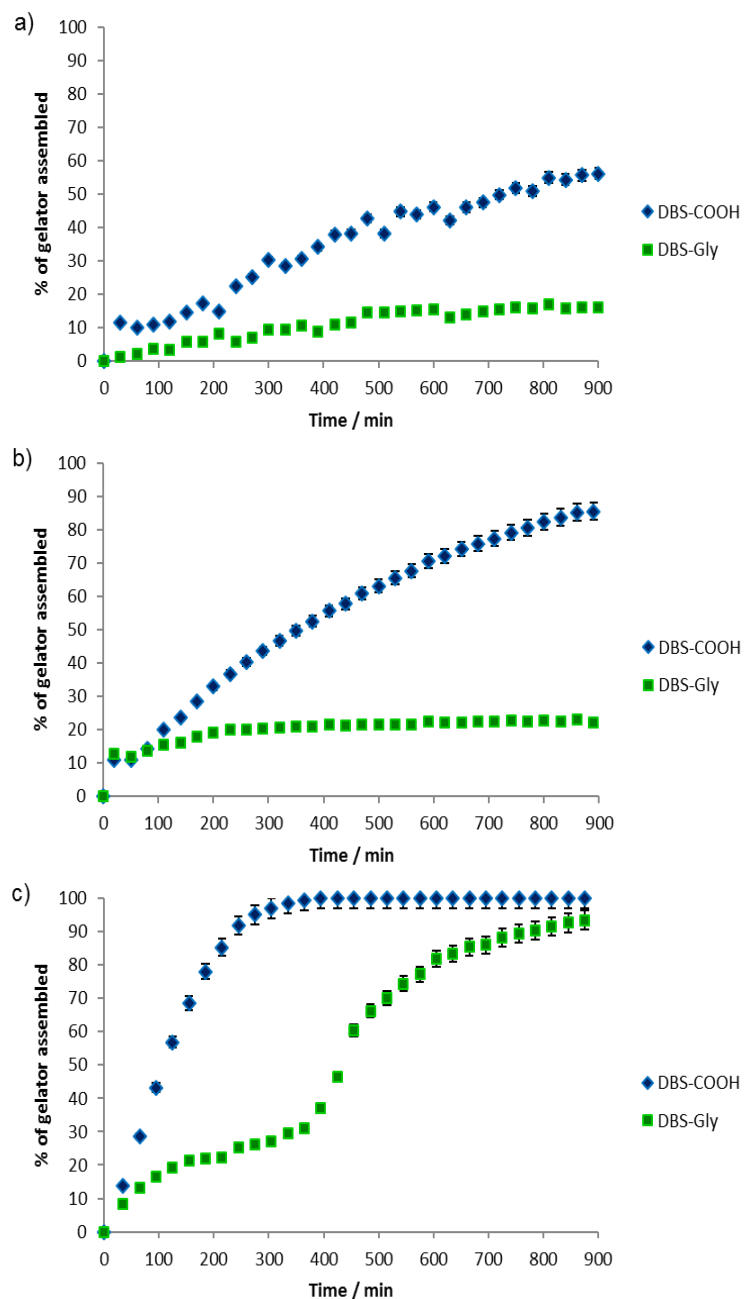
Figure 4.15: % of gelator assembled into a solid-like network for multi-component systems of DBS-Gly (8.03 mM) and DBS-CO$_2$H (10.08 mM) with a) 22.5 mM, b) 32.0 mM, and c) 80.3 mM GdL.

Figure 4.15 clearly shows that with an increasing the amount of GdL, an increased percentage of the two gelators was assembled. Assembly of DBS-CO$_2$H is initially favoured, particularly at low concentrations of GdL (Figure 4.15a). With more GdL, after an extended period of time, *ca.* 90% of DBS-CO$_2$H has assembled, but only *ca.* 20% of DBS-Gly is in the solid-like state (Figure 4.15b). It should be noted that there is an initial rapid assembly of both gelators, possibly attributed to the 'burst' release of protons from hydrolysis of GdL by residual excess NaOH. When using a large excess of GdL (Figure 4.15c), continuous gradual assembly of DBS-CO$_2$H was observed up to *ca.* 300 minutes, at which point 100% of the gelator was incorporated into the solid-like network. Up to this point, only *ca.* 20% of DBS-Gly had been immobilized. After this point, at *ca.* 400 minutes, the DBS-Gly, which prior to this point had a much slower rate of assembly, began to rapidly assemble. This is presumably as the pH drops to the pK_a value of DBS-Gly and triggers self-assembly. By the end of the experiment, over 90% of DBS-Gly had also been immobilized.

It can be clearly concluded that there is a good degree of stepwise kinetic control over the assembly when the pH is slowly lowered, with DBS-CO$_2$H primarily assembling first, and only a small amount (*ca.* 20%) of DBS-Gly assembly concurrent with that of DBS-CO$_2$H. It is not easily possible to say whether these small amounts of DBS-Gly start to form their own assemblies or co-assemble into the DBS-CO$_2$H nanofibres, followed by separate DBS-Gly nanofibres. Nonetheless, these experiments provide strong evidence that these two gelators can, to a large extent, kinetically self-sort, one followed by the other, rather than concurrently co-assembling into mixed fibres.

4.4.4. CD studies of multi-component hydrogels of DBS-Gly and DBS-CO$_2$H

The samples of multi-component systems prepared for CD were made using sub-gelation amounts of the gelators, in this case 0.045% wt/vol of each, and therefore (as in Chapters 2 and 3) what was observed was the assembly of organised nanofibres within the sample but not the formation of a full sample-spanning network. Samples of each individual gelator at 0.045% wt/vol were also prepared, and all three CD spectra are compared in Figure 4.16a. On standing a sample of DBS-CO$_2$H for five hours after the addition of GdL, the CD spectrum recorded for DBS- CO$_2$H showed that (as previously observed) the aromatic rings experienced a chiral microenvironment, as confirmed by the observation of a CD band with a maximum intensity of *ca.* -18 mdeg at 263 nm. The major peak at *ca.* 220 nm was assigned to the presence of GdL. As noted before, the presence of the GdL peak unfortunately masked any signals that might be present in the DBS-Gly sample. For the multi-component system, a peak was observed at *ca.* 260 nm, corresponding to the chiral microenvironment experienced by the aromatic rings of DBS-CO$_2$H, but with a significantly lower intensity of *ca.* -4 mdeg; this peak was also somewhat overlapped by the major peak corresponding to GdL. However, this lowering of intensity could have also been caused by overlap with a CD signal corresponding to DBS-Gly, which may lie somewhere in the region of 230-250 nm.

Alternatively, the observed differences may be due to differences in the HT values (Figure 4.16b), though these are not particularly significant in the region examined in the plots.
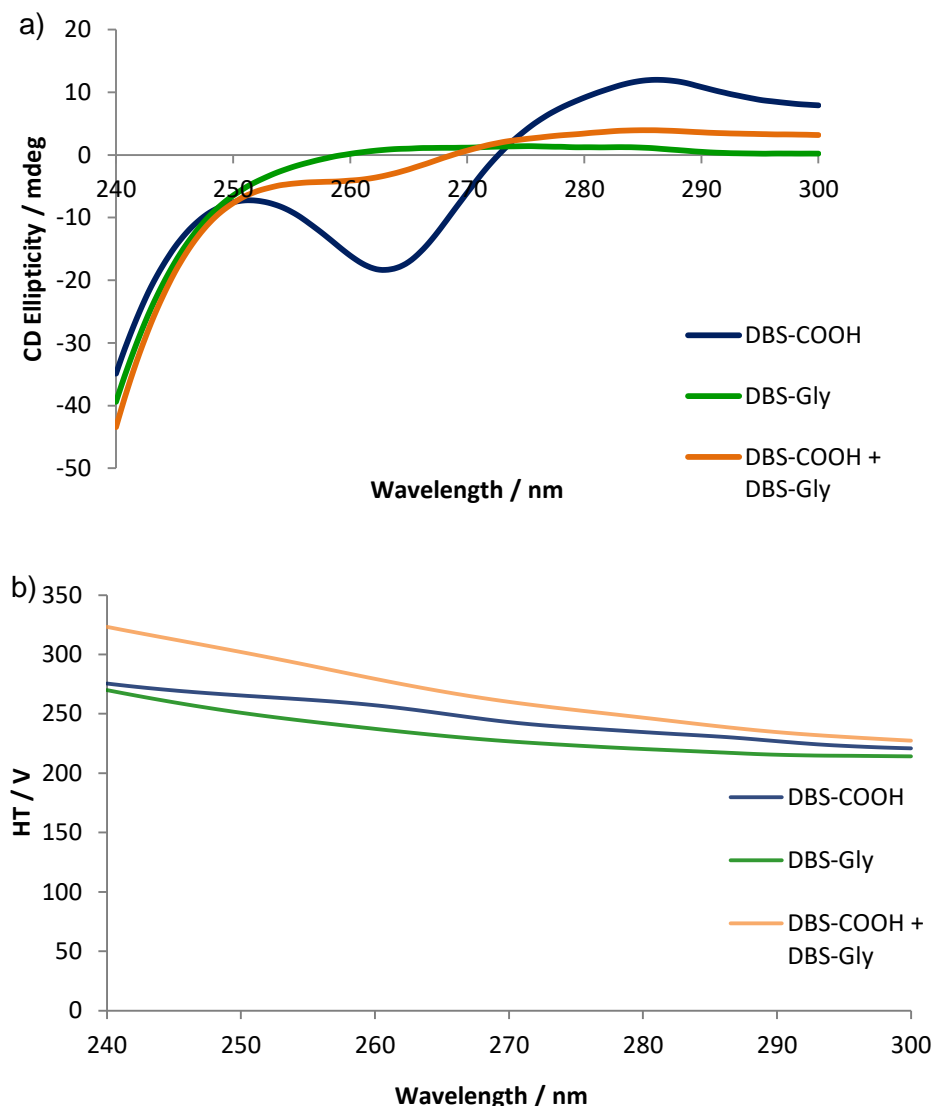
Figure 4.16: a) CD spectra of DBS-CO$_2$H (0.045% wt/vol) (blue), DBS-Gly (0.045% wt/vol) (green), and a multi-component mixture of DBS-CO$_2$H and DBS-Gly (0.045% wt/vol each) (orange), all using GdL (8 mg mL^{-1}) as the acidifying agent. The major band from gluconic acid can be seen to start to appear below 250 nm; b) HT data.

To circumvent the issue with the gluconic acid band, CD was used to investigate the nanofibres formed from DBS-CO$_2$H and DBS-Gly using HCl$_{(aq)}$ (final concentration 0.03 mM) as the acidifying agent (Figure 4.17). For DBS-CO$_2$H, a CD band with a maximum intensity of *ca.* -18 mdeg at 262 nm was observed, closely matching that seen when GdL was used. For DBS-Gly, a number of broader CD bands were seen, notably at 275 nm (*ca.* -3 mdeg) and 242 nm (*ca.* +3 mdeg) – neither of which were observed when using GdL, though the latter of these was similar to that seen when using the heat/cool method (Figure 4.9).
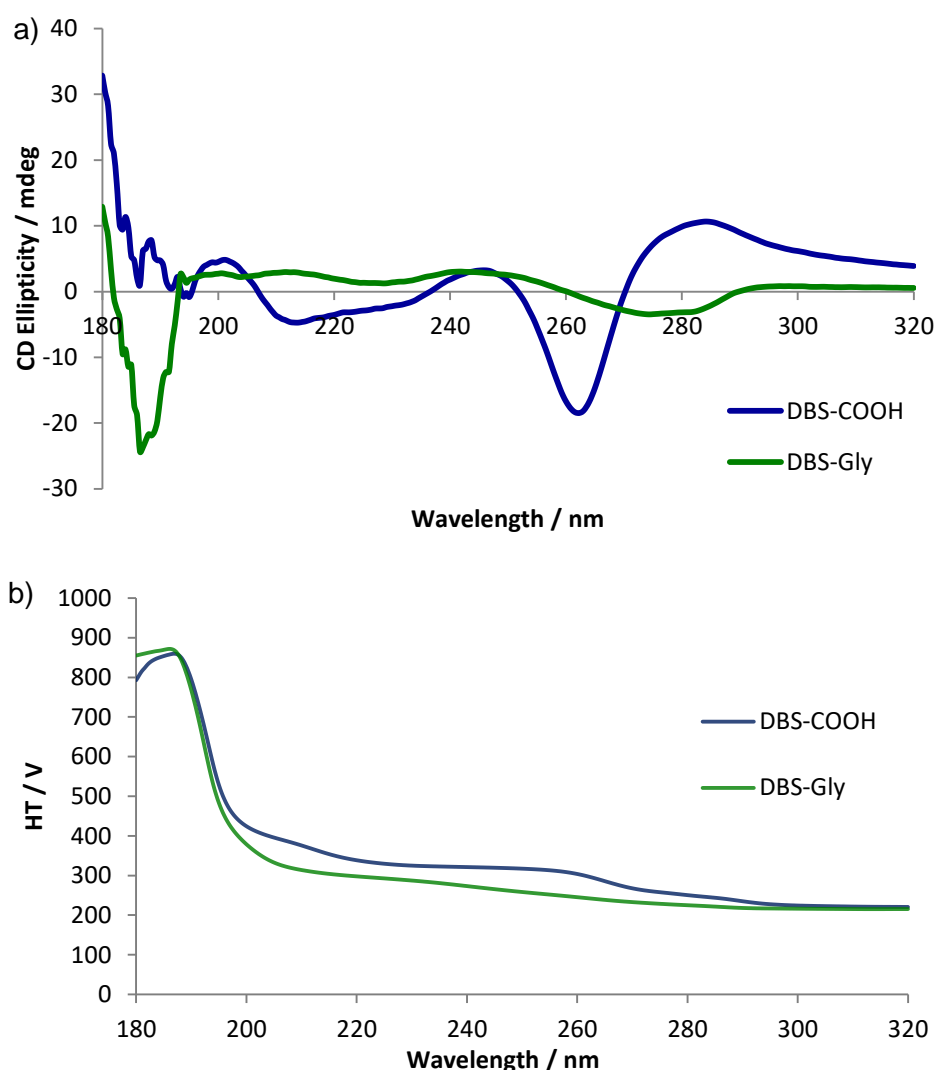
Figure 4.17: a) CD spectra of DBS-CO$_2$H (0.045% wt/vol) and DBS-Gly (0.045% wt/vol) using HCl (0.03 mM) as acidifying agent; a number of CD bands are now visible for DBS-Gly (notably at *ca*. 275 nm and 242 nm); b) HT data.

A CD spectrum of the multi-component system with HCl was also recorded, and compared to a calculated addition of the two separate CD spectra for DBS-CO$_2$H and DBS-Gly with HCl (Figure 4.18). The calculated spectrum showed two maximum absorbances – one at 262 nm (*ca*. -10 mdeg), corresponding to the absorbance from DBS-CO$_2$H, and another at 245 nm (*ca*. +3 mdeg), corresponding to the absorbance from DBS-Gly. The experimental spectrum resembled the overall shape of the calculated spectrum, but the values of λ_{max} and CD ellipticity were somewhat different. It is assumed that the maximum at 259 nm (*ca*. -16 mdeg) corresponds to DBS-CO$_2$H, whilst the maximum at 229 nm (*ca*. +5 mdeg) corresponds to DBS-Gly. Whilst the former value is not too dissimilar from the calculated values, suggesting that DBS-CO$_2$H still assembles into distinct nanofibres, the latter is significantly different – it may be the case that the self-assembled

135

nanofibres adopt slightly different structures when in the presence of another gelator. The HT data is similar for both the individual components (Figure 4.16b) and the multi-component system (Figure 4.17b), suggesting differences in HT are not the cause. These results do, however, explain the decrease in CD ellipticity observed for the DBS-CO$_2$H band in the multi-component system when GdL is used as the acidifier (Figure 4.16) – the DBS-Gly band's proximity causes a reduction in peak intensity. Whilst not as conclusive as the results from NMR studies, these results do somewhat support the likelihood of some self-sorting between the two LMWGs.
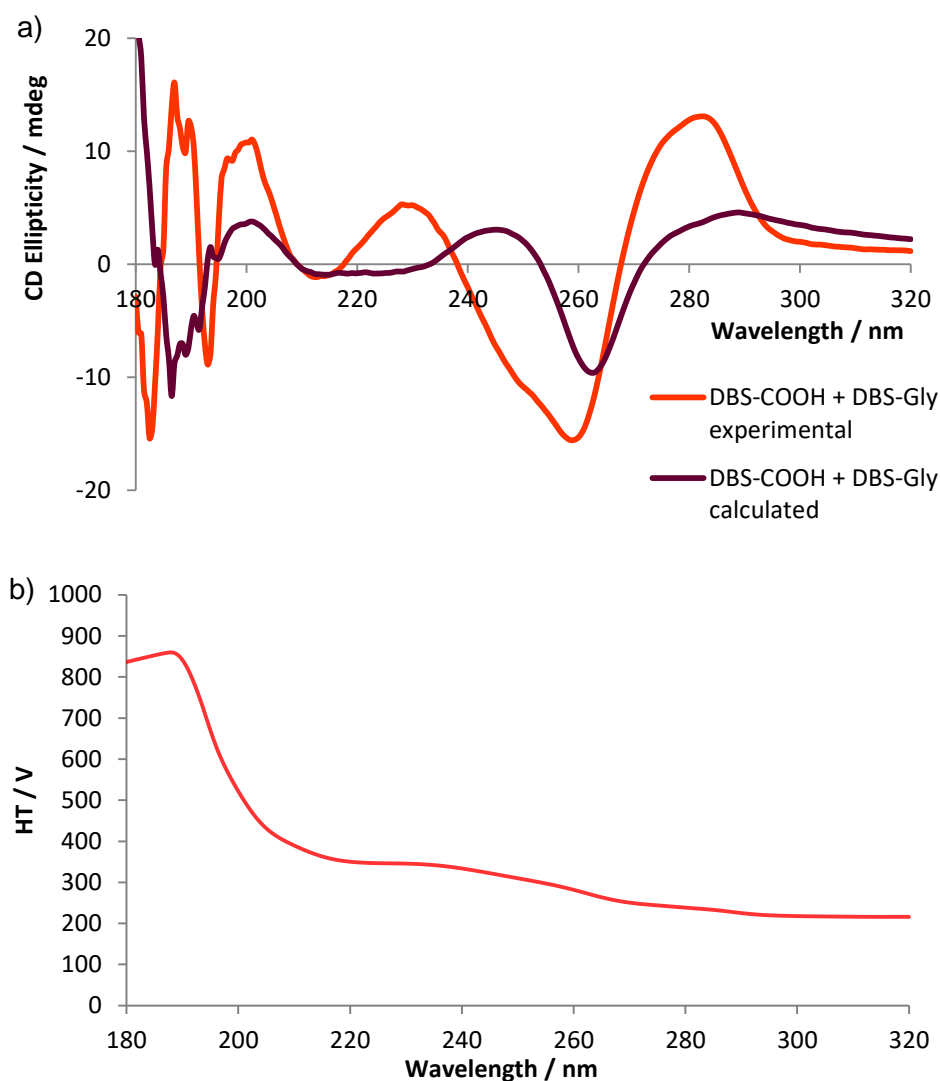
Figure 4.18: Calculated (purple) and experimental (orange) CD spectra for a multi-component mixture of DBS-CO$_2$H and DBS-Gly (0.045% wt/vol each), prepared using HCl (0.03 mM) as the acidifying agent; b) experimental HT data.

4.4.5. SEM imaging of multi-component hydrogels of DBS-Gly and DBS-CO$_2$H

The nanostructure of each of the constituent component gel and the multi-component gel were examined and compared using SEM. Samples were prepared by freeze-drying in liquid nitrogen, followed by lyophilising overnight (see 2.4.4 for a discussion on the limitations on the information

that can be obtained from freeze-drying samples for SEM). The nanofibres formed in each case were fairly similar, suggesting that the two gelators do not inhibit one another's self-assembly into nanofibres. However, self-sorting could not clearly be imaged due to the similarity of the two nanostructures.
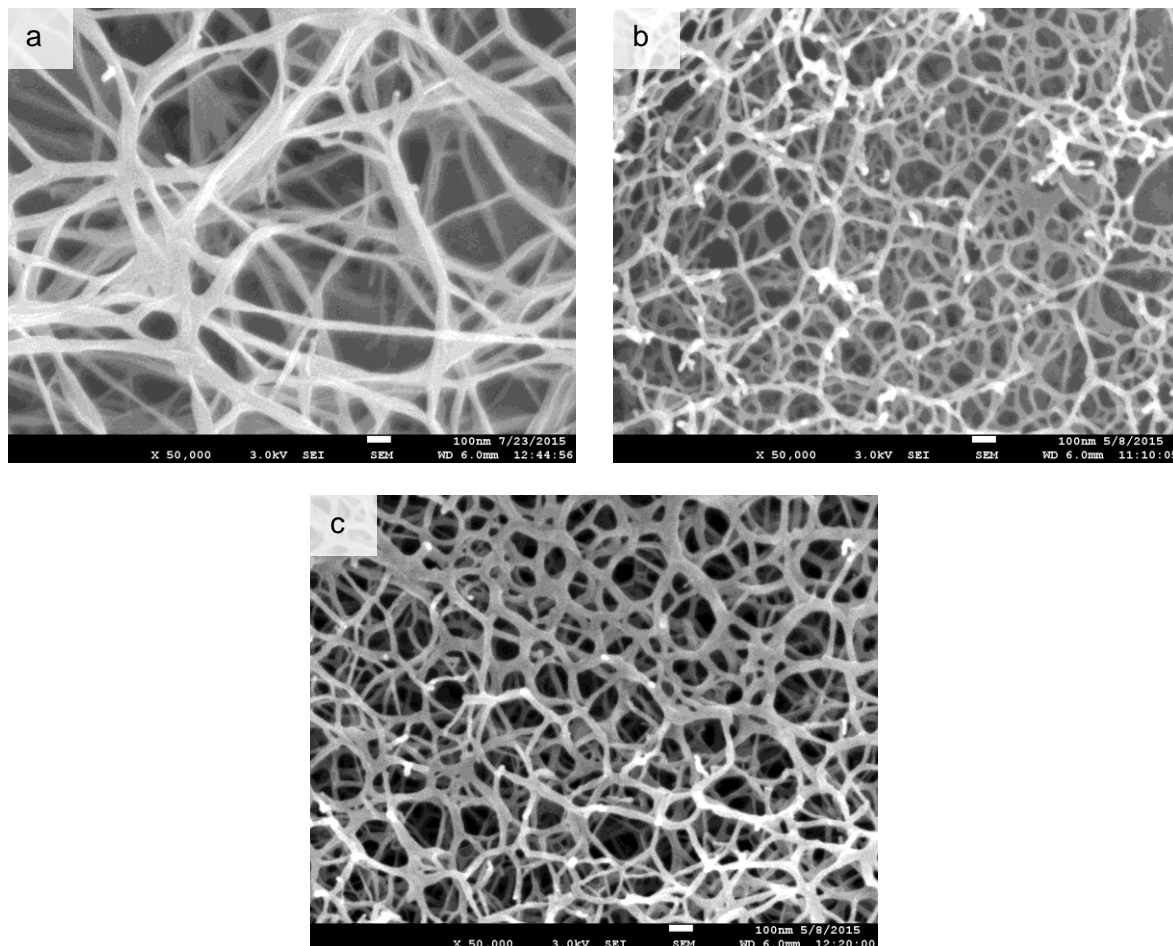
Figure 4.19: images of a) DBS-CO₂H (0.40% wt/vol); b) DBS-Gly (0.45% wt/vol); c) multi-component gel of DBS-CO₂H and DBS-Gly (0.45% wt/vol each). Scale bars = 100 nm.

4.4.6. Rheological studies of multi-component hydrogels of DBS-Gly and DBS-CO₂H

Rheology was used to compare the relative materials properties of the two individual gels to the multi-component gel. In all cases, gels were prepared by making the pre-gel solution using the standard method; gelation was then carried out directly on the lower plate of the rheometer, using a sealed bottomless glass vial as a mould to hold 500 µL of the solution. The solution was left overnight, after which gels *ca.* 1.5 mm thick had formed. As described in previous chapters, this method was necessary because the fragile gels could not be transferred by hand to the plate.

After sample loading, amplitude sweep analyses were carried out. These were performed at a frequency of 1 Hz, with shear strain amplitude increasing from 0.01% to 100%, though all of the runs were halted well before 100% shear strain was reached as the limit of the LVR had been

reached before this point. Typical results are shown in Figure 4.20; results from other runs were within ± 10% of the values presented here. In all cases, it can clearly be seen that the values of the storage modulus G' are significantly larger than those of the loss modulus G'', confirming that the materials are indeed gels in nature. Clearly the gel of DBS-CO$_2$H has a greater G' than DBS-Gly, and further, it maintains its gel properties to a higher shear strain (*ca.* 8% vs. *ca.* 2%). For the multi-component gel, somewhat surprising is that the values of G' and G'' sit in between those for the two individual gels, as does the limit of the LVR. As such it can be suggested that the multi-component gel has intermediate rheological behaviour between its constituent components.
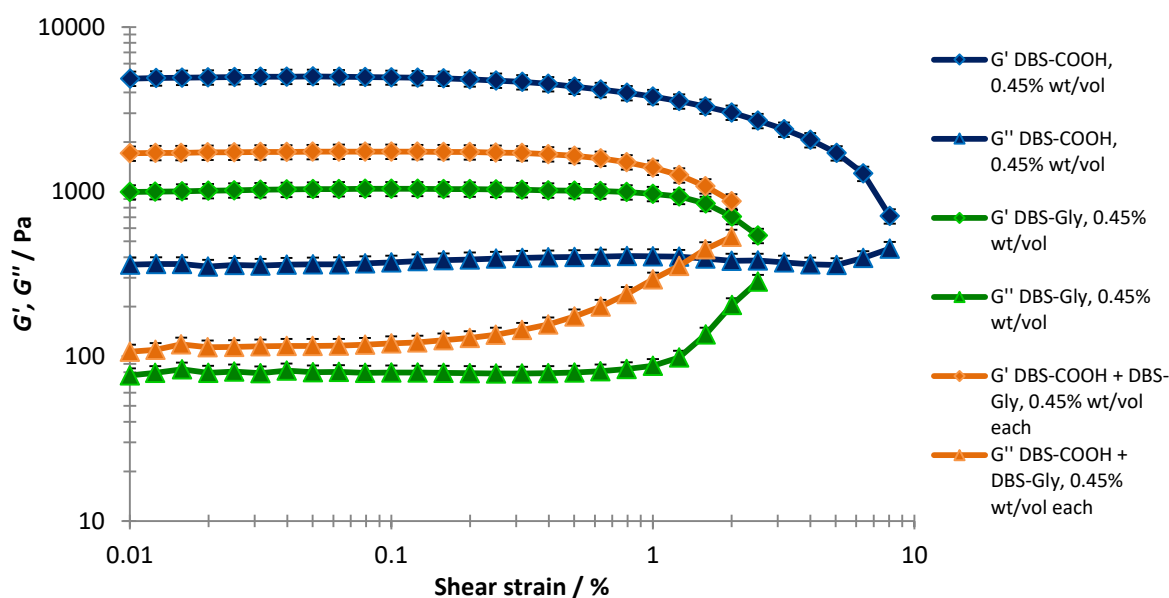
Figure 4.20: Comparison of typical results from amplitude sweep rheological analysis of DBS-CO$_2$H, DBS-Gly, and multi-component DBS-CO$_2$H + DBS-Gly hydrogels.

Further mechanical analysis was conducted through a frequency sweep, at which the shear strain was kept constant at 0.3% – this value was chosen as it was within the limit of the LVR for all the gels analysed. The frequency itself was varied between 0.1 and 10 Hz; typical results are compared in Figure 4.21; results from other runs were within ± 10% of the values presented here.
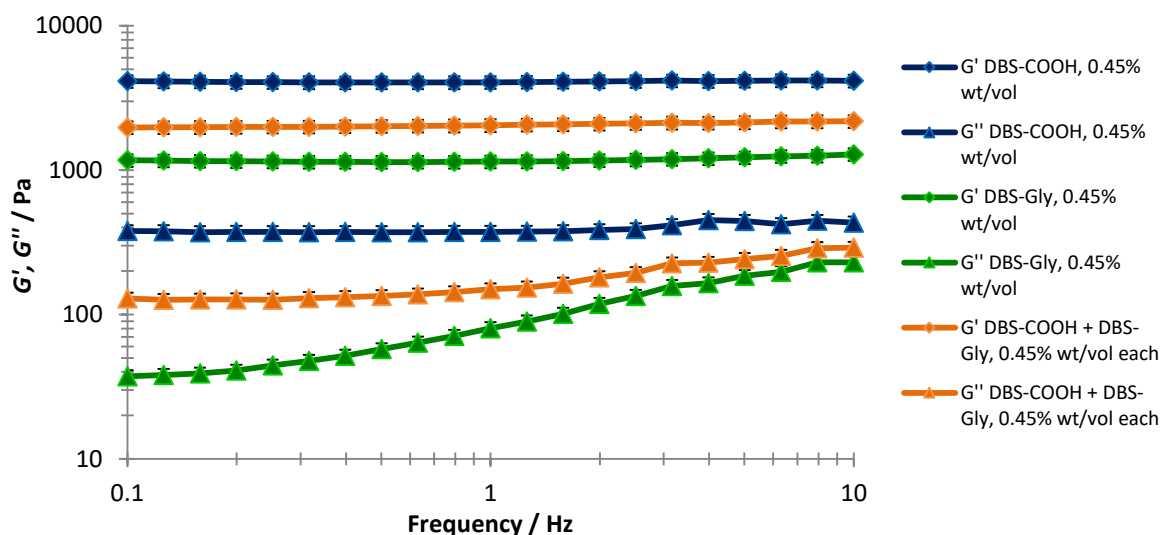
Figure 4.21: Comparison of typical results from frequency sweep rheological analysis of DBS-CO$_2$H, DBS-Gly, and multi-component DBS-CO$_2$H + DBS-Gly hydrogels.

From the frequency sweep analysis in Figure 4.21, comparing *G'* at 1 Hz, the strongest gel as characterized by *G'* was DBS-CO$_2$H (4060 Pa); DBS-Gly was significantly weaker (1140 Pa). Interestingly, the mixed two-component gel was somewhat intermediate between the two in terms of rheological performance (*G'* = 2040 Pa), suggesting that the fibres of DBS-Gly present within the two-component gel may prevent DBS-CO$_2$H from forming its most optimal sample-spanning network. Similar effects have also been observed when mixing self-assembled gels with polymers, the presence of which can somewhat disrupt the formation of a sample-spanning network.[84,85]

4.5. Conclusions and Outlook

In this chapter, the first known examples of DBS-derivatives functionalised with amino acids have been described. Whilst only one compound (DBS-Gly) showed gelation ability, there is clearly scope for further investigation into the synthesis of further derivatives with other amino acids. There would likely need to be some more refinement of the synthesis procedure, as it is believed that slight variations were the cause of the variable gelation properties of DBS-Gly – notably whether or not each batch could function as a heat/cool LMWG. Additionally, attempts were made to synthesis DBS-derivatives with alanine and aspartic acid, though these were not obtained successfully, possibly due to solubility in the chosen solvents – such issues would need to be considered in future work. Importantly though, the incorporation of amino acids into DBS LMWGs potentially opens this class of gelator to a potentially wide range of biomedical applications.

Due to the issues of solubility affecting its ability to act as a heat/cool LMWG, DBS-Gly was primarily treated as a pH-responsive LMWG. It was seen to function similarly to DBS-CO$_2$H,

though with some differences in its nanoscale arrangement, as evidenced by differing Avrami number and CD spectra.

The key difference examined here between DBS-Gly and DBS-CO$_2$H was in the values of pK_a, which were *ca.* 4.3 and *ca.* 5.4 respectively. This enabled the two LMWGs to undergo partial kinetic self-sorting, which was observed by NMR. DBS-CO$_2$H primarily assembled first after addition of GdL, followed by the assembly of DBS-Gly as the pH neared its pK_a. The multi-component gel was seen to have a similar morphology to each individual gel, and rheological properties which were intermediate between the two. Future work on these self-sorting systems could involve the use of another pH-responsive LMWG in place of either of the two used here, potentially one which would give a greater difference in pK_a, and hence possibly distinct instead of partial self-sorting. It could also be feasible to investigate a combination of three or more pH-responsive LMWGs with differing pK_a values, or to investigate alternative methods of acidification and how this might affect the rate of assembly or the self-sorting ability of the gelators.

5. Chapter 5: Photoactivation of DBS-derived low-molecular-weight gelators

The work in this chapter was carried out in conjunction with MChem Student Oliver J. Daubney, and results were published in D. J. Cornwell, O. J. Daubney and D. K. Smith, *J. Am. Chem. Soc.*, 2015, **137**, 15486–15492.

5.1. Introduction

In Chapter 3, the use of UV light to photopattern a PG network was examined; when the patterned PG network was used in combination with a pH responsive LMWG network, a material termed a multidomain gel was produced. Photopatterning of PGs is a widely used and reported method for gaining spatial resolution in gel materials, particularly in the biomedical field;[230,232,256–261] in contrast, photoresponsiveness – let alone photopatterning – of LMWGs has rarely been reported.

There are two main methods by which LWMGs can be made photoresponsive, and potentially photopatterned: a) by incorporation of photoresponsive moieties into the structure of the LMWG to directly trigger gelation, or b) through the use of a light-responsive compound, such as a photoacid generator (PAG) to trigger the gelation event indirectly.

5.1.1. Photoresponsive LMWGs

A popular mechanism for photoresponsive LMWG gelation is to use photo-induced *cis-trans* isomerisation of a double bond with the structure of the gelator to switch gelation "on" or "off". Zinić and co-workers investigated an early example of such a LMWG, exploiting the irreversible UV light (in presence of bromine) induced *cis* to *trans* isomerisation to switch non-gelling microspheres of bis(phenylalanine) maleic acid amides to gelling bis(phenylalanine) fumaric acid amides.[262] Hamachi and co-workers similarly used *cis-trans* isomerism with glycolipid-based LMWGs; under visible light in the presence of bromine, the LMWG network was switched on, whilst under UV irradiation the gel converted to a sol.[263] Photopatterning was achieved in these materials through selective exposure to UV light through a mask to negatively etch out a pattern. Hamachi *et al* developed their photoresponsive systems further by designing LMWGs to respond to light, temperature, Ca^{2+} ions and pH; in doing so these LMWGs could be used to construct physical "logic gates" where multiple stimuli (e.g., light and Ca^{2+}) were needed for the gel to form.[264]

An alternative mechanism for photoresponsiveness was investigated by Zhang and co-workers, who investigated LMWGs formed from peptides linked to a tetrazole-containing moiety; upon exposure to UV, the tetrazole moiety underwent intramolecular photoclick ligation to form a pyrazoline ring.[265] This rearrangement resulted in a gel-sol transition; using a photomask during the

exposure allowed for etching of microchannels into the gel, which could be used for growing cells within.

The above systems were limited to 2D photopatterning (where photopatterning was possible); Hamachi and co-workers, having also developed photoresponsive dipeptide-based LMWGs,[266] investigated the possibility of obtaining 3D photopatterned materials through the use of two-photon polymerisation techniques.[267] The LMWG used contained a dimethylaminocoumarin-4-yl-methoxycarbony, which had suitable responsive absorbance for 2PP. This responsive group was cleaved from the dipeptide segment of the LMWG when activated at the focal point of the two lasers used in 2PP, causing a gel-sol transition. The 2PP technique allowed for much more detailed and higher resolution 3D patterning in the gels, and could be used to selectively mobilise nanobeads or bacteria.

5.1.2. LMWGs with photoacid generators

PAGS are a type of molecule which upon exposure to light (either visible or UV) undergo photolysis, with one of the products being an acid. PAGs are therefore of particular use for promoting gelation in certain pH-responsive LMWG systems. Surprisingly though, very little work has been carried out in this area. Adams and co-workers used the PAG diphenyliodonium nitrate (DPIN) in combination with pH-responsive dipeptide LMWGs, and observed formation of gels after exposure to low-intensity UV light for 14 hours.[268] With a higher-intensity UV light, lower exposure time and a photomask, photopatterning was also shown to be possible.

Van Esch and co-workers investigated a different PAG, derived from spiropyran, which generated acid upon exposure to visible light.[269] With this PAG, the generated protons catalysed the formation of a trishydrazone LMWG from a trishydrazide and a benzaldehyde derivative, and a gel was seen to form after 100 minutes of exposure; photopatterning was also possible at reasonable resolutions (100 µm). A disadvantage of this system, however, is that the PAG still functioned as a catalyst for the gelation in the absence of visible light, albeit at a slower rate and with a weaker gel being formed.

5.1.3. Photo-induced gelation of DBS-derived LMWGs

Given that both DBS-CO$_2$H and DBS-Gly are both pH-responsive LMWG, it seemed reasonable to presume that one or both of them could undergo photo-induced gelation with the use of a PAG as the proton source. This chapter therefore examines the gelation of both LWMGs using the PAG DPIN.

5.2.   Photoacid generator diphenyliodonium nitrate

DPIN was selected as the PAG of choice due to it being commercially available, and water soluble. DPIN is activated under UV light, where absorption of a photon causes homolytic cleavage of one Ar-I bond, generating iodide and phenyl radicals. The highly reactive phenyl radical is quenched through reaction with water to form phenol and a protonated iodide, which then decays to iodobenzene, releasing an acidic proton – in combination with the nitrate, this effectively generates an equivalent of nitric acid (Scheme 5.1).[270,271]
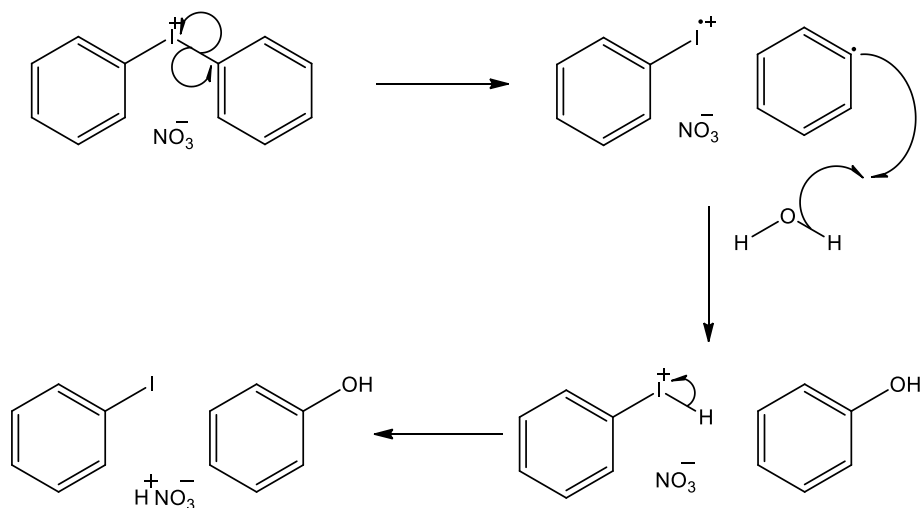
Scheme 5.1: Mechanism for the activation of DPIN in aqueous solution.

The λ_{max} of DPIN as supplied was determined by UV-vis spectroscopy to be 287 nm (Figure 5.1); other investigations with DPIN have yielded similar λ_{max} values.[268]
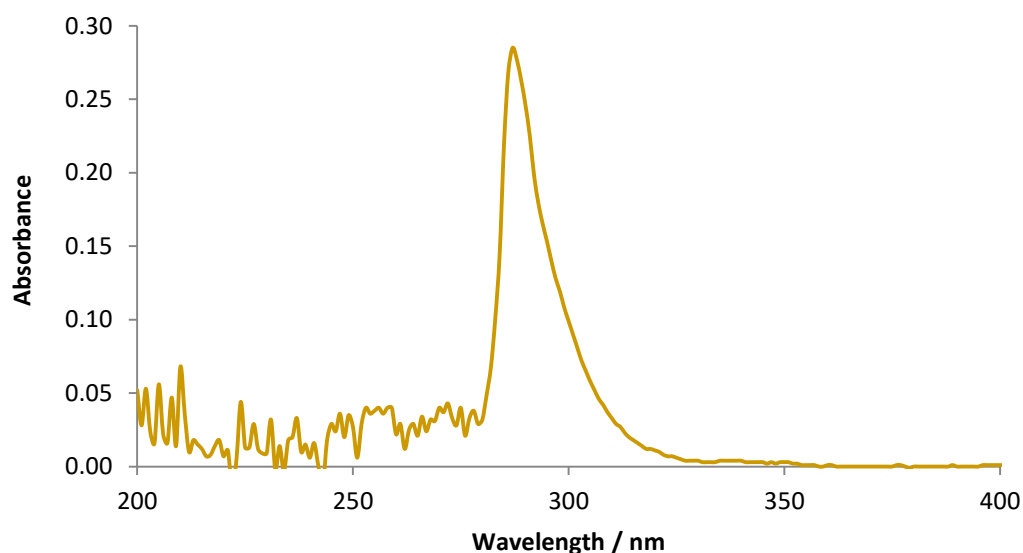
Figure 5.1: UV-vis spectrum of PAG diphenyliodonium nitrate (DPIN), 1.5 mM in H$_2$O. From this spectrum, λ_{max} = 287 nm.

To determine the pH activity of DPIN, 48 mg was dissolve in 6 mL deionised water; the initial pH was recorded as *ca.* 6.8. Upon exposure to low-intensity UV light (254 nm) for two hours, the pH was observed to drop to *ca.* 2.6, with the main drop of *ca.* 3 pH units occurring within the first 20 minutes (Figure 5.2). The activation of DPIN is accompanied by the formation of a white precipitate, attributable to the formation of insoluble iodobenzene as one of the by-products.
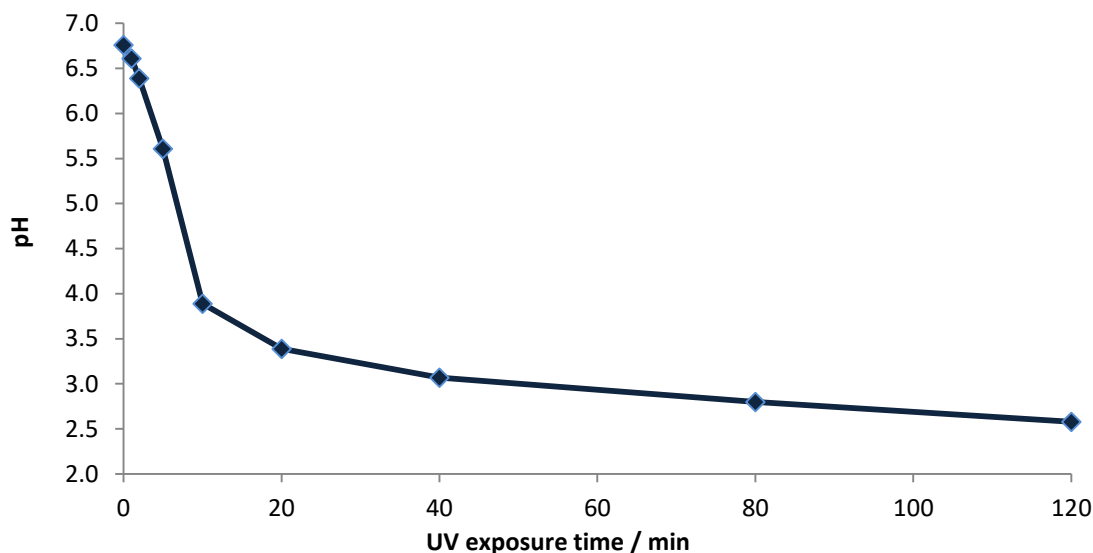
Figure 5.2: Change in pH over time as DPIN solution (8 mg mL^{-1}) is exposed to UV light (254 nm).

5.3. Initial studies of DBS-CO$_2$H using DPIN as PAG, with low-intensity UV light

5.3.1. System optimisation

When DPIN is used in combination with DBS-CO$_2$H or DBS-Gly, the starting pH of the solution would be between *ca.* 10 and 11.5, due to the use of NaOH$_{(aq)}$ to deprotonate the LMWGs and render them fully soluble prior to reprotonation to trigger gelation. To assess the effect of this on the overall acidification of the system by use of DPIN, the pH of solutions of DBS-CO$_2$H (0.1% wt/vol or 0.4% wt/vol), NaOH$_{(aq)}$ (minimum amount of 0.5 M required to dissolve DBS-CO$_2$H) and DPIN (8 mg mL-1) were monitored upon exposure to low-intensity UV light (254 nm) over the course of 2 hours (Figure 5.3). The concentration of 8 mg mL^{-1} of DPIN was selected as it was reasoned to be able to generate a sufficient excess of protons to counter the excess NaOH. The initial pH of the solution of 0.1% wt/vol DBS-CO$_2$H was *ca.* 7.5; after 2 hours of exposure to UV, this had dropped to *ca.* 5.2. Some formation of gel-like precipitate was observed (along with the white iodobenzene precipitate), though as the concentration of LMWG used was below the MGC, and stirring was used between pH measurements, no full sample-network was formed. For the solution of 0.4% wt/vol DBS-CO$_2$H, the starting pH was *ca.* 10.5; after 2 hours of UV exposure,

this had only dropped to *ca.* 9.2. Clearly the much higher starting pH prevented the protons generated from activation of DPIN from pushing the system past the equivalence point.
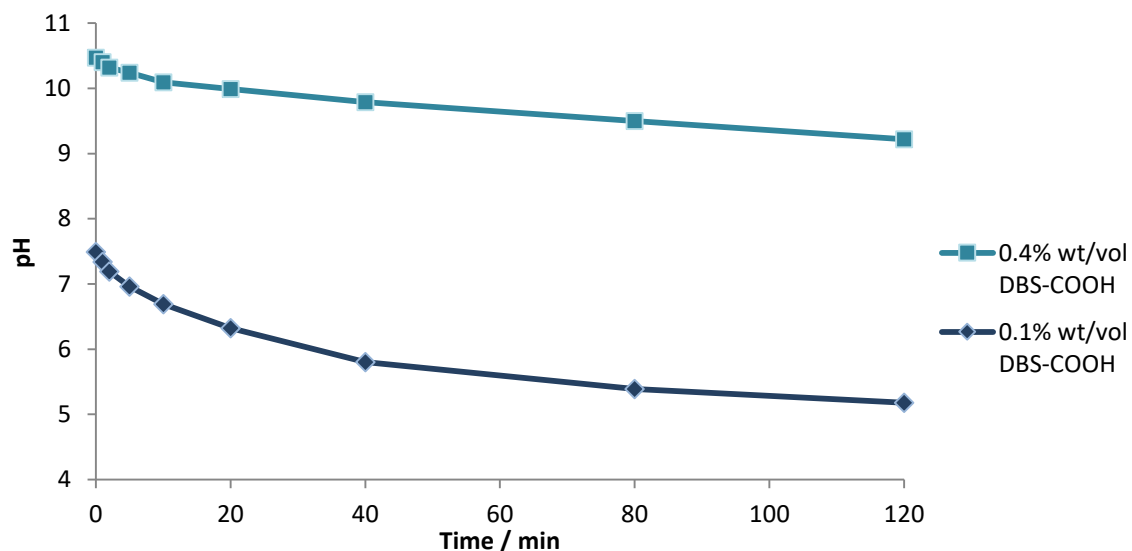
Figure 5.3: Change in pH over time as DBS-CO$_2$H/DPIN solutions are exposed to UV light (254 nm).

To improve the level of reprotonation of DBS-CO$_2$H, it was reasoned that addition of a small amount of HCl prior to DPIN activation would help to neutralise excess NaOH, and also push the initial pH of the system down to between *ca.* 5.8 and 6.8 – still above the pKa of DBS-CO$_2$H (*ca.* 5.4), and around the starting pH of a solution of just DPIN (*ca.* 6.8 in Figure 5.2). HCl (0.5 M) was added in varying amounts (1.5-2.5 μL mL^{-1}) to the basic DBS-CO$_2$H (0.2% wt/vol) and DPIN (8 mg mL^{-1}) solutions, then the pH change upon exposure to low-intensity UV light over 2 hours was monitored (Figure 5.4). For all the systems, partial gel was observed after UV exposure – the stirring required for pH measurements prevented full gelation of the solution. The concentration of HCl (0.5 M) selected for further studies was 2.5 μL mL^{-1}, as the final pH of this system (*ca.* 5.3) was below the pKa of DBS-CO$_2$H.
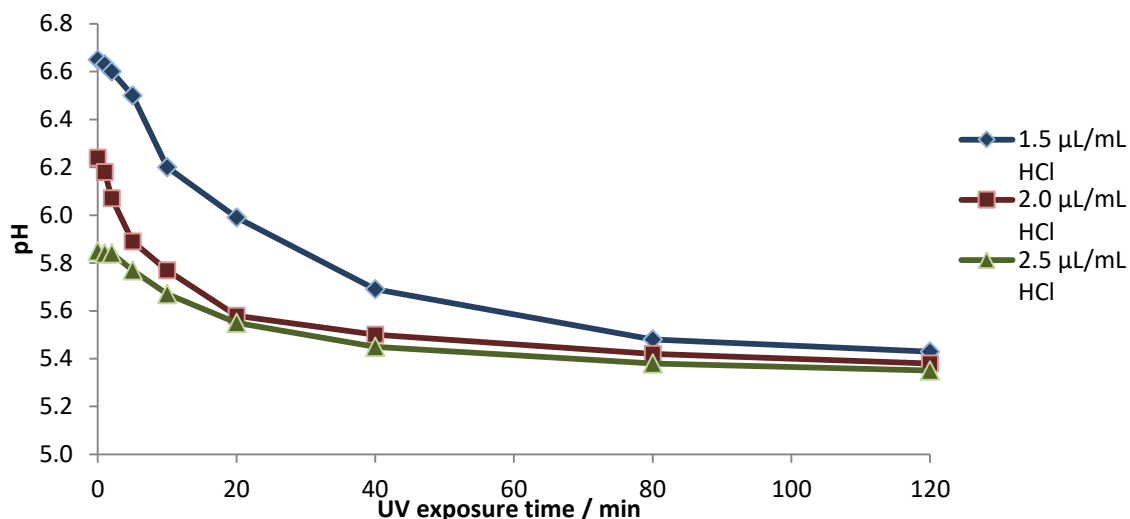
Figure 5.4: Change in pH over time for DBS-CO$_2$H/DPIN systems (0.2% wt/vol, 8 mg mL^{-1}) with varying amounts of HCl (0.5 M) added.

5.3.2. Gelation studies of DBS-CO$_2$H using DPIN as PAG, with low-intensity UV light

To attempt to form gels of DBS-CO$_2$H using DPIN as the acidifying agent, known amounts of DBS-CO$_2$H were weighed into 2.5 mL sample vials, followed by addition of water and the minimum amount of NaOH$_{(aq)}$ (0.5 M) to give a volume of 125 μL; to this, 125 μL of 16 mg mL^{-1} DPIN solution with 5μL mL^{-1} HCl (0.5 M) was added (so final amounts of DPIN and HCl (0.5 M) were 8 mg mL^{-1} and 2.5 μL mL^{-1} respectively), bringing the total volume of solution to 250 μL. The vials were placed under UV light (254 nm, from a 'TLC' lamp) for 8 hours to activate the PAG and allow sufficient time for gelation to take place. After this time, opaque, gel-like membranes were observed to have formed at the surfaces of the solutions, whilst the free liquid beneath was discoloured; the membranes were capable of holding the liquid in place during tube inversion (Figure 5.5).
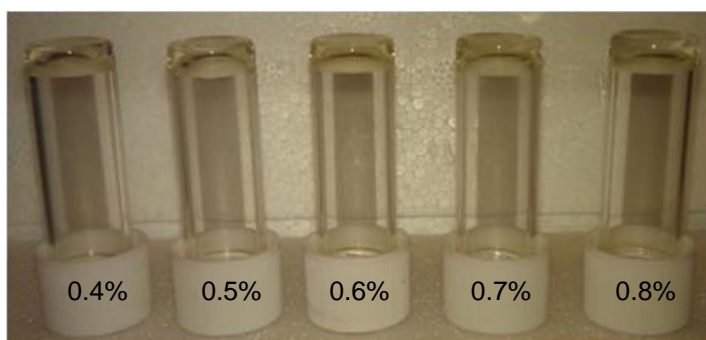
Figure 5.5: DBS-CO$_2$H (varying % wt/vol) and DPIN (8 mg mL^{-1}) systems after 8 hours of exposure to UV (254 nm); the gel-like membranes formed at the surface of the solution prevent flow of the remaining solution upon tube inversion.

There was clearly a problem with the method used – specifically, a shallow depth of light penetration, which meant that only in the upper part of the solution was DPIN sufficiently activated

146

to promote acidification of the system and that gelation was kinetically faster than pH equilibrium through the sample, hence a gel only forms at the surface (the discolouration of the non-gelled solution was likely due to formation of smaller amounts of iodobenzene). Investigating this further, a solution of 0.4% wt/vol of DBS-CO$_2$H with 8 mg/mL DPIN was placed into a 5 × 5 cm glass mould at a depth of *ca.* 2 mm, then exposed to UV light for 8 hours. Again, this formed only a thin opaque membrane on the surface of the solution. This led to the conclusion that as well as the problem with depth penetration, there was also an issue with the intensity of the light, which could possibly be limiting the amount of DPIN activated.

5.4. Gelation studies of DBS-CO$_2$H and DBS-Gly using DPIN as PAG, with high-intensity UV light

For subsequent studies of gelation using DPIN, the low-intensity UV lamp was swapped for the high-intensity UV lamp previously used for the gelation of PEGDM (Chapter 3); the broad spectrum of the available lamp, λ ≈ 300-400 nm, is slightly above the λ$_{max}$ of DPIN (287 nm), though it still overlaps with DPIN's absorbance (see Figure 5.1).

5.4.1. Formation of gels of DBS-CO$_2$H and DBS-Gly using DPIN as PAG, with high-intensity UV light

Solutions of DBS-CO$_2$H and DPIN were prepared by first dissolving 64 mg of DPIN in 3.98 mL water, followed by the addition of 20 μL of HCl$_{(aq)}$ (0.5 M). Separately, 24 mg of DBS-CO$_2$H was sonicated in 2.89 mL of water, followed by the addition of 110 μL of NaOH$_{(aq)}$ to dissolve. Then, 3 mL of the DPIN solution was added to the DBS-CO$_2$H solution to give a final volume of 6 mL, with concentrations of DBS-CO$_2$H at 0.4% wt/vol, and DPIN at 8 mg/mL. The solution was divided into samples vials at different volumes: 0.25 mL, 0.5 mL, and 1 mL. The samples were placed in a cold water bath (to prevent UV-induced heating effects) below the high-intensity UV lamp, and exposed to UV for 2 hours. After this time, opaque suspensions of partial gels were observed (Figure 5.6); as seen before with the low-intensity UV light, there was not sufficient depth penetration or exposure to fully gelate the samples. However, the suspensions produced by this method were significantly more homogeneous, suggesting that the light was able to reach most of the solution.

147
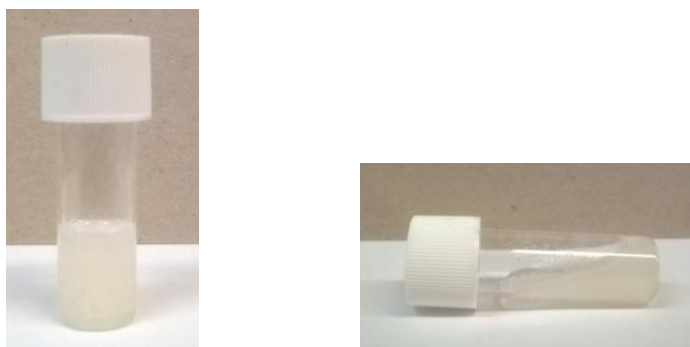
Figure 5.6: Suspensions of partial gels produced from solutions (1 mL volumes) of DBS-CO₂H (0.4% wt/vol) and DPIN (8 mg mL⁻¹) after exposure to high intensity UV light; the partial gel nature can be seen when the vial is placed on its side (right).

A solution of DBS-CO$_2$H and DPIN was prepared with the same quantities as above, but this time 5 mL was poured into a 5 × 5 cm glass mould. This was placed under UV light for 2 hours, after which a weak, opaque gel was observed to have formed (Figure 5.7). This showed that photoactivation of DBS-CO$_2$H was clearly most effective in shallow samples and containers, so that good penetration of UV light could be achieved, leading to homogeneous dispersion of the LMWG nanofibers and hence formation of a sample-spanning network.
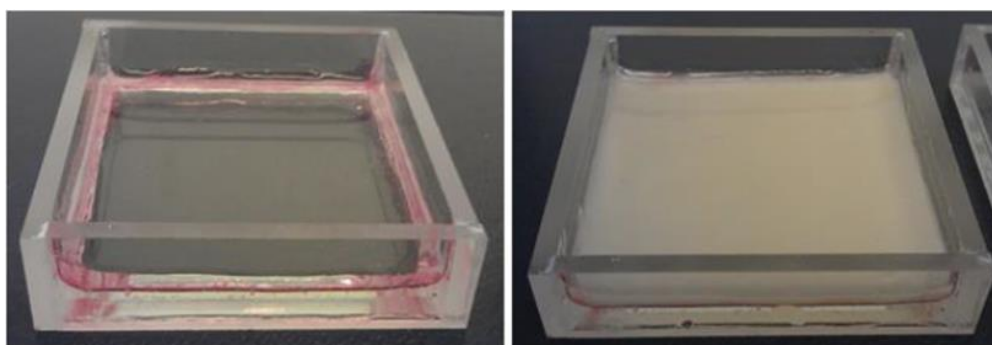
Figure 5.7: System of DBS-CO₂H (0.4% wt/vol) and DPIN (8 mg mL⁻¹) in a 5 × 5 cm glass mould before (left) and after (right) exposure to UV light; after exposure, a weak, opaque hydrogel is formed.

The gelation of DBS-Gly in combination with DPIN was similarly investigated. 64 mg of DPIN was dissolved in 3.98 mL of water, followed by the addition of 20 µL HCl$_{(aq)}$ (0.5 M). Separately, 22.5 mg DBS-Gly was sonicated in 2.33 mL of water, then dissolved through the addition of 170 µL of NaOH$_{(aq)}$ (0.5 M). 2.5 mL of the DPIN solution was added to the DBS-Gly solution, to give a total volume of 6 mL, with concentrations of DBS-Gly at 0.45% wt/vol, and DPIN at 8 mg/mL. The solution was divided into samples vials at different volumes: 0.25 mL, 0.5 mL, and 1 mL. The samples were placed in a cold water bath below the high-intensity UV lamp, and exposed to UV for 2 hours. After this time, opaque suspensions of partial gels were observed, similar to those seen for the systems of DBS-CO$_2$H with DPIN (Figure 5.8a and b). On using an identically prepared

solution, this time pouring 5 mL into a 5 × 5 cm glass mould, a weak, opaque hydrogel was formed (Figure 5.8c). Again, the observations here show that photoactivation was clearly most effective in shallow samples and containers.
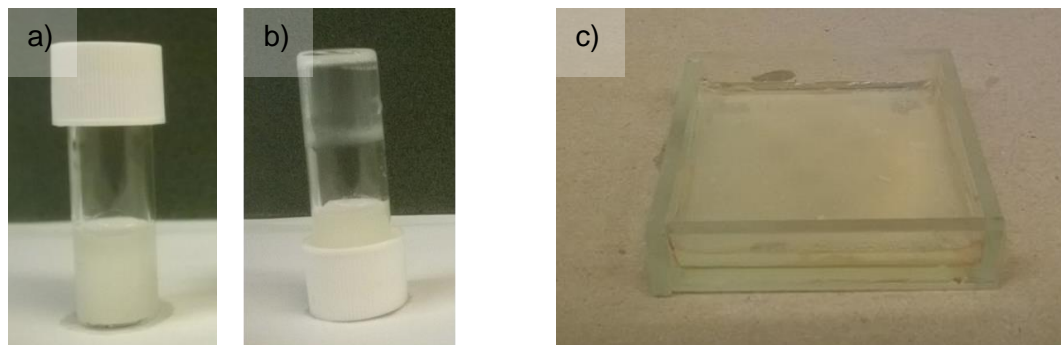
Figure 5.8: a) and b) suspensions of partial gel of DBS-Gly (0.4% wt/vol) using DPIN (8 mg mL^{-1}) as acidifying agent made in vials; c) weak, opaque hydrogel of DBS-Gly (0.4% wt/vol) using DPIN (8 mg/mL) made in glass mould.

The mechanical weakness of these gels formed in the moulds made T_{gel} and rheological studies difficult. From simple table-top observations, the gels appeared to be significantly weaker than those made using GdL as the acidifying agent. It is known that the mechanical properties of acid-functionalised gels can be affected by the kinetics of gelation;[272] given that DPIN activates the system in ≤ 2 hours (when using high-intensity UV light), it is unsurprising that there are some mechanical differences dependent on the method of activation.

5.4.2. ^{1}H NMR studies of DBS-CO$_2$H and DBS-Gly using DPIN as PAG

5.4.2.1. DBS-CO$_2$H

NMR samples of DBS-CO$_2$H with DPIN were prepared by first dissolving DPIN (8 mg) in 497.5 µL of D$_2$O, containing of 2 µL mL^{-1} DMSO as internal standard, followed by addition of 2.5 µL HCl$_{(aq)}$ (0.5 M). Separately, 4 mg of DBS-CO$_2$H was dissolved in 466 µL D$_2$O (also containing 2 µL mL^{-1} DMSO as internal standard) through the addition of 34 µL NaOH$_{(aq)}$ (0.5 M). The two solutions were mixed, and 700 µL was transferred to an NMR tube; a spectrum of the solution was then recorded. The NMR tube was then placed under UV light for 1 hour, after which a second spectrum was recorded. Comparing the two spectra (Figure 5.9) revealed that all of the DBS-CO$_2$H had been reprotonated, and therefore presumably incorporated into a sample-spanning solid-like network.
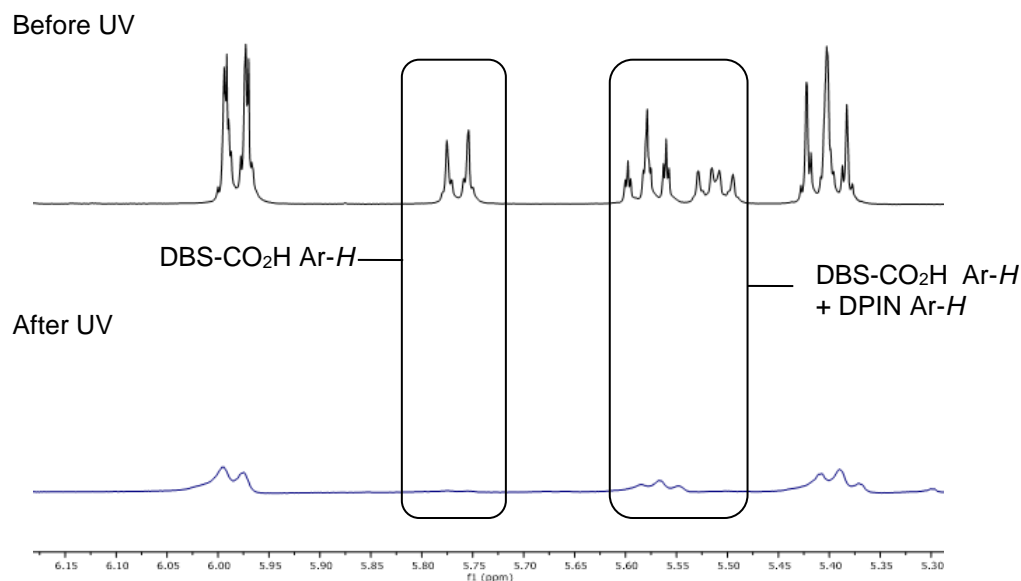
Figure 5.9: ^{1}H NMR of DBS-CO$_2$H system with 8mg mL^{-1} DPIN as acidifying agent, before and after UV exposure of 1 hour. The lack of DBS-CO$_2$H Ar-*H* peaks signifies that all the LMWG has been reprotonated. Unlabelled peaks correspond to Ar-*H* protons of DPIN.

NMR was then used to follow the kinetics of DBS-CO$_2$H assembly into solid-like nanostructures on photoactivation. To achieve this, samples of DBS-CO$_2$H with DPIN were prepared by first dissolving DPIN (80 mg) in 4.975 mL of D$_2$O, containing of 2 µL mL^{-1} DMSO as internal standard, followed by addition of 25 µL HCl$_{(aq)}$ (0.5 M). Separately, 40 mg of DBS-CO$_2$H was dissolved in 4.66 mL D$_2$O (also containing 2 µL mL^{-1} DMSO as internal standard) through the addition of 340 µL NaOH$_{(aq)}$ (0.5 M). The two solutions were mixed, then 13 separate 700 µL volumes were transferred to NMR tubes. One tube was left uncured, whilst the other 12 were cured under UV light, with one tube being removed every 5 minutes over the course of 1 hour for NMR spectra to be recorded. The concentration of mobile DBS-CO$_2$H in each sample was determined, and plotted against time (Figure 5.10a). From this, the Avrami exponent was calculated to be n = 0.99 (Figure 5.10b) - close enough (within the margins of experimental error) to a value of 1 to suggest the fibres exhibit much more 1D growth in this case, as opposed to the more 2D growth when GdL was used as the acidifying agent – potentially as the different kinetics of formation lead to different nanostructures[272] (though see section 2.4.2 for comments on the use of the Avrami model with pH-responsive LMWGs).
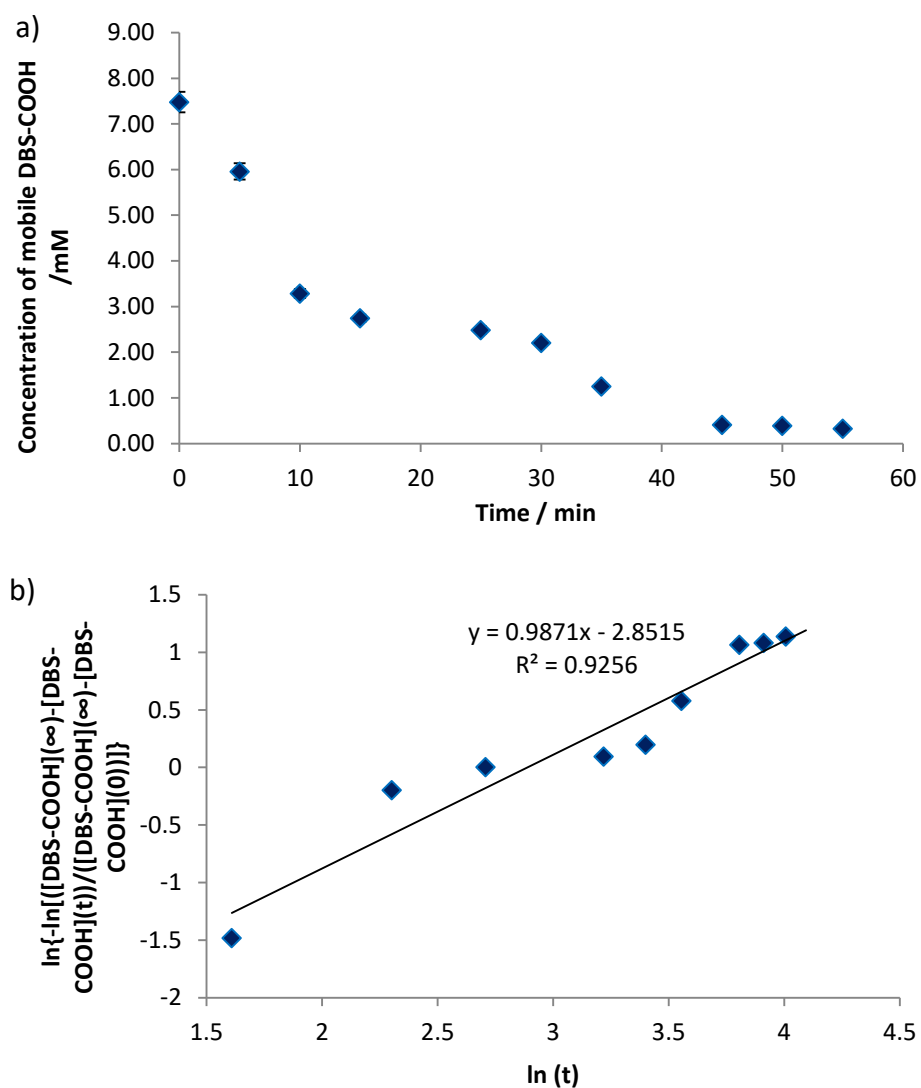
Figure 5.10: a) Plot of average rate of formation of the DBS-CO₂H network when using DPIN as the acidifying agent, as monitored by ¹H NMR; b) Avrami plot for formation of DBS-CO₂H network, n = gradient of line = 0.99.

5.4.2.2. DBS-Gly

Systems of DBS-Gly with DPIN were similarly investigated by NMR, being prepared by the same method as described above, though with 0.45% wt/vol of the LMWG. Comparing the two spectra (Figure 5.11) revealed that most of the DBS-Gly had been reprotonated, and therefore presumably incorporated into a sample-spanning solid-like network.
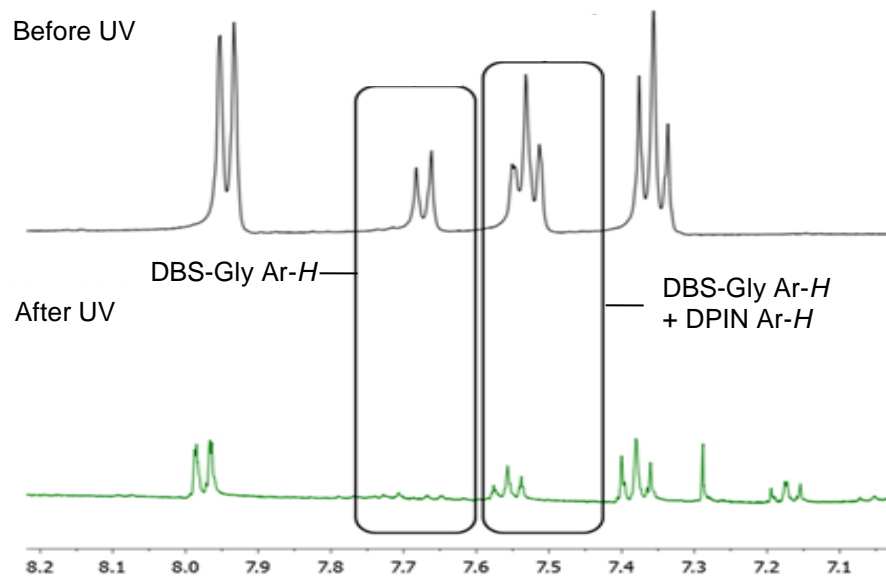
Figure 5.11: ¹H NMR of DBS-Gly system with 8mg mL⁻¹ DPIN as acidifying agent, before and after UV exposure of 1 hour. The significant reduction of DBS-Gly Ar-*H* peaks signifies that most of the LMWG has been reprotonated. Unlabelled peaks correspond to Ar-*H* protons of DPIN.

NMR was then used to follow the kinetics of DBS-Gly assembly into solid-like nanostructures on photoactivation, again using the same method as was used for DBS-CO$_2$H but with 0.45% wt/vol of DBS-Gly. The concentration of mobile DBS-Gly in each sample was determined, and plotted against time (a). From this, the Avrami exponent was calculated to be n = 1.08 (b), very similar to the value when GdL was used (n = 1.06), indicating that DBS-Gly assembled into mostly 1D nanostructures; in contrast to the results of this experiment with DBS-CO$_2$H, the kinetics of assembly when using DPIN did not appear to have a significant effect on the nanostructure (though again, see section 2.4.2 for comments on the use of the Avrami model with pH-responsive LMWGs).
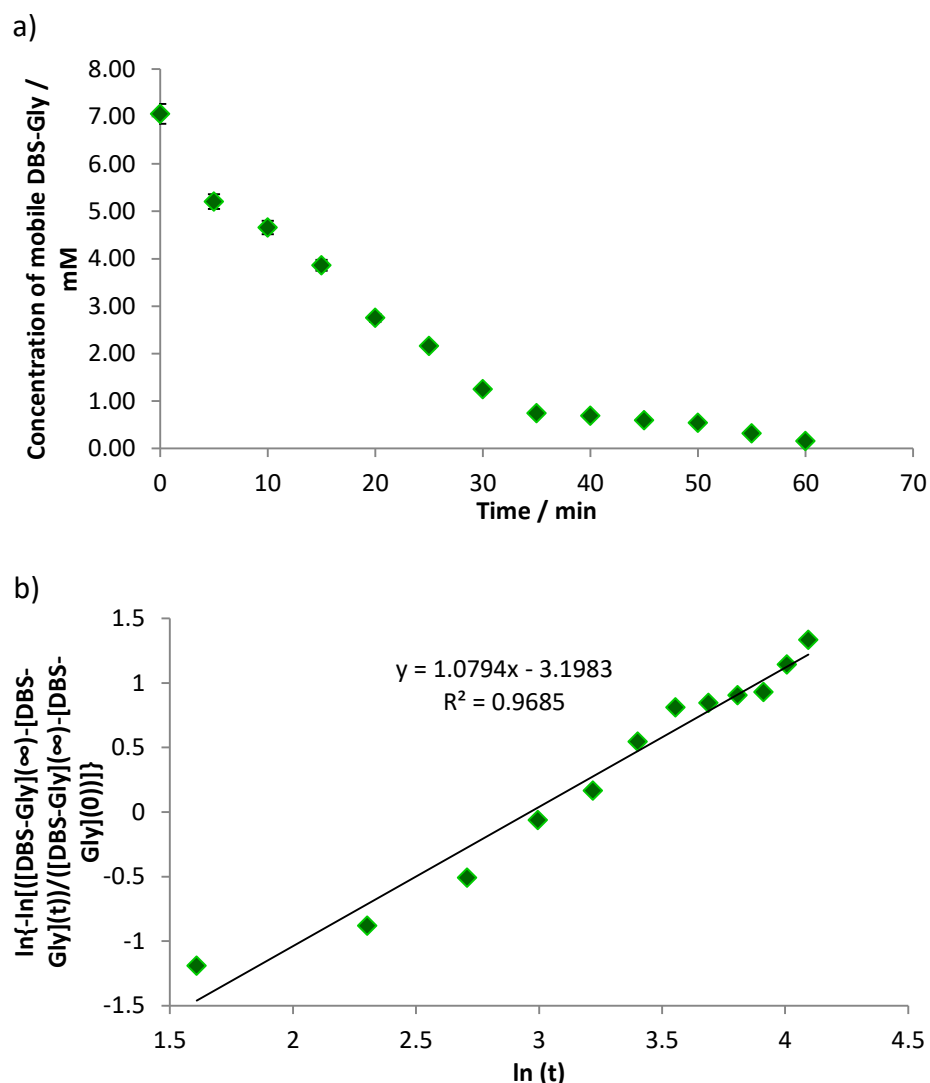
Figure 5.12: a) Plot of average rate of formation of the DBS-Gly network when using DPIN as the acidifying agent, as monitored by ^{1}H NMR; b) Avrami plot for formation of DBS-CO$_2$H network, n = gradient of line = 1.08.

5.4.3. CD studies of DBS-CO$_2$H and DBS-Gly using DPIN as PAG

Studying systems where DPIN was used to activate DBS-CO$_2$H and DBS-Gly was only partially useful for two reasons: a) a CD spectrum of DPIN (at a concentration of 0.8 mg mL^{-1}) after 2 hours of exposure to UV shows strong CD signals in the region of 180-240 nm, which overlaps with some of the CD signals from the LMWGs, and b) the strong signals in between 180-240 nm caused the detector in the CD instrument to become saturated for this region.

5.4.3.1. DBS-CO$_2$H

Samples of DBS-CO$_2$H with DPIN were prepared for CD by dissolving 3.2 mg of DPIN in 1.999 mL of water; to this was added 1 μL of HCl$_{(aq)}$ (0.5 M) to make a DPIN stock solution. 0.4 mg DBS-CO$_2$H was dissolved in 500 μL of water through the addition of 3.7 μL NaOH$_{(aq)}$ (0.5 M),

followed by sonication. 500 μL of the DPIN stock solution was added to the DBS-CO$_2$H solution, and this was then cured under UV light for 2 hours to produce a suspension of nanofibers. The CD spectra recorded for samples prepared as such showed a CD band with a maximum at *ca.* 260 nm with an intensity of *ca.* -36 mdeg (Figure 5.13), similar to that observed when GdL was used as the acidifying agent (see Chapter 2 – data added for comparison in Figure 5.13) – though as a higher concentration of DBS-CO$_2$H was used in this study it might have been expected that the intensity would be higher, but the close proximity of the CD bands generated by DPIN and its products likely cause some reduction of intensity; it should also be noted that the value of HT rapidly increases from *ca.* 300 V to above 800 V below 250 nm – attributable to the high absorbance of DPIN. Nonetheless, this study shows that very similar chiral nanostructures are formed when using either GdL or DPIN as the acidifying agent – though the results from NMR would suggest that the nanostructures are maybe less branched/aggregated when DPIN is used.
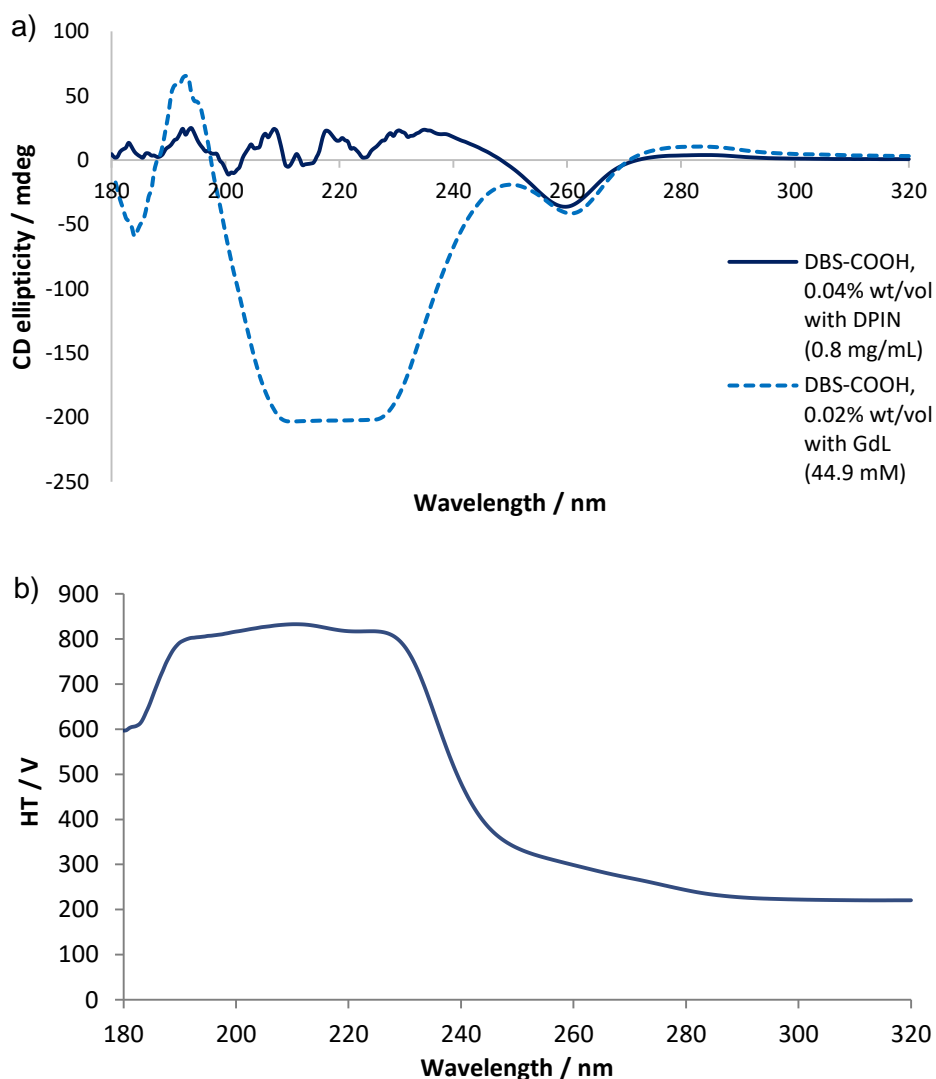
Figure 5.13: a) CD spectra of DBS-CO$_2$H when prepared using DPIN as then acidifying agent (solid line) or GdL as the acidifying agent (dashed line); b) HT data for DBS-CO$_2$H and DPIN system.

5.4.3.2. DBS-Gly

Samples of DBS-Gly with DPIN were prepared for CD by making a stock solution of DPIN as described above. 0.45 mg DBS-Gly was dissolved in 500 μL of water through the addition of 3.4 μL NaOH$_{(aq)}$ (0.5 M), followed by sonication. 500 μL of the DPIN stock solution was added to the DBS-Gly solution, and this was then cured under UV light for 2 hours to produce a suspension of nanofibers. Unfortunately, the strong CD bands generated from DPIN and its products appeared to mask any CD bands associated with the chiral nanostructures of DBS-Gly (Figure 5.14a) – these would have been expected to have maxima at *ca.* 275 and 242 nm (based on observations in Chapter 4). Additionally, bands for DBS-Gly would likely lie in the region where the detector becomes saturated (below 250 nm), as seen from the HT data recorded (Figure 5.14b).
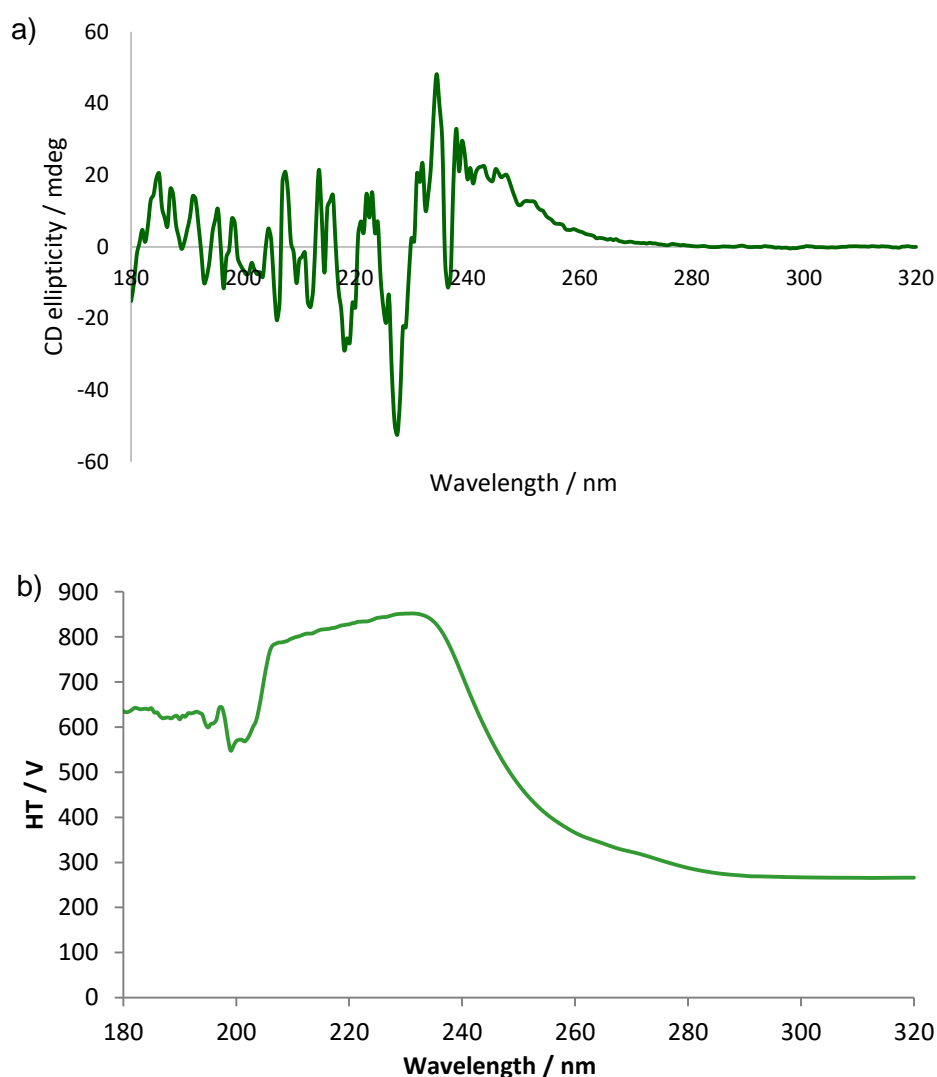
Figure 5.14: a) CD spectra of DBS-Gly (0.045% wt/vol) using DPIN (0.8 mg/mL) as the acidifying agent; the CD bands of DPIN appeared to mask the CD bands of DBS-Gly; b) HT data.

155

5.4.4.   SEM imaging of hydrogels of DBS-CO₂H and DBS-Gly using DPIN as PAG

Due to the difficulties in producing stable gels of DBS-CO$_2$H or DBS-Gly activated by DPIN in vials, samples for SEM were prepared from partial-gel suspensions of DBS-CO$_2$H or DBS-Gly with DPIN (prepared as described in section 5.4.1). This meant that the freeze-drying method used previously was not practical in this case. To prepare these samples, a small amount of the suspensions were applied to metal SEM stubs, and these were then dried under ambient conditions to yield dried-down xerogels. The samples were then sputter-coated with a thin layer of palladium to prevent sample charging, before imaging with a field emission gun scanning electron microscope (FEG-SEM).

5.4.4.1. DBS-CO₂H

The preparation method used meant that the network of gel fibres collapsed down into dense layers, as opposed to the expanded structure seen when freeze-drying was used. From the images taken of DBS-CO$_2$H (Figure 5.15), the fibres are not particularly well-defined in the overall sheet-like appearance of the xerogels; but there are fibre-like structures visible.
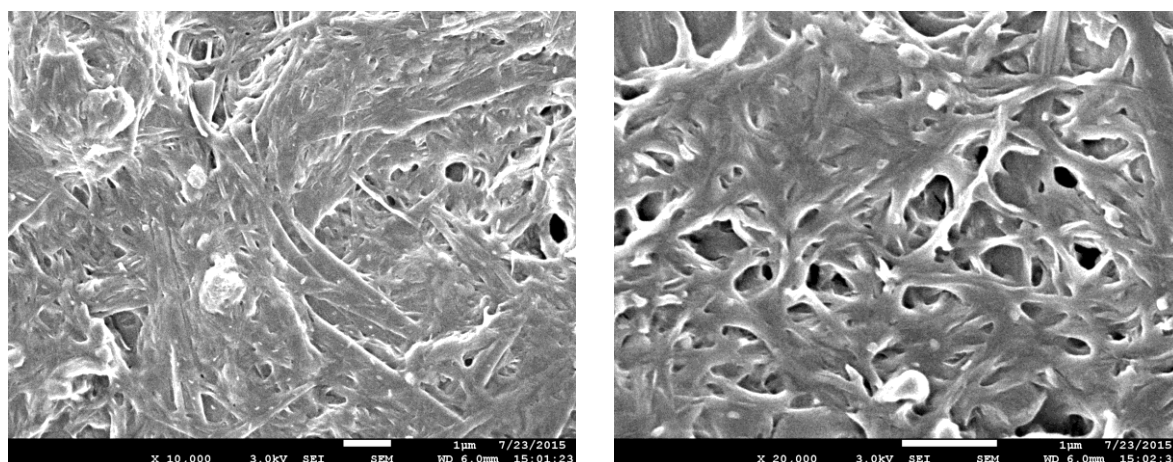
Figure 5.15: SEM images of the xerogels of DBS-CO₂H partial gels produced using DPIN as PAG. Scale bars = 1 μm.

5.4.4.2. DBS-Gly

The images of DBS-Gly xerogels also show the presence of some fibres; they appear to be relatively unbranched in nature, in agreement with the Avrami number n = 1.08 from the NMR experiments, which indicated that the nanofibers formed should be largely 1 dimensional.
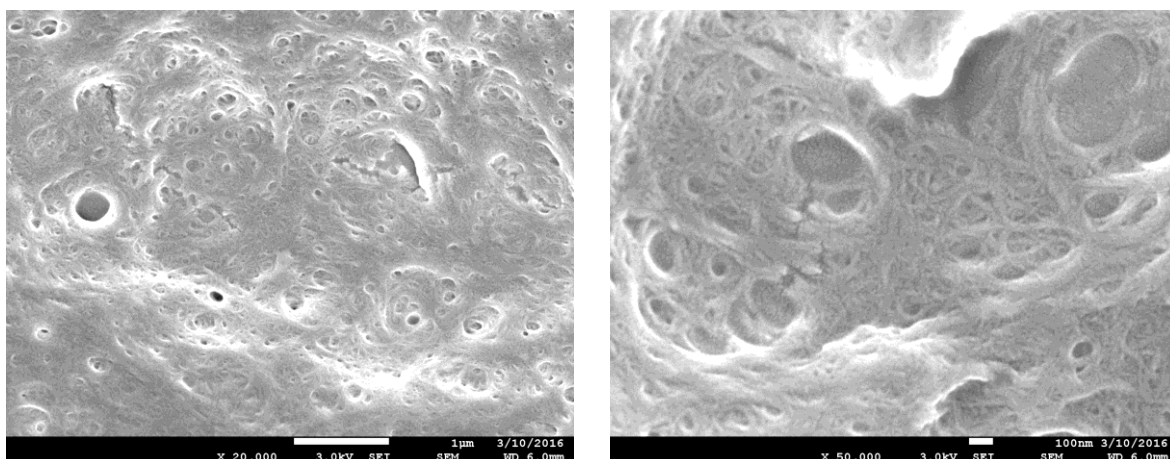
Figure 5.16: SEM images of the xerogels of DBS-Gly partial gels produced using DPIN as PAG. Scale bars = 1 μm (left) and 100 nm (right).

5.5. Dual activation of DBS-CO$_2$H and DBS-Gly hydrogels using GdL and DPIN

In Chapter 4, it was demonstrated that a multi-component gel of DBS-CO$_2$H and DBS-Gly has a two-step activation process, with the majority of the DBS-CO$_2$H network forming before the DBS-Gly network. It was therefore reasoned that it might be possible to use two different proton sources to trigger the assembly of the two different LMWG networks independently – specifically, that GdL hydrolysis would mostly cause formation of the DBS-CO$_2$H network, then with activation of DPIN by UV light the assembly of the DBS-Gly network would occur, forming the dual-network gel (Scheme 5.2). With gluconic acid (produced from GdL hydrolysis) and nitric acid (product of DPIN activation) having pK_a values of 3.86 and – 1.4 respectively, these acidification agents appeared to be well-suited for this stepwise protonation of DBS-CO$_2$H and DBS-Gly, which have pK_a values of 5.4 and 4.3, respectively.
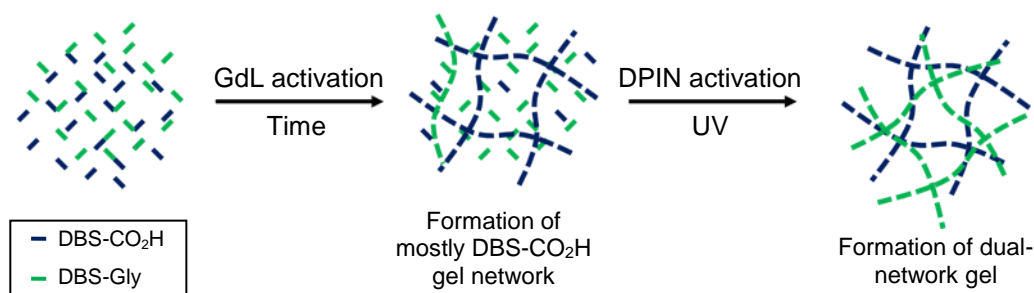
Scheme 5.2: Formation of dual-network gel of DBS-CO$_2$H and DBS-Gly through a two-step activation process using GdL followed by DPIN.

5.5.1. ^{1}H NMR studies of multi-component system with dual activation

From the ^{1}H NMR studies of the multi-component system in Chapter 4, it was observed that a concentration of 32.0 mM (5.7 mg mL^{-1}) of GdL was sufficient to cause *ca.* 90% of DBS-CO$_2$H and only *ca.* 20% of DBS-Gly (when both were at 0.45% wt/vol) to assemble into solid-like nanostructures; hence these concentrations of GdL and the two LMWGs were selected for the dual activation studies. The concentration of DPIN selected was 23.3 mM (8 mg mL-1), as this was known to be sufficient to cause complete (or near complete) formation of either DBS-CO$_2$H or DBS-Gly when they were present at 0.45% wt/vol.

To prepare the samples for NMR, 32 mg of DPIN was dissolved in 2 mL D$_2$O (with 2 µL mL^{-1} DMSO as an internal standard) to make a stock solution. 3.15 mg of both DBS-CO$_2$H and DBS-Gly were suspended by sonication in 0.3 mL D$_2$O (with 2 µL mL^{-1} DMSO as an internal standard) in 2.5 mL vials, followed by addition of 51 µL of NaOH$_{(aq)}$ (0.5 M) to dissolve. 350 µL of DPIN stock solution was then added, followed by 4 mg GdL. The solutions were immediately transferred to NMR tubes and placed in the spectrometer to record an initial spectrum. The tubes were then allowed to stand overnight, after which a second spectrum was recorded. The tubes were then placed under high-intensity UV light for 1 hour, and then a final NMR spectrum was recorded.

From these spectra (Figure 5.17), it was unfortunately somewhat difficult to accurately quantify how much of each gelator was incorporated into the network at any given time, due to the presence of the aromatic signals from DPIN and the overlap between signals. However, the disappearance of the signals could still be qualitatively observed. After being left overnight, the resonances associated with DBS-CO$_2$H were significantly reduced compared to those of DBS-Gly, as a result of the DBS-CO$_2$H being favourably reprotonated by the protons generated from GdL hydrolysis. After the exposure to UV light, the signals corresponding to both LMWGs had decreased further; those for DBS-Gly decreased very significantly, and those corresponding to the small remaining amount of DBS-CO$_2$H had disappeared completely.

This NMR experiment therefore supported the view that in the first activation step, GdL primarily activates DBS-CO$_2$H, and then in the second activation step, DPIN primarily activates DBS-Gly, with the two nanoscale networks being formed stepwise in the two individual steps. This study also showed that 1 hour of photoirradiation was sufficient for photoinitiated gelation to be complete, indicating no problems with slow kinetics in this system, in contrast to other examples of photoacid-activated gels.[268]
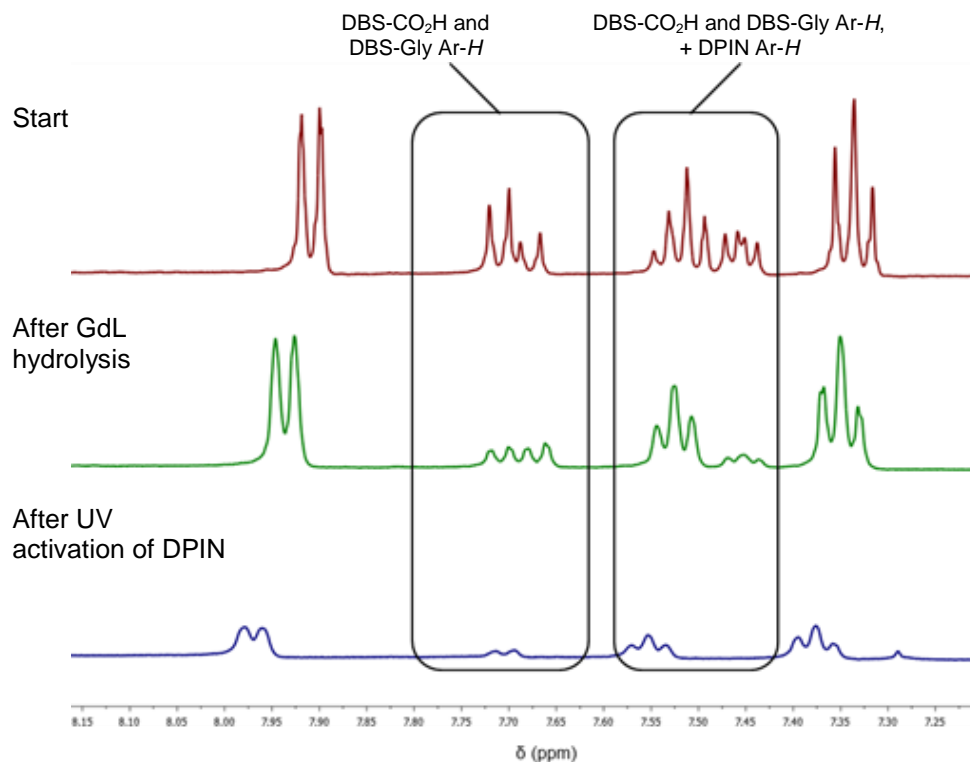
Figure 5.17: ^{1}H NMR spectra (aromatic region) for multicomponent gel of DBS-CO$_2$H and DBS-Gly (both 0.45% wt/vol), incorporating GdL (32.0 mM) and DPIN (23.3 mM) as proton sources. Spectra were recorded after initial preparation of the solution (top, red), after GdL hydrolysis (centre, green) and after UV activation of DPIN (bottom, blue). The highlighted peaks decrease in intensity after each proton source has been activated, showing incorporation of the LMWGs into solid-like networks.

5.5.2. Rheological studies of multi-component systems with dual activation

Rheological studies of these multi-component gels were attempted; as the gels were soft and quite fragile, they needed to produced directly on the rheometer plate. It was possible to analyse a gel formed after the first step (GdL hydrolysis), however, after UV curing to activate DPIN, the gel was observed to have significantly shrunk, due to heat-induced evaporation, even with measures in place to cool the sample. Therefore, due to this change in sample volume, there could be no accurate comparison of the gels before and after UV curing.

5.5.3. SEM images of multi-component systems with dual activation

Samples were prepared for SEM by first dissolving 24 mg of DPIN in 1.5 ml of water to make a stock solution. Then, 11.25 mg of both DBS-CO$_2$H and DBS-Gly were suspended in 1.25 mL of water by sonication, followed by the addition of 130 µl NaOH$_{(aq)}$ (0.5 M) to dissolve the solid. Next, 1.25 mL of DPIN stock was added to the DBS solution, followed by 20 mg of GdL. This solution was then divided into two 1.5 mL volumes in 8 mL vials. The vials were left overnight for

GdL hydrolysis to occur, after which a gel was observed to have formed. One sample was then cured under UV light for 1 hour (with a water bath used for cooling to prevent UV-induced heating effects from affecting gelation) to activate DPIN, after which time the gel had become visibly opaque.

A small portion of the gel was then freeze dried and coated in gold/palladium as described in Chapter 2. It was possible to use the freeze-drying method here as stable gels were formed, rather than the very weak gels or suspensions of partial gels when only DPIN was used as the proton source (see 2.4.4 though for a discussion on the limitations on the information that can be obtained from freeze-drying samples for SEM).

The SEM images of the multi-component gels both before and after UV activation of DPIN (Figure 5.18) show that the networks are very similar in appearance, indicating that the activation of DPIN does not have any major effects on the already formed nanostructure, nor are the nanostructures of (mostly) DBS-Gly formed as a result DPIN activation significantly different to those formed when GdL was used as a proton source.
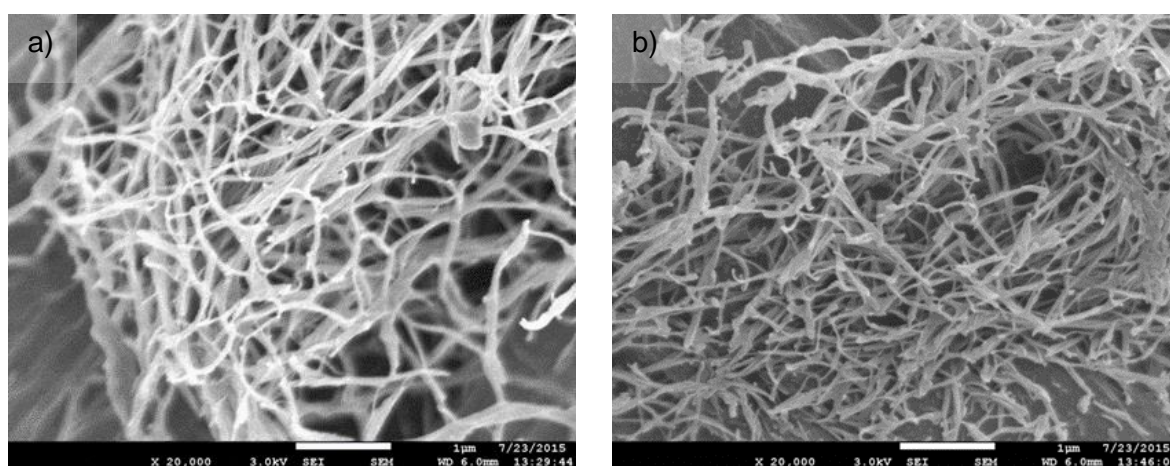
Figure 5.18: SEM images of multi-component gels of DBS-CO2H and DBS-Gly (0.45% wt/vol each), a) after GdL hydrolysis, and b) after both GdL hydrolysis and activation of DPIN. Scale bars = 1 μm.

5.6. Photopatterning to achieve spatial control in multi-component gels using dual activation methodology

The possibility of photopatterning these multi-component systems using the two different activators to achieve spatial control by positively "writing" one network into the other was then investigated. It was reasoned that the rapid kinetics of the photo-induced gelation combined with the assembly of DBS-Gly within a pre-formed gel of DBS-CO2H, hence preventing convection effects,[260] could potentially lead to excellent spatial resolution and precise control over the formation of multidomain gels (Scheme 5.3).
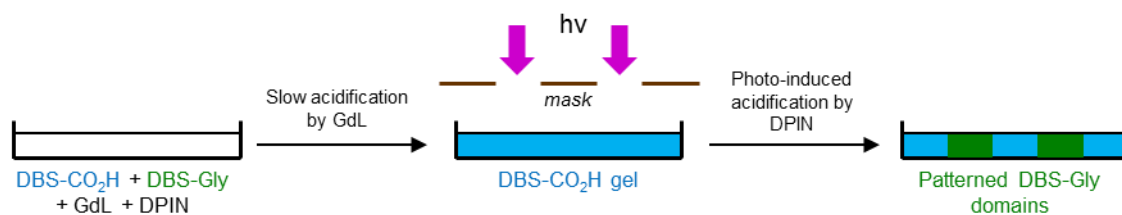
Scheme 5.3: Fabrication of photopatterned multi-component multidomain gels by two-step acidification process; in the first step, GdL activates DBS-CO₂H network formation, then in the second step UV activation of DPIN activates DBS-Gly network formation in the exposed regions.

5.6.1. Preparation of photopatterned multi-component, multidomain gels using dual activation methodology

To prepare such gels, 48 mg of DPIN was dissolved in 3 ml of water to make a stock solution. 22.5 mg of both DBS-CO₂H and DBS-Gly were suspended in 2.5 mL of water by sonication, followed by addition of 255 µl NaOH$_{(aq)}$ (0.5 M) to dissolve the solid. 2.5 mL of the DPIN stock was then added, followed by 20 mg of GdL. The solution was then transferred to a 5×5 cm square glass dish, and left overnight after which a translucent gel was observed to have formed. The NMR study described above, and the physical appearance of the gel, would support the view that the solid-like network of this material consisted mostly of a DBS-CO₂H network, with some (*ca.* 20%) DBS-Gly. A mask was then placed over the top of the mould, and the gel exposed to UV light for 1 hour – enough time to complete photo-initiated gelation as indicated by the previous NMR study. The mould was cooled in a water bath to prevent UV-induced heating effects from disrupting gelation. After photoirradiation, an opaque, well-resolved pattern was formed within the gel (Figure 5.19), indicating that only in those regions exposed to UV light through the mask was the PAG activated.
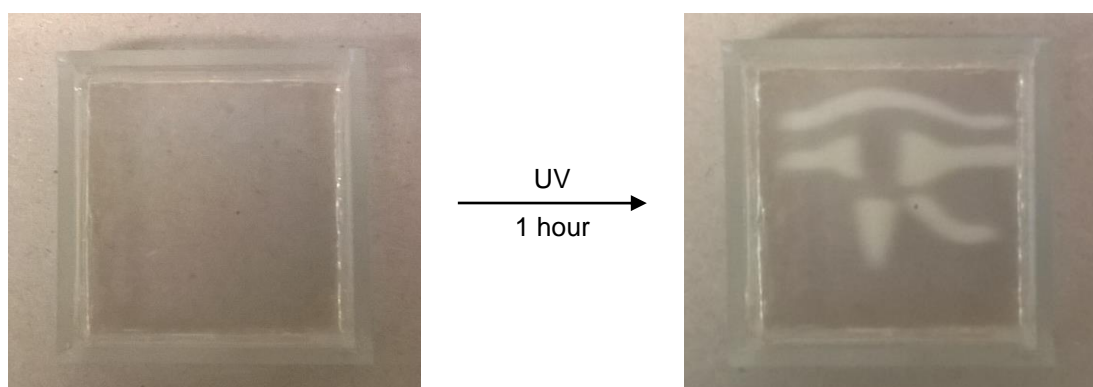
Figure 5.19: Photopatterning of a multi-component gel of DBS-CO₂H and DBS-Gly in 5×5 cm mould. After formation of a translucent gel (left) using GdL as the proton source, exposure to UV through a mask activates DPIN on the exposed regions, visualised by the gel changing from translucent to opaque as the second network forms (right).

To ensure that the protons generated by photoactivation of the PAG remained predominantly in the patterned region, and did not diffuse out to cause DBS-Gly network formation outside of the

patterned region, a control experiment using Congo Red as a pH indicator was performed. For this experiment, a photopatterned gel was prepared (following the above method) in which one half was exposed to UV light during curing, and the other half masked. After curing, the indicator was applied in small portions across the gel to determine whether there was a pH gradient across the material, or if the pH was distinct between the two domains. It was observed that in the domain where DPIN was not activated, the indicator remained bright red in colour, indicating a pH above *ca*. 5, whilst in the domain where the PAG was activated, the indicator became a red-purple colour, indicating a pH of *ca*. 4. Even after several hours, the colours did not appear to change, suggesting that in regions where DPIN is activated, the protons generated do not diffuse out, even after some time. This is supportive of the idea that the protons generated from activation of DPIN are associated with the self-assembled, solid-like DBS-Gly network, limiting their diffusion out of the photopatterned regions.
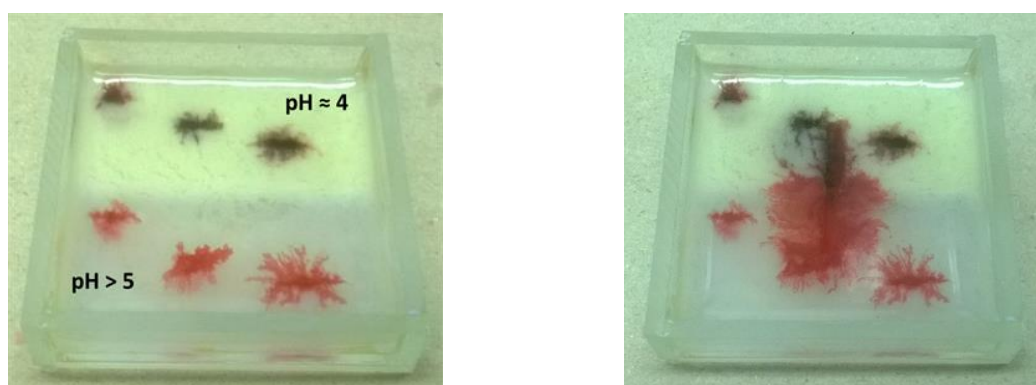
Figure 5.20: Photopatterned multi-component gel of DBS-CO$_2$H and DBS-Gly in which one half has been exposed to UV to activate DPIN (upper, opaque half) whilst one half was left unexposed (lower, translucent half). Congo Red indicator has been applied, showing that pH > 5 in the unexposed region, and pH ≈ 4 in the photopatterned region, indicating that the protons generated during DPIN activation remain in the patterned region (left). A line of Congo Red indicator was then applied to span the two regions, further showing the distinct difference in pH between the two regions (right).

5.7. Conclusions and Outlook

In this chapter, it has been shown that photochemical activation of carboxylic acid-functionalised derivatives of DBS is possible, using the PAG DPIN, which can be activated by UV light. At suitable sample depths, it was possible to form sample-spanning solid-like networks of self-assembled nanofibres for both DBS-CO$_2$H and DBS-Gly, and hence hydrogels. NMR studies showed that the use of the PAG as the proton source at suitable concentrations led to full reprotonation of the LMWGs, with the kinetics of assembly from this method leading to primarily 1D nanofibres being formed.

Most importantly, it has been demonstrated that it is possible to use two different proton sources – GdL and DPIN – in combination with one another to achieve a two-step dual activation process

of a multi-component gel of DBS-CO$_2$H and DPIN, in which the protons generated from GdL in the first step mainly drive formation of the DBS-CO$_2$H network, whilst the protons generated from DPIN in the second step drive the formation of the DBS-Gly network. Performing the second step of this process through a photo mask allowed for positive photopatterning of one LMWG network within the other, leading to a multidomain, spatially resolved supramolecular gel, in which there is also a degree of temporal control over when each network is formed (particularly the second network).

Concurrent with this research, Adams and co-workers published a similar study into spatially-resolved multi-component gels where the patterning was achieved by exposure to UV light.[273] These gels were formed from two structurally different LMWGS, one based on stilbene, the other a naphthalene dipeptide. Both LMWGs were pH-responsive, and having suitably differing pK_a values, their reprotonation occurred at different pHs; this allowed for production of a self-sorted multi-component gel. The stilbene-based gelator was also responsive to UV light, under which it would undergo isomerisation from *trans* to *cis* structure; the *cis* isomer was not an effective LMWG, and gels of just the stilbene-based gelator would undergo a *gel-sol* transition on exposure to UV. Hence, if the multi-component gel was exposed to UV through a mask, only in the exposed areas was the stilbene-based LMWG network broken down, leading to a gel photopatterned through a negative etching approach.

Spatial and temporal control over the formation of different networks in multi-component gels is also potentially achievable by other methods. Adams and co-workers have also investigated the use of an electrochemical method, in which an electrode was used to oxidise hydroquinone, releasing protons to trigger the gelation of pH-responsive dipeptide-based gelators, with the gel forming on the electrode surface.[274] Temporal control could be introduced to multi-component gels by the choice of the current applied to the electrode, determining the pH at a given time and if it was sufficient to promote gelator of one or both gelators in the multi-component system. Spatial control could be achieved by forming a layer of a gel of one LMWG on the electrode, then placing it into a solution of another LMWG and electrochemically triggering gelation.

Whilst both of these above systems achieved spatial resolution in the gels, they are not without potential problems. In the first example,[273] both gel networks needed to be formed before the "negative etching" patterning could be carried out; this could limit the overall detail possible in the patterning, particularly if most of the photodegradable network was required to be removed. In the second example,[274] achieving spatial resolution required removal and insertion of the gel-coated electrode, which disturbs the sample. The system described in this chapter does not have these associated problems, although the self-sorting of each network is not quite as good; future development would likely require this issue to be addressed. Additionally, it should be noted that

DPIN is not very biocompatible – a more biologically-friendly PAG would need to be used/developed if these materials were to be used in biomedical applications.

Looking further to the future of these systems, there is considerable potential for them. There is scope for morphological design using this photopatterning approach, limited only by the possibilities of photoactivation. This photo-activated approach to gelation could also be very simply combined with other different hydrogels (both LMWG and PG based) – for example those activated by heat-cool cycles rather than pH control. Such materials could be viable for controlled release or tissue engineering applications (if the issue of PAG biocompatibility is addressed). Furthermore, the use two-photon methods to activate the PAG could give rise to truly three dimensional multi-domain supramolecular gel architectures.

6. Chapter 6: Photopatterned Multidomain Multi-Component Hybrid Hydrogels

6.1.   Introduction

In Chapter 3, the spatial patterning of a hybrid hydrogel of DBS-CO$_2$H and PEGDM was examined, forming a material with two distinct regions, which was termed a multidomain gel. In Chapters 4 and 5, multi-component, self-sorting hydrogels of DBS-CO$_2$H and DBS-Gly were investigated, in particular it was demonstrated how to gain some degree of temporal control over the formation of the networks, and how orthogonally activated proton sources could be used to gain spatial control over the formation of the networks, to create a photopatterned multi-component, multidomain gel.

In this final research chapter, the possibility of combining both of the systems described above is examined. Firstly, the patterning of a LMWG within a PG matrix will be briefly examined. Secondly, as there is as yet no example in literature of a hybrid hydrogel containing three or more independent gel networks, the formation of such a gel will then be studied. Finally, this will be followed by an investigation into multidomain materials with three or more domains, which should in theory be possible to achieve with sequential use of activation methods for each of the three networks (i.e., PI for PEGDM, GdL for DBS-CO$_2$H, and DPIN for DBS-Gly).

6.2.   Photopatterned multidomain hydrogels of PEGDM and a LMWG

The main concern of combining the photoactivated PEGDM gel with the photoactivation of either DBS-CO$_2$H or DBS-Gly is that the same high-intensity UV lamp was used to activate both PI and DPIN to initiate gel network formation. Placing a solution of PEGDM with one of the LMWGs under the lamp would therefore result in both PI and DPIN being activated, so formation of both gel networks would begin at the same time. However, from kinetic experiments in Chapter 5, it is clear that complete DPIN-driven formation of the LMWG network takes significantly longer than the PI-driven formation of the complete PEGDM network (*ca.* 60 minutes vs. *ca.* 10 minutes). It was therefore reasoned that it might be possible to still obtain a reasonably resolution in a patterned hybrid gel using the same principles of kinetically controlled self-sorting as have previously been applied to pH-mediated gelation events.[29,30]

6.2.1.   Preparation of hybrid and photopatterned hybrid hydrogels of DBS-CO$_2$H and PEGDM

In Chapter 5, it was observed that photoactivation of either DBS-CO$_2$H or DBS-Gly through a PAG was most effective in shallow samples and containers. Therefore, the hybrid gels incorporating DPIN were only prepared in shallow glass moulds, as opposed to glass sample vials.

First, a hybrid gel with full bulk sample-spanning networks of both gelator networks was prepared to ensure that DPIN could be sufficiently activated. To achieve this, first a solution of DPIN (64 mg) in deionised water (3.98 mL) and HCl (20 μL, 0.5 M) was prepared, then 3 mL was added to a separately prepared solution of DBS-CO$_2$H (24 mg) in deionised water (2.8 mL) and NaOH$_{(aq)}$ (200 μL, 0.5 M). To this, 300 mg of PEGDM and 3 mg PI were added. Then, 5 mL of the resulting solution was poured into a 5 × 5 cm glass mould, followed by curing under high-intensity UV light for 1 hour (with cooling by ice to prevent any potential heat-induced effects). After this time, a robust, white, opaque gel was formed (Figure 6.1), the opaqueness confirming activation of the DPIN – and presumably formation of a network of DBS-CO$_2$H fibres.
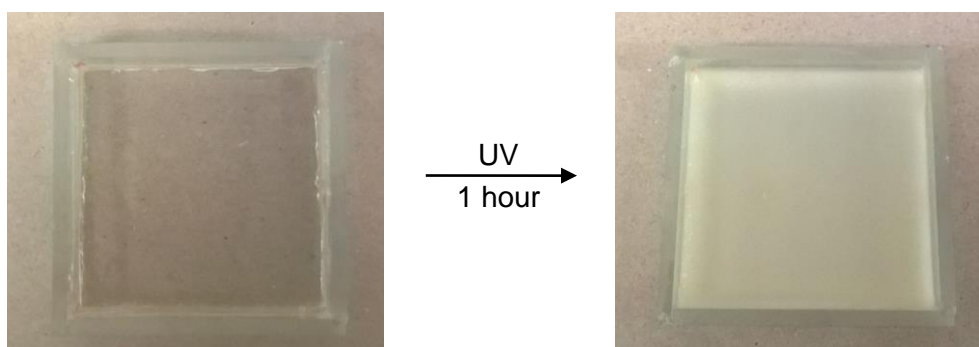
Figure 6.1: Formation of a hybrid hydrogel of DBS-CO$_2$H and PEGDM through photoactivation of both networks (PI-initiated for PEGDM, DPIN-initiated for DBS-CO$_2$H); a clear solution (left) becomes an opaque gel after 1 hour of exposure to high-intensity UV light.

Next, the resolution of patterning in the hybrid hydrogel was tested. A solution was prepared as described above, and poured into a 5 × 5 cm glass mould. This was then cured under UV for 10 mins, after which a robust, slightly translucent gel had formed, consistent with the polymerisation of the PEGDM polymer gel. A mask with a series of circles was then placed over the gel, and the sample was cured for another 50 minutes. After this time, opaque circular patterns were clearly visible in the final material (Figure 6.2) – indicating that significant further DPIN activation still takes place even after the initial ten minutes of photoirradiation, enough to produce good spatial resolution of both the patterning, and presumably the density of the DBS-CO$_2$H networks between patterned and "non-patterned" domains.
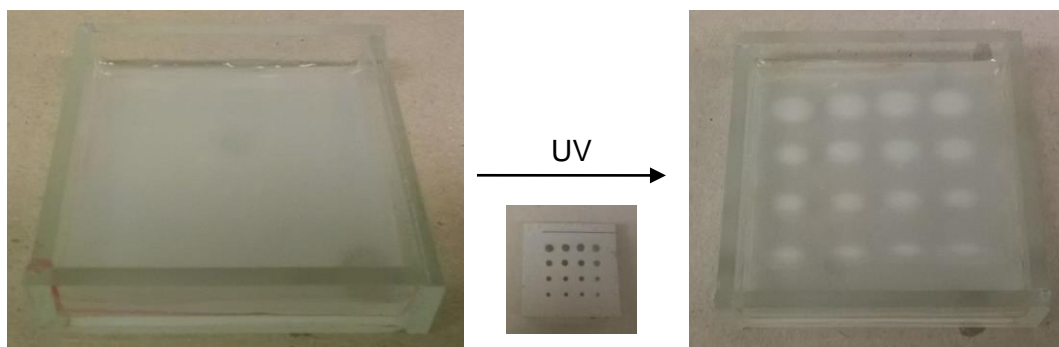
Figure 6.2: Formation of a photopatterned hybrid hydrogel of DBS-CO₂H and PEGDM through photoactivation of both networks; after 10 minutes of UV curing a translucent gel is formed (left); after application of a mask (centre) and 50 minutes of further UV curing, a pattern is visible in the gel (right).

Additionally, an alternative to using a cardboard mask for photopatterning was investigated, using patterns printed on acetate with a laser printer, inspired by the work of West and co-workers.[209] The advantage of making masks in this way is that it very simply allows for much more complex patterns to be generated than could possibly be cut out of cardboard. In these investigations, solutions of PEGDM, DBS-CO₂H, PI and DPIN were prepared as described above, then cured under UV for 10 minutes to gelate the PEGDM network, before the acetate was placed over the gel. An example mask and photopatterned gel are shown in Figure 6.3. This method showed great promise for creating patterns with greater resolution, though as can be seen, some of the finer detail was lost in the final photopatterned gel. From measurements, it appeared that good resolution was lost for any part of the pattern less than 1 mm in width.
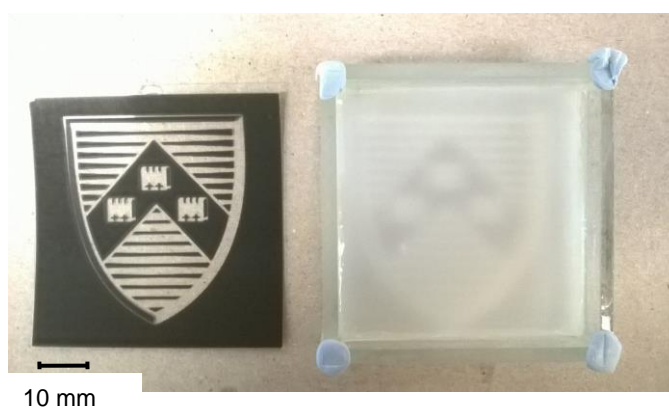
Figure 6.3: Photopatterned hybrid hydrogel of DBS-CO₂H and PEGDM through photoactivation of both networks; after formation of the PEGDM gel, the acetate photomask (left) was placed over the gel and after 50 minutes of further UV curing, a detailed pattern is visible in the gel (right). Scale bar = 10 mm.

6.2.2. Rheological studies of hybrid hydrogels of DBS-CO₂H and PEGDM

Unfortunately, rheological studies were not possible for these samples, due to the shrinking problems previously discussed in Chapter 5.

6.2.3. ^{1}H NMR studies of hybrid hydrogels of DBS-CO$_2$H and PEGDM

To prepare samples for NMR analysis, first DPIN (8 mg) was dissolved in 497.5 µL of D$_2$O, containing of 2 µL mL^{-1} DMSO as internal standard, followed by the addition of 2.5 µL HCl$_{(aq)}$ (0.5 M). Separately, 4 mg of DBS-CO$_2$H was dissolved in 466 µL D$_2$O (also containing 2 µL mL^{-1} DMSO as internal standard) through the addition of 34 µL NaOH$_{(aq)}$ (0.5 M). The two solutions were mixed, then 50 mg of PEGDM and 0.5 mg PI were added. 700 µL of the solution was transferred to an NMR tube; a spectrum of the solution was then recorded. The NMR tube was then placed under UV light for 1 hour, after which a second spectrum was recorded. Comparing the two spectra (Figure 6.4) revealed that nearly all of the DBS-CO$_2$H had been reprotonated, and had disappeared from the NMR spectrum, presumably being incorporated into a solid-like network.
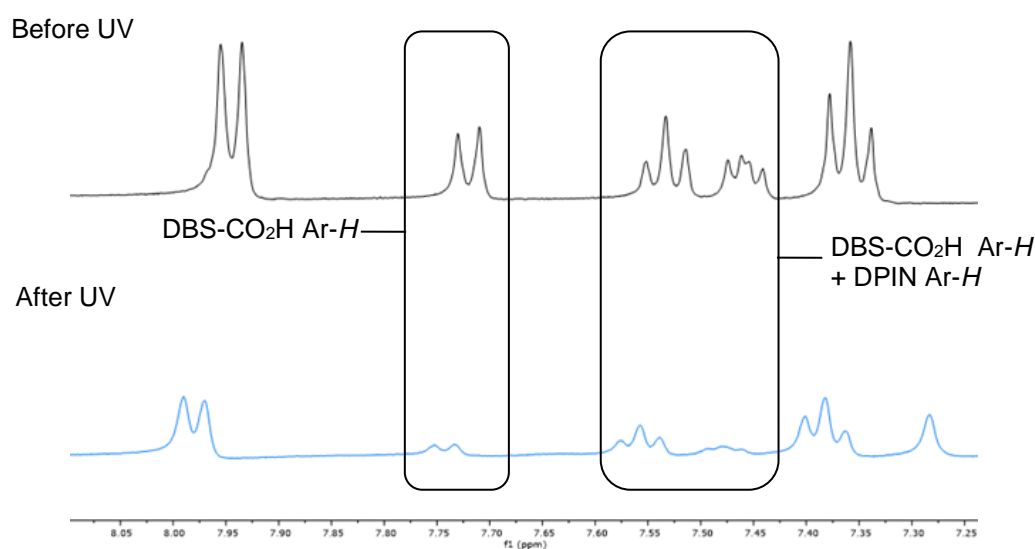
Figure 6.4: ^{1}**H NMR of DBS-CO$_2$H and PEGDM hybrid system with 8mg mL^{-1} DPIN as acidifying agent, before and after UV exposure of 1 hour. The significant reduction of DBS-CO$_2$H Ar-*H* peaks signifies that nearly all the LMWG has been reprotonated. Unlabelled peaks correspond to Ar-*H* protons of DPIN.**

NMR was then used to follow the kinetics of DBS-CO$_2$H assembly into solid-like nanostructures on photoactivation in the presence of PEGDM. To achieve this, samples of DBS-CO$_2$H with DPIN were prepared by first dissolving DPIN (160 mg) in 9.95 mL of D$_2$O, containing of 2 µL mL^{-1} DMSO as internal standard, followed by addition of 50 µL HCl$_{(aq)}$ (0.5 M). Separately, 80 mg of DBS-CO$_2$H was dissolved in 9.32 mL D$_2$O (also containing 2 µL mL^{-1} DMSO as internal standard) through the addition of 680 µL NaOH$_{(aq)}$ (0.5 M). The two solutions were mixed, 1 g of PEGDM and 10 mg of PI were added, and then 26 separate 700 µL volumes were transferred to NMR tubes. One tube was left uncured, whilst the other 25 were cured under UV light, with one tube being removed every 2 minutes over the course of 50 minutes for NMR spectra to be recorded. The concentration of mobile DBS-CO$_2$H in each sample was determined, and plotted against time (Figure 6.5). Interestingly, the assembly of DBS-CO$_2$H by photoactivation

with DPIN appeared to occur much faster in the presence of PEGDM than in the absence of it (25 minutes compared to 60 seen in Figure 5.10 in Chapter 5). This is also different from when GdL was used as the proton source – in that case, the assembly of DBS-CO$_2$H occurred at a much slower rate in the presence of PEGDM (see Figure 3.8 in Chapter 3). It is unclear as to why this should be the case, as the increased viscosity of the solution from addition of the polymer is often thought to limit diffusion;[84,85,107,181] it may be that there is energy transfer from activated PI to DPIN, increasing the rate of DPIN hydrolysis, and therefore the rate of DBS-CO$_2$H network formation. What these results also show is that there is immediate assembly of DBS-CO$_2$H, through activation of DPIN upon exposure of the sample to UV. This does mean the patterned gels in section 6.2.1 are not fully kinetically self-sorted, as both regions contain both gel networks – though the patterned domain should have a much greater percentage of assembled LMWG network.
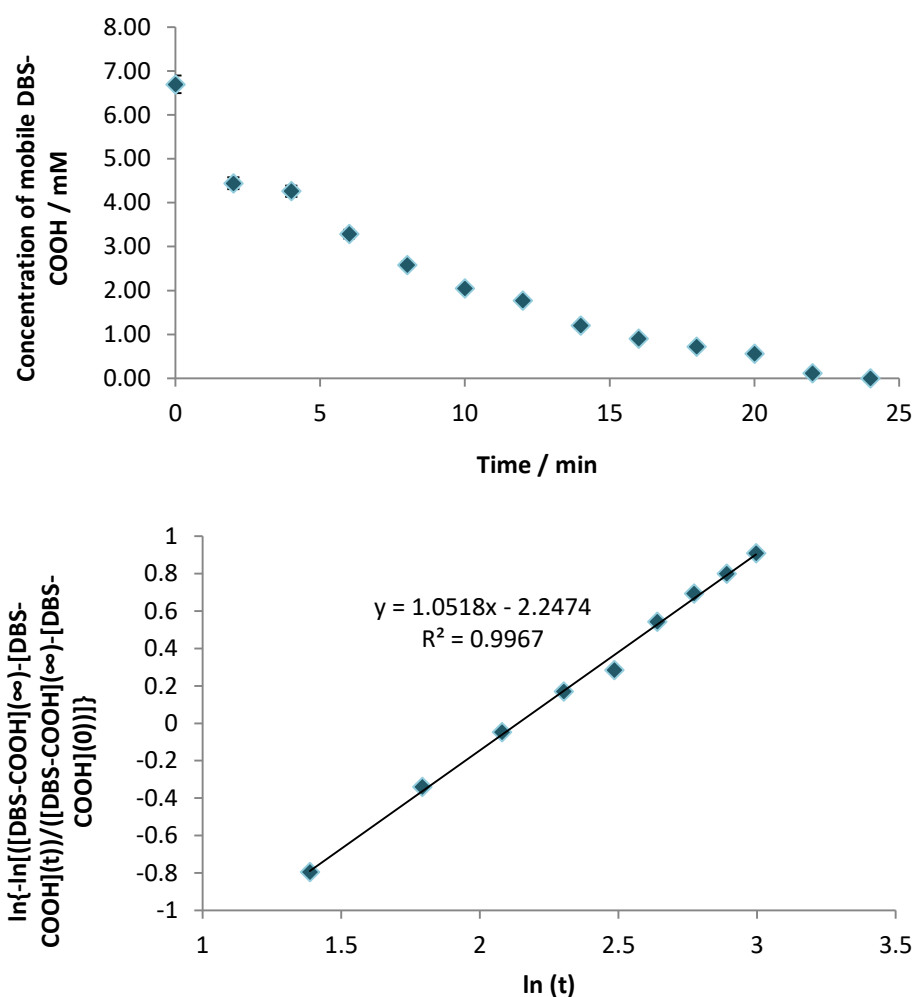
Figure 6.5: a) Plot of average rate of formation of the DBS-CO$_2$H network when using DPIN as the acidifying agent, in the presence of PEGDM, as monitored by ^{1}H NMR; b) Avrami plot for formation of DBS-CO$_2$H network, n = gradient of line = 1.05.

169

From the data, the Avrami exponent was calculated to be n = 1.05 - close enough in value (within the margins of experimental error) to that for DBS-CO$_2$H assembly activated by DPIN in the absence of PEGDM to suggest no significant difference in the assembly mechanism for the nanostructures (though see section 2.4.2 for comments on the use of the Avrami model with pH-responsive LMWGs).

6.2.4. CD studies of hybrid hydrogels of DBS-CO$_2$H and PEGDM

Unfortunately, CD spectroscopy studies of these hybrid hydrogels were not possible due to the strong bands corresponding to DPIN obscuring any bands associated with DBS-CO$_2$H.

6.2.5. SEM imaging of hybrid hydrogels of DBS-CO$_2$H and PEGDM

SEM was used to confirm the presence of nanofibres in the hybrid gels. The sample was prepared from very a small volume of gel made in a sample vial to the following method: 16 mg of DPIN was dissolved in 0.995 µL deionised water, followed by the addition of 5 µL of HCl$_{(aq)}$ (0.5 M). Separately, 2 mg of DBS-CO$_2$H was suspended in 232 µL of deionised water by sonication, followed by the addition of 18 µL NaOH$_{(aq)}$ (0.5 M) to dissolve the solid. 250 µL of the DPIN solution was added to the DBS-CO$_2$H solution, followed by 25 mg of PEGDM and 0.25 mg of PI. This solution was cured in an uncapped 2.5 mL sample vial under UV for 1 hour to produce a robust, opaque hydrogel. The gel was then prepared for SEM by the previously described freeze-drying method (see 2.4.4 for a discussion on the limitations on the information that can be obtained from freeze-drying samples for SEM).

From the SEM images in Figure 6.6, it can be clearly seen that there is indeed a fibrous nanostructure present in the hybrid hydrogel; these fibres are attributable to DBS-CO$_2$H, and they appear to be embedded/coated in the more film-like nanostructure formed by PEGDM. This would suggest that both PG and LMWG networks are present in the hybrid material.
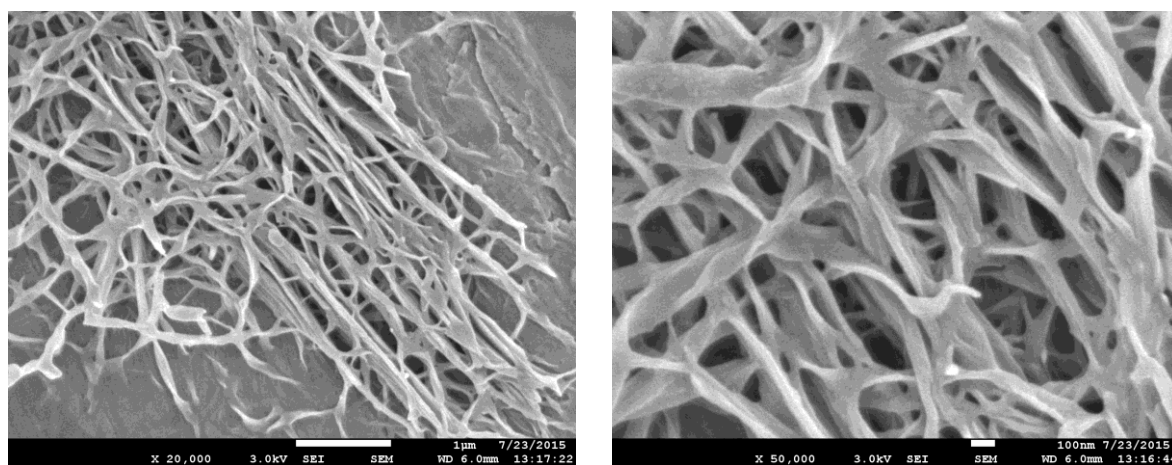
Figure 6.6: SEM images of the xerogels of hybrid hydrogels of DBS-CO$_2$H and PEGDM, produced using DPIN as PAG. Scale bars = 1 µm (left) and 100 nm (right).

6.3. Multi-component hybrid hydrogels of DBS-CO₂H, DBS-Gly and PEGDM with single proton source

Investigations then moved on to examine the controlled assembly of systems containing three gelators – one PG and two LMWGs. To begin with, multi-component hybrid hydrogels of PEGDM, DBS-CO$_2$H and DBS-Gly were prepared using only GdL as the proton source for the LMWGs, to ascertain if all three gelators (particularly the two pH-responsive LMWGs) would be able to form their independent networks in this multi-gelator system.

6.3.1. Preparation and T_{gel} studies of multi-component hybrid hydrogels with single proton source

To prepare the gels, 0.45% wt/vol of both DBS-CO$_2$H and DBS-Gly were added to a 1 mL solution of PEGDM (5% wt/vol) and PI (0.05% wt vol) in 2.5 mL sample vials, followed by sonication to disperse the solid. NaOH$_{(aq)}$ (0.5 M) was added in 10 µL aliquots to dissolve DBS-CO$_2$H, followed by GdL (18 mg). The uncapped vials were then cured under UV light for 10 minutes to obtain a clear PEGDM hydrogel, which was then left overnight for gelation of DBS-CO$_2$H and DBS-Gly to occur; by the next day, the gel had gone from clear to translucent, indicative of the formation of the LMWG networks (Figure 6.7) – though not indicative of the total percentage of each LMWG in the network, or indeed whether they were self-sorted.
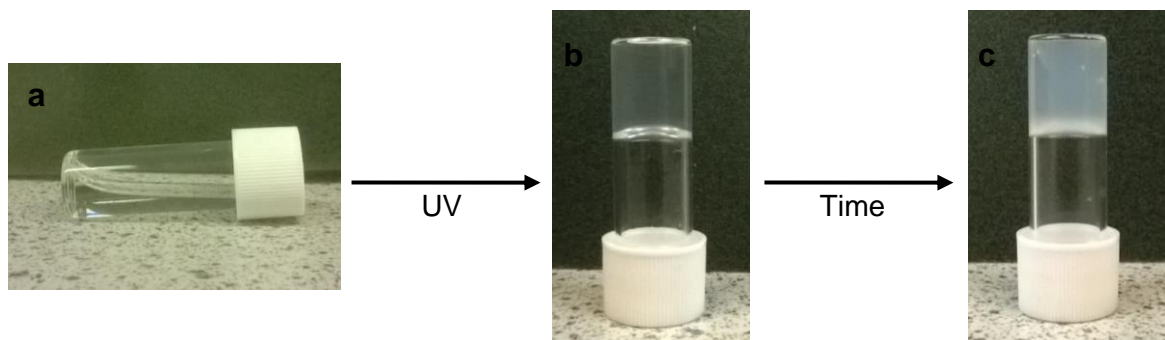
Figure 6.7: Formation of multi-component hybrid hydrogels of DBS-CO₂H, DBS-Gly and PEGDM; photoirradiation of a solution of all three gelators with PI and GdL (a) triggers photopolymerisation to form the crosslinked PEGDM network and to yield a clear gel (b); the gel goes from clear to translucent (c) as the LMWG networks forms over time with the slow hydrolysis of GdL.

Like the previously investigated PEGDM, and hybrid DBS-CO$_2$H and PEGDM hydrogels, the multi-component hybrid gels of DBS-CO$_2$H, DBS-Gly and PEGDM did not have T_{gel} values, nor showed any visible changes upon heating, attributable to both the robust nature of the crosslinked PEGDM gel and the thermal stability of the DBS-CO$_2$H and DBS-Gly networks.

6.3.2. Rheological studies of multi-component hybrid hydrogels with single proton source

6.3.2.1. Sample preparation

Samples were prepared for rheological analysis by the method described in Chapter 3 – i.e., simply adding 1 mL of the PEGDM containing solution to a sample vial with a diameter of 20 mm before UV curing. The solutions were prepared as described in section 6.3.1, using 50 mg (5% wt/vol) PEGDM, 0.5 mg (0.05% wt/vol) PI, 4.5 mg (0.45% wt/vol) DBS-CO$_2$H, 4.5 mg DBS-Gly (0.45% wt/vol) and 18 mg GdL. After UV curing, the gels were left overnight for hydrolysis of GdL to occur, leading to formation of the LMWG networks. The disc of prepared gel (*ca.* 3 mm in thickness) was then carefully removed from the vial before being placed on the rheometer.

6.3.2.2. Rheological measurements

After sample loading, the first tests to be performed were amplitude sweeps in order to determine the LVR for the various hydrogels. These were performed at a frequency of 1 Hz, with shear strain amplitude increasing from 0.01% to 100%. The typical results (blue data) were compared to those for a PEGDM gel (purple data) and a multi-component gel of DBS-CO$_2$H and DBS-Gly (orange data, previously presented in Chapters 3 and 4 respectively) (Figure 6.8); results from other runs were within ± 10% of the values presented here.
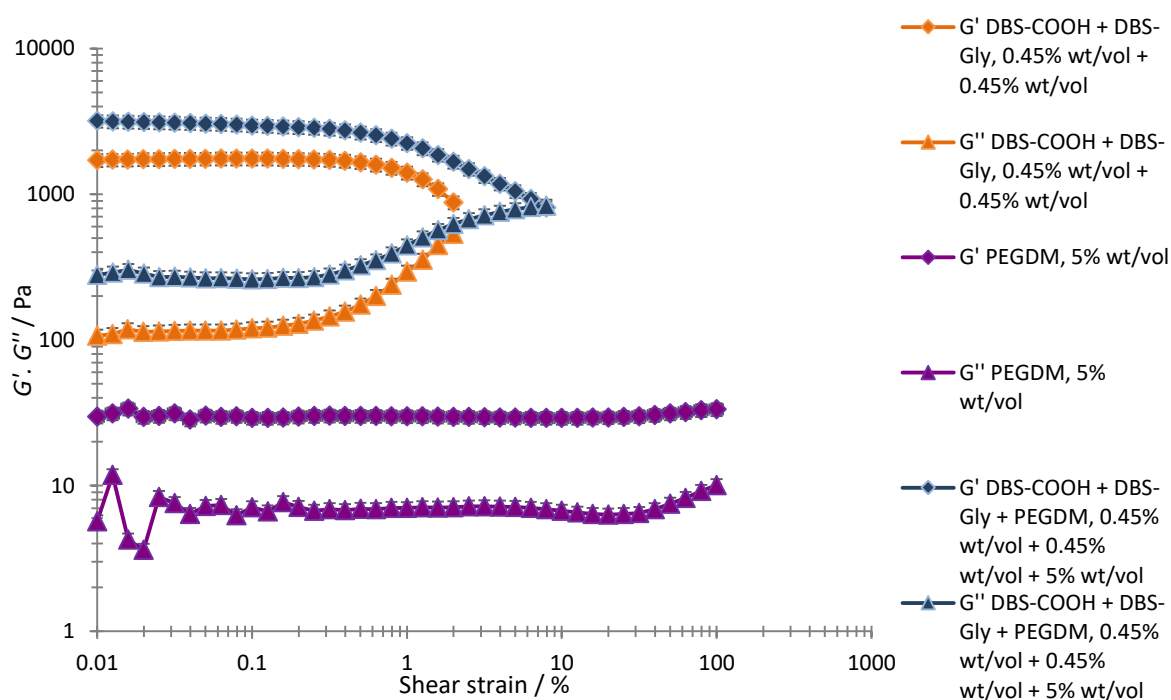
Figure 6.8: Comparison of typical results from amplitude sweep rheological analysis of DBS-CO$_2$H and DBS-Gly multi-component hydrogel, PEGDM hydrogel, and DBS-CO$_2$H, DBS-Gly and PEGDM hybrid hydrogel.

Figure 6.8 shows that, for the hybrid hydrogel of DBS-CO$_2$H, DBS-Gly and PEGDM, the values of the storage modulus *G'* are significantly larger than those of the loss modulus *G''*,

confirming the materials are definitely gels. In this case, the values of G' and G'' for the hybrid hydrogel are greater than those for either of the two individual gels; the hybrid hydrogel of DBS-CO$_2$H and PEGDM in Chapter 3 had values in between its two constituent components – possibly the much greater % wt/vol of LMWGs in the hybrid here give it better rheological properties in terms of G'. The LVR is also greater than that of the DBS-CO$_2$H and DBS-Gly multi-component gel, though there remains a notable crossover in the values of G' and G'' at *ca*. 8% shear strain, marking the breakdown of the gel. However, once again the PEGDM quite clearly increases the resistance to shear strain of the hydrogel, and its mechanical robustness and ability to be handled – in this case enhancing from *ca.* 2% strain to 6.5% strain.

Further mechanical analysis was conducted through a frequency sweep, at which the shear strain was kept constant at 0.3%. The frequency itself was again only varied between 0.1 and 1 Hz in this case, due to higher frequencies causing "slipping" of the rheometer geometry with PEGDM samples, producing unreliable results. The typical results (Figure 6.9) were again compared to those for a PEGDM gel (purple) and a multi-component gel of DBS-CO$_2$H and DBS-Gly (orange); results from other runs were within ± 10% of the values presented here.
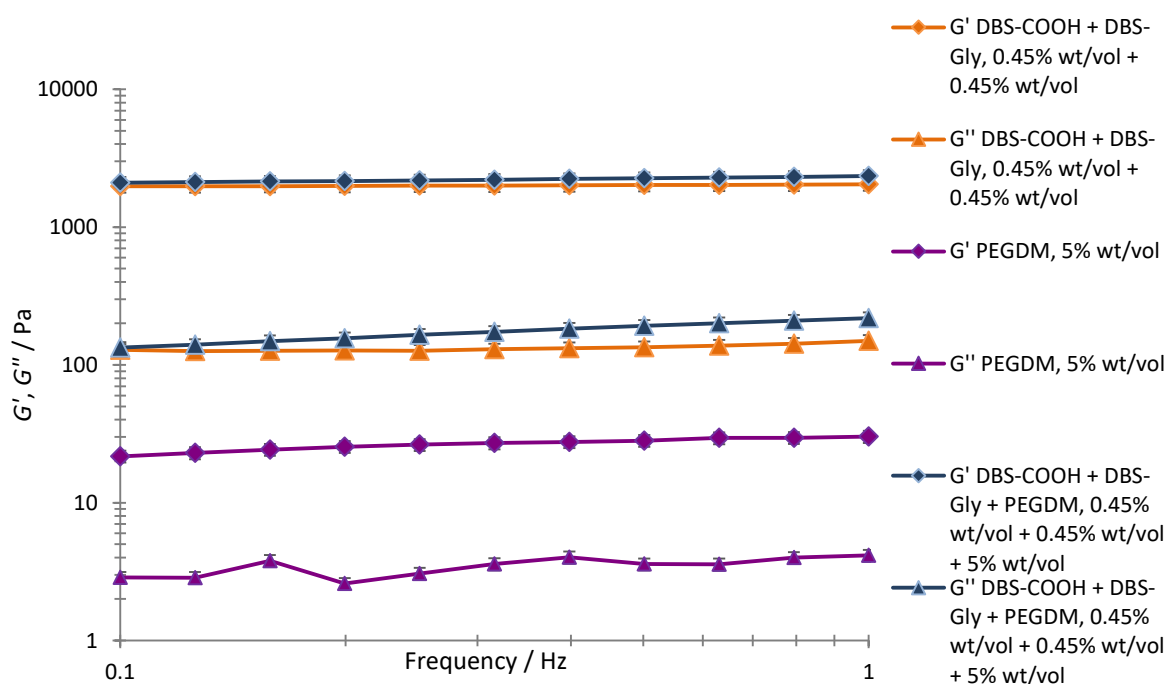
Figure 6.9: Comparison of typical results from frequency sweep rheological analysis of DBS-CO₂H and DBS-Gly multi-component hydrogel, PEGDM hydrogel, and DBS-CO₂H, DBS-Gly and PEGDM hybrid hydrogel.

From the frequency sweep analysis, it can be seen that at 1 Hz, the G' value for the hybrid gel is 2352 Pa, whilst the value of G' for DBS-CO$_2$H and DBS-Gly multi-component gel is only slightly less at 2044 Pa. As with the results from the amplitude sweep, it seems likely that the closeness in these values, rather than the hybrid value being significantly less that the multi-component value, is

due to the greater % wt/vol of LMWGs in the hybrid than in the previous rheological studies. In this case, the greater % wt/vol of the LMWGs has more of a contribution to the overall rheological profile of the material, countering the effects of the higher %wt/vol of the PEGDM – there is a much denser network of the rigid LMWG fibres to reinforce the overall solid-like structure of the gel. As the *G'* values for the hybrid and multi-component gel are so close, it cannot be concluded that the hybrid necessarily has a higher *G'* value, as the difference is within the range of accepted experimental error/ variation for this technique.

6.3.3. ^{1}H NMR studies of multi-component hybrid hydrogels with single proton source

Hybrid hydrogels of DBS-CO$_2$H, DBS-Gly and PEGDM were prepared for ^{1}H NMR studies by adding D$_2$O (0.7 mL) to DBS-CO$_2$H (3.15 mg) and DBS-Gly (3.15 mg), followed by sonication to disperse the solid. NaOH$_{(aq)}$ (0.5 M) was added in 10 µL aliquots to dissolve all solid, and DMSO (1.4 µl) was added as an internal standard. GdL (12.6 mg), PEGDM (35 mg) and PI (0.35 mg) were then added, and the solution was transferred to an NMR tube. UV photopolymerisation was then carried out by placing the NMR tube under UV light for 10 minutes.

Using the "snapshot" method, recording spectra immediately after UV curing and again after the sample was left for 24 hours for GdL hydrolysis to occur, it was seen that, as for with previous hybrid gels, nearly all of the DBS-CO$_2$H and DBS-Gly were immobilised and incorporated into LMWG networks (Figure 6.10).
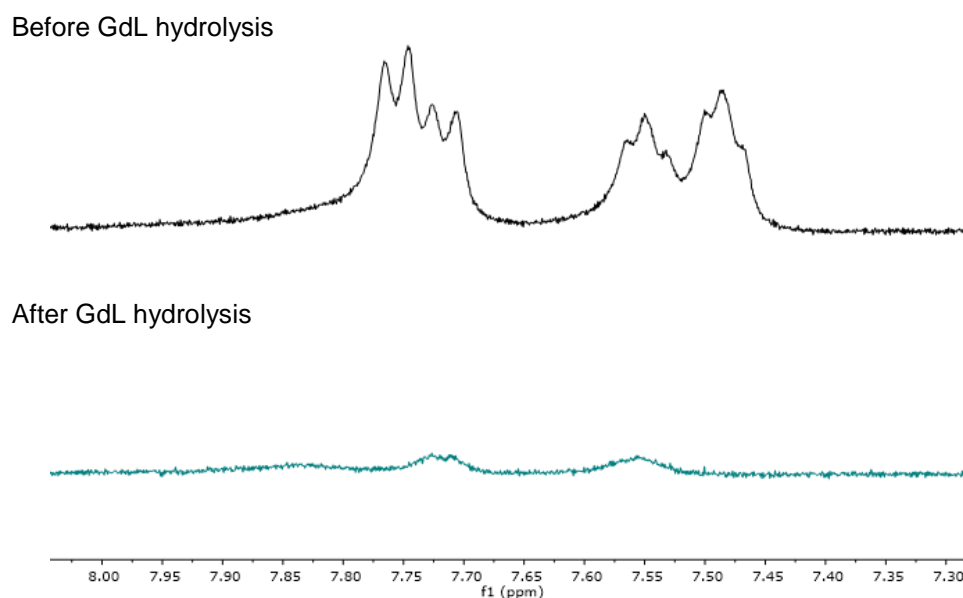
Figure 6.10: ^{1}H NMR spectra (aromatic region) for multi-component gel of DBS-CO$_2$H and DBS-Gly (both 0.45% wt/vol) and PEGDM (5% wt/vol), using GdL (101 mM) as proton source. Spectra were recorded after initial preparation of the PEGDM gel (top, black), and after GdL hydrolysis (bottom, blue).

More detailed kinetic information was then obtained by recording ^{1}H NMR spectra every 30 minutes following the addition of GdL and photopolymerisation, and plotting the concentration of mobile LMWGs versus time (Figure 6.11a). Unfortunately, due to experimental limitations, spectra could only be recorded up to 14 hours; whilst this was sufficient time for DBS-CO$_2$H to form a complete network, it was not enough time for DBS-Gly to do the same (though from the above experiment DBS-Gly is evidently almost completely in a solid-like network after 24 hours). This represents a marked increase in the amount of time needed for each LMWG to forms its network compared to being individual gelators (Chapters 2 and 4) or in a multi-component system with a similar excess of GdL (Chapter 4). This is again most likely due to the increase in the viscosity of the solution brought about by the presence of the polymerised PEGDM limiting the rate of diffusion.[84,85,107,181]
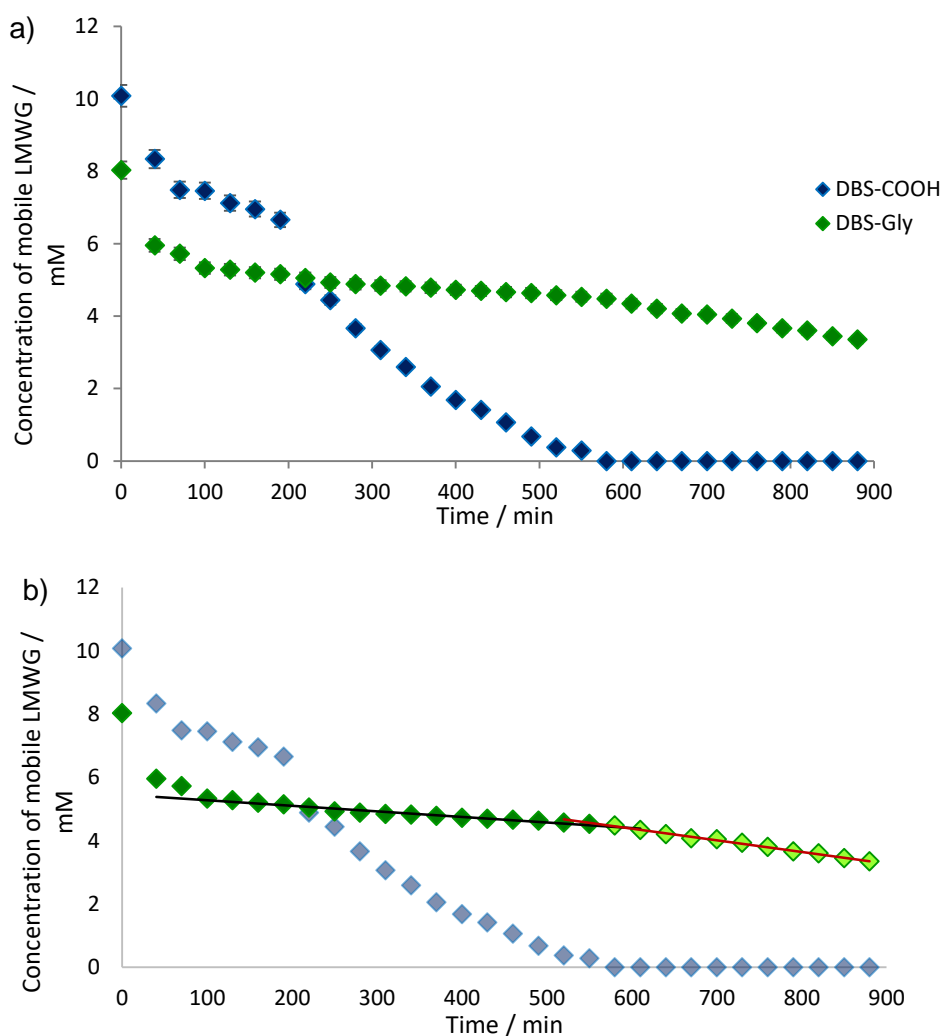
Figure 6.11: a) Plot of average rate of formation of the DBS-CO$_2$H (blue) and DBS-Gly (green) networks in the presence of PEGDM; b) the same plot with the two different periods of assembly of DBS-Gly highlighted (dark green diamonds and black line, light green diamonds and red line).

Unlike previous kinetic experiments, the data in this case could not be satisfactorily fitted to Avrami's kinetic model;[160–163] this is due to one of the required parameters being the concentration of LMWG at the start of fibre growth. For DBS-Gly fibres, as can been seen in Figure 6.11b (similar to that in Figure 4.15 in Chapter 4), there are two distinct periods of assembly – a relatively slow assembly whilst DBS-CO$_2$H undergoes more rapid assembly, then a slightly more rapid assembly of DBS-Gly once DBS-CO$_2$H is completely assembled into a network. As the rates of assembly in these two periods are different, it could be said that DBS-Gly assembly does not properly start until after complete assembly of DBS-CO$_2$H – so this would mean the starting concentration of DBS-Gly is not 8.03 mM, but whatever the concentration is at the time its more rapid assembly begins. This value is quite subjective, which means very variable Avrami numbers (n) could be derived, so the accuracy of any of these values would be questionable; this is especially the case as the assembly rate of DBS-Gly is quite low.

6.3.4. CD studies of multi-component hybrid hydrogels with single proton source

Samples of the hybrid system prepared for CD were prepared with sub-gelation amounts of the gelators (0.045% wt/vol DBS-CO$_2$H, 0.045% wt/vol DBS-Gly and 0.5% wt/wt PEGDM), so as previously discussed in other chapters, what was observed by this technique was not the formation of a sample-spanning network, but the assembly of the nanofibres.

From the spectrum (Figure 6.12) of the system of DBS-CO$_2$H (0.045% wt/vol), DBS-Gly (0.045% wt/vol) and PEGDM (0.5% wt/vol) after standing for 5 hours, a CD band at with a maximum at *ca.* 261, associated with DBS-CO$_2$H, was clearly visible. The intensity of this band was much greater (*ca.* -168 mdeg) than any previously observed; this may be in part due to increased concentration of DBS-CO$_2$H compared to when previously examine by CD in the presence of a PG (0.045% wt/vol in this case versus 0.02% previously), or due to the presence of PEGDM allowing the DBS-CO$_2$H nanofibres to access a more thermodynamically stable form, or even possibly due to some co-assembly with DBS-Gly. Alternatively, it could be due to a much greater value of HT than previously observed for any other sample with DBS-CO$_2$H – in this case the value of HT at 260 nm was *ca.* 500 V, compared to the previously seen values of *ca.* 300 V or less. As with previous CD analysis of samples with DBS-Gly and GdL, the band(s) associated with DBS-Gly were unfortunately obscured by the broad band associated with gluconic acid. What this study did show is that at least DBS-CO$_2$H was able to access a similar chiral nanostructure to that previously seen when combined with either DBS-Gly or PEGDM.
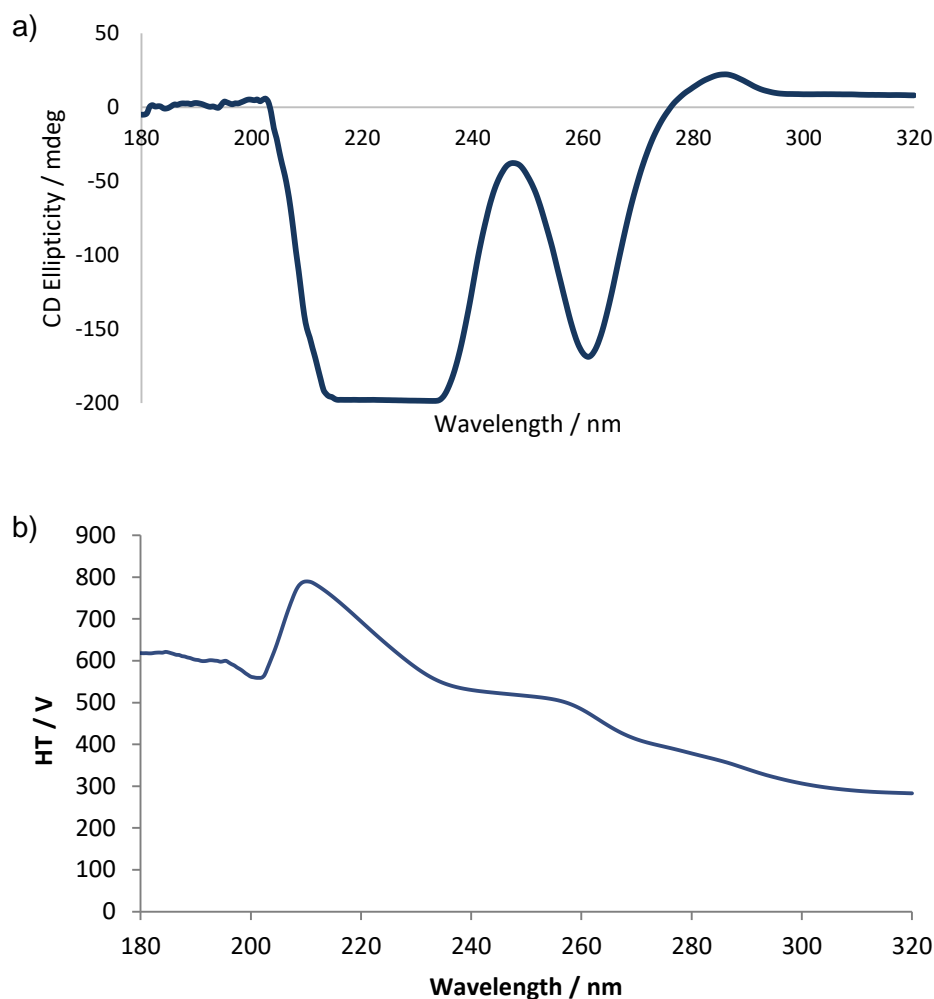
Figure 6.12: a) CD spectrum of hybrid system of DBS-CO₂H (0.045% wt/vol), DBS-Gly (0.045% wt/vol) and PEGDM (0.5% wt/vol) after standing for 5 hours; b) HT data.

6.3.5.   SEM imaging of multi-component hybrid hydrogels with single proton source

Samples for SEM were prepared by the previously described freeze-drying method (see 2.4.4 for a discussion on the limitations on the information that can be obtained from freeze-drying samples for SEM). The xerogel of the multi-component hybrid hydrogel (Figure 6.13) clearly showed a LMWG fibre network coated with or embedded within the polymer films of PEGDM. Whilst this also does not confirm self-sorting of the two LMWG networks, it does show that the material is indeed a hybrid gel in terms of its nanoscale morphology.

177
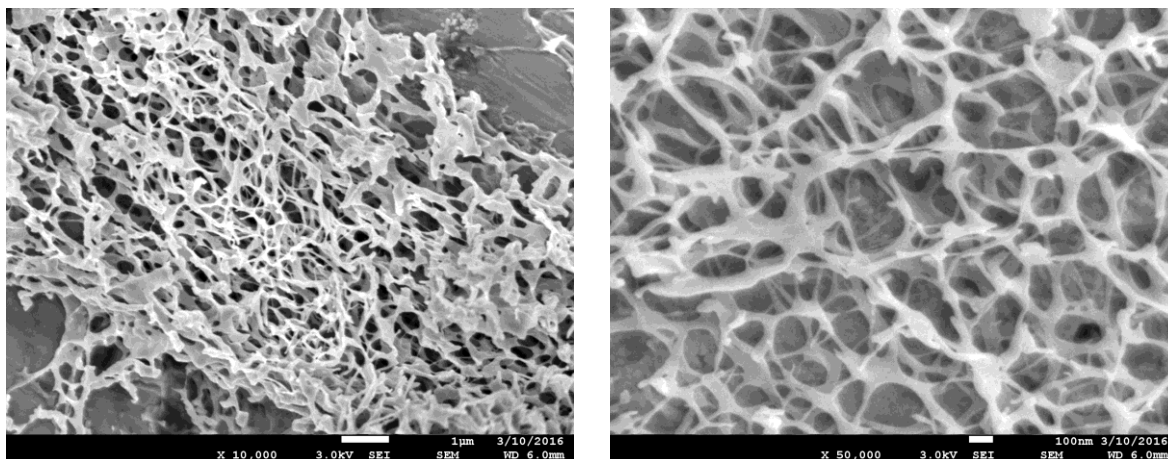
Figure 6.13: SEM images of xerogels of multi-component hybrid hydrogels of DBS-CO₂H (0.45% wt/vol), DBS-Gly (0.45% wt/vol) and PEGDM (5 % wt/vol); scale bars = 1 μm (left) and 100 nm (right).

6.4. Multi-component hybrid hydrogels of DBS-CO₂H, DBS-Gly and PEGDM with two proton sources

Having satisfactorily ascertained that all three gelators could form their networks in the same sample, the next step was to introduce DPIN as a second proton source for driving assembly of (chiefly) the DBS-Gly network.

6.4.1. Preparation of multi-component hybrid hydrogels with two proton sources

From Chapter 5, it was observed that photoactivation of either DBS-CO₂H or DBS-Gly through a PAG was most effective in shallow samples and containers. Therefore, the multi-component hybrid gels incorporating DPIN were only prepared in shallow glass moulds, as opposed to glass sample vials.

Initially, multi-component hybrid hydrogels with full sample-spanning networks of each gelator were prepared. To achieve this, first, 48 mg of DPIN was dissolved in 3 mL of deionised water. Separately, 22.5 mg of both DBS-CO₂H and DBS-Gly were dissolved in 2.245 mL deionised water, followed by sonication to disperse the solid and then addition of 255 μL NaOH$_{(aq)}$ (0.5 M) to dissolve. 2.5 mL of the DPIN solution was added to the LMWG solution, followed by 250 mg of PEGDM, 2.5 mg of PI, and 20 mg of GdL (calculated to be sufficient to form most of the DBS-CO₂H network but not the DBS-Gly network). The solution was poured into a 5 × 5 cm glass mould, and then cured under UV light (with cooling in an ice bath) for 10 minutes to form a robust, slightly translucent gel. The mould was then left to sit (covered, to prevent drying out) overnight for GdL hydrolysis to occur. The next day, the gel was observed to be slightly more translucent in appearance, indicative of the formation of a LMWG network. The gel was then cured under UV for

178

a further 50 minutes (again with cooling) to activate the remaining DPIN, with the final gel being robust, and opaque in appearance, indicative of the activation of DPIN and presumably further LMWG network formation (Figure 6.14).
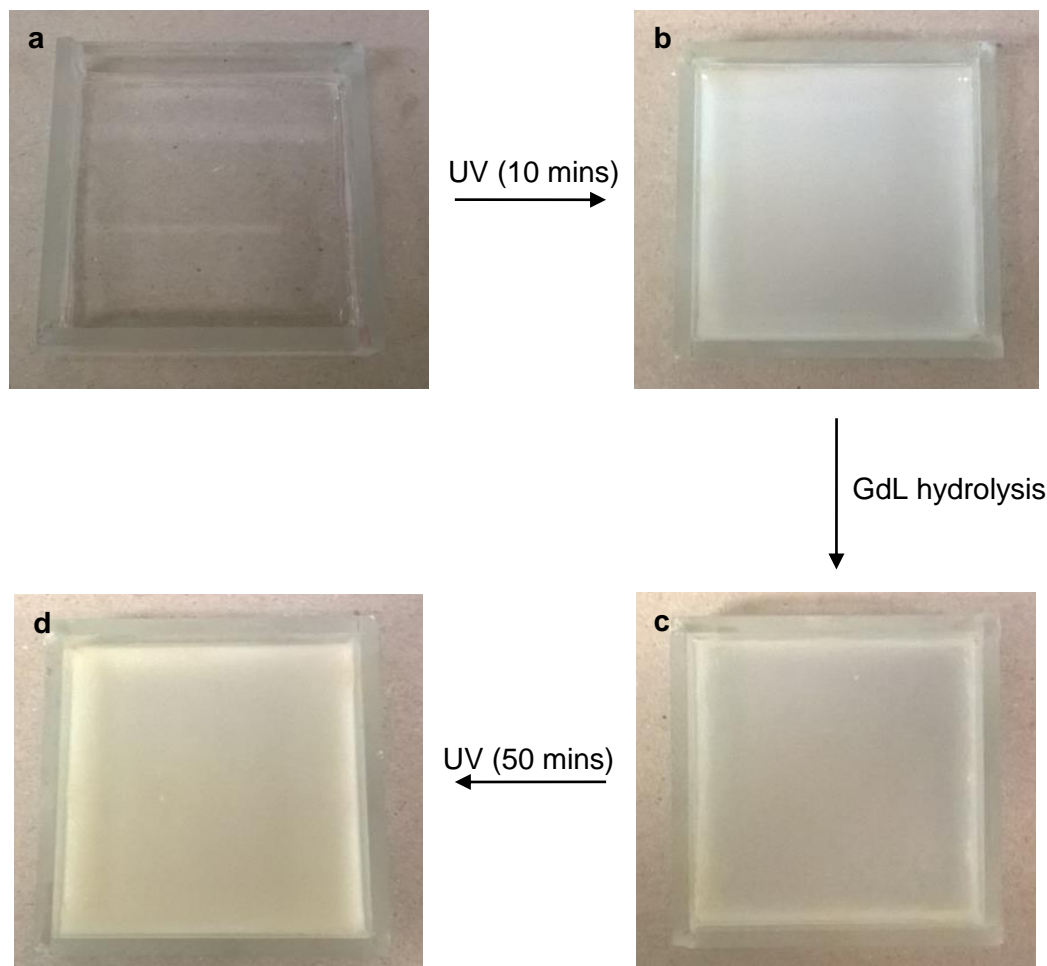
Figure 6.14: Stepwise formation of a multi-component hybrid hydrogel of DBS-CO$_2$H, DBS-Gly and PEGDM. A solution of all three gelators and PI, GdL and DPIN (a) is cured under UV light for 10 minutes to form a complete PEGDM gel (with a small amount of DPIN activation) (b); the gel is then left overnight for GdL to hydrolyse, and partial formation of the LMWG networks (mostly DBS-CO$_2$H) takes place (c); further curing under UV for 60 minutes then activates the remaining DPIN and LMWG network formation is completed, accompanied by production of iodobenzene, changing the gel from translucent to opaque (d).

6.4.2. Rheology of multi-component hybrid hydrogels with two proton sources

Unfortunately, rheological studies were not possible for these samples, again due to the shrinking problems previously mentioned.

6.4.3. ¹H NMR studies of multi-component hybrid hydrogels with two proton sources

Samples were prepared for NMR by first dissolving 8 mg of DPIN in 0.5 mL D$_2$O (with 2 µL mL^{-1} DMSO as an internal standard). Separately, 3.15 mg of both DBS-CO$_2$H and DBS-Gly were suspended by sonication in 0.3 mL D$_2$O, followed by addition of 51 µL of NaOH$_{(aq)}$ (0.5 M) to dissolve the solid. 0.35 mL of the DPIN solution was added to the LMWG solution, followed by 35 mg of PEGDM, 0.35 mg PI, and 4 mg of GdL. The solution was transferred to an NMR tube and cured under UV for 5 minutes to gelate PEGDM, after which an NMR spectrum was recorded. The NMR tube was then allowed to sit overnight for GdL hydrolysis to occur, then a second spectrum was recorded. Finally, the tube was then cured under UV for a further 30 minutes to sufficiently activate DPIN, and a third spectrum was then recorded.

From these spectra (Figure 6.15), it was unfortunately somewhat difficult – as in Chapter 5 – to accurately quantify how much of each gelator was incorporated into the network at any given time, due to again the presence of the aromatic signals from DPIN, the overlap between signals, and some broadening of the signals on this occasion. However, it was again possible to qualitatively observe the disappearance of the signals. After the initial, short UV curing to gelate PEGDM, resonances associated with both gelators and DPIN are clearly visible, as peaks associated with PEGDM (excluding the large resonance associated with the polymer chain CH$_2$s) had disappeared. After being left overnight, some of these resonances were significantly reduced, suggesting that DBS-CO$_2$H had been reprotonated by GdL hydrolysis. After the second, longer exposure to UV light, the signals corresponding to both LMWGs, and DPIN, had decreased further, as well as shifting upfield – the reason for this is unclear. Ultimately this experiment shows that the majority of the LWMG molecules were successfully reprotonated and incorporated into solid-like aggregates in a stepwise manner, therefore it seems plausible that there are three largely independent gel networks present in this material.
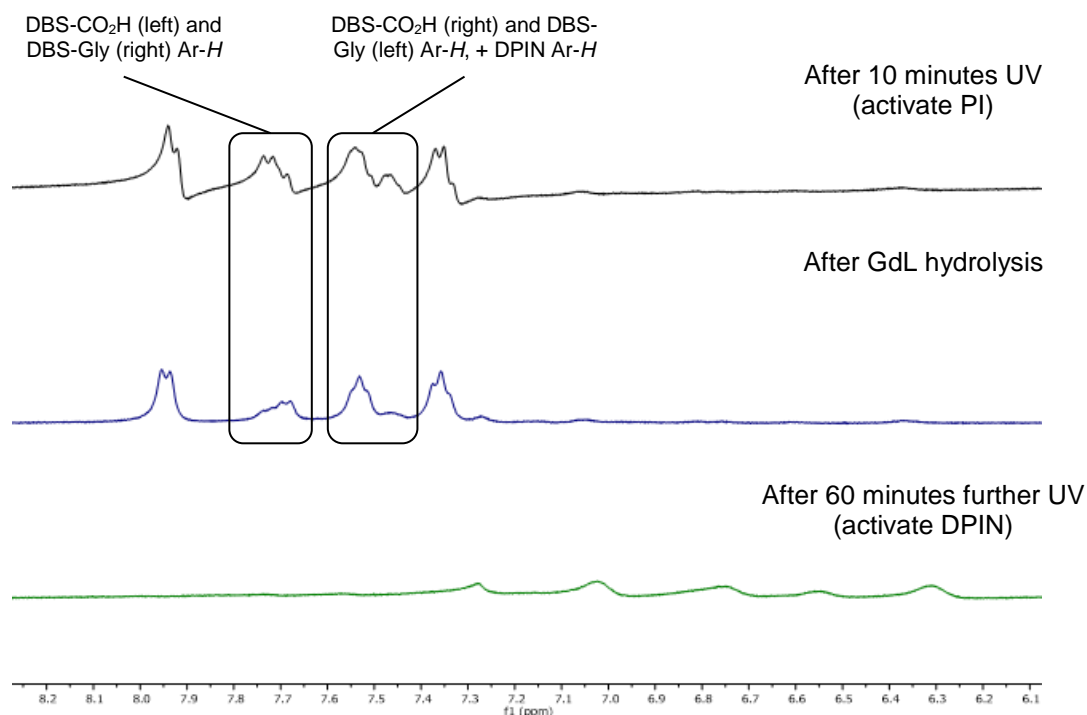
Figure 6.15: ^{1}H NMR spectra (aromatic region) for multi-component hybrid hydrogel of DBS-CO$_2$H, DBS-Gly and PEGDM (0.45% wt/vol of both LMWGs, 5% wt/vol PG), incorporating GdL (32.0 mM) and DPIN (23.3 mM) as proton sources. Spectra were recorded after initial UV curing of the solution (top, black), after GdL hydrolysis (centre, blue) and after UV activation of DPIN (bottom, green). The highlighted peaks in the first two spectra show a decrease in intensity after GdL has been activated; though the peaks are shifted upfield in the final spectrum, their further significant decrease indicates further incorporation of the LMWGs into solid-like networks. The peaks for DBS-CO2H and DBS-Gly overlap; the relevant "side" of each multiplet is assigned to the Ar-*H* of each LMWG. Unlabelled peaks correspond to Ar-*H* protons of DPIN.

6.4.4. CD studies of multi-component hybrid hydrogels with two proton sources

Unfortunately, CD spectroscopy studies of these multi-component hybrid hydrogels were not possible due to the strong bands corresponding to DPIN obscuring any bands associated with DBS-CO$_2$H and DBS-Gly.

6.4.5. SEM imaging of multi-component hybrid hydrogels with two proton sources

SEM was used to confirm the presence of nanofibres in the hybrid gels. The sample was prepared from very a small volume of gel made in a sample vial to the following method: 8 mg of DPIN was dissolved in 0.925 µL deionised water, followed by the addition of 4.5 mg of both DBS-CO$_2$H and DBS-Gly. The sample was then sonicated to suspended the solid, then 75 µL of NaOH$_{(aq)}$ (0.5 M) was added to dissolve. This was followed by 50 mg of PEGDM, 0.5 mg of PI, and 4 mg of GdL. The solution was divided into two 0.5 mL volumes in separate 2.5 mL sample vials, and cured under UV for 10 minutes to achieve gelation of PEGDM. The samples were then left overnight for hydrolysis of GdL to occur, after which only one sample was then further cured

under UV for another 50 minutes to ensure full activation of DPIN. The gels were then prepared for SEM by the previously described freeze-drying method (see 2.4.4 for a discussion on the limitations on the information that can be obtained from freeze-drying samples for SEM).

The SEM images of the hybrid multi-component gels both before and after UV activation of DPIN (Figure 6.16) show that the networks are very similar in appearance, on both occasions appearing to be coated/embedded within the more film-like nanostructure of PEGDM. Though the nanostructure of the gel before DPIN activation appears to be more "globular" in nature (Figure 6.16a and b), this may be due to variations in the freeze-drying process, or potentially due to there being less LMWG network present, hence it would be more thickly coated in the polymer upon freeze-drying. Importantly though, these images show again that the activation of DPIN does not have any major effects on the already formed nanostructure.

After GdL hydrolysis:
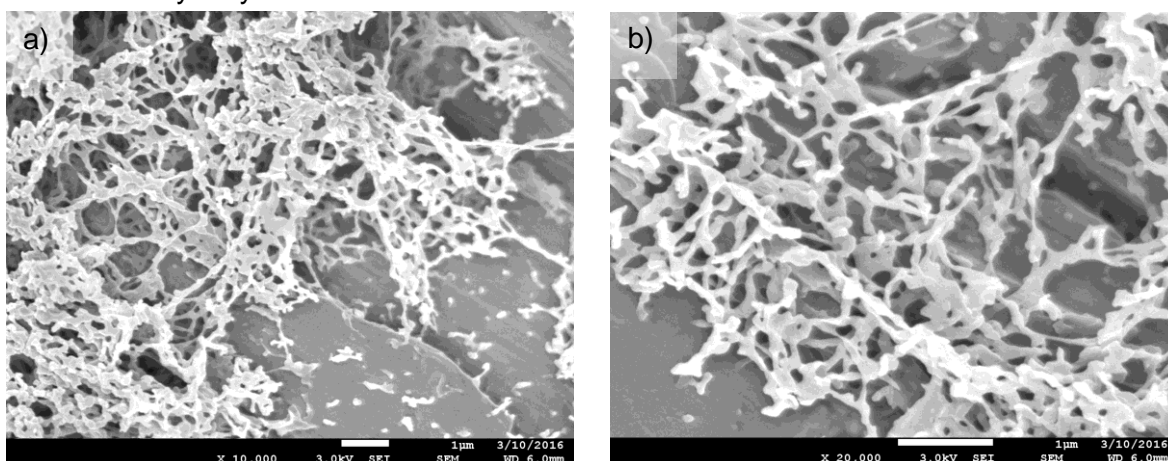
After DPIN activation:
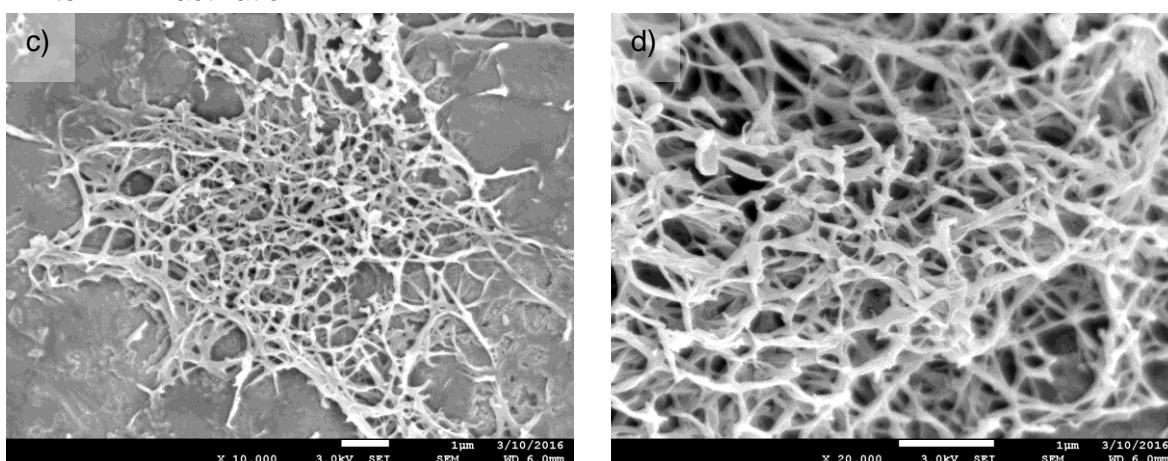
Figure 6.16: SEM images of multi-component hybrid hydrogels of DBS-CO$_2$H, DBS-Gly (0.45% wt/vol each) and PEGDM (5% wt/vol), a) + b) after GdL hydrolysis, and c) + d) after both GdL hydrolysis and activation of DPIN. Scale bars = 1 µm.

6.4.6. Photopatterning of multi-component hybrid hydrogels with two proton sources

6.4.6.1. Three-domain multi-component hybrid hydrogel

For preliminary investigations into photopatterning, a solution of the three gelators (DBS-CO_2H, DBS-Gly and PEGDM), along with the activating agents PI, GdL and DPIN, was prepared according to the procedure given in section 6.4.1. This solution was then poured into a 5×5 cm glass mould, and a mask obscuring half of the sample was placed over it. The solution was then cured under UV light for ten minutes to gelate PEGDM, after which it was left overnight for hydrolysis of GdL to occur. The next day, the mask was rotated 90°, and the sample was cured under UV again, this time for a further 50 minutes, to fully activate DPIN – this would also activate PI in the previously masked region and cause further formation of PEGDM networks. The final gel is shown in Figure 6.17.

It was hoped that by this procedure what would be achieved was a gel with the following three different domains:

1. A domain consisting of all three gelator networks.
2. A domain consisting of PEGDM and mostly DBS-CO_2H networks (activated by GdL hydrolysis), gelling free DBS-Gly and inactivated DPIN.
3. A domain consisting of just mostly DBS-CO_2H gelling a solution of PEGDM, free DBS-Gly and inactivated DPIN.

"Domain 1": DBS-CO_2H, DBS-Gly and PEGDM networks
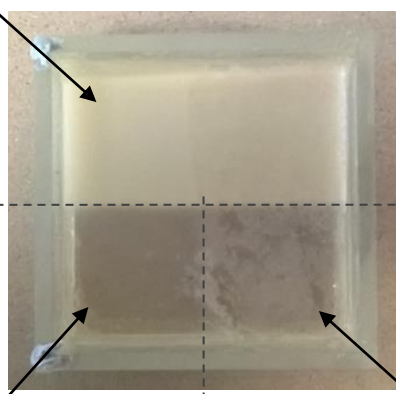
"Domain 2": DBS-CO_2H and PEGDM networks gelling free DBS-Gly

"Domain 3": DBS-CO_2H network gelling free PEGDM and DBS-Gly – this domain was very fragile

Figure 6.17: Photopatterned multidomain, multi-component hybrid hydrogel of DBS-CO_2H, DBS-Gly and PEGDM. Each domain is labelled to show which gel networks are present and which gelators remain largely free in solution.

Whilst this was achieved, it should be noted that after GdL hydrolysis (but before the second UV cure), the two domains without a PEGDM network (2 and 3) were observed to be very fragile in nature, and broke with just a slight disturbance of the mould. This was in contrast to when the multi-component gel of DBS-CO$_2$H and DBS-Gly using GdL and DPIN as proton sources was produced with the same concentrations of GdL and DPIN (see Chapter 5) – in that case the gel formed after just GdL hydrolysis, though soft, was reasonably stable. It is known that the presence of PEGDM seems to limit the diffusion of the mobile LWMG, causing the kinetics of network formation to be slower and having some effect on the final nanostructure – it is possible that these effects are the cause of the weakening of the gel formed through GdL hydrolysis in this case. Whilst a weak gel was not observed in the case of the multidomain gels of DBS-CO$_2$H and PEGDM in Chapter 3, it should be noted that in those gels GdL was present in excess, which would lead to a faster rate of formation of the LMWG network than when a controlled amount of GdL was used (as is done here).

6.4.6.2. Four-domain multi-component hybrid hydrogel

As the presence of PEGDM in the domains where it was designed to remain inactivated was not essential to the final gel, it was reasoned that after the first UV curing the non-gelled solution could be poured off and replaced by a solution of DBS-CO$_2$H and DBS-Gly (with GdL and DPIN) before GdL hydrolysis and subsequent DPIN activation. In this way, a true 4-domain gel could be achieved, and it would potentially improve the mechanical properties of the non-hybrid domains.

To this end, a solution of all three gelators, plus PI, GdL and DPIN was prepared as described above, poured in to a 5 × 5 cm glass mould, half-obscured with a mask, then cured under UV light for 10 minutes. After this time, the mould was half-filled with a PEGDM gel, and the remaining solution was poured off. It was replaced with 2.5 mL of a solution, prepared from DBS-CO$_2$H (11.25 mg), DBS-Gly (11.25 mg), DPIN (20 mg), GdL (10 mg), and NaOH$_{(aq)}$ (0.5 M, 130 µL) in 2.37 mL of deionised water. The mould was then allowed to sit overnight for GdL hydrolysis to occur, followed by the mask being rotated 90° the next day before a further 50 minutes UV curing to activate DPIN. The process of making this gel is shown in Figure 6.18.

It was hoped that this procedure would yield a gel with the following four different domains:

1. A domain consisting of all three gelator networks.
2. A domain consisting of PEGDM and mostly DBS-CO$_2$H networks (activated by GdL hydrolysis), gelling free DBS-Gly and inactivated DPIN.
3. A domain consisting of just mostly DBS-CO$_2$H gelling a solution of free DBS-Gly and inactivated DPIN.
4. A domain consisting of DBS-CO$_2$H and DBS-Gly networks (activated by GdL and DPIN).

Pleasingly, a gel with the appearance of four distinct domains was produced – this is shown in Figure 6.18d, with each domain labelled as above. Additionally, after GdL hydrolysis, the gel of DBS-CO$_2$H without PEGDM was on this occasion observed to be significantly less fragile. The only drawback to this method is that the second solution would often flow a little over the PEGDM gel before gelation, hence the four domains were not as neatly defined as in the three-domain gel. Despite this, after the second UV curing, this material could be considered a true four-domain multi-component hybrid hydrogel.
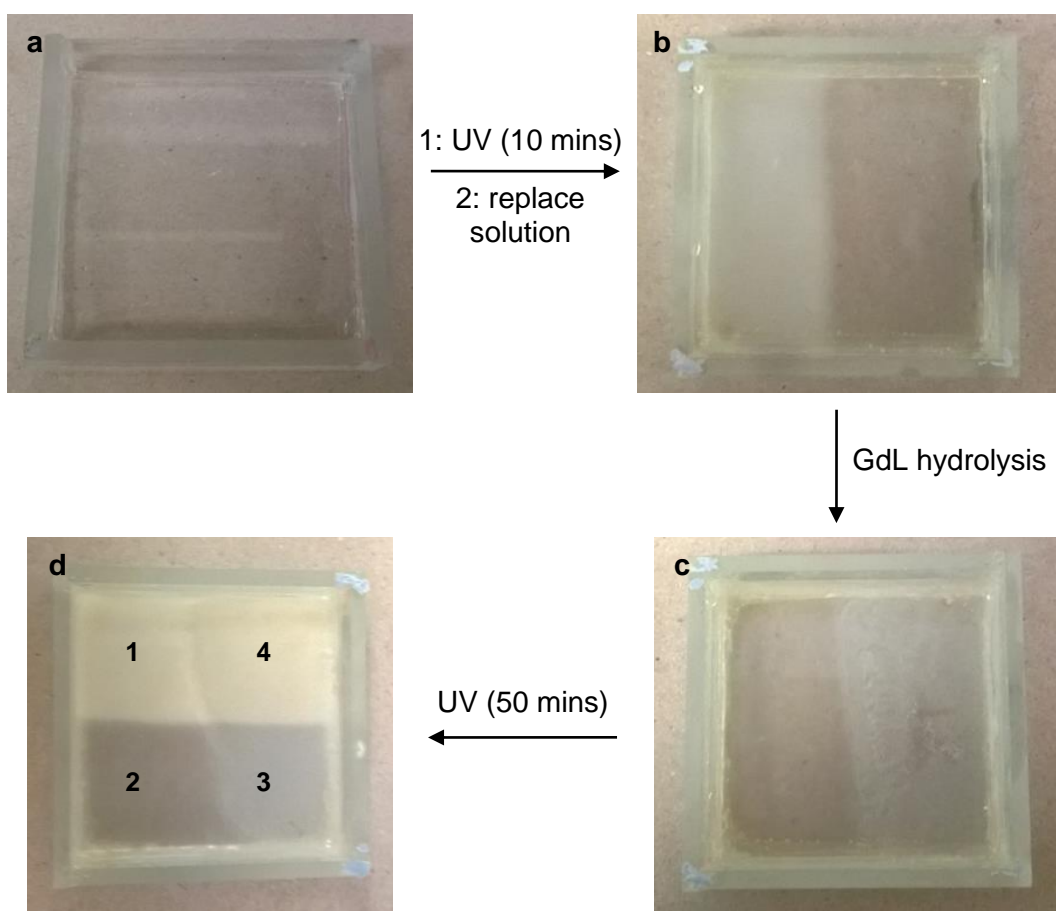
Figure 6.18: Stepwise formation of a four-domain multi-component hybrid hydrogel of DBS-CO$_2$H, DBS-Gly and PEGDM. A solution of all three gelators and PI, GdL and DPIN (a) is cured under UV light (with a mask obscuring half of the sample) for 10 minutes to form a complete PEGDM gel (with a small amount of DPIN activation), after which the remaining solution is poured away and replaced by one containing DBS-CO$_2$H, DBS-Gly, GdL and DPIN (b); the sample is then left overnight for GdL to hydrolyse, and partial formation of the LMWG networks (mostly DBS-CO$_2$H) takes place (c); further curing under UV (with the mask now rotated 90°) for 50 minutes then activates the remaining DPIN and LMWG network formation is completed, accompanied by production of iodobenzene, changing the gel from translucent to opaque, and completing formation of the four-domain gel (d); each domain is labelled according to the list given above.

6.5. Conclusions and Outlook

The hydrogels studied in this chapter have bridged the gap between the hybrid hydrogels examined in Chapters 2 and 3, and the multi-component gels in Chapters 4 and 5. To begin with, the two methods of photoactivating gel networks, DPIN and PI, were combined to yield multidomain gels of DBS-CO$_2$H and PEGDM. Due to the wavelength of UV used, both PI and DPIN were activated concurrently, meaning that in a patterned gel, both domains actually contained some of both networks. However, as DPIN takes much longer to be full activated, this meant that in photopatterning a good degree of kinetic resolution between domains could be achieved in the final gel. With these gels, it was also demonstrated that laser-printed acetate masks could be used in place of cardboard masks, allowing for more complex patterns to be produced – such complexity would be very useful in gels patterned for use in applications such as tissue engineering.

In the second main section of this chapter, the first (to current knowledge) example of a multi-component hybrid hydrogel containing three separate (or at least largely separate) networks was presented. Whilst not contributing much in the way of any functionality, this is an important development with regards to showing that three separate gel networks can potentially exist in the same material – particularly when one of those networks is a PG.

Finally, a multi-component hybrid hydrogel utilising both methods of forming the LMWG networks within a PG network was studied. The main problem with this material was not that it was a challenge to produce, but more that it was a challenge to analyse by the methods used for other gels. This was largely due to there being many components present in the one material, which led to overlaps between signals observed by spectroscopic methods, meaning a fuller understanding could not be easily obtained for the interactions (or lack of) between the gelators and their networks or the kinetics of gelation; rheology was also not possible for these samples as the heat from the UV lamp during photoactivation of DPIN caused the gels to shrink, preventing accurate comparisons between gels before and after DPIN activation. In spite of this, qualitative analysis suggested that all three gelators did indeed form their networks. Knowing this, and by carefully controlled stepwise activation of PI, GdL and DPIN within different regions, hydrogels with three and four domains were successfully produced – again, to current knowledge, this has not previously been achieved. Though the patterns produced were reasonably crude, it is highly likely that using laser-printed acetate masks would allow for much more complex patterning in these materials. The other main drawback still to be addressed is that both UV responsive component, PI and DPIN, activate at the same time – this could be easily rectified by using UV lamps with much more specific ranges than the high-intensity UV lamp that was available during this work, or by

changing one of the photoactivation agents such that it is activated at a significantly different wavelength.

Though these three- and four-domain hybrid hydrogels are very much "proof of principle systems", they are examples of gels in which there is both spatial and temporal resolution – the location and time of formation of each gel network being controlled. There is much scope for their future development, which could eventually yield materials very suitable for complex tissue engineering, where each domain allows for different stem cell differentiation depending on the materials properties of the domain,[275] potentially allowing for growth of replacement organs *ex-vivo*. Suggested future work and possible applications for these materials will be discussed in the next chapter.

7. Chapter 7: Conclusions and Future Work

Three main aims for this project were outlined in the introduction: (i) the combination of a LMWG with a PG to yield a material that could be described as responsive yet also robust; (ii) to achieve spatial resolution by controlling the formation of one gel network in space in the presence of another gel network; and (iii) to achieve temporal resolution by controlling the formation of gel networks in time. It could also be said that there were three main avenues of investigation for achieving these aims: simple hybrid hydrogels, multi-component hydrogels, and more complex multi-component hybrid hydrogels. In this concluding chapter, each avenue of investigation will be considered again, examining the key findings and how the aims were addressed. Whilst much of the work presented here has been very much "proof-of-principle" fundamental research, there is scope to use the increased understanding of these hybrid and multi-component gels for potential development into applications in the future, which will also be discussed.

7.1. Chapters 2 and 3: Simple hybrid hydrogels

The investigations into hybrid hydrogels began in Chapter 2 with the combination of the pH-responsive LMWG DBS-CO_2H and the thermally-responsive PG agarose. It was demonstrated that the LMWG retained its ability to self-assemble within the gel formed by the PG – making this material one of the first known examples of a hybrid gel where the two networks were formed by orthogonal methods, allowing for much better examination of the assembly of the LMWG network and the effects the PG network had on it. The unique property of this hybrid hydrogel, compared to other examples,[106–108,181,182] was that it was the first known example of a responsive yet robust hybrid hydrogel, in which the LMWG network could be repeatedly switched on or off (through addition of acid or base) whilst the PG network remained intact (Figure 7.1). As such, the aim of responsive yet robust hybrid hydrogels was achieved.[276]
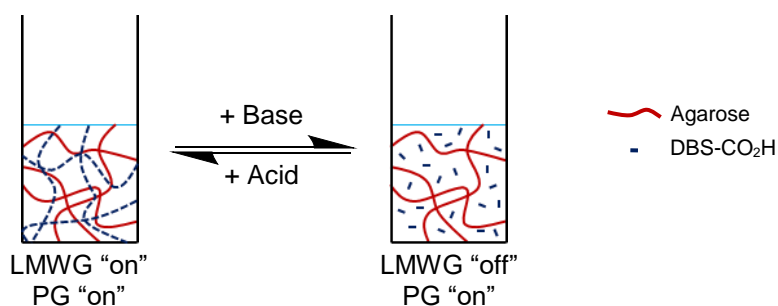
Figure 7.1: Illustration of the principle of the responsive yet robust hybrid hydrogel produced from the combination of DBS-CO_2H and agarose.

Following this, in Chapter 3, DBS-CO_2H was combined with the synthetic PG PEGDM – the first known example of a hybrid hydrogel utilising a synthetic PG. In this hybrid hydrogel, the

presence of the PG was shown to have a much greater effect on the assembly of the LMWG – something which will need to be taken into consideration for more complex systems. The functionality of this gel was again related to the properties of both its constituent networks. Firstly, as PEGDM gels are formed by exposure to UV light, controlled photoirradiation allowed for different regions to be spatially patterned, yielding materials with two distinct regions, termed multidomain gels – so in this way the second aim of spatially resolved gels was also achieved (Figure 7.2). Secondly, the controlled release of dyes from the hybrid gels was found to depend on both the density of the PG network, and potential interactions between the dye and the LMWG network.[277]

Solution of LMWG, PG, PI and GdL

Apply mask

UV

PG network forms in exposed region

GdL hydrolysis

LMWG networks forms throughout material
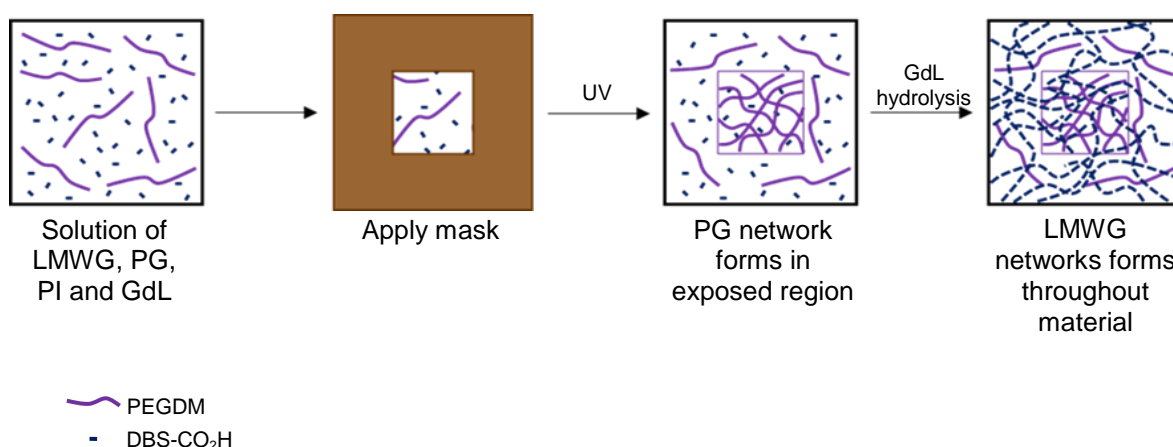
PEGDM
DBS-CO$_2$H

Figure 7.2: Illustration of the principle of making a multidomain hybrid hydrogel from the combination of DBS-CO$_2$H and PEGDM.

The controlled release applications of these simple hybrid hydrogels are perhaps the most amenable to be investigated in the near future. From the responsive yet robust system, it could be envisaged that a drug bound to the DBS-CO$_2$H network when at acidic pH would be preferentially released under basic conditions, as the gradual disassembly of the LMWG network would trigger diffusion of the drug out of the unaffected polymer gel. Either agarose, PEGDM, or another orthogonally assembling gelator could be used as the PG – the rate of diffusion would also be determined by the % wt/vol of the PG used. Such drugs to be bound to the DBS-CO$_2$H network would likely need a functional group to interact with the peripheral carboxylic acids of the LMWG fibres, such as an amine, and the conformation and size of the drug molecule would also need to be considered for effective release. Similar studies have shown that anti-inflammatory drugs interacting with DBS-CONHNH$_2$ (DBS-hydrazine) via hydrogen-bonding interactions were preferentially released at pH 8 (intestinal pH);[278] future work could use this gelator in place of, or in combination with, DBS-CO$_2$H and a PG.

For actual biomedical use the biocompatibility of these materials needs to be seriously considered. As a biopolymer (particularly one that is used in food) agarose is known to be very

biocompatible;[5] the biocompatibility of PEGDM can be improved by modifications (usually through insertion of enzymatically responsive groups between the photopolymerisable methacrylate groups and the poly(ethylene glycol) chain).[195–201] Therefore the main work in this area would be to ascertain the biocompatibility of DBS-CO$_2$H – the compound is not capable of supporting cell cultures, due to the LWMG network requiring a relatively acidic pH to form,[279] though this would not prevent its use in drug delivery applications, where positive interactions with cells are less critical, and toxicity (or lack of it) is the key issue. It is certainly the case that the DBS framework itself is non-toxic, being widely used in consumer products, such as deodorant sticks.[128–133,135,136]

7.2. Chapters 4 and 5: Multi-component hydrogels

The search for more biocompatible DBS-derived LMWGs was an initial drive into the investigation of coupling amino acids to DBS-CO$_2$H, which yielded the new LMWG DBS-Gly.[280] Although this is the only DBS-amino acid compound capable of gelation found so far, there still exists significant scope for investigation of other DBS-amino acid compounds as potential LMWGs, though some improvements to the synthesis procedure may be required to overcome issues including the solubility of intermediates, and the final solubility profile of the DBS-amino acid compounds. This work could potentially lead to obtaining of DBS-derivatives that act as heat-cool hydrogelators, rather than requiring a pH-mediated gel-forming stimulus. If these improvements were successful, it would be interesting to examine the coupling of di- or tri-peptides to DBS-CO$_2$H; a particular target could be the cell-adhesion sequence RGD (arginine-glycine-aspartic acid).

Whilst certain batches of DBS-Gly could act as heat-cool LMWGs, it was found to work most reproducibly as a pH-responsive LMWG. It was also found to have a significantly different pK_a value to DBS-CO$_2$H, which allowed for a mixture of the two gelators to at least partially kinetically self-sort. A degree of temporal control over when each network formed was possible by controlling the amount of the acidifying agent GdL that was used. This temporal control was taken further by introducing a second proton source in the form of the photoacid generator DPIN to achieve a two-step dual activation process, where protons generated from GdL mainly drove formation of DBS-CO$_2$H, then the protons from DPIN activation mainly drove formation of the DBS-Gly network (Figure 7.3). Therefore, as it could be chosen when the DBS-Gly network was formed, this was another form of temporal control over network formation, and hence in this way the third aim of the project was achieved.[280]

Solution of both | Network of | Networks of
LMWGs, GdL | predominantly | both LMWGS
and DPIN | one LMWG |
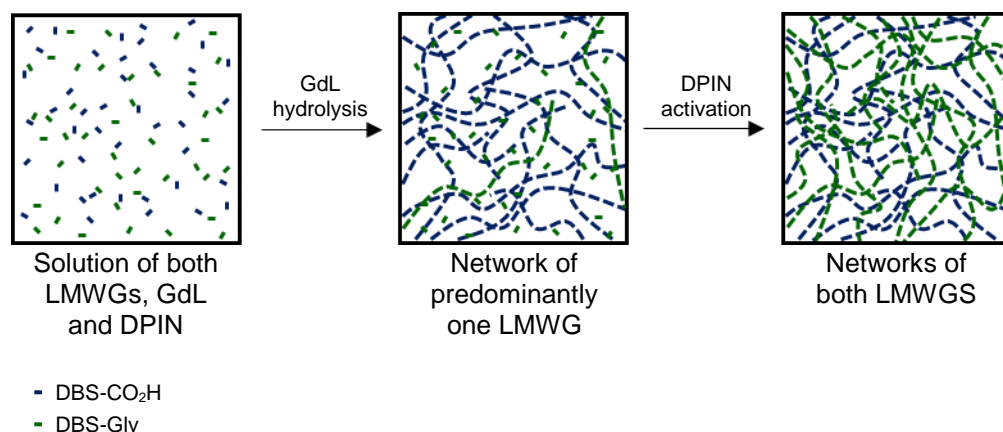
- DBS-CO$_2$H
- DBS-Gly

Figure 7.3: Illustration of the principle of gaining temporal resolution in multi-component gels through the hydrolysis of GdL, followed by activation of DPIN with a combination of the LMWGs DBS-CO$_2$H and DBS-Gly.

In addition to the temporal patterning, as the second proton generation step required UV light, simultaneous spatial patterning of the DBS-Gly network was possible, yielding a multidomain, multi-component hydrogel. This material also constituted the first known example of a photopatterned multi-component gel in which the pattern was positively "written in".[280] This method of photopatterning could ultimately allow for much more complex patterned materials than the 2D bulk-patterned gels produced in this project – for example, using 2PP methods would allow for incorporation of much finer detail and true 3D patterning.[230–232]

Such complex patterned materials could have great potential in tissue engineering applications, where different domains could direct the growth and proliferation of cells in different ways. Obviously, as previously discussed, both DBS-CO$_2$H and DBS-Gly would likely not be suitable for these applications due to their need to be formed at acidic pH values, so again more biocompatible LMWGs would be needed. Additionally, the PAG DPIN is also not biocompatible; investigations in the near future would likely need to centre around finding a more biologically-friendly PAG. These could begin with an examination of the spiropyran-derived PAG used by van Esch and co-workers.[269]

7.3.　Chapter 6: Complex multi-component hybrid hydrogels

In the final part of the project, the combination in several ways of the two previous main classes of hydrogels was studied. These investigations yielded PEGDM gels with photopatterned regions of DBS-CO$_2$H when DPIN was used as the proton source, three-gelator multi-component hybrid gels using GdL as the proton source, and finally multi-component hybrid hydrogels of DBS-CO$_2$H, DBS-Gly and PEGDM using the two-step proton generation method (Figure 7.4). The latter set of

hydrogels marked the first known examples of three- and four-domain gels, demonstrating how several orthogonally activated gel networks can be combined and patterned in one material.
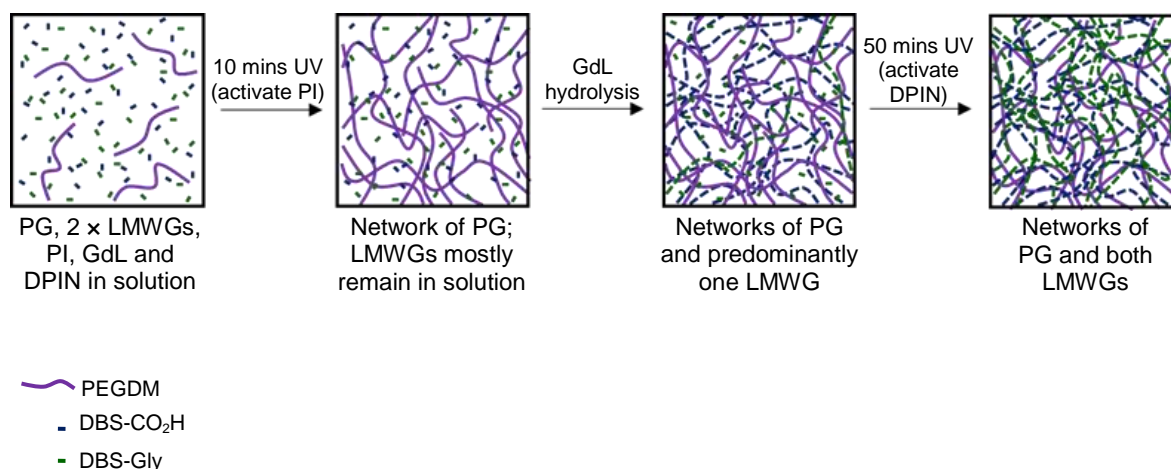
Figure 7.4: Illustration of the procedure for producing a multi-component hybrid hydrogel through activation of PI, followed by hydrolysis of GdL, followed by activation of DPIN, for a combination of the LMWGs DBS-CO₂H and DBS-Gly and the PG PEGDM.

Whilst showing some exciting possibilities, the results from this chapter also showed that the more components are present in these hybrid systems, the more complicated they become to analyse. Work in the near future will need to focus on ways to generate clearer NMR spectra and alternative ways to produce sample for rheology to better understand the interactions between the three networks and how the presence of one affects the formation and properties of the other two.

The other main issue that requires work is to achieve sufficient difference between the activation wavelengths of the photoinitiator for the PG network, and the chosen PAG; in the hybrid gels here, both were activated at very similar wavelengths (though this was also due to the experimental limitations, i.e., only one high-intensity UV lamp was available). The previously mentioned spiropyran-derived PAG is activated at visible light wavelengths,[269] so this could be a potential starting point for such investigations. Alternatively, use of 2PP methods, where the activation of the photoinitiator or PAG would be confined to a specific point receiving a specific wavelength, would also potentially overcome this problem.

Nonetheless, these materials represent an interesting move forward in the production of gels with spatial and temporal control over the formation of networks. Again, there is particular scope to use such materials in tissue engineering applications – or at very least the understanding of how to make such materials for tissue engineering, given again that the gels examined here are not likely to be biocompatible. Such complex patterned gels with multiple domains – especially if patterned in 3D as opposed to 2D – would be potentially ideal environments for the growth of stem cells, which are known to differentiate according to the mechanical properties of their surrounding

environments,[275] so in this way complex tissues could be grown. Again, with patterning in 3D, it could also be possible to make gels for drug delivery applications in which the multiple domains have different kinetics of release depending on the networks present in each domain, controlling release through interactions with the networks, through how easily the drug diffuses though the networks, and how easily each domain is degraded to release the drug.

7.4. Summary

Altogether, the work in this project has contributed much to the understanding of how hybrid and multi-component gels can be produced, how the gelators in them interact with or are affected by each other, and how functionality can be added to the materials, particularly by photopatterning methods. As such, the experiments described in this thesis have opened up wholly new areas in gel-phase materials research. It is hoped that the principles elucidated here will go on to open up new applications of such materials in high-tech biomedical processes, and prompt further investigations into the understanding of this relatively new class of materials that is hybrid gels.

8. Chapter 8: Experimental

For each main section, experimental procedures are presented largely according to their order of appearance in this thesis.

8.1. General Experimental Methods

All compounds required for synthesis and analysis were purchased from standard commercial suppliers, and used without further purification. Proton and carbon NMR spectra were recorded on a Jeol ECX 400 spectrometer ([1]H 400 MHz, [13]C 100 MHz). A Bruker 500 ([1]H 500 MHz) was used for the longer kinetics experiments. Samples were recorded as solutions in deuterated NMR solvents as stated and chemical shifts (δ) are quoted in parts per million. Coupling constant values (J) are given in Hz. The level of assignment of ^{1}H NMR spectra was achieved using model compounds, literature data and standard knowledge of ^{1}H NMR. DEPT experiments were used to assist in the assignment of ^{13}C NMR spectra. Positive and negative ion ESI and MALDI mass spectra were recorded on a Bruker solariX FTMS 9.4T mass spectrometer. ATR-FTIR spectra were recorded on a PerkinElmer Spectrum Two FT-IR spectrometer. Melting points were measured on a Stuart SMP3 melting point apparatus and are uncorrected. Transparent glass screw-capped vials (2.5 or 8.5 mL) were used in the preparation of gels. T_{gel} values were recorded using a high precision thermoregulated oil bath. Rheological measurements were recorded using a Malvern Instruments Kinexus Pro+ rheometer fitted with a parallel plate geometry at 25°C; data were processed using rSpace software. Circular dichroism spectra were recorded on a Jasco J810 CD spectrophotometer fitted with a Peltier temperature control unit using a quartz cell with a path length of 1 mm, and using the following settings: Data Pitch = 0.5 nm, Scanning Mode = continuous, Scanning Speed = 100 nm min^{-1}, Response = 1 s, Bandwidth = 2 nm, Accumulation = 5, or = 3 in kinetics experiments. SEM was carried out on a JEOL JSM-7600F FEG-SEM. TEM was performed on copper-backed TEM grids using a FEI Tecnai 12 BioTWIN G2 fitted with a CCD camera; samples were stained with a 1% uranyl acetate solution. SEM and TEM images were collected by Meg Stark at the Biology Technology Facility, University of York. UV-vis absorbance was measured on a Shimadzu UV-2401 PC spectrophotometer. pH readings were carried out using a Hanna Instruments Checker® pH Tester HI98103, calibrated to pH values 4 and 7 using buffer solutions.

8.1.1. ^{1}H NMR assignment of sugar C*H* resonances for DBS-derivative

To aid in the assignment of sugar C*H* resonances in the ^{1}H NMR spectra of the DBS-derivatives, each sugar C*H* is numbered according to Figure 8.1. Fully assigned spectra of DBS-CO$_2$Me and DBS-CO$_2$H are presented in the Appendix.
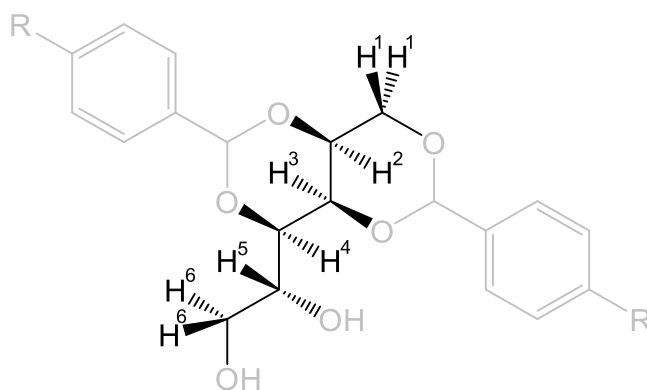
Figure 8.1: Numbering of sugar C*H* resonances as used in ¹H NMR assignment of DBS-derived compounds.

8.2. Synthesis procedures

8.2.1. Synthesis and characterisation of DBS-CO₂Me

Synthesis of DBS-CO₂Me was achieved by adapting previously published methods for the synthesis of DBS-derivatives.[114,120]
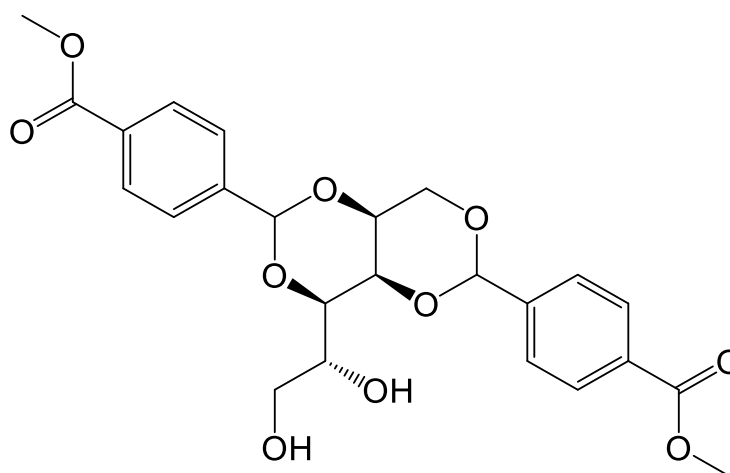
Chemical Formula: $C_{24}H_{26}O_{10}$
Molecular Weight: 474.46

D-Sorbitol (4.90 g, 26.9 mmol) was weighed into a 3-necked round-bottom flask fitted with Dean-Stark apparatus. Cyclohexane (35 mL) and methanol (10 mL) were added, and the mixture was stirred under N_2 at 50ºC for 20 min. 4-Methylcarboxybenzaldehyde (7.50 g, 45.7 mmol) and *p*-toluene sulfonic acid hydrate (1.00 g, 5.3 mmol) were dissolved in methanol (20 mL) and stirred for 20 min at room temperature, before being added dropwise to the D-sorbitol mixture. The reaction temperature was increased to 70ºC, and was stirred for 2 h, until most of the solvent was removed. The white paste formed was washed with methanol (3 x 100 mL). The crude product was dried under high vacuum for 2 h, then air-dried overnight. Mono- and trisubstituted derivatives

were removed by washing with boiling water (4 x 100 mL) and boiling DCM (3 x 100 mL) respectively. Yield: 8.37 g (17.6 mmol, 77%).

M.p: 210-213°C. ^{1}H NMR (400 MHz, DMSO-d_6): δ 8.00-7.97 (m, ArH, 4H), 7.63-7.58 (m, ArH, 4H), 5.76 (s, Ar-CH, 2H), 4.96 (d, CHOH, J = 5.6, 1H), 4.50 (br, CH$_2$OH, 1H), 4.26-4.17 (m, sugar H^1 & H^3, 3H (overlap)), 4.01 (app s, sugar H^2, 1H), 3.89 (app d, sugar H^4, J = 9.2, 1H), 3.85 (s, OCH_3, 6H), 3.79 (br, sugar H^5, 1H), 3.63-3.60 (app d, sugar H^6, J = 10.4, 1H), 3.48-3.45 (m, sugar H^6, 1H). ^{13}C NMR (400 MHz, DMSO-d_6): δ 166.00 (COO), 143.33 (aromatic p-C), 143.06 (aromatic p-C), 129.77 (aromatic o-C), 129.72 (aromatic o-C), 129.04 (aromatic o-C), 128.95 (aromatic o-C), 126.50 (aromatic m-C), 98.54 (Ph-C), 98.46 (Ph-C), 77.58 (CH), 70.18 (CH), 69.31 (CH$_2$), 68.53 (CH), 67.59 (CH), 62.56 (CH$_2$), 52.21 (CH$_3$). ν_{max} (cm^{-1}) (solid): 3241m, 2956w, 1723s, 1435w, 1399m, 1276s, 1167w, 1093s, 1018s, 856m, 835m, 750s, 707m. ESI-MS (m/z) calc. for C$_{24}$H$_{27}$O$_{10}$ 475.1599; found 475.1603 (100% [M+H]$^+$), 497.1431 (35% [M+Na]$^+$).

8.2.2. Synthesis and characterisation of DBS-CO$_2$H
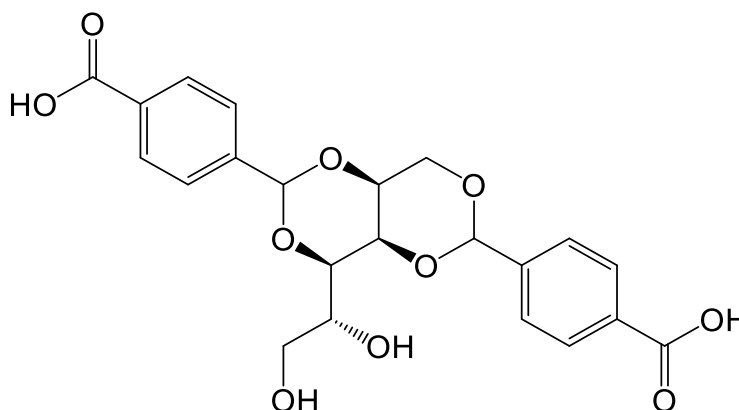
Chemical Formula: C$_{22}$H$_{22}$O$_{10}$
Molecular Weight: 446.41

1,3:2,4-Dibenzylidene-D-sorbitol-p,p'-dimethylester (1.20 g, 2.5 mmol) was dissolved in methanol (35 mL), and NaOH$_{(aq)}$ (35 mL, 1 M) was added to the solution. The mixture was heated overnight at 80°C under reflux. The methanol was removed by rotary evaporation, and deionised water (50 mL) was added. The mixture was acidified to pH 3 with NaHSO$_4$, causing a white, stable gel to form. The product was filtered using a sintered funnel, and washed thoroughly with deionised water (4 x 100 mL). The product was dried under high vacuum, and was then finally dried to a constant weight in a vacuum oven at 50°C for 2 d. Yield: 0.79 g (1.8 mmol, 69%).

^{1}H NMR (400 MHz, DMSO-d_6): δ 7.97-7.95 (m, ArH, 4H), 7.60-7.56 (m, ArH, 4H), 5.75 (s, Ar-CH, 2H), 4.25-4.17 (m, sugar H^1 & H^3, 3H (overlap)), 4.00 (app s, sugar H^2, 1H), 3.89 (app d, sugar H^4, J = 9.6, 1H), 3.80-3.77 (m, sugar H^5, 1H), 3.62 (app d, sugar H^6, J = 10.4, 1H), 3.48-3.44

(dd, sugar H^6, J = 11.2, 5.2, 1H). ^{13}C NMR (100 MHz, DMSO-d_6): δ 167.16 (*C*OOH), 142.93 (aromatic *p-C*), 142.65 (aromatic *p-C*), 131.03 (aromatic *o-C*), 130.97 (aromatic *o-C*), 129.20 (aromatic *o-C*), 129.11 (aromatic *o-C*), 126.34 (aromatic *m-C*), 98.67 (Ph-*C*), 77.56 (*C*H), 70.19 (*C*H), 69.34 (*C*H$_2$), 68.53 (*C*H), 67.64 (*C*H), 62.60 (*C*H$_2$). v_{max} (cm^{-1}) (solid): 3245*m*, 2880*m*, 1722*m*, 1466*w*, 1341*m*, 1279*m*, 1095*s*, 841*m*, 750*w*, 707*w*. ESI-MS (*m/z*) calc. for C$_{22}$H$_{12}$O$_{10}$ 445.1140; found 445.1143 (100% [M-H]$^-$).

8.2.3. Synthesis and characterisation of PEGDM

Synthesis of PEGDM was carried out by following a previously reported method.[202]

Chemical Formula: C$_{2n+8}$H$_{4n+10}$O$_{n+3}$
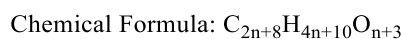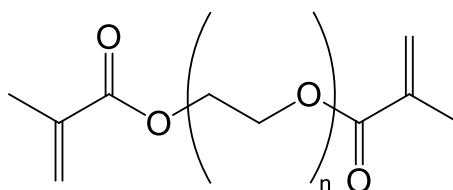
PEG 8000 (8 g, 1 mmol), methacrylic anhydride (0.34 g, 2.2 mmol) and triethylamine (0.15 g, 1.4 mmol) were reacted in dry DCM (15 mL) over activated molecular sieves (3 g) for 4 days at room temperature. The solution was filtered over alumina and precipitated by addition of diethyl ether (800 mL). The product was filtered, and then dried under vacuum to obtain a white solid. Yield: 5.98 g (0.6 mmol, 74%).

M.p: 61-63°C. ^{1}H NMR (400 MHz, CDCl$_3$): δ = 6.11 (app s, =C*H*, 2H), 5.55 (app t, =C*H*, J = 1.6, 2H), 4.29-4.27 (m, OC*H$_2$*, 4H), 3.81-3.43 (m, polymer chain OC*H$_2$*), 1.93 (s, C*H$_3$*, 6H). ^{13}C NMR (400 MHz, CDCl$_3$): δ = 169.99 (*C*OO), 136.19 (*C*=CH$_2$), 125.82 (C=*C*H$_2$), 70.62 (O*C*H$_2$), 69.18 (O*C*H$_2$), 63.94 (O*C*H$_2$), 18.40 (*C*H$_3$). v_{max} (cm^{-1}) (solid): 2882*s*, 1716*w*, 1467*w*, 1341*m*, 1279*w*, 1241*w*, 1097*s*, 961*m*. MALDI-MS (*m/z*): found (average) 9313.4386 (C$_4$H$_5$O$_{1.5}$)$_2$(C$_2$H$_4$O)$_{208}$ (100% [M-H]$^+$).

8.2.4. Synthesis and characterisation of DBS-GlyOMe
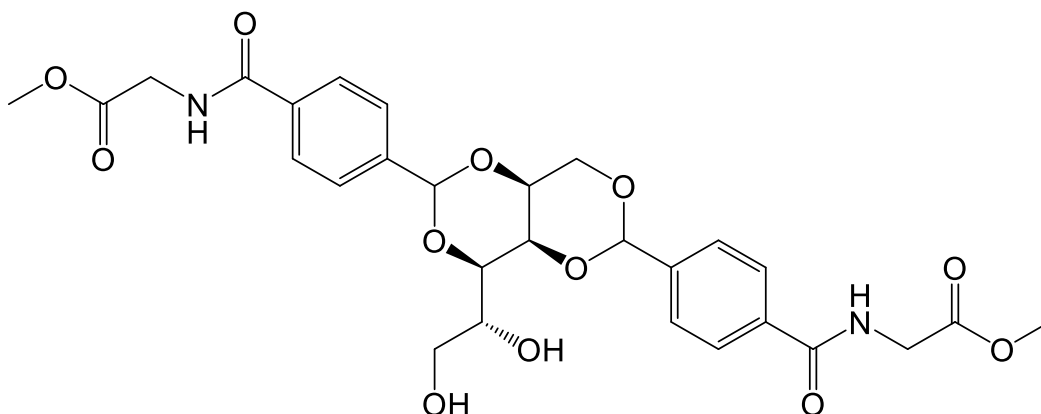
Chemical Formula: $C_{28}H_{32}N_2O_{12}$
Molecular Weight: 588.57

DBS-CO_2H (500 mg, 1.1 mmol) was dissolved in DMF (12 mL) with addition of DIPEA (780 µL, 4.5 mmol). The solution was cooled to 0°C, then TBTU (720 mg, 2.2 mmol) was added as a solid, with DMF (4 mL) used to wash residual TBTU into the flask. The reaction was stirred for 20 minutes, and then glycine methyl ester hydrochloride (282 mg, 2.2 mmol) was added with a further portion of DMF (4 mL). The reaction was stirred for a further 30 minutes at 0°C, then at room temperature for 3 days. DMF was removed by rotary evaporation to give an orange residue. A solid was precipitated by the addition of water (50 mL), and collected over a sinter funnel. The solid was washed with water (3 × 50 mL) and DCM (2 × 50 mL), and then dried under high vacuum for 1 d, followed by drying to constant weight in a vacuum oven at 70°C for 1 d. Yield: 440 mg (0.7 mmol, 67%) as yellow-brown solid.

M.p.: 228-231°C. ^{1}H NMR (400 MHz, DMSO-d_6): δ = 8.99 (t, NH, J = 5.8, 2H), 7.89-7.87 (m, ArH, 4H), 7.58-7.54 (m, ArH, 4H), 5.74 (s, Ar-CH, 2H), 4.94 (d, CHOH, J = 5.6, 1H), 4.47 (t, CH_2OH, J = 5.4, 1H), 4.23-4.19 (m, sugar H^1 & H^3, 3H (overlap)), 4.01-3.99 (m, sugar H^2 and CH_2, 5H (overlap)), 3.88 (app d, sugar H^4, J = 9.2, 1H), 3.80-3.79 (m, sugar H^5, 1H), 3.65 (s, CH_3, 6H), 3.65-3.62 (m, sugar H^6, 1H (overlap with previous)), 3.47-3.46 (m, sugar H^6, 1H). ^{13}C NMR (400 MHz, DMSO-d_6): δ = 170.92 (CONH), 166.80 (COO), 142.22 (aromatic p-C), 141.95 (aromatic p-C), 134.31 (aromatic p-C), 134.23 (aromatic p-C), 127.62 (aromatic o-C), 127.54 (aromatic o-C), 126.73 (aromatic m-C), 126.66 (aromatic m-C), 99.26 (Ph-C), 99.21 (Ph-C), 78.13 (CH), 70.72 (CH), 69.82 (CH$_2$), 69.07 (CH), 68.15 (CH), 63.11 (CH$_2$), 52.30 (CH$_3$), 41.76 (CH$_2$). v_{max} (cm^{-1}) (solid): 3333m, 2949w, 1739s, 1643s, 1544s, 1505w, 1400w, 1369w, 1342w, 1215s, 1165w, 1094s, 1018s, 850m, 751m. ESI-MS (m/z) calc. for $C_{28}H_{33}N_2O_{12}$ 589.2028; found 589.2035 (5% [M+H]$^+$), 611.1839 (100% [M+Na]$^+$).

8.2.5. Synthesis and characterisation of DBS-Gly
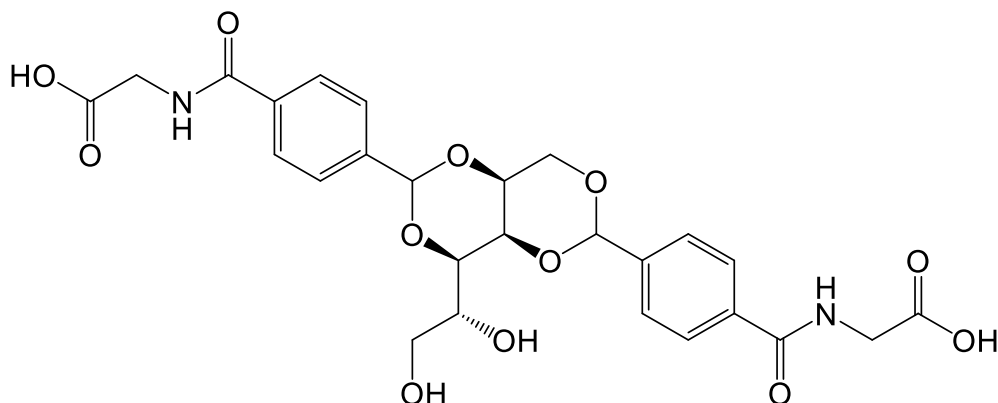
Chemical Formula: $C_{26}H_{28}N_2O_{12}$
Molecular Weight: 560.51

DBS-GlyOMe (190 mg, 0.32 mmol) was suspended in MeOH (25 mL) and H_2O (10 mL). $NaOH_{(aq)}$ (1.33 mL, 0.5 M, 0.66 mmol) was added, and the reaction was stirred overnight at room temperature. MeOH was removed by rotary evaporation, and the mixture was acidified to *ca*. pH 2 with $NaHSO_4$ until a white, stable gel formed. The product was filtered using a sintered funnel, and washed thoroughly with water (4×50 mL). The product was dried under high vacuum, and then finally dried to constant weight in a vacuum oven at 70°C for 1 d. Yield: 117 mg (0.2 mmol, 65%) as pale brown solid.

^{1}H NMR (400 MHz, DMSO-d_6): δ 8.80 (t, N*H*, *J* = 4.8, 2H), 7.89-7.87 (m, Ar*H*, 4H), 7.58-7.54 (m, Ar*H*, 4H), 5.74 (s, Ar-C*H*, 2H), 4.94 (br, CHO*H*, 1H), 4.48 (br, CH$_2$O*H*, 1H), 4.25-4.20 (m, sugar H^1 & H^3, 3H (overlap)), 4.00 (app s, sugar H^2, 1H), 3.92-3.88 (m, C*H$_2$* and sugar H^4, 5H (overlap)), 3.82-3.79 (m, sugar H^5, 1H), 3.64-3.60 (m, sugar H^6, 1H), 3.49-3.45 (m, sugar H^6, 1H). ^{13}C NMR (400 MHz, DMSO-d_6): δ 171.86 (*C*ONH), 166.65 (*C*OO), 142.08 (aromatic *p-C*), 141.81 (aromatic *p-C*), 134.58 (aromatic *p-C*), 134.50 (aromatic *p-C*), 127.58 (aromatic *o-C*), 127.51 (aromatic *o-C*), 126.62 (aromatic *m-C*), 99.30 (Ph-*C*), 99.24 (Ph-*C*), 78.15 (*C*H), 70.72 (*C*H), 69.84 (*C*H$_2$), 69.07 (*C*H), 68.15 (*C*H), 63.11 (*C*H$_2$), 41.82 (*C*H$_2$). v_{max} (cm^{-1}) (solid): 3335*s*, 2931*w*, 1713*m*, 1644*s*, 1539*s*, 1505*w*, 1398*m*, 1340*w*, 1218*s*, 1165*m*, 1093*s*, 998*s*, 805*m*, 749*m*. ESI-MS (*m/z*) calc. for $C_{26}H_{27}N_2O_{12}$ 559.1569; found 559.1592 (100% [M-H]$^-$), 581.1431 (30% [(M-2H)+Na]$^-$).

8.2.6. Synthesis and characterisation of DBS-PheOMe
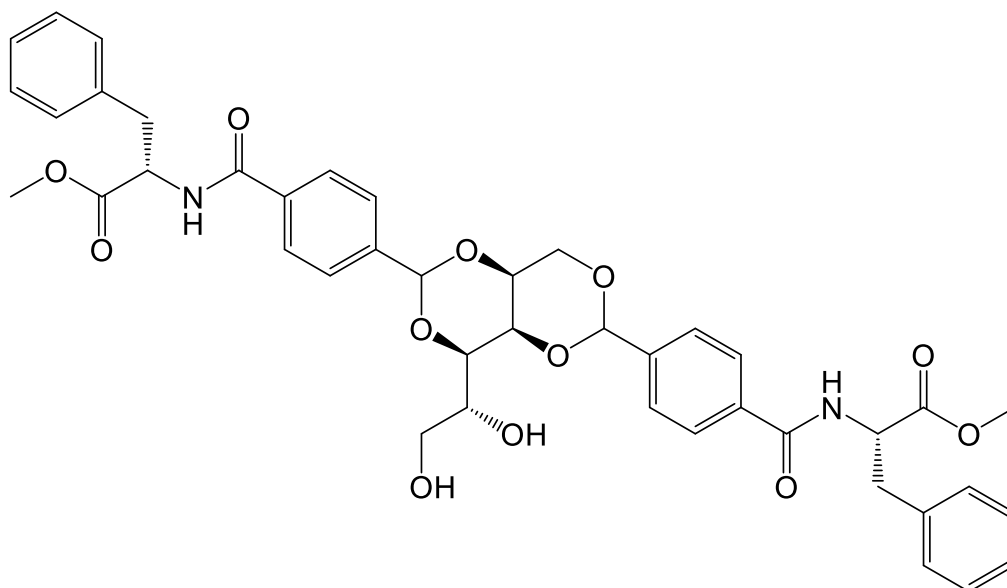
Chemical Formula: $C_{42}H_{44}N_2O_{12}$
Molecular Weight: 768.82

DBS-CO_2H (500 mg, 1.1 mmol) was dissolved in DMF (12 mL) with addition of DIPEA (780 µL, 4.4 mmol). The solution was cooled to 0°C, then TBTU (720 mg, 2.2 mmol) was added as a solid, with DMF (4 mL) used to wash residual TBTU into the flask. The reaction was stirred for 20 minutes, and then L-phenylalanine methyl ester hydrochloride (485 mg, 2.2 mmol) was added with a further portion of DMF (4 mL). The reaction was stirred for a further 30 minutes at 0°C, then at room temperature for 3 days. DMF was removed by rotary evaporation to give an orange residue. A solid was precipitated by the addition of water (50 mL), and collected over a sinter funnel. The product was washed with water (3 × 50 mL), and then dried under high vacuum for 1 d, followed by drying to constant weight in a vacuum oven at 60°C for 1 d. Yield: 585 mg (0.76 mmol, 68%) as orange-brown solid.

M.p.: 194-197°C. ^1H NMR (400 MHz, $CDCl_3$): δ = 7.67-7.63 (m, Ar*H*, 4H), 7.54-7.50 (m, Ar*H*, 4H), 7.27-7.23 (m, Ar*H*, 6H), 7.10-7.08 (m, Ar*H*, 4H), 6.70 (t, N*H*, *J* = 7.0, 2H), 5.61 (s, Ar-C*H*, 1H), 5.58 (s, Ar-C*H*, 1H), 5.05-5.02 (m, C*H*, 2H), 4.34 (d, sugar H^2, *J* = 12.0, 1H), 4.12-4.07 (m, sugar H^1 & H^3, 3H (overlap)), 3.94 (dd, sugar H^4, *J* = 8.4, 1.6, 1H), 3.83 (app d, sugar H^5, *J* = 3.2 , 1H), 3.80 (app s, sugar H^6, 1H), 3.76 (app d, sugar H^6, *J* = 4.8, 1H), 3.74-3.72 (m, C*H*₃, 6H), 3.26 (app ddd, ArC*H*, *J* = 14.0, 5.6, 2.8, 1H), 3.18 (app dd, ArC*H*, *J* = 14.0, 5.6, 1H). ^{13}C NMR (400 MHz, DMSO-d_6): δ = 172.00 (*C*ONH), 166.57 (*C*OO), 141.33 (aromatic *p-C*), 141.07 (aromatic *p-C*), 135.74 (aromatic *C*), 134.22 (aromatic *p-C*), 134.14 (aromatic *p-C*), 129.25 (aromatic *C*H), 128.62 (aromatic *C*H), 127.19 (aromatic *C*H), 126.92 (aromatic *m-C*), 126.88 (aromatic *m-C*H), 126.66 (aromatic *o-C*), 126.59 (aromatic *o-C*), 99.81 (Ph-*C*), 99.73 (Ph-*C*), 77.87 (*C*H), 70.41 (*C*H), 69.93 (*C*H₂), 68.98 (*C*H), 68.37 (*C*H), 63.14 (*C*H₂), 53.54 (*C*H), 52.44 (*C*H₃), 37.74 (*C*H₂).

v_{max} (cm^{-1}) (solid): 3315m, 2951w, 1738s, 1645s, 1536s, 1497m, 1436w, 1340w, 1217s, 1168w, 1092s, 1019s, 852m, 747m, 700s. ESI-MS (m/z) calc. for $C_{42}H_{45}N_2O_{12}$ 769.2967; found 769.2976 (10% [M+H]$^+$), 791.2781 (100%, [M+Na]$^+$).

8.2.7. Synthesis and characterisation of DBS-Phe
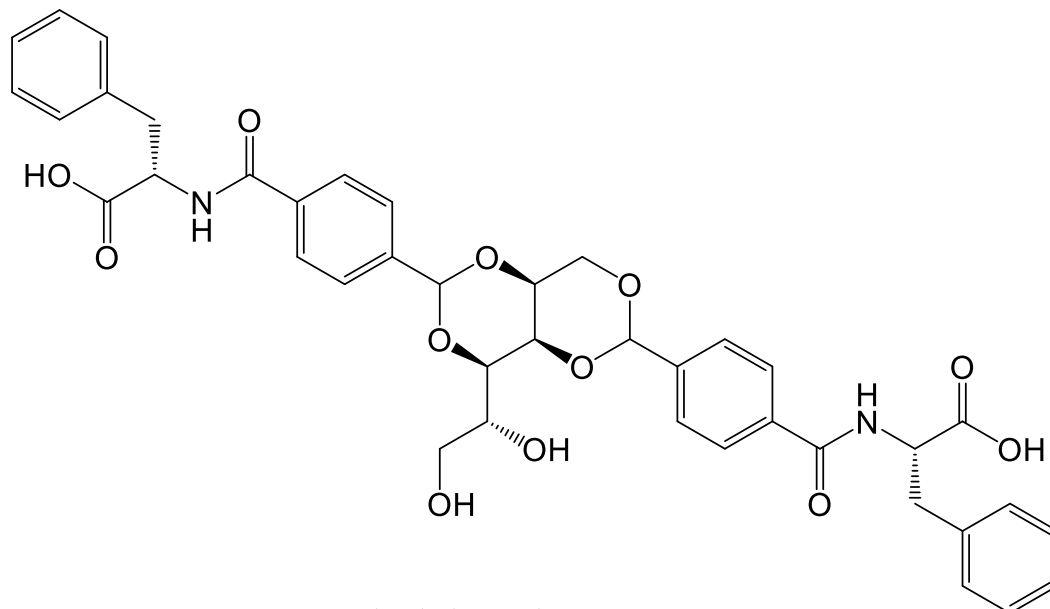
Chemical Formula: $C_{40}H_{40}N_2O_{12}$
Molecular Weight: 740.76

DBS-PheOMe (150 mg, 0.2 mmol) was suspended in MeOH (15 mL) and H_2O (15 mL). NaOH (0.78 mL, 0.5 M, 0.4 mmol) was added, and the reaction was stirred overnight at room temperature. MeOH was removed by rotary evaporation, and the mixture was acidified with NaHSO$_4$ to cause a white precipitate to form. The product was filtered using a sintered funnel, and washed thoroughly with water (4 × 50 mL). The product was dried under high vacuum, and then finally dried to constant weight in a vacuum oven at 60ºC for 1 d. Yield: 102 mg (0.14 mmol, 69%) as white solid.

^{1}H NMR (400 MHz, CDCl$_3$): δ = 8.70 (d, NH, J = 8.0, 2H), 7.79-7.76 (m, ArH, 4H), 7.52-7.47 (m, ArH, 4H), 7.28-7.21 (m, ArH, 6H), 7.15-7.12 (m, ArH, 4H), 5.68 (s, Ar-CH, 2H), (s, Ar-CH, 1H), 4.89 (br, CHOH, 1H), 4.60-4.54 (m, CH, 2H), 4.42 (br, CH$_2$OH, 1H), 4.21-4.15 (m, sugar H^1 & H^3, 3H (overlap)), 3.96 (app s, sugar H^2, 1H), 3.84 (app d, sugar H^4, J = 10.0, 1H), 3.75 (br, sugar H^5, 1H), 3.57 (app d, sugar H^6, J = 10.8, 1H), 3.43 (br, sugar H^6, 1H), 3.15 (dd, ArCH, J = 13.6, 4.4, 1H), 3.07-3.00 (m, ArCH, 1H). ^{13}C NMR (400 MHz, DMSO-d_6): δ = 172.68 (CONH), 165.45 (COO), 141.05 (aromatic p-C), 140.77 (aromatic p-C), 137.67 (aromatic C), 133.59 (aromatic C), 133.51 (aromatic p-C), 128.60 (aromatic CH), 127.70 (aromatic CH), 126.66 (aromatic CH), 126.58 (aromatic CH), 125.87 (aromatic m-C), 125.58 (aromatic o-CH), 125.49 (aromatic o-CH), 98.25 (Ph-C), 77.11 (CH), 69.68 (CH), 68.59 (CH$_2$), 67.99 (CH), 67.11 (CH), 62.07 (CH$_2$), 53.75 (CH), 35.79 (CH$_2$). v_{max} (cm^{-1}) (solid): 3321m, 2931w, 1729s, 1643s, 1531s,

1498s, 1394w, 1340m, 1219w, 1168w, 1094s, 1019s, 852m, 756m, 701s. ESI-MS (m/z) calc. for $C_{40}H_{39}N_2O_{12}$ 739.2508; found 739.2533 (100% [M-H]$^-$), 761.2354 (20%, [(M-2H)+Na]$^-$).

8.2.8. Synthesis and characterisation of DBS-TrpOMe
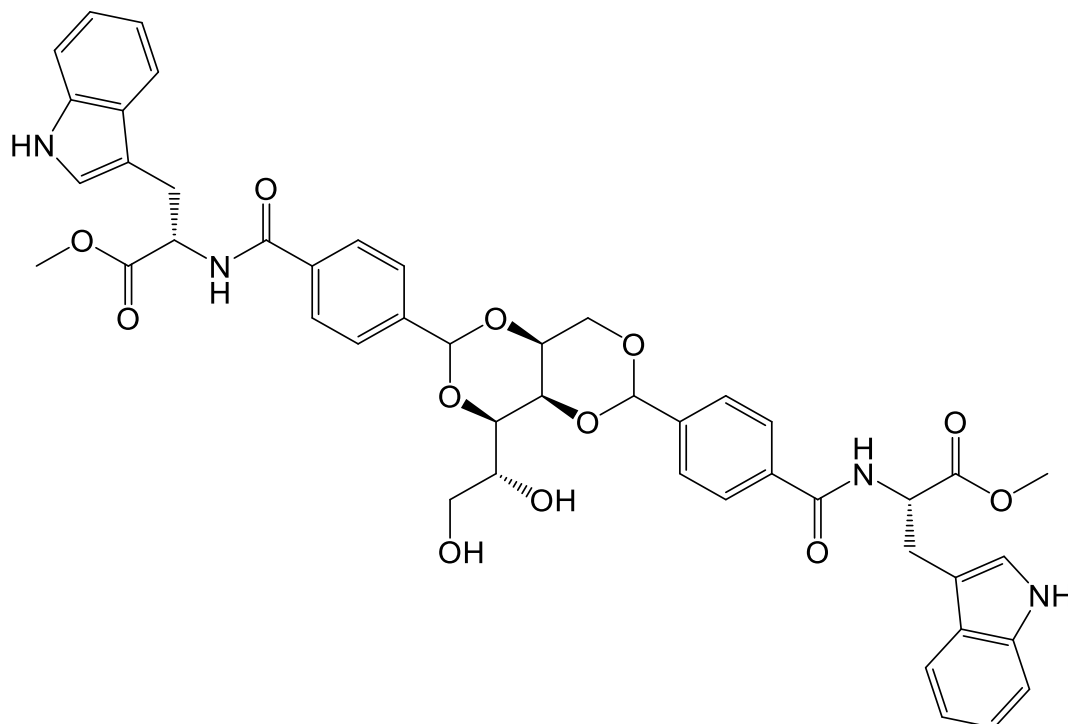
Chemical Formula: $C_{46}H_{46}N_4O_{12}$
Molecular Weight: 846.89

DBS-CO$_2$H (100 mg, 0.22 mmol) was dissolved in DMF (10 mL) with addition of DIPEA (156 µL, 0.88 mmol). The solution was cooled to 0°C, then TBTU (144 mg, 0.44 mmol) was added as a solid, with DMF (4 mL) used to wash residual TBTU into the flask. The reaction was stirred for 20 minutes, and then L-tryptophan methyl ester hydrochloride (114 mg, 0.44 mmol) was added with a further portion of DMF (4 mL). The reaction was stirred for a further 30 minutes at 0°C, then at room temperature for 3 days. DMF was removed by rotary evaporation to give an orange residue. A solid was precipitated by the addition of water (30 mL), and collected over a sinter funnel. The solid was washed with water (3 × 30 mL) and DCM (2 × 30 mL), and then dried under high vacuum for 1 d, followed by drying to constant weight in a vacuum oven at 70°C for 1 d. Yield: 184 mg (0.22 mmol, 97%) as pale brown solid.

M.p.: 134-137°C. ^{1}H NMR (400 MHz, DMSO-d_6): δ = 10.84 (s, NH, 2H) 8.85 (d, NH, J = 5.6, 2H), 7.85 (d, ArH, J = 6.8, 4H), 7.56-7.52 (m, ArH, 4H), 7.33 (d, ArH, J = 6.8, 2H), 7.20 (s, ArH, 2H), 7.06-6.99 (m, ArH, 4H), 5.73 (s, Ar-CH, 2H), 4.93 (br, CHOH, 1H), 4.69-4.68 (m, CH, 2H), 4.47 (br, CH$_2$OH, 1H), 4.22-4.19 (m, sugar H^1 & H^3, 3H (overlap)), 3.99 (app s, sugar H^2, 1H), 3.89 (app d, sugar H^4, J = 8.4, 1H), 3.79-3.77 (m, sugar H^5, 1H), 3.63-3.57 (m, CH_3 and sugar H^6

7H (overlap), 3.46 (br, sugar H^6, 1H (partial overlap with H_2O from NMR solvent)) 3.29-3.21 (m, CH_2, 4H (partial overlap with H_2O from NMR solvent)). ^{13}C NMR (400 MHz, DMSO-d_6): δ = 172.06 (CONH), 165.61 (COO), 141.16 (aromatic p-C), 140.89 (aromatic p-C), 135.61 (aromatic C), 133.29 (aromatic m-C), 126.77 (aromatic C), 126.70 (aromatic p-C), 126.57 (aromatic p-C), 125.52 (aromatic o-C), 123.12 (aromatic CH), 120.51 (aromatic CH), 117.96 (aromatic CH), 117.53 (aromatic CH), 111.00 (aromatic CH), 109.43 (aromatic C), 98.24 (Ph-C), 98.20 (Ph-C), 79.53 (CH), 69.69 (CH), 68.80 (CH$_2$), 68.04 (CH), 67.18 (CH), 62.09 (CH$_2$), 53.40 (CH), 51.45 (CH$_3$), 26.14 (CH$_2$). v_{max} (cm^{-1}) (solid): 3401m, 2940w, 1732s, 1644s, 1530s, 1500m, 1436w, 1340m, 1218w, 1168m, 1093s, 1018s, 852m, 744s, 587w, 545m. ESI-MS (m/z) calc. for $C_{46}H_{46}N_4NaO_{12}$ 869.3004; found 869.2987 (100% [M+Na]$^+$).

8.2.9. Synthesis and characterisation of DBS-Trp
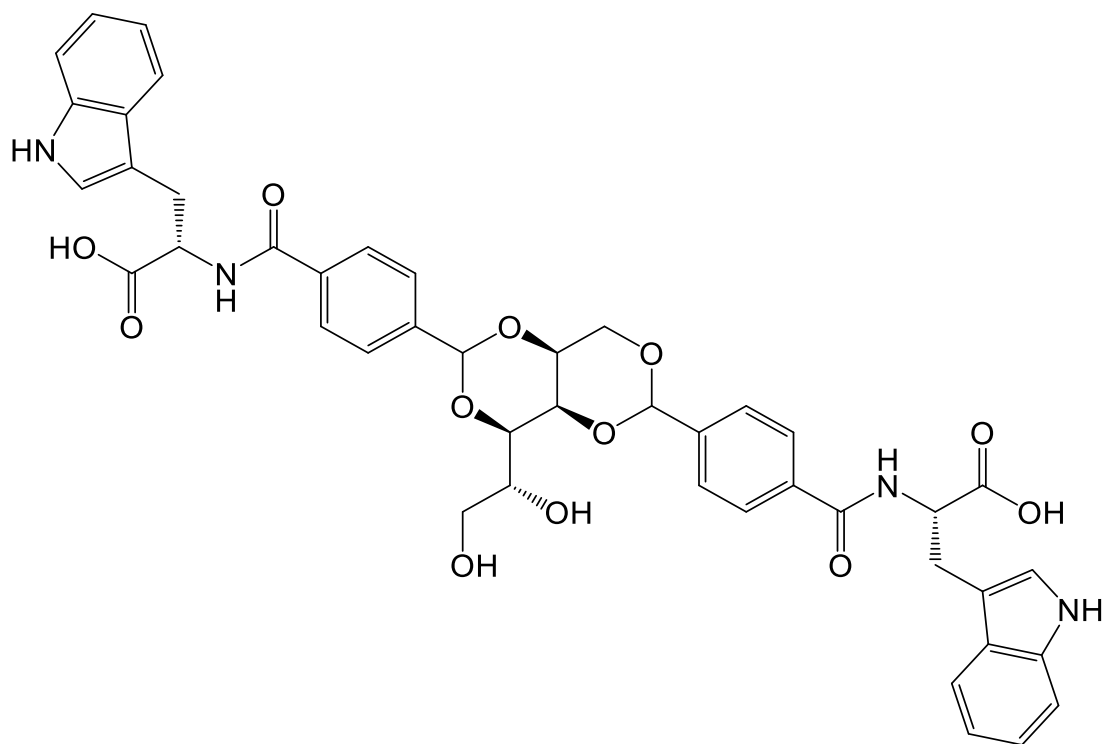
Chemical Formula: $C_{44}H_{42}N_4O_{12}$
Molecular Weight: 818.84

DBS-TrpOMe (150 mg, 0.18 mmol) was suspended in MeOH (20 mL) and H_2O (10 mL). NaOH (0.72 mL, 0.5 M, 0.36 mmol) was added, and the reaction was stirred overnight at room temperature. MeOH was removed by rotary evaporation, and the mixture was acidified with NaHSO$_4$ until a white, stable gel formed (pH ≈ 2). The product was filtered using a sintered funnel, and washed thoroughly with water (4 × 50 mL). The product was dried under high vacuum, and then finally dried to constant weight in a vacuum oven at 60°C for 1 d. Yield: 75 mg (0.1 mmol, 52%) as pale brown solid.

^{1}H NMR (400 MHz, DMSO-d_6): δ = 10.81 (s, NH, 2H) 8.68 (d, N*H*, *J* = 7.6, 2H), 7.84 (d, Ar*H*, *J* = 6.8, 4H), 7.61-7.50 (m, Ar*H*, 6H), 7.32 (d, Ar*H*, *J* = 8.0, 2H), 7.19 (s, Ar*H*, 2H), 7.06-6.98 (m, Ar*H*, 4H), 5.72 (s, Ar-C*H*, 2H), 4.93 (br, CHO*H*, 1H), 4.68-4.63 (m, C*H*, 2H), 4.47 (br, CH$_2$O*H*, 1H), 4.24-4.19 (m, sugar H^1 & H^3, 3H (overlap)), 3.98 (s, sugar H^2, 1H), 3.89 (app d, sugar H^4, *J* = 9.2, 1H), 3.79-3.77 (m, sugar H^5, 1H), 3.62 (app d, sugar H^6, *J* = 10.4, 1H), 3.30-3.18 (m, C*H$_2$*, 4H (partial overlap with H$_2$O from NMR solvent)); one sugar H^6 proton signal obscured by H$_2$O from NMR solvent. ^{13}C NMR (400 MHz, DMSO-d_6): δ = 173.28 (*C*ONH), 165.72 (*C*OOH), 141.26 (aromatic *p*-*C*), 140.98 (aromatic *p*-*C*), 135.81 (aromatic *C*), 133.87 (aromatic *m*-*C*), 126.93 (aromatic *C*), 126.86 (aromatic *p*-*C*), 125.69 (aromatic *o*-*C*), 123.32 (aromatic *C*H), 120.67 (aromatic *C*H), 118.13 (aromatic *C*H), 117.87 (aromatic *C*H), 111.17 (aromatic *C*H), 110.12 (aromatic *C*), 98.48 (Ph-*C*), 77.35 (*C*H), 69.92 (*C*H), 69.04 (*C*H$_2$), 68.25 (*C*H), 67.36 (*C*H), 62.35 (*C*H$_2$), 53.46 (*C*H), 26.39 (*C*H$_2$). v_{max} (cm^{-1}) (solid): 3398*m*, 2922*w*, 1725*m*, 1638*s*, 1529*s*, 1499*m*, 1394*w*, 1340*m*, 1220*m*, 1166*w*, 1092*s*, 1017*m*, 851*m*, 744*s*, 544*m*. ESI-MS (*m/z*) calc. for C$_{44}$H$_{41}$N$_4$O$_{12}$ 817.2726; found 817.2756 (100% [M-H]$^-$), 839.2597 (35% [(M-2H)+Na]$^-$.

### 8.2.10. Attempted synthesis of DBS-AlaOMe
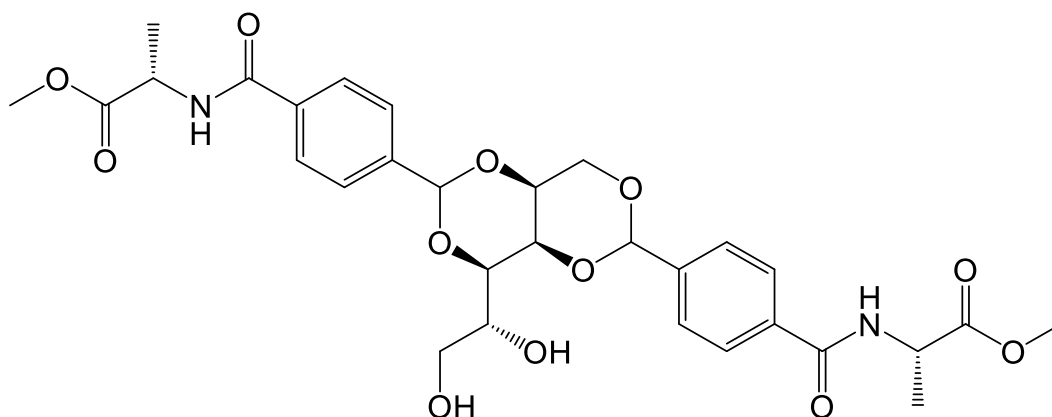
Chemical Formula: C$_{30}$H$_{36}$N$_2$O$_{12}$
Molecular Weight: 616.62

DBS-CO$_2$H (500 mg, 1.1 mmol) was dissolved in DMF (12 mL) with addition of DIPEA (780 µL, 4.4 mmol). The solution was cooled to 0°C, then TBTU (720 mg, 2.2 mmol) was added as a solid, with DMF (4 mL) used to wash residual TBTU into the flask. The reaction was stirred for 20 minutes, and then L-alanine methyl ester hydrochloride (314 mg, 2.2 mmol) was added with a further portion of DMF (4 mL). The reaction was stirred for a further 30 minutes at 0°C, then at room temperature for 3 days. DMF was removed by rotary evaporation to give an orange residue. Water (30 mL) was added to attempt precipitation of product, followed by further portions of water

(20 mL) when no precipitate was seen; however, product remained dissolved even after addition of > 100 mL water. The reaction was not purified further.

8.2.11. Attempted synthesis of DBS-Asp(OMe)₂
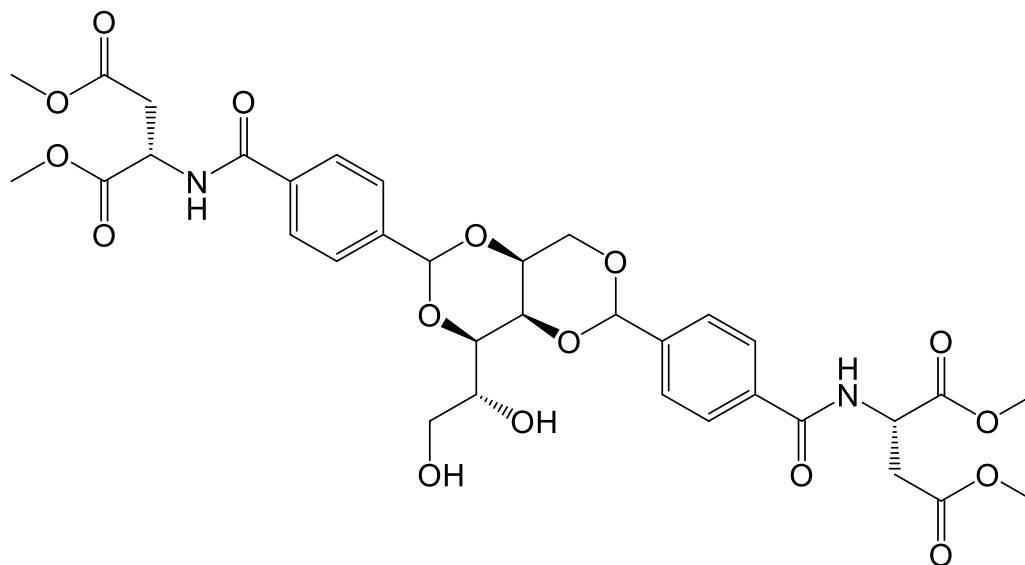
Chemical Formula: $C_{34}H_{40}N_2O_{16}$
Molecular Weight: 732.69

DBS-CO₂H (250 mg, 0.55 mmol) was dissolved in DMF (8 mL) with addition of DIPEA (390 μL, 2.2 mmol). The solution was cooled to 0°C, then TBTU (360 mg, 1.1 mmol) was added as a solid, with DMF (2 mL) used to wash residual TBTU into the flask. The reaction was stirred for 20 minutes, and then L-aspartic acid dimethyl ester hydrochloride (222 mg, 1.1 mmol) was added with a further portion of DMF (2 mL). The reaction was stirred for a further 30 minutes at 0°C, then at room temperature for 3 days. DMF was removed by rotary evaporation to give an orange residue. Water (20 mL) was added to attempt precipitation of product, followed by further portions of water (15 mL) when no precipitate was seen; however, product remained dissolved even after addition of > 100 mL water. The reaction was not purified further.

8.3. Standard gelation protocols to produce gels in sample vials

8.3.1. DBS-CO₂H hydrogels

1 mL H₂O was added to a known mass of DBS-CO₂H in 2.5 mL sample vials. The vials were then sonicated to disperse the solid, and 10 μL aliquots of 0.5 M NaOH₍ₐq₎ were added to dissolve (pH ≈ 11). The solutions were then transferred to vials containing 6 or 8 mg of GdL, followed by shaking to dissolve. The vials were then left overnight for gelation to occur. Final pH values of the gels were 3-4, depending on amount of GdL used.

8.3.2. Agarose hydrogels

1 mL H_2O was added to a known mass of agarose in a 2.5 mL sample vial. The capped vial was then heated to 90°C in an oil bath, and held at this temperature for 5 minutes, with shaking every minute to dissolve the agarose. The solutions were removed from the oil bath and allowed to cool to room temperature, upon which a clear gel was formed after *ca.* 20 minutes

8.3.3. DBS-CO₂H and agarose hybrid hydrogels

1 mL H_2O was added to a known mass of DBS-CO₂H in 2.5 mL sample vials. The vials were then sonicated to disperse the solid, and 10 µL aliquots of 0.5 M NaOH$_{(aq)}$ were added to dissolve (pH ≈ 11). Agarose (5 mg) was then added. The capped vials were then heated to 90°C in an oil bath, and held at this temperature for 5 minutes, with shaking every minute to dissolve the agarose. The solutions were then cooled to 50°C, at which temperature they were removed from the oil bath and GdL (6-8 mg) was added, followed by shaking to dissolve. The vials were left overnight for gelation to occur. Final pH values of the gels were 3-4, depending on amount of GdL used.

8.3.4. PEGDM hydrogels

PEGDM was dissolved at varying % wt/vols in 1 mL a 0.05% wt/vol aqueous solution of 2-hydroxy-4′-(2-hydroxyethoxy)-2-methylpropiophenone (photoinitiator, PI) in 2.5 mL sample vials. The solutions were cured in the uncapped vials under a long wavelength UV lamp for 10 minutes to obtain hydrogels.

8.3.5. DBS-CO₂H and PEGDM hybrid hydrogels

PEGDM (50 mg) was dissolved in 1 mL a 0.05% wt/vol aqueous solution of 2-hydroxy-4′-(2-hydroxyethoxy)-2-methylpropiophenone (photoinitiator, PI) in 2.5 mL sample vials. Varying known masses of DBS-CO₂H were added, and the vials were then sonicated to disperse the solid; 10 µL aliquots of 0.5 M NaOH$_{(aq)}$ were added to dissolve (pH ≈ 11). The solutions were then transferred to vials containing 6 or 8 mg of GdL, followed by shaking to dissolve. The solutions were cured in the uncapped vials under a long wavelength UV source for 10 minutes to obtain transparent gels. The vials were then capped and left overnight for DBS-CO₂H gelation to occur. Final pH values of the gels were 3-4, depending on amount of GdL used.

8.3.6. DBS-Gly hydrogels, heat-cool method

1 mL of H_2O was added to a known mass of DBS-Gly in a 2.5 mL glass sample vial. The sealed vial was then heated to 95°C in a thermoregulated oil bath, with shaking every few minutes to fully dissolve the LMWG. The vial was removed from the oil bath and cooled to room temperature with an optically transparent gel forming after *ca.* 30 minutes.

8.3.7. DBS-Gly hydrogels, pH-change method

1 mL H_2O was added to a known mass of DBS-Gly in 2.5 mL sample vials. The vials were then sonicated to disperse the solid, and 10 µL aliquots of 0.5 M $NaOH_{(aq)}$ were added to dissolve (pH ≈ 11). The solutions were then transferred to vials containing ≥10 mg of GdL, followed by shaking to dissolve. The vials were then left overnight for gelation to occur.

8.3.8. DBS-CO₂H and DBS-Gly multi-component hydrogels

1 mL H_2O was added DBS-Gly (4.5 mg) and DBS-CO₂H (4.5 mg) in a 2.5 mL sample vial. The vial was then sonicated to disperse the solid, and 10 µL aliquots of 0.5 M $NaOH_{(aq)}$ were added to dissolve (pH ≈ 11). The solution was then transferred to a vial containing 18 mg of GdL, followed by shaking to dissolve. The vial was then left overnight for gelation to occur.

8.3.9. DBS-CO₂H, DBS-Gly and PEGDM multi-component hybrid hydrogels with single proton source

DBS-CO₂H and DBS-Gly (4.5 mg of both) were added to a 1 mL solution of PEGDM (5% wt/vol) and PI (0.05% wt vol) in 2.5 mL sample vials, followed by sonication to disperse the solid. $NaOH_{(aq)}$ (0.5 M) was added in 10 µL aliquots to dissolve DBS-CO₂H, followed by GdL (18 mg). The uncapped vials were then cured under UV light for 10 minutes to obtain a clear PEGDM hydrogel, which was then left overnight for gelation of DBS-CO₂H and DBS-Gly to occur.

8.4. T_{gel} procedure

To record T_{gel} values, gel samples were first prepared in 2.5 mL sample vials as described on section 8.3. The vials were then placed in a thermoregulated oil bath, which was then heated from 20°C at a rate of 1°C min⁻¹. Vials were carefully removed every minute, inverted, and replaced until a gel-sol transition was observed.

8.5. Rheology sample preparation

Note: For the preparation of agarose-containing gels for rheology, special vials were made. These consisted of an 8 mL sample vial where the base had been cleanly removed, and could be reattached with heat-shrink tape. After preparation of gel within the vial, the base could be removed to give a disc of gel *ca*. 20 mm in diameter – the same diameter as the selected upper plate geometry of the rheometer.

8.5.1. DBS-CO₂H hydrogels

Solutions were prepared according to the method described in section 8.3.1; gelation was carried out directly on the lower plate of the rheometer, using a sealed bottomless glass vial as a mould to hold 0.5 – 1 mL of the solution. This method produced gels *ca*. 1.5 – 3 mm thick.

8.5.2. Agarose hydrogels

0.5% wt/vol worth of agarose was dissolved in H_2O at 95°C; 500 μL volumes of this hot solution were then transferred to preparation vials and allowed to cool; discs *ca*. 1.5 mm thick were formed.

8.5.3. DBS-CO₂H and agarose hybrid hydrogels

Hot solutions were prepared as described in section 8.3.3; after addition of GdL, 500 μL volumes of the solution were then transferred to preparation vials and allowed to cool. This method produced discs of gels *ca*. 1.5 mm thick.

8.5.4. PEGDM hydrogels

PEGDM (50 mg) and PI (0.5 mg) were dissolved in 1 mL H_2O; the solution was transferred to an 8.5 mL sample vial and cured under UV light for 10 minutes. The disc of gel (*ca.* 3 mm in thickness) was then carefully removed from the vial and placed onto the lower plate of the rheometer.

8.5.5. DBS-CO₂H and PEGDM hybrid hydrogels

Solutions were prepared as described in section 8.3.5; 1 mL volumes were transferred to 8.5 mL sample vials, before being cured under UV light for 10 minutes. The vials were then left overnight. The disc of prepared gel (*ca.* 3 mm in thickness) was then carefully removed from the vial before being placed on the rheometer.

8.5.6. DBS-Gly

Solutions were prepared by the pH-change method as described in section 8.3.7; gelation was carried out directly on the lower plate of the rheometer, using a sealed bottomless glass vial as a mould to hold 0.5 – 1 mL of the solution. This method produced gels *ca*. 1.5 – 3 mm thick.

8.5.7. DBS-CO₂H and DBS-Gly multi-component hydrogels

Solutions were prepared as described in section 8.3.8; gelation was carried out directly on the lower plate of the rheometer, using a sealed bottomless glass vial as a mould to hold 0.5 – 1 mL of the solution. This method produced gels *ca*. 1.5 – 3 mm thick.

8.5.8. DBS-CO₂H, DBS-Gly and PEGDM multi-component hybrid hydrogels with single proton source

Solutions were prepared as described in section 8.3.9; 1 mL volumes of the solutions were transferred to 8.5 mL sample vials before being cured under UV light for 10 minutes. The vials were then left overnight. The disc of prepared gel (*ca.* 3 mm in thickness) was then carefully removed from the vial before being placed on the rheometer.

8.6. NMR sample preparation

8.6.1. DBS-CO₂H hydrogels with GdL

DBS-CO$_2$H (1.4 mg) was suspended in 0.7 mL D$_2$O with sonication. NaOH$_{(aq)}$ (21 μ, 0.5 M) was added to dissolve all solid and DMSO (1.4 µl) was added to act as an internal standard. The solution was then transferred to a vial containing GdL (5.6 mg), followed by shaking. The sample was then immediately transferred to a NMR tube for spectra to be recorded.

8.6.2. DBS-CO₂H and agarose hybrid hydrogels

DBS-CO$_2$H (2.0 mg) was suspended in 1 mL D$_2$O with sonication. NaOH$_{(aq)}$ (30 µl, 0.5 M) was added to dissolve all solid and DMSO (2 µl) was added to act as an internal standard. The solution was then transferred to a vial containing agarose (5 mg), which was then heated to 90°C in a thermoregulated oil bath to dissolve the agarose. The solution was then cooled to 50°C, and transferred to a vial containing 8 mg of GdL (8 mg), followed by shaking to dissolve. *Ca.* 0.7 mL was then immediately transferred to a NMR tube for spectra to be recorded.

8.6.3. PEGDM hydrogels

PEGDM (35 mg) and PI (0.35 mg) were dissolved in 0.7 mL D$_2$O; DMSO (1.4 µl) was added to act as an internal standard. The solution was transferred to a NMR tube and a spectrum was recorded. The tube was then cured under UV light for 10 minutes, followed by recording of a second spectrum.

8.6.4. DBS-CO₂H and PEGDM hybrid hydrogels

DBS-CO$_2$H (1.4 mg) was suspended in 0.7 mL D$_2$O with sonication. NaOH$_{(aq)}$ (21 µl, 0.5 M) was added to dissolve all solid and DMSO (1.4 µl) was added to act as an internal standard. PEGDM (35 mg), PI (0.35 mg) and GdL (5.6 mg) were then added, followed by shaking to dissolve. The solution was transferred to a NMR tube and cured under UV light for 10 minutes, after which NMR spectra were recorded.

8.6.5. DBS-Gly hydrogels, heat cool method

DBS-Gly (1 mg) was suspended in 1 mL D$_2$O by sonication, with 2 µL DMSO added as an internal standard. The solution was heated to 95°C in a thermoregulated oil bath, with shaking every few minutes until all solid had dissolved. *Ca.* 0.7 ml of the hot solution was transferred to a NMR tube and allowed to cool to a gel, after which NMR spectra were recorded.

8.6.6. DBS-Gly hydrogels, pH-change method with GdL

DBS-Gly (3.15 mg) was suspended in 0.7 mL D$_2$O with sonication. NaOH$_{(aq)}$ (42 µl, 0.5 M) was added to dissolve all solid and DMSO (1.4 µl) was added to act as an internal standard. The

solution was then transferred to a vial containing GdL (7 mg), followed by shaking. The sample was then immediately transferred to a NMR tube for spectra to be recorded.

8.6.7. DBS-CO₂H and DBS-Gly multi-component hydrogels with GdL

DBS-CO$_2$H and DBS-Gly (3.15 mg of both) were suspended by sonication in 0.65 mL D$_2$O, followed by addition of 51 µL of NaOH$_{(aq)}$ (0.5 M) to dissolve, and DMSO (1.4 µL) to act as an internal standard. GdL (12.6 mg) was then added with shaking, and the solution was immediately transferred to a NMR tube, and spectra were recorded.

8.6.8. DBS-CO₂H hydrogels with DPIN

DPIN (8 mg) was dissolved in 497.5 µL D$_2$O (with 2 µL mL^{-1} DMSO added as internal standard), followed by addition of HCl$_{(aq)}$ (2.5 µL, 0.5 M). Separately, DBS-CO$_2$H (4 mg) was dissolved in 466 µL D$_2$O (with 2 µL mL^{-1} DMSO as internal standard) through the addition of NaOH$_{(aq)}$ (34 µL, 0.5 M). The two solutions were mixed, and 700 µL was transferred to a NMR tube. An initial ^{1}H NMR spectra was recorded, after which the tube was cured for 30 minutes under UV light. A second spectra was then recorded.

8.6.9. DBS-Gly hydrogels with DPIN

DPIN (8 mg) was dissolved in 497.5 µL D$_2$O (with 2 µL mL^{-1} DMSO added as internal standard), followed by addition of HCl$_{(aq)}$ (2.5 µL, 0.5 M). Separately, DBS-Gly (4.5 mg) was dissolved in 461 µL D$_2$O (with 2 µL mL^{-1} DMSO as internal standard) through the addition of NaOH$_{(aq)}$ (39 µL, 0.5 M). The two solutions were mixed, and 700 µL was transferred to a NMR tube. An initial ^{1}H NMR spectra was recorded, after which the tube was cured for 30 minutes under UV light. A second spectra was then recorded.

8.6.10. DBS-CO₂H and DBS-Gly multi-component hydrogels with dual proton source

DPIN (32 mg) was dissolved in 2 mL D$_2$O (with 2 µL mL^{-1} DMSO as an internal standard) to make a stock solution. DBS-CO$_2$H and DBS-Gly (3.15 mg of both) were suspended by sonication in 0.3 mL D$_2$O (with 2 µL mL^{-1} DMSO as an internal standard), followed by addition of 51 µL of NaOH$_{(aq)}$ (0.5 M) to dissolve. 350 µL of DPIN stock solution was then added, followed by 4 mg GdL. The solution was immediately transferred to a NMR tube and placed in the spectrometer to record an initial spectrum. The tube was then allowed to stand overnight, after which a second spectrum was recorded. The tube was then cured under UV light for 1 hour, and then a third and final NMR spectrum was recorded.

8.6.11. DBS-CO₂H and PEGDM hybrid hydrogel with DPIN

DPIN (8 mg) was dissolved in 497.5 µL of D$_2$O, containing of 2 µL mL^{-1} DMSO as internal standard, followed by the addition of HCl$_{(aq)}$ (2.5 µL, 0.5 M). Separately, DBS-CO$_2$H (4 mg) was

dissolved in 466 µL D$_2$O (also containing 2 µL mL^{-1} DMSO as internal standard) through the addition of 34 µL NaOH$_{(aq)}$ (0.5 M). The two solutions were mixed, then PEGDM (50 mg) and PI (0.5 mg) were added. 700 µL of the solution was transferred to an NMR tube, and a spectrum of the solution was then recorded. The NMR tube was then cured under UV light for 1 hour, after which a second spectrum was recorded.

8.6.12. DBS-CO$_2$H, DBS-Gly and PEGDM multi-component hybrid hydrogel with single proton source

DBS-CO$_2$H and DBS-Gly (3.15 mg of both) were suspended in 0.7 mL D$_2$O by sonication, followed by the addition of NaOH$_{(aq)}$ (0.5 M) in 10 µL aliquots to dissolve all solid; DMSO (1.4 µl) was added as an internal standard. GdL (12.6 mg), PEGDM (35 mg) and PI (0.35 mg) were then added, and the solution was transferred to an NMR tube. UV photopolymerisation was then carried out by placing the NMR tube under UV light for 10 minutes.

8.6.13. DBS-CO$_2$H, DBS-Gly and PEGDM multi-component hybrid hydrogel with dual proton source

DPIN (8 mg) was dissolved in 0.5 mL D$_2$O (with 2 µL mL^{-1} DMSO as an internal standard). Separately, DBS-CO$_2$H and DBS-Gly (3.15 mg of both) were suspended by sonication in 0.3 mL D$_2$O, followed by addition of NaOH$_{(aq)}$ (51 µL, 0.5 M) to dissolve the solid. 0.35 mL of the DPIN solution was added to the LMWG solution, followed by PEGDM (35 mg), PI (0.35 mg), and GdL (4 mg). The solution was transferred to an NMR tube and cured under UV for 5 minutes to cause gelation of PEGDM, after which an NMR spectrum was recorded. The NMR tube was then allowed to sit overnight for GdL hydrolysis to occur, then a second spectrum was recorded. Finally, the tube was then cured under UV for a further 30 minutes to sufficiently activate DPIN, and a third spectrum was then recorded.

8.7. NMR kinetics and VT experiments

8.7.1. DBS-CO$_2$H hydrogels with GdL

Samples were prepared as described in section 8.6.1; spectra were recorded every 30 minutes for a period of 14 hours in total, with the time of GdL addition being considered the start point of gelation.

8.7.2. DBS-CO$_2$H and agarose hybrid hydrogels

Samples were prepared as described in section 8.6.2; spectra were recorded every 30 minutes for a period of 14 hours in total, with the time of GdL addition being considered the start point of gelation.

8.7.3. DBS-CO₂H and PEGDM hybrid hydrogels

Samples were prepared as described in section 8.6.4; spectra were recorded every 30 minutes for a period of 14 hours in total, with the time of GdL addition being considered the start point of gelation.

8.7.4. DBS-Gly hydrogels, heat-cool method VT experiments

Samples were prepared as described in section 8.6.5; after gelation, the NMR tube was placed in the spectrometer and spectra were recorded at temperatures from 25 – 75°C (at 10°C intervals).

8.7.5. DBS-Gly hydrogels, pH-change method with GdL

Samples were prepared as described in section 8.6.68.6.4; spectra were recorded every 30 minutes for a period of 14 hours in total, with the time of GdL addition being considered the start point of gelation.

8.7.6. DBS-CO₂H and DBS-Gly multi-component hydrogels, varying amounts of GdL

DBS-Gly and DBS-CO₂H (3.15 mg of both) were suspended by sonication in 0.65 mL D_2O (with 2 µL mL^{-1} DMSO as an internal standard), followed by addition of NaOH$_{(aq)}$ (51 µL, 0.5 M) to dissolve. GdL was then added in known amounts, and the solutions were immediately transferred to NMR tubes and placed in the spectrometer. Spectra were recorded every 30 minutes for a period of 14 hours.

8.7.7. DBS-CO₂H hydrogels with DPIN

DPIN (80 mg) was dissolved in 4.975 mL of D_2O (with 2 µL mL^{-1} DMSO as internal standard), followed by addition of HCl$_{(aq)}$ (25 µL, 0.5 M). Separately, DBS-CO₂H (40 mg) was dissolved in 4.66 mL D_2O (also containing 2 µL mL^{-1} DMSO as internal standard) through the addition of NaOH$_{(aq)}$ (340 µL, 0.5 M). The two solutions were mixed, then 13 separate 700 µL volumes were transferred to NMR tubes. One tube was left uncured, whilst the other 12 were cured under UV light, with one tube being removed every 5 minutes over the course of 1 hour for NMR spectra to be recorded.

8.7.8. DBS-Gly hydrogels with DPIN

DPIN (80 mg) was dissolved in 4.975 mL of D_2O (with 2 µL mL^{-1} DMSO as internal standard), followed by addition of HCl$_{(aq)}$ (25 µL, 0.5 M). Separately, DBS-Gly (45 mg) was dissolved in 4.61 mL D_2O (also containing 2 µL mL^{-1} DMSO as internal standard) through the addition of NaOH$_{(aq)}$ (390 µL, 0.5 M). The two solutions were mixed, then 13 separate 700 µL volumes were transferred to NMR tubes. One tube was left uncured, whilst the other 12 were cured under UV light, with one tube being removed every 5 minutes over the course of 1 hour for NMR spectra to be recorded.

8.7.9. DBS-CO₂H and PEGDM hybrid hydrogels with DPIN

DPIN (160 mg) was dissolved in 9.95 mL of D_2O, (with 2 µL mL^{-1} DMSO as internal standard), followed by addition of $HCl_{(aq)}$ (50 µL, 0.5 M). Separately, DBS-CO₂H (80 mg) was dissolved in 9.32 mL D_2O (also containing 2 µL mL^{-1} DMSO as internal standard) through the addition of $NaOH_{(aq)}$ (680 µL, 0.5 M). The two solutions were mixed, and PEGDM (1 g) and PI (10 mg) were added, and then 26 separate 700 µL volumes were transferred to NMR tubes. One tube was left uncured, whilst the other 25 were cured under UV light, with one tube being removed every 2 minutes over the course of 50 minutes for NMR spectra to be recorded.

8.7.10. DBS-CO₂H, DBS-Gly and PEGDM multi-component hybrid hydrogels with single proton source

Samples were prepared as described in section 8.6.12; spectra were recorded every 30 minutes for a period of 14 hours in total, with the time of GdL addition being considered the start point of gelation.

8.8. CD sample preparation

8.8.1. DBS-CO₂H with GdL

DBS-CO₂H (0.2 or 0.45 mg) was dispersed in H_2O (1 mL) by sonication. $NaOH_{(aq)}$ (20 µL, 0.5 M) was added to dissolve the solid and bring the pH to *ca.* 11. GdL (8 mg) was then added, followed by shaking to dissolve. The solution was allowed to stand for five hours, before 400 µL was transferred to a CD cuvette for spectra to be recorded.

8.8.2. Agarose

Agarose (0.5 mg) was added to 1 mL H_2O in a sample vial. The capped vial was then heated to 90°C in an oil bath, and held at this temperature for 5 minutes, with shaking every minute to dissolve the agarose. The vial was then removed from the oil bath, and allowed to stand for five hours, before 400 µL was transferred to a CD cuvette for spectra to be recorded.

8.8.3. DBS-CO₂H and agarose hybrid system

DBS-CO₂H (0.2 mg) was dispersed in H_2O (1 mL) by sonication. $NaOH_{(aq)}$ (20 µL, 0.5 M) was added to dissolve the solid and bring the pH to *ca.* 11. Agarose (0.5 mg) was then added. The capped vial was then heated to 90°C in an oil bath, and held at this temperature for 5 minutes, with shaking every minute to dissolve the agarose. The solution was then cooled to 50°C, at which temperature it was removed from the oil bath and GdL (8 mg) was added, followed by shaking to dissolve. The solution was allowed to stand for five hours, before 400 µL was transferred to a CD cuvette for spectra to be recorded.

8.8.4.   PEGDM

PEGDM (5 mg) was dissolved in 1 mL of 0.05% wt/vol aqueous solution of PI in a sample vial. The uncapped vial was then cured under UV light for 10 minutes. After standing for 5 hours, 400 µL was transferred to a CD cuvette for spectra to be recorded.

8.8.5.   DBS-CO$_2$H and PEGDM hybrid system

PEGDM (5 mg) was dissolved in 1 mL of 0.05% wt/vol aqueous solution of PI in a sample vial. DBS-CO$_2$H (0.2 mg) was added and dispersed by sonication. NaOH$_{(aq)}$ (20 µl 0.5 M) was added to dissolve the solid and bring the pH to *ca*. 11. The uncapped vial was then cured under UV light for 10 minutes. The solution then transferred to a vial containing GdL (8 mg), followed by shaking to dissolve. After standing for 5 hours, 400 µL was transferred to a CD cuvette for spectra to be recorded.

8.8.6.   DBS-Gly, heat-cool method

1 mL of H$_2$O was added to DBS-Gly (0.1 or 0.5 mg) in a 2.5 mL glass sample vial. The sealed vial was then heated to 95°C in a thermoregulated oil bath, with shaking every few minutes to fully dissolve the LMWG. The vial was removed from the oil bath and cooled to room temperature, then allowed to stand for 5 hours, after which 400 µL was transferred to a CD cuvette for spectra to be recorded.

8.8.7.   DBS-CO$_2$H and DBS-Gly multi-component system with GdL

DBS-CO$_2$H and DBS-Gly (0.45 mg of both) were dispersed in 1 mL H$_2$O by sonication. NaOH$_{(aq)}$ (20 µl 0.5 M) was added to dissolve the solid and bring the pH to *ca*. 11. The solution was transferred to a vial containing 8 mg GdL, followed by shaking to dissolve. The solution was allowed to stand for 5 hours, then 400 µl was transferred to a CD cuvette for spectra to be recorded.

8.8.8.   DBS-CO$_2$H with HCl

DBS-CO$_2$H (0.45 mg) was dispersed in 940 µl H$_2$O by sonication. NaOH$_{(aq)}$ (20 µl 0.5 M) was added to dissolve the solid and bring the pH to *ca*. 11. HCl$_{(aq)}$ (0.5 M, 60 µl) was then added dropwise with gentle stirring. 400 µl was transferred to a CD cuvette for spectra to be recorded.

8.8.9.   DBS-Gly with HCl

DBS-Gly (0.45 mg) was dispersed in 940 µl H$_2$O by sonication. NaOH$_{(aq)}$ (20 µl 0.5 M) was added to dissolve the solid and bring the pH to *ca*. 11. HCl$_{(aq)}$ (0.5 M, 60 µl) was then added dropwise with gentle stirring. 400 µl was transferred to a CD cuvette for spectra to be recorded.

8.8.10. DBS-CO₂H and DBS-Gly multi-component system with HCl

DBS-CO$_2$H and DBS-Gly (0.45 mg of both) was dispersed in 940 µl H$_2$O by sonication. 20 µl 0.5 M NaOH$_{(aq)}$ was added to dissolve the solid and bring the pH to *ca*. 11. HCl$_{(aq)}$ (0.5 M, 60 µl) was then added dropwise with gentle stirring. 400 µl was transferred to a CD cuvette for spectra to be recorded.

8.8.11. DBS-CO₂H with DPIN

DPIN (3.2 mg) was dissolved in 1.999 mL of water, along with 1 µL of HCl$_{(aq)}$ (0.5 M) to make a DPIN stock solution. DBS-CO$_2$H (0.4 mg) was dissolved in 500 µL of H$_2$O through the addition of NaOH$_{(aq)}$ (3.7 µL, 0.5 M), followed by sonication. 500 µL of the DPIN stock solution was added to the DBS-CO$_2$H solution, and this was then cured under UV light for 2 hours to produce a suspension of nanofibers. 400 µl was transferred to a CD cuvette for spectra to be recorded.

8.8.12. DBS-Gly with DPIN

DPIN (3.2 mg) was dissolved in 1.999 mL of water, along with 1 µL of HCl$_{(aq)}$ (0.5 M) to make a DPIN stock solution. DBS-Gly (0.45 mg) was dissolved in 500 µL of H$_2$O through the addition of NaOH$_{(aq)}$ (3.4 µL, 0.5 M), followed by sonication. 500 µL of the DPIN stock solution was added to the DBS-Gly solution, and this was then cured under UV light for 2 hours to produce a suspension of nanofibers. 400 µl was transferred to a CD cuvette for spectra to be recorded.

8.8.13. DBS-CO₂H, DBS-Gly and PEGDM multi-component hybrid system

DBS-CO$_2$H and DBS-Gly (0.45 mg of both) were dispersed in 1 mL H$_2$O by sonication. NaOH$_{(aq)}$ (20 µl 0.5 M) was added to dissolve the solid and bring the pH to *ca*. 11. PEGDM (5 mg), PI (0.05 mg) and GdL (8 mg) were then added, followed by shaking to dissolve. The solution was allowed to stand for 5 hours, then 400 µl was transferred to a CD cuvette for spectra to be recorded.

8.9. CD kinetics and VT experiments

8.9.1. DBS-CO₂H with GdL

DBS-CO$_2$H (0.2 mg) was dispersed in H$_2$O (1 mL) by sonication. NaOH$_{(aq)}$ (20 µL, 0.5 M) was added to dissolve the solid and bring the pH to *ca*. 11. GdL (8 mg) was then added, followed by shaking to dissolve. 400 µL of the solution was immediately transferred to a CD cuvette for spectra to be recorded every 5 minutes for up to 2 hours.

8.9.2. DBS-CO₂H and agarose hybrid system

DBS-CO$_2$H (0.2 mg) was dispersed in H$_2$O (1 mL) by sonication. NaOH$_{(aq)}$ (20 µL, 0.5 M) was added to dissolve the solid and bring the pH to *ca*. 11. Agarose (0.5 mg) was then added. The capped vial was then heated to 90°C in an oil bath, and held at this temperature for 5 minutes, with

shaking every minute to dissolve the agarose. The solution was then cooled to 50°C, at which temperature it was removed from the oil bath and GdL (8 mg) was added, followed by shaking to dissolve. 400 µL of the solution was immediately transferred to a CD cuvette for spectra to be recorded every 5 minutes for up to 80 minutes.

8.9.3. DBS-CO₂H and PEGDM hybrid system

PEGDM (5 mg) was dissolved in 1 mL of 0.05% wt/vol aqueous solution of PI in a sample vial. DBS-CO$_2$H (0.2 mg) was added and dispersed by sonication. NaOH$_{(aq)}$ (20 µl 0.5 M) was added to dissolve the solid and bring the pH to *ca.* 11. The uncapped vial was then cured under UV light for 10 minutes. The solution then transferred to a vial containing GdL (8 mg), followed by shaking to dissolve. 400 µL of the solution was immediately transferred to a CD cuvette for spectra to be recorded every 5 minutes for up to 2 hours.

8.9.4. DBS-Gly, heat-cool method VT experiment

1 mL of H$_2$O was added to DBS-Gly (0.1 or 0.5 mg) in a 2.5 mL glass sample vial. The sealed vial was then heated to 95°C in a thermoregulated oil bath, with shaking every few minutes to fully dissolve the LMWG. The vial was removed from the oil bath and cooled to room temperature, then 400 µL was transferred to a CD cuvette for spectra to be recorded, starting at 20°C and increasing temperature in 10°C increments up to 90°C.

8.10. Responsive yet robust experiment procedures

8.10.1. Table-top method

1 mL H$_2$O was added to DBS-CO$_2$H (2 mg) in a 2.5 mL sample vial. The vial was then sonicated to disperse the solid, and 10 µL aliquots of 0.5 M NaOH$_{(aq)}$ were added to dissolve (pH ≈ 11). Agarose (5 mg) was then added. The capped vial was then heated to 90°C in an oil bath, and held at this temperature for 5 minutes, with shaking every minute to dissolve the agarose. The solution was then cooled to 50°C, at which temperature they were removed from the oil bath and GdL (8 mg) and universal indicator (20 µL) were added, followed by shaking to dissolve. The vials were left overnight for gelation to occur, with the final gel being orange in colour due to the acidic pH. NaOH$_{(aq)}$ (0.054 M, 1 mL) was then applied to the top of the gel, and allowed to diffuse in. When the gel was fully blue, indicating basic pH (after *ca.* 24 hours), the supernatant solution was removed, and a solution of GdL (14 mg dissolved in 0.5 mL) was applied and allowed to diffuse; the gel would become orange again (returned to acidic pH) after *ca.* 24 hours.

8.10.2. NMR method

DBS-CO$_2$H (2 mg) was dispersed in 1 mL D$_2$O by sonication. NaOH$_{(aq)}$ (30 µl, 0.5 M) was then added along with DMSO (2 µl) to act as an internal standard. The solution was transferred to a vial containing agarose (5 mg), which was then heated to 90°C in a thermoregulated oil bath. The solution was cooled to 50°C, and transferred to a vial containing GdL (8 mg), and shaken. A sample (0.5 ml) was then immediately transferred to a NMR tube and placed in the spectrometer to record the initial concentration of mobile DBS-CO$_2$H. After leaving the tube overnight for DBS-CO$_2$H to fully gelate, a spectrum was again recorded. NaOH (20.8 mg) was dissolved in D$_2$O (1 mL, to give 0.54 M). 100 µL of this solution was added onto the top of the gel sample in the NMR tube and allowed to diffuse into the gel. Spectra were recorded periodically, until it was deemed that all the DBS-CO$_2$H was mobile again (*ca.* 36 hours). The supernatant NaOH solution was then removed by pipette. GdL (8 mg) was dissolved in D$_2$O (100 µl), then added onto the top of the gel sample in the NMR tube, and allowed to diffuse, with spectra being recorded periodically until it was deemed that all the DBS-CO$_2$H was again immobilised in a gelator network (*ca.* 4 days).

8.11. pK_a titrations

8.11.1. DBS-CO$_2$H

DBS-CO$_2$H (20 mg) was dispersed in 10 mL H$_2$O by sonication, followed by addition of NaOH$_{(aq)}$ (170 µL, 0.5 M) to dissolve the solid. 5 mL of this solution was used for each titration. To the solution, aliquots of HCl (0.1 M) were added in 20 µL volumes with gentle stirring. The pH values were recorded from a pH meter once the readings had stabilised (*ca.* 10 minutes).

8.11.2. DBS-Gly

DBS-Gly (20 mg) was dispersed in 10 mL H$_2$O by sonication, followed by addition of NaOH$_{(aq)}$ (173 µL, 0.5 M) to dissolve the solid. 5 mL of this solution was used for each titration. To the solution, aliquots of HCl (0.1 M) were added in 15 µL volumes with gentle stirring. The pH values were recorded from a pH meter once the readings had stabilised (*ca.* 10 minutes).

8.12. UV curing and photopatterning procedures

8.12.1. General equipment and setup for UV curing

High-intensity UV curing was carried out using a UV Light Technology Ltd. UV-F 400B lamp. Photopatterned gels were standardly made in a 5 × 5 × 1 cm glass mould, made from 5 mm thick glass, glued together using LOCTITE EA 3430 epoxy adhesive.

During UV curing, the mould was cured in a cooling tray using the following setup: an 8 cm glass petri dish was packed with ice, and placed upside down in a 15 cm petri dish; the square

mould was sat on top of the 8 cm petri dish, and then more ice was packed around the mould (see Figure 8.2). In photopatterning experiments, a mask made from either cardboard or laser-printed acetate was sat across the top of the glass mould.
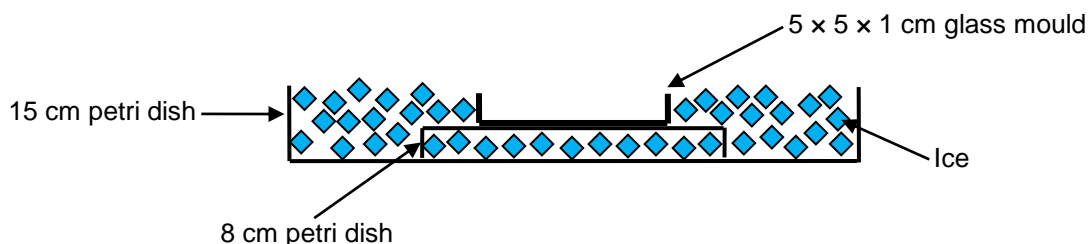
Figure 8.2: Typical setup of a cooling tray used for cooling glass mould and gel during UV curing.

8.12.2. Procedure for hybrid hydrogels of DBS-CO$_2$H and PEGDM with GdL as proton source

5 mg of PI was dissolved in 10 mL H$_2$O. 500 mg of PEGDM was added and stirred to dissolve. 20 mg DBS-CO$_2$H was then added, followed by sonication to disperse and addition of 0.3 mL NaOH$_{(aq)}$ (0.5 M) to dissolve DBS-CO$_2$H. 80 mg of GdL was added with stirring, then the solution was transferred to a 5 x 5 x 1 cm square glass mould. A cardboard mask was placed over the top so that only part of the gel was exposed. The mould was then sat in a cooling tray (to minimise heating) and placed under a long-wavelength UV lamp. The solution was cured for 20 mins, after which the exposed region of the solution had formed a gel. The mould was then transferred to a petri dish, covered (to prevent evaporation) and left overnight for DBS-CO$_2$H to gelate the remaining solution.

8.12.3. Procedure for multi-component hydrogels of DBS-CO$_2$H and DBS-Gly with dual proton source

48 mg of DPIN was dissolved in 3 mL H$_2$O to make a stock solution. 22.5 mg of both DBS-Gly and DBS-CO$_2$H were suspended in 2.5 mL H$_2$O by sonication, followed by addition of 255 µl NaOH$_{(aq)}$ (0.5 M) to dissolve DBS-CO$_2$H and DBS-Gly. 2.5 mL of DPIN stock was then added, followed by 20 mg of GdL. The solution was then transferred to a 5 x 5 x 1 cm square glass mould; the mould was then transferred to a petri dish, covered (to prevent evaporation) and left overnight for GdL hydrolysis to occur. The next day, the mould was removed from the petri dish, and a cardboard mask was placed over the top so that only part of the gel was exposed. The mould was then sat in the cooling tray (to minimise heating), and placed under a long-wavelength UV lamp and cured for 1 hour, after which the exposed region of the solution had become visibly opaque.

8.12.4. Procedure for hybrid hydrogels of DBS-CO₂H and PEGDM with DPIN as proton source

64 mg of DPIN was dissolved in 3.98 mL H_2O with 20 µL $HCl_{(aq)}$ (0.5 M) to make a stock solution. 24 mg of DBS-CO₂H was suspended by sonication in 2.8 mL H_2O, then 0.2 mL of $NaOH_{(aq)}$ (0.5 M) was added to dissolve DBS-CO₂H. 3 mL of DPIN stock was added to the DBS-CO₂H solution, followed by 3 mg of PI and 300 mg of PEGDM, with stirring. The solution was transferred to a 5 x 5 x 1 cm square glass mould. The dish was then sat in a cooling tray (to minimise heating) and placed under a long-wavelength UV lamp. The solution was cured for 10 mins to gelate PEGDM, after which a mask (cardboard or acetate) could be applied before a further 50 minutes curing to fully activate DPIN and form a patterned hydrogel.

8.12.5. Procedure for multi-component hybrid hydrogels of DBS-CO₂H, DBS-Gly and PEGDM

8.12.5.1. Multi-component hybrid hydrogels with three domains

48 mg of DPIN was dissolved in 3 mL of H_2O to make a stock solution. Separately, 22.5 mg of both DBS-CO₂H and DBS-Gly were dissolved in 2.245 mL H_2O, followed by sonication to disperse the solid, followed by addition of 255 µL $NaOH_{(aq)}$ (0.5 M) to dissolve the solid. 2.5 mL of the DPIN stock solution was added to the LMWG solution, followed by 250 mg of PEGDM, 2.5 mg of PI, and 20 mg of GdL with stirring. The solution was poured into a 5 x 5 x 1 cm square glass mould, then sat in a cooling tray (to minimise heating) and cured under UV light for 10 minutes; a mask could be applied during this step to pattern the formation of the PEGDM network. The mould was then transferred to a petri dish, covered (to prevent evaporation) and left overnight for GdL hydrolysis to occur. The next day, the mould was removed from the petri dish, sat in a cooling tray, and then cured under UV for a further 50 minutes to activate the remaining DPIN; a mask could also be applied during this step to pattern the formation of the DBS-Gly and further PEGDM networks.

8.12.5.2. Multi-component hybrid hydrogels with four domains

48 mg of DPIN was dissolved in 3 mL of H_2O to make a stock solution. Separately, 22.5 mg of both DBS-CO₂H and DBS-Gly were dissolved in 2.245 mL H_2O, followed by sonication to disperse the solid, followed by addition of 255 µL $NaOH_{(aq)}$ (0.5 M) to dissolve the solid. 2.5 mL of the DPIN stock solution was added to the LMWG solution, followed by 250 mg of PEGDM, 2.5 mg of PI, and 20 mg of GdL with stirring. The solution was poured into a 5 x 5 x 1 cm glass mould, and sat in a cooling tray (to minimise heating). A mask was applied over the solution, which was then cured under UV light for 10 minutes. The non-gelled solution was then poured away. 11.25 mg of both DBS-CO₂H and DBS-Gly were suspended in 2.37 mL of H_2O by sonication, followed by addition of 130 µL of $NaOH_{(aq)}$ (0.5 M) to dissolve the solid. 20 mg of DPIN and 10 mg of GdL

was then added to this solution with stirring. The solution was then poured into the mould to fill the voids from removal of the first solution. The mould was then transferred to a petri dish, covered (to prevent evaporation) and left overnight for GdL hydrolysis to occur. The next day, the mould was removed from the petri dish, sat in a cooling tray, and then cured under UV for a further 50 minutes to activate the remaining DPIN; a mask could also be applied during this step to pattern formation of the DBS-Gly networks.

8.13. SEM sample preparation

8.13.1. Freeze-drying method

Gels were prepared as described in section 8.3, or as described in section 8.10 for gels which could not be produced in 1 mL volumes in sample vials – in these cases, 0.5 mL of solution was cured in a 2.5 mL sample vial.

Gels were then prepared for SEM by freeze-drying; this was carried out by Meg Stark at the Biology Technology Facility, University of York, using the method described below.

The gel was spread using a mounted needle on a thin piece of copper shim (to act as support); excess liquid was removed with filter paper. The gel was frozen on the copper support by submersion in nitrogen slush (*ca.* -210°C); after this water was removed from the gel by lyophilising on a Peltier stage, with a maximum temperature of -50°C. Once dry, the gel was knocked off the shim with a mounted needle, and the shim was mounted on an SEM stub using a carbon sticky tab. The sample was then sputter-coated with a thin layer (< 12 nm) of gold/palladium coating to prevent sample charging, before SEM imaging.

8.13.2. Ambient drying method

Suspensions were prepared as described below. To prepare the sample for SEM a small amount of the suspensions were applied to metal SEM stubs, and these were then dried under ambient conditions to yield dried-down xerogels. The samples were then sputter-coated with a thin layer of palladium to prevent sample charging before SEM imaging.

8.13.2.1. *DBS-CO2H with DPIN*

DPIN (8 mg) was dissolved in 497.5 µL H_2O, followed by addition of $HCl_{(aq)}$ (2.5 µL, 0.5 M). Separately, DBS-CO_2H (4 mg) was dissolved in 466 µL H_2O through the addition of $NaOH_{(aq)}$ (34 µL, 0.5 M) and sonication. The two solutions were mixed, then cured under UV light for 2 hours.

DPIN (8 mg) was dissolved in 497.5 µL H_2O, followed by addition of $HCl_{(aq)}$ (2.5 µL, 0.5 M). Separately, DBS-Gly (4.5 mg) was dissolved in 461 µL H_2O through the addition of $NaOH_{(aq)}$ (39 µL, 0.5 M) and sonication. The two solutions were mixed, then cured under UV light for 2 hours.

8.14. TEM sample preparation

8.14.1. DBS-CO₂H hydrogels, with or without MB dye

Gels were prepared as described in section 8.3.1; for gels containing methylene blue chloride, 0.1 mg mL^{-1} of the dye was added at the same time as GdL.

To prepare samples for TEM, a small portion of gel was removed with a spatula and 'drop-cast' onto a heat-treated copper TEM grip. Excess material was removed using filter paper and left to dry for 20 minutes prior to imaging. A uranyl acetate stain was used for contrast.

8.15. UV-vis experiments

8.15.1. Controlled release from PEGDM hydrogels and DBS-CO₂H and PEGDM hybrid hydrogels

8.15.1.1. *Calibration*

0.5 mg of the selected dye (either methylene blue chloride, malachite green oxalate, or Direct Red 80) was dissolved in 5 mL pH7 phosphate-buffered saline (PBS). 0.5 mL of this solution was then added to 29.5 mL PBS to make a stock solution. 1 mL volumes of solutions were prepared from this stock in dilutions ranging from 1 in 10 to 9 in 10. Calibration plots (Figure 8.3, Figure 8.4 and Figure 8.5) were then recorded using these solutions and the undiluted stock.
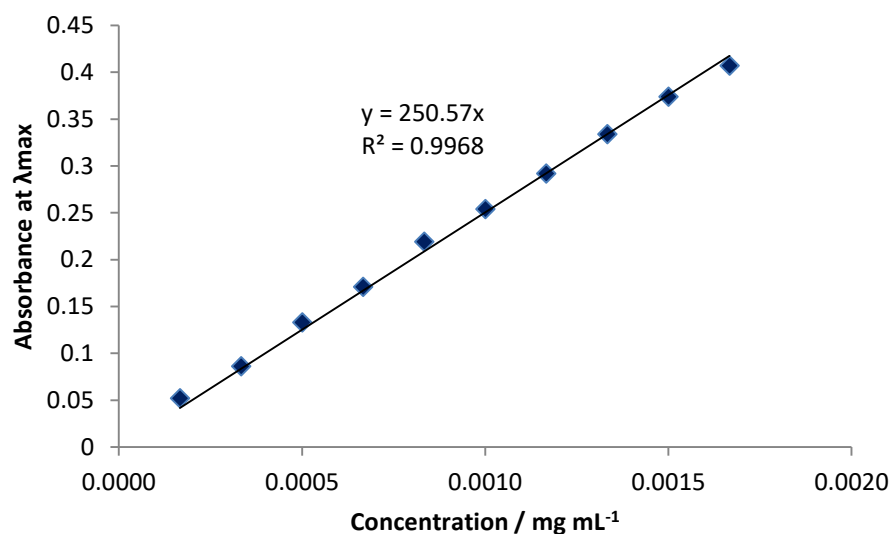
Figure 8.3: Calibration plot of methylene blue for controlled release, λ_{max} = 663 nm.

y = 109.08x
R² = 0.9989

Absorbance at λmax

Concentration of malachite green / mg mL⁻¹
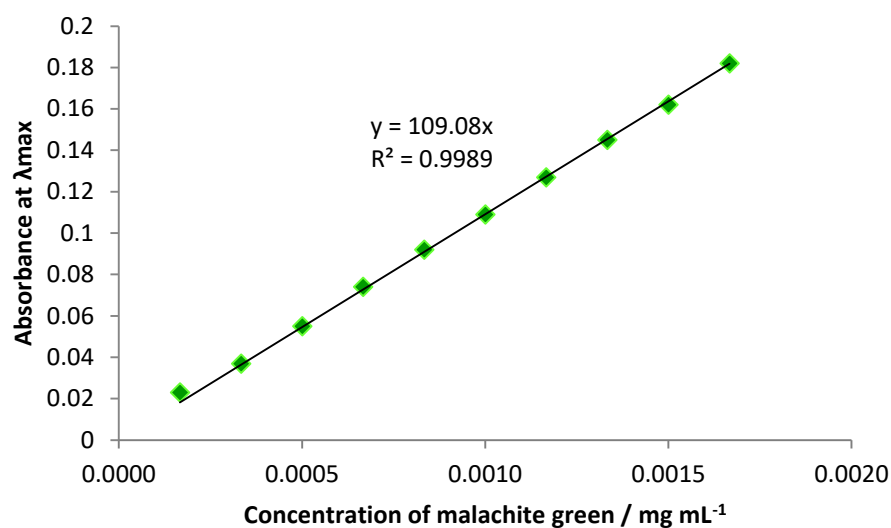
Figure 8.4: Calibration plot of malachite green for controlled release, λ_{max} = 617 nm.

y = 26.197x
R² = 0.995

Absorbance a λmax

Concentration of Direct Red 80 / mg mL⁻¹
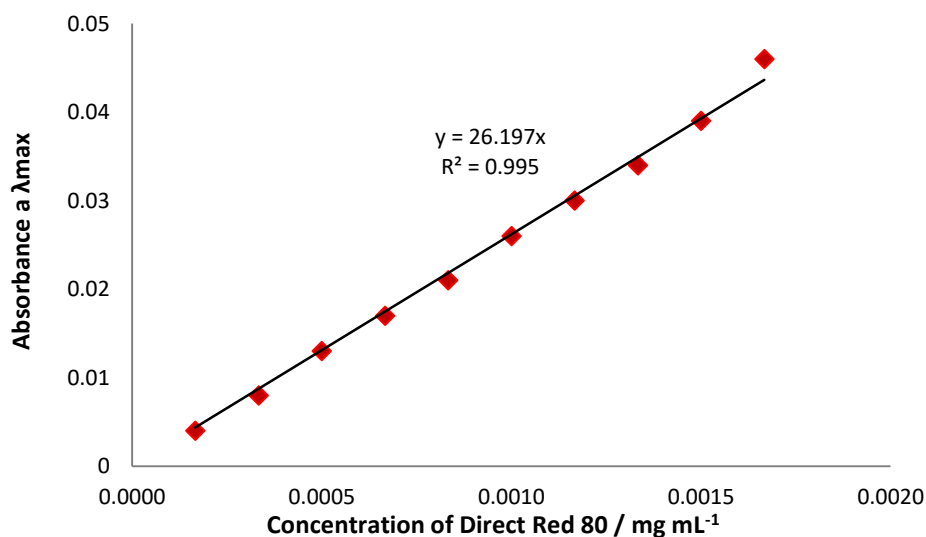
Figure 8.5: Calibration plot of Direct Red 80 for controlled release, λ_{max} = 541 nm.

8.15.1.2. Controlled release procedure

For PEGDM gels, 0.1 mg of selected dye (methylene blue chloride, malachite green oxalate or Direct Red 80) was dissolved in 1 mL H_2O. To this solution was added 0.5 mg PI and 50 mg PEGDM. The solutions were cured in uncapped 2.5 mL vials under a long wavelength UV source for 10 minutes to obtain gels.

For hybrid gels, 0.1 mg of selected dye (methylene blue chloride, malachite green oxalate or Direct Red 80) was dissolved in 1 mL H_2O. To this solution was added 0.5 mg PI and 50 mg PEGDM. 2 mg of DBS-CO_2H was then added, followed by sonication to disperse and addition of

NaOH (0.5 M in 10 μL aliquots) to dissolve. The solutions were then transferred to vials containing 8 mg of GdL, followed by shaking to dissolve. The solutions were cured in uncapped 2.5 mL vials under a long wavelength UV source for 10 minutes in order to polymerise the PEGDM network. The vials were then capped and left overnight for DBS-CO$_2$H gelation to occur.

The prepared gels were cut in half horizontally to yield two cylindrical gels of 0.5 mL in volume. The gel was then submerged in 30 mL of pH 7 phosphate buffer solution. A 2 mL sample was taken every hour for 7 hours to be analysed by UV-vis spectroscopy, then returned to the bulk solution. A final sample was taken at 24 hours. Absorbance of MB was measured at 663 nm, absorbance of MG at 617 nm, and absorbance of DR80 at 541 nm. Using the calibration plots the concentration, and thus percentage, of dye released was calculated.

8.15.2. Adsorption of MB and MG dyes onto DBS-CO$_2$H

8.15.2.1. *Calibration*

2 mg of the selected dye (either methylene blue chloride or malachite green oxalate) was dissolved in 100 mL H$_2$O. 1 mL volumes of solutions were prepared from this stock in dilutions 20%, 40%, 60%, 80% and 100%. Calibration plots (Figure 8.6 and Figure 8.7) were then recorded using these solutions.
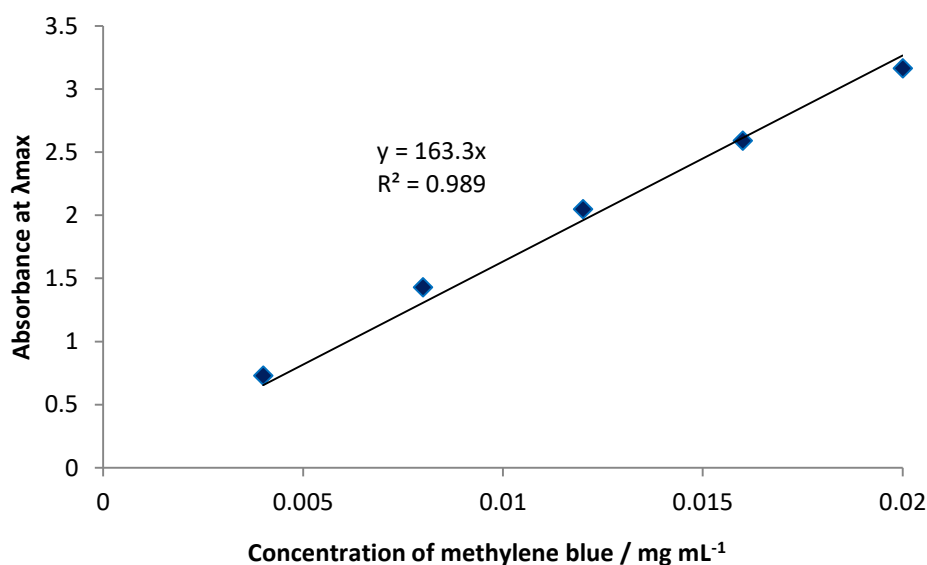
Figure 8.6: Calibration plot of methylene blue for adsorption, λ$_{max}$ = 663 nm.
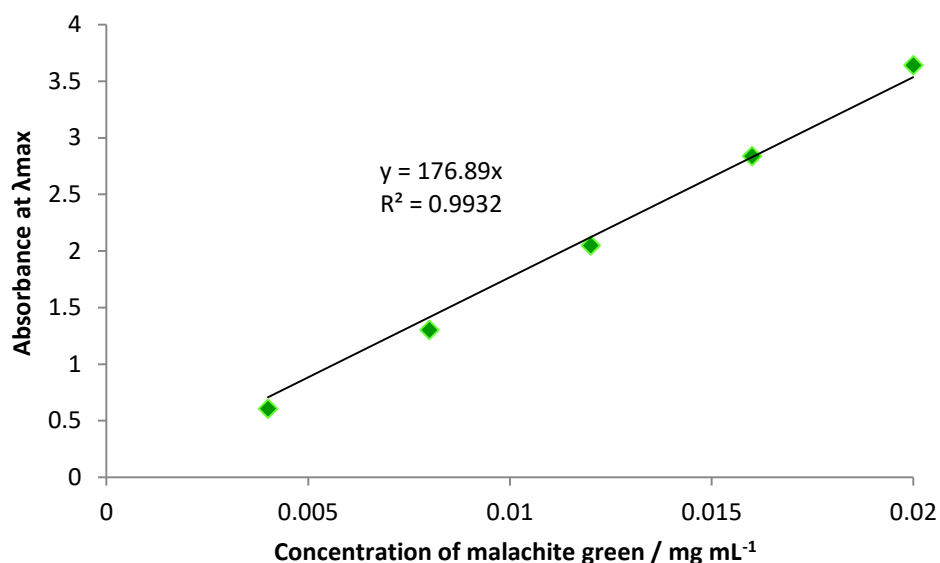
Figure 8.7: Calibration plot of malachite green for adsorption, λ_{max} = 617 nm.

8.15.2.2. Adsorption procedure

0.5 mL H$_2$O was added to 3 mg of DBS-CO$_2$H in sample vials. The vials were then sonicated to disperse the solid, and 10 µL aliquots of NaOH$_{(aq)}$ (0.5 M) were added to dissolve. The solutions were then transferred to 8 mL sample vials containing 13 mg of GdL, followed by shaking to dissolve. The vials were then left overnight for gelation to occur.

Dye solutions were prepared by dissolving 200 µg of either methylene blue chloride (MB) or malachite green oxalate (MG) in 10 mL of H$_2$O (to give a concentration of 20 µg mL^{-1}). 4 mL of dye solution was added to the top of each gel. The systems were allowed to stand undisturbed at room temperature for a total of 24 hours. At 0, 2, 4, 6 and 24 hours, a 2 mL aliquot of the supernatant solution was taken for UV-vis spectroscopy, then returned to the bulk solution. Absorbance was measured at maximum absorbance wavelength of 663 nm for MB, and at 617 nm for MG. Using the calibration plots, the percentage of dye adsorbed was calculated.

Appendix

Exemplar assigned ^{1}H NMR spectra

DBS-CO₂Me:
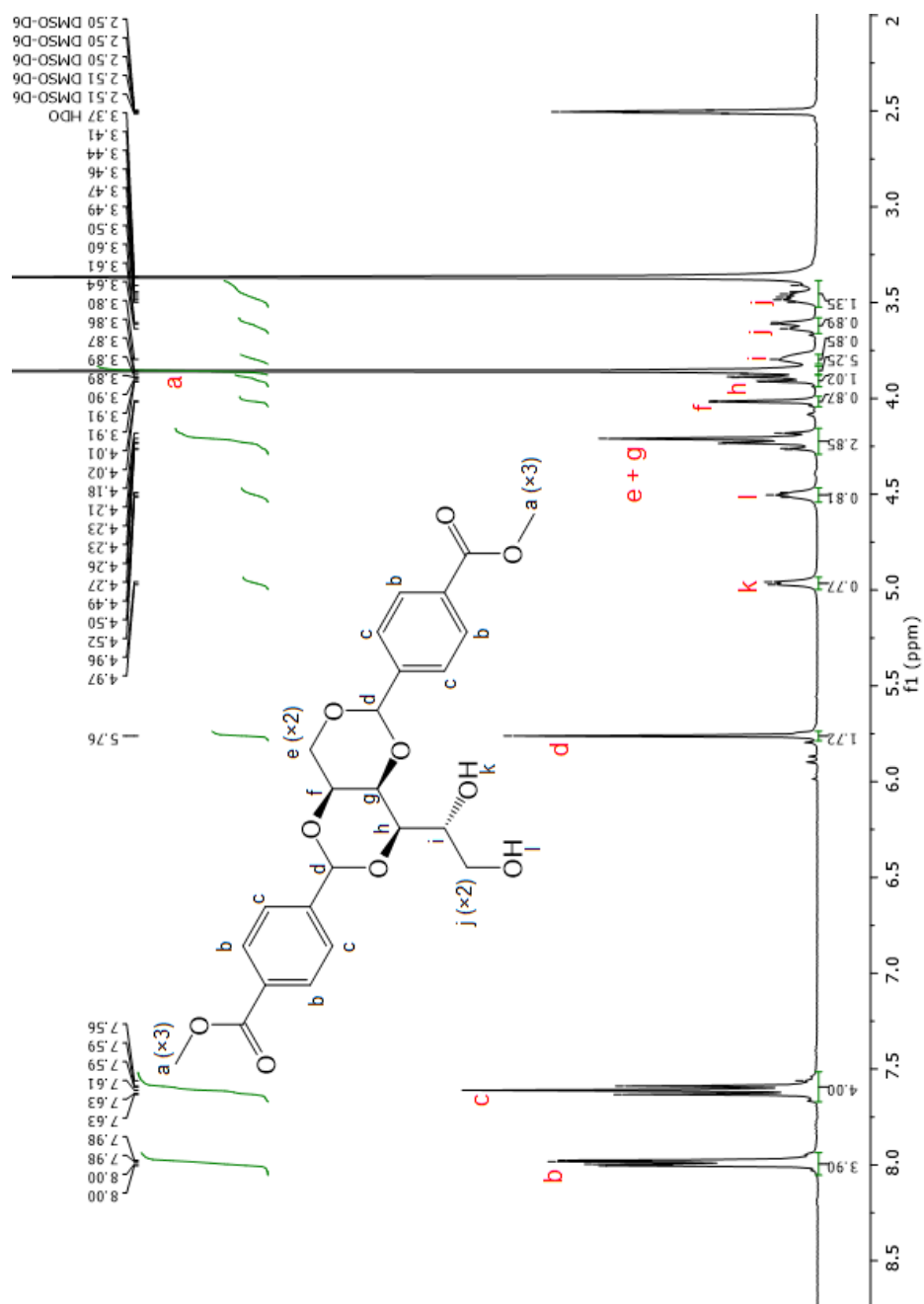
DBS-CO₂H:
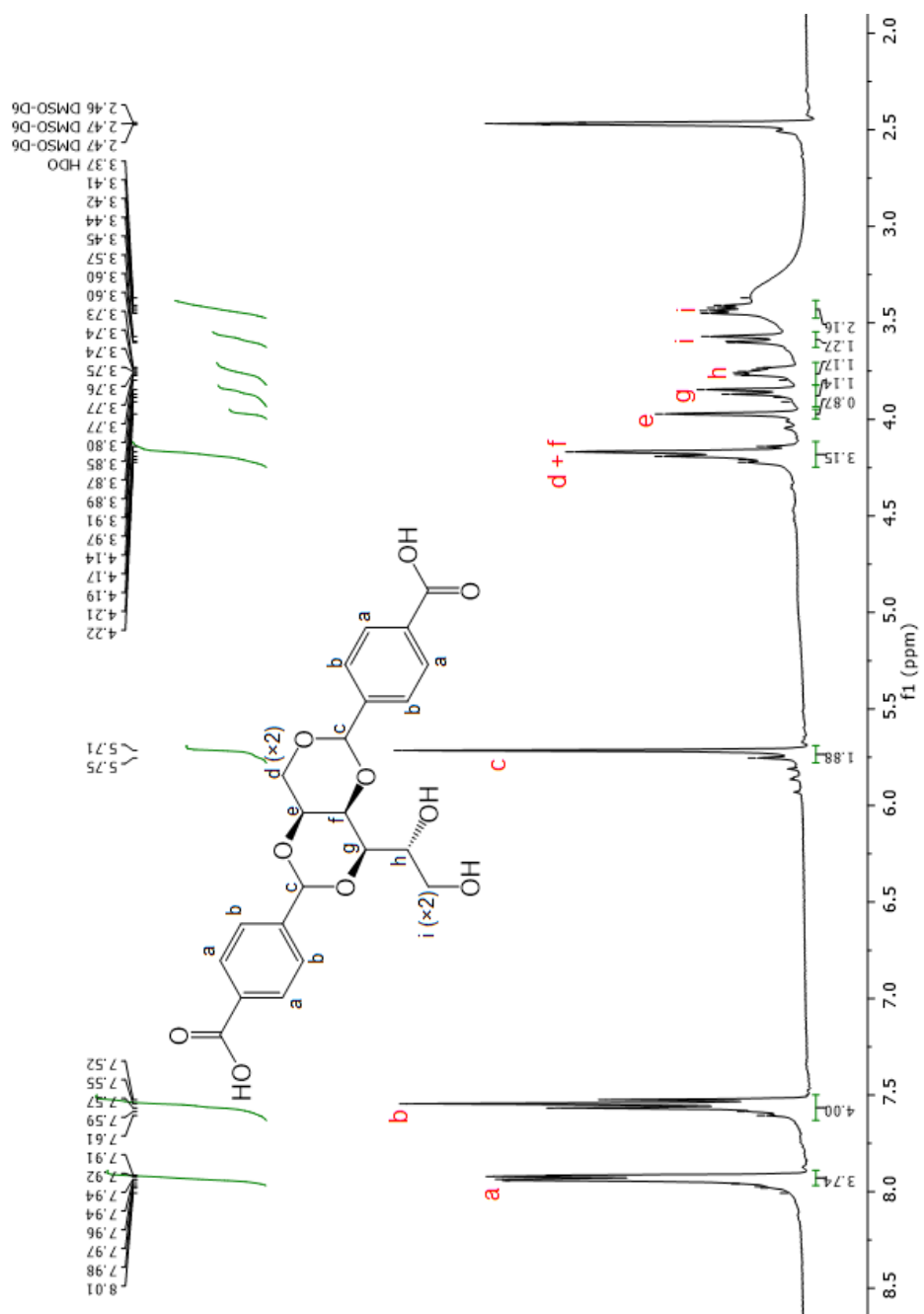
PEGDM:

Maldi MS spectra

PEGDM:
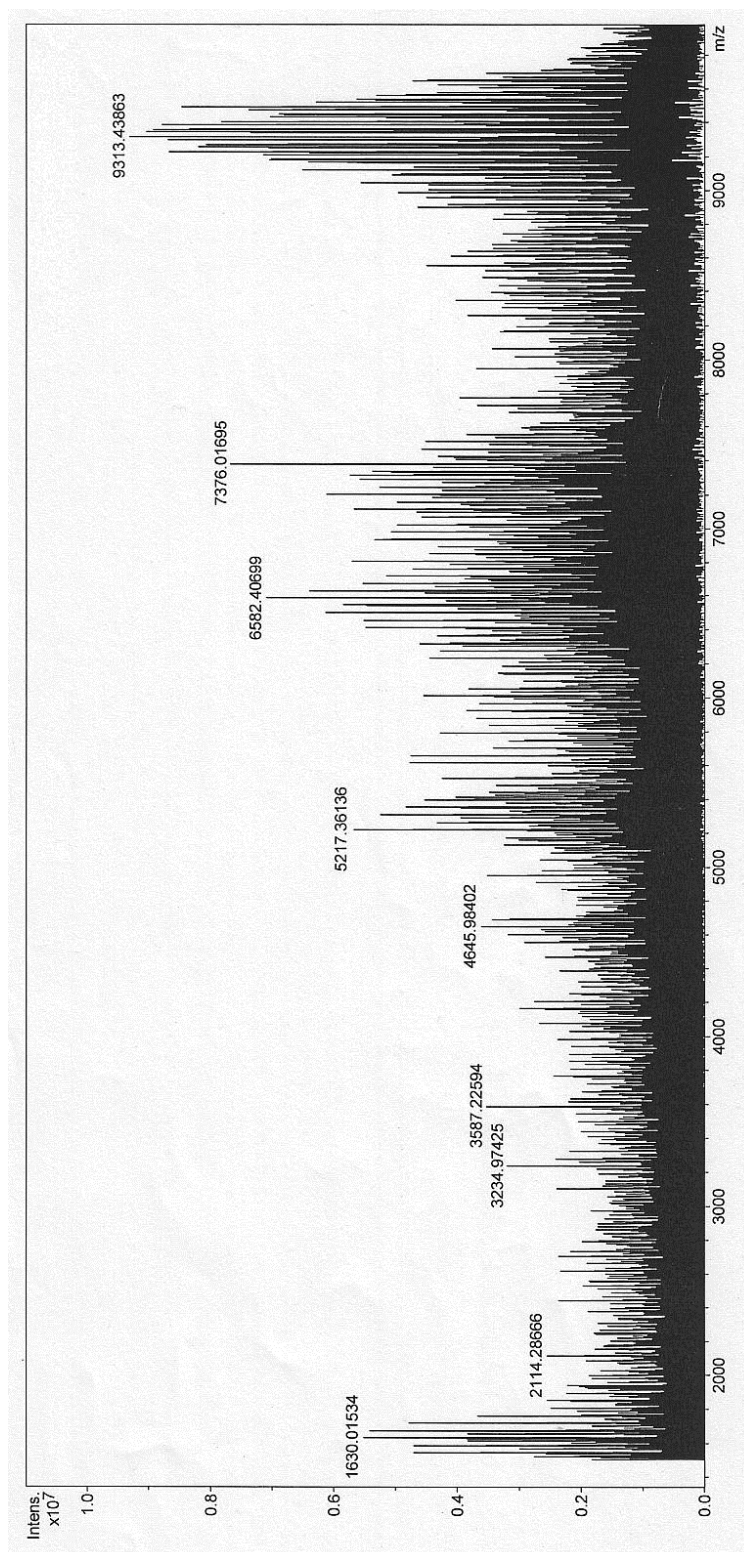
List of Abbreviations

Ar	aromatic
app	apparent (NMR)
aq	aqueous
br	broad (NMR)
CD	circular dichroism spectroscopy
CDCl$_3$	deuterated chloroform
d	doublet (NMR)
dd	doublet of doublets (NMR)
ddd	double doublet of doublets (NMR)
D$_2$O	deuterated water (heavy water)
DBS	1,3:2,4-dibenzylidene-D-sorbitol
DBS-Ala	1,3:2,4-dibenzylidene-D-sorbitol-*p,p'*-dicarbonyl alanine
DBS-AlaOMe	1,3:2,4-dibenzylidene-D-sorbitol-*p,p'*-dicarbonyl alanine methyl ester
DBS-Asp	1,3:2,4-dibenzylidene-D-sorbitol-*p,p'*-dicarbonyl aspartic acid
DBS-Asp(OMe)$_2$	1,3:2,4-dibenzylidene-D-sorbitol-*p,p'*-dicarbonyl aspartic acid dimethyl ester
DBS-CO$_2$H	1,3:2,4-dibenzylidene-D-sorbitol-*p,p'*-dicarboxylic acid
DBS-CO$_2$Me	1,3:2,4-dibenzylidene-D-sorbitol-*p,p'*-dimethyl ester
DBS-Gly	1,3:2,4-dibenzylidene-D-sorbitol-*p,p'*-dicarbonyl glycine
DBS-GlyOMe	1,3:2,4-dibenzylidene-D-sorbitol-*p,p'*-dicarbonyl glycine methyl ester
DBS-Phe	1,3:2,4-dibenzylidene-D-sorbitol-*p,p'*-dicarbonyl phenylalanine

DBS-PheOMe	1,3:2,4-dibenzylidene-D-sorbitol-*p*,*p'*-dicrbonyl phenylalanine methyl ester
DBS-Trp	1,3:2,4-dibenzylidene-D-sorbitol-*p*,*p'*-dicarbonyl tryptophan
DBS-TrpOMe	1,3:2,4-dibenzylidene-D-sorbitol-*p*,*p'*-dicarbonyl tryptophan methyl ester
DCM	dichloromethane
DEPT	distortionless enhancement by polarization transfer
DIPEA	diisopropylethylamine
DMSO	dimethylsulfoxide
DMSO-*d6*	deuterated dimethylsulfoxide
DPIN	diphenyliodonium nitrate
DR80	Direct Red 80
Eq.	equation
eq/equiv	equivalent
ESI-MS	electrospray ionisation mass spectrometry
FEG-SEM	field emission gun scanning electron microscopy
FT-IR	Fourier transform infrared spectroscopy
G'	storage modulus
G''	loss modulus
GdL	glucono-δ-lactone
HCl	hydrochloric acid
HOD	partially deuterated water (one hydrogen atom, one deuterium atom)
HT	high tension voltage

Hz	hertz
IR	infrared
J	coupling constant (in hertz)
K	Kelvin
LMWG	low-molecular-weight gelator
LVR	linear viscoelastic region
M	moles per dm^3
m	multiplet (NMR)
m	medium (IR)
MGC	minimum gelator concentration
M.p.	melting point
m/z	mass to charge ratio
MALDI-MS	matrix-assisted laser desorption/ionisation
MB	methylene blue (chloride)
mdeg	millidegrees
MG	malachite green (oxalate)
mg	milligrams
min	minutes
mL	millilitres
mM	millimoles per dm^3
MS	mass spectrometry

MW	molecular weight
NaHSO₄	sodium hydrogen sulfate
NaOH	sodium hydroxide
nm	nanometre
NMR	nuclear magnetic resonance (spectroscopy)
Pa	Pascal
PAG	photoacid generator
PEG	poly(ethylene glycol)
PEGDM	poly(ethylene glycol) dimethacrylate, here commonly used to refer to PEGDM synthesised from PEG 8000
PG	polymer gelator
pH	negative logarithm of the concentration of hydrogen ions
PI	photoinitiator, here used to refer to 2-hydroxy-4′-(2-hydroxyethoxy)-2-methylpropiophenone
pK_a	negative logarithm of the acid disassociation constant
ppm	parts per million
***p*-TsOH**	*para*-toluene sulfonic acid (monohydrate)
q	quartet (NMR)
R	gas constant, 8.314 J K^{-1} mol^{-1}
RGD	arginine-glycine-aspartic acid tripeptide
rt	room temperature
s	singlet (NMR)

s	strong (IR)
SEM	scanning electron microscopy
sol	solution
t	time **or** triplet (NMR)
TBTU	O-(Benzotriazol-1-yl)-N,N,N',N'-tetramethyluronium tetrafluoroborate
TEA	triethylamine
TEM	transmission electron microscopy
T_{gel}	gel-sol transition temperature
UV	ultraviolet
UV-vis	ultraviolet visible (spectroscopy)
VT	variable temperature
w	weak (IR)
wt/vol	weight to volume ratio
ΔH	change in enthalpy
ΔS	change in entropy
δ	NMR chemical shift (in ppm)
λ_{max}	wavelength at maximum intensity
μg	micrograms
μL	microlitres
ν_{max}	wavenumber at maximum peak intensity

References

1   P. Terech and R. G. Weiss, *Chem. Rev.*, 1997, **97**, 3133–3160.

2   H. B. Bohidar, P. Dubin and Y. Osada, Eds., *Polymer Gels: Fundamentals and Applications*, American Chemical Society, Washington DC, 2002.

3   M. Suzuki and K. Hanabusa, *Chem. Soc. Rev.*, 2010, **39**, 455–463.

4   E. A. Appel, J. del Barrio, X. J. Loh and O. A. Scherman, *Chem. Soc. Rev.*, 2012, **41**, 6195–6214.

5   K. Y. Lee and D. J. Mooney, *Chem. Rev.*, 2001, **101**, 1869–1880.

6   J. Jagur-Grodzinski, *Polym. Adv. Technol.*, 2010, **21**, 27–47.

7   I. Gibas and H. Janik, *Chem. Chem. Technol.*, 2010, **4**, 297–304.

8   R. G. Weiss and P. Terech, Eds., *Molecular Gels: Materials with Self-Assembled Fibrillar Networks*, Springer, Dordrecht, Netherlands, 2006.

9   L. A. Estroff and A. D. Hamilton, *Chem. Rev.*, 2004, **104**, 1201–1218.

10 M. de Loos, B. L. Feringa and J. H. Van Esch, *Eur. J. Org. Chem.*, 2005, 3615–3631.

11 J. H. Van Esch, *Langmuir*, 2009, **25**, 8392–8394.

12 J. W. Steed, *Chem. Commun.*, 2011, **47**, 1379–1383.

13 L. E. Buerkle and S. J. Rowan, *Chem. Soc. Rev.*, 2012, **41**, 6089–6102.

14 A. R. Hirst, B. Escuder, J. F. Miravet and D. K. Smith, *Angew. Chem. Int. Ed.*, 2008, **47**, 8002–8018.

15 N. M. Sangeetha and U. Maitra, *Chem. Soc. Rev.*, 2005, **34**, 821–836.

16 S. Banerjee, R. K. Das and U. Maitra, *J. Mater. Chem.*, 2009, **19**, 6649–6687.

17 J. H. Fuhrhop and C. Boettcher, *J. Am. Chem. Soc.*, 1990, **112**, 1768–1776.

18 A. R. Hirst, B. Huang, V. Castelletto, I. W. Hamley and D. K. Smith, *Chem. Eur. J.*, 2007, **13**, 2180–2188.

19 J. R. Moffat and D. K. Smith, *Chem. Commun.*, 2009, 316–318.

20 J. A. Foster, R. M. Edkins, G. J. Cameron, N. Colgin, K. Fucke, S. Ridgeway, A. G. Crawford, T. B. Marder, A. Beeby, S. L. Cobb and J. W. Steed, *Chem. Eur. J*, 2014, **20**, 279–291.

21 S. Cicchi, G. Ghini, L. Lascialfari, A. Brandi, F. Betti, D. Berti, P. Baglioni, L. Di Bari, G.

Pescitelli, M. Mannini and A. Caneschi, *Soft Matter*, 2010, **6**, 1655–1661.

22   M. R. Molla, A. Das and S. Ghosh, *Chem. Eur. J.*, 2010, **16**, 10084–10093.

23   A. Das and S. Ghosh, *Chem. Commun.*, 2011, **47**, 8922–8924.

24   A. Das, M. R. Molla and S. Ghosh, *J. Chem. Sci.*, 2011, **123**, 963–973.

25   M. R. Molla, A. Das and S. Ghosh, *Chem. Commun.*, 2011, **47**, 8934–8936.

26   A. Das, M. R. Molla, A. Banerjee, A. Paul and S. Ghosh, *Chem. Eur. J.*, 2011, **17**, 6061–6066.

27   K. Sugiyasu, S. Kawano, N. Fujita and S. Shinkai, *Chem. Mater.*, 2008, **20**, 3871–3873.

28   R. Afrasiabi and H. B. Kraatz, *Chem. Eur. J.*, 2013, **19**, 15862–15871.

29   K. L. Morris, L. Chen, J. Raeburn, O. R. Sellick, P. Cotanda, A. Paul, P. C. Griffiths, S. M. King, R. K. O'Reilly, L. C. Serpell and D. J. Adams, *Nat. Commun.*, 2013, **4**, 1480.

30   C. Colquhoun, E. R. Draper, E. G. B. Eden, B. N. Cattoz, K. L. Morris, L. Chen, T. O. McDonald, A. E. Terry, P. C. Griffiths, L. C. Serpell and D. J. Adams, *Nanoscale*, 2014, **6**, 13719–13725.

31   M. M. Smith and D. K. Smith, *Soft Matter*, 2011, **7**, 4856–4860.

32   D. G. Velázquez and R. Luque, *Chem. Eur. J.*, 2011, **17**, 3847–3849.

33   P. Xing, X. Chu, S. Li, F. Xin, M. Ma and A. Hao, *New J. Chem.*, 2013, **37**, 3949–3955.

34   X. Yan, F. Wang, B. Zheng and F. Huang, *Chem. Soc. Rev.*, 2012, **41**, 6042.

35   M. de Loos, J. van Esch, I. Stokroos, R. M. Kellog and B. L. Feringa, *J. Am. Chem. Soc.*, 1997, **7863**, 12675–12676.

36   H. Eimura, M. Yoshio, Y. Shoji, K. Hanabusa and T. Kato, *Polym. J.*, 2012, **44**, 594–599.

37   M. George and R. G. Weiss, *Chem. Mater.*, 2003, **15**, 2879–2888.

38   C. Kim, S. J. Lee, I. H. Lee and K. T. Kim, *Chem. Mater.*, 2003, **15**, 3638–3642.

39   M. Shirakawa, N. Fujita and S. Shinkai, *J. Am. Chem. Soc.*, 2005, **127**, 4164–4165.

40   K. Aoki, M. Kudo and N. Tamaoki, *Org. Lett.*, 2004, **6**, 429–430.

41   O. J. Dautel, M. Robitzer, J. Le and J. E. Moreau, *J. Am. Chem. Soc.*, 2006, **128**, 16213–16223.

42   N. Fujita, Y. Sakamoto, M. Shirakawa, M. Ojima, A. Fujii, M. Ozaki and S. Shinkai, *J. Am. Chem. Soc.*, 2007, **129**, 4134–4135.

43 E. Jahnke, I. Lieberwirth, N. Severin, J. P. Rabe and H. Frauenrath, *Angew. Chem. Int. Ed.*, 2006, **45**, 5383–5386.

44 E. Jahnke, N. Severin, P. Kreutzkamp, J. P. Rabe and H. Frauenrath, *Adv. Mater.*, 2008, **20**, 409–414.

45 J. Nagasawa, M. Kudo and S. Hayashi, *Langmuir*, 2004, **6**, 7907–7916.

46 X. Nie and G. Wang, *J. Org. Chem.*, 2006, **71**, 4734–4741.

47 C. S. Love, V. Chechik, D. K. Smith, I. Ashworth and C. Brennan, *Chem. Commun.*, 2005, **45**, 5647–5649.

48 J. R. Moffat, I. A. Coates, F. J. Leng and D. K. Smith, *Langmuir*, 2009, **25**, 8786–8793.

49 D. D. Díaz, K. Rajagopal, E. Strable, J. Schneider and M. G. Finn, *J. Am. Chem. Soc.*, 2006, **128**, 6056–7.

50 D. D. Díaz, J. J. Cid, P. Vázquez and T. Torres, *Chem. Eur. J.*, 2008, **14**, 9261–9273.

51 D. D. Díaz, E. Morin, E. M. Schön, G. Budin, A. Wagner and J.-S. Remy, *J. Mater. Chem.*, 2011, **21**, 641–644.

52 M.-O. M. Piepenbrock, N. Clarke, J. A. Foster and J. W. Steed, *Chem. Commun.*, 2011, **47**, 2095–2097.

53 P. Kubiak, S. Awhida, C. Hotchen, W. Deng, B. M. Alston, T. O. McDonald, D. J. Adams and P. J. Cameron, *Chem. Commun.*, 2015, **51**, 10427–10430.

54 H. Gankema, M. A. Hempenius, M. Möller, G. Johansson and V. Percec, *Macromol. Symp.*, 1996, **102**, 381–390.

55 U. Beginn, S. Keinath and M. Möller, *Macromol. Chem. Phys.*, 1998, **119**, 2379–2384.

56 U. Beginn, S. Sheiko and M. Möller, *Macromol. Chem. Phys.*, 2000, **201**, 1008–1015.

57 W. Gu, L. Lu, G. B. Chapman and R. G. Weiss, *Chem. Commun.*, 1997, **1**, 543–544.

58 R. J. H. Hafkamp, B. P. A. Kokke, I. M. Danke, H. P. M. Geurts, A. E. Rowan, M. C. Feiters and R. J. M. Nolte, *Microscopy*, 1997, 545–546.

59 G. Tan, M. Singh, J. He, V. T. John and G. L. McPherson, *Langmuir*, 2005, **21**, 9322–9326.

60 M. I. Burguete, F. Galindo, R. Gavara, M. A. Izquierdo, J. C. Lima, S. V Luis, A. J. Parola and F. Pina, *Langmuir*, 2008, **24**, 9795–9803.

61 J. A. Foster, D. W. Johnson, M.-O. M. Pipenbrock and J. W. Steed, *New J. Chem.*, 2014, **38**, 927–932.

62   F.-X. Simon, N. S. Khelfallah, M. Schmutz, N. Díaz and P. J. Mésini, *J. Am. Chem. Soc.*, 2007, **129**, 3788–3789.

63   J. C. Stendahl, L. Li, E. R. Zubarev, Y.-R. Chen and S. I. Stupp, *Adv. Mater.*, 2002, **14**, 1540–1543.

64   E. R. Zubarev, M. U. Pralle, E. D. Stone and S. I. Stupp, *Adv. Mater.*, 2002, **14**, 198–203.

65   J. C. Stendahl, E. R. Zubarev, M. S. Arnold, M. C. Hersam, H.-J. Sue and S. I. Stupp, *Adv. Funct. Mater.*, 2005, **15**, 487–493.

66   J. R. Moffat, G. J. Seeley, J. T. Carter, A. Burgess and D. K. Smith, *Chem. Commun.*, 2008, 4601–4603.

67   J. R. Moffat and D. K. Smith, *Chem. Commun.*, 2011, **47**, 11864–11866.

68   H. Kim and J. Y. Chang, *Langmuir*, 2014, **30**, 13673–13679.

69   E. A. Wilder, K. S. Wilson, J. B. Quinn, D. Skrtic and J. M. Antonucci, *Chem. Mater.*, 2005, **17**, 2946–2952.

70   S. H. Kang, B. M. Jung and J. Y. Chang, *Adv. Mater.*, 2007, **19**, 2780–2784.

71   S. H. Kang, B. M. Jung, W. J. Kim and J. Y. Chang, *Chem. Mater.*, 2008, **20**, 5532–5540.

72   S. Zhang, X. Fu, H. Wang and Y. Yang, *J. Sep. Sci.*, 2008, **31**, 3782–3787.

73   G. Vasapollo, R. Del Sole, L. Mergola, M. R. Lazzoi, A. Scardino, S. Scorrano and G. Mele, *Int. J. Mol. Sci.*, 2011, **12**, 5908–5945.

74   D. A. Stone, L. Hsu, N. R. Wheeler, E. Wilusz, W. Zukas, G. E. Wnek and L. T. J. Korley, *Soft Matter*, 2011, **7**, 2449–2455.

75   Y. Zhang, R. Zhou, J. Shi, N. Zhou, I. R. Epstein and B. Xu, *J. Phys. Chem. B*, 2013, **117**, 6566–6573.

76   K. Hanabusa, A. Itoh, M. Kimura and H. Shirai, *Chem. Lett.*, 1999, 767–768.

77   X.-Y. Liu and P. D. Sawant, *Angew. Chem. Int. Ed.*, 2002, **41**, 3641–3645.

78   X.-Y. Liu, P. D. Sawant, W.-B. Tan, I. B. M. Noor, C. Pramesti and B.-H. Chen, *J. Am. Chem. Soc.*, 2002, **124**, 15055–15063.

79   J.-L. Li and X.-Y. Liu, *J. Phys. Chem. B*, 2009, **113**, 15467–15472.

80   J.-L. Li, B. Yuan, X.-Y. Liu, X.-G. Wang and R.-Y. Wang, *Cryst. Growth Des.*, 2011, **11**, 3227–3234.

81   J. Cui, Z. Shen and X. Wan, *Langmuir*, 2010, **26**, 97–103.

82   P. Chakraborty, B. Roy, P. Bairi and A. K. Nandi, *J. Mater. Chem.*, 2012, **22**, 20291–20298.

83   P. Chakraborty, S. Das, S. Mondal, P. Bairi and A. K. Nandi, *Langmuir*, 2016, **32**, 1871–1880.

84   L. Chen, S. Revel, K. Morris, D. G. Spiller, L. C. Serpell and D. J. Adams, *Chem. Commun.*, 2010, **46**, 6738–6740.

85   G. Pont, L. Chen, D. G. Spiller and D. J. Adams, *Soft Matter*, 2012, **8**, 7797–7802.

86   C. Yang, M. Bian and Z. Yang, *Biomater. Sci.*, 2014, **2**, 651–654.

87   N. Javid, S. Roy, M. Zelzer, Z. Yang, J. Sefcik and R. V Ulijn, *Biomacromolecules*, 2013, **14**, 4368–4376.

88   Y. J. Adhia, T. H. Schloemer, M. T. Perez and A. J. McNeil, *Soft Matter*, 2012, **8**, 430–434.

89   H. Kobayashi, M. Amaike, J. H. Jung, A. Friggeri, S. Shinkai and D. N. Reinhoudt, *Chem. Commun.*, 2001, 1038–1039.

90   M. Gradzielski, *J. Phys. Condens. Matter*, 2003, **15**, R655–R697.

91   M. Numata, K. Sugiyasu, T. Kishida, S. Haraguchi, N. Fujita, S. M. Park, Y. J. Yun, B. H. Kim and S. Shinkai, *Org. Biomol. Chem.*, 2008, **6**, 712–718.

92   Z. Zhang, M. Yang, X. Zhang, L. Zhang, B. Liu, P. Zheng and W. Wang, *Chem. Eur. J.*, 2009, **15**, 2352–2361.

93   Z. Zhang, M. Yang, C. Hu, B. Liu, M. Hu, X. Zhang, W. Wang, Y. Zhou and H. Wang, *New J. Chem.*, 2011, **35**, 103–110.

94   A. E. Way, A. B. Korpusik, T. B. Dorsey, L. E. Buerkle, H. A. von Recum and S. J. Rowan, *Macromolecules*, 2014, **47**, 1810–1818.

95   P. Chakraborty, S. Mondal, S. Khara, P. Bairi and A. K. Nandi, *J. Phys. Chem. B*, 2015, **119**, 5933–5944.

96   W.-C. Lai and C.-C. Chen, *Soft Matter*, 2014, **10**, 312–319.

97   P. Chakraborty, P. Bairi, B. Roy and A. K. Nandi, *Appl. Mater. Interfaces*, 2014, **6**, 3615–3622.

98   Q. Wang, X. Xiao, Y. Hu, H. Wang and Y. Yang, *RSC Adv.*, 2014, **4**, 22380–22386.

99   E. S. Dragan, *Chem. Eng. J.*, 2014, **243**, 572–590.

100   M. Shivashankar and B. K. Mandal, *Int. J. Pharm. Pharm. Sci.*, 2012, **4**, 1–7.

101   M. A. Haque, T. Kurokawa and J. P. Gong, *Polymer*, 2012, **53**, 1805–1822.

102 P. Li, X.-Q. Dou, Y.-T. Tang, S. Zhu, J. Gu, C.-L. Feng and D. Zhang, *J. Colloid. Interface Sci.*, 2012, **387**, 115–122.

103 P. Li, Z. Yin, X.-Q. Dou, G. Zhou and C.-L. Feng, *Appl. Mater. Interfaces*, 2014, **6**, 7948–7952.

104 L. L. Hyland, M. B. Taraban, Y. Feng, B. Hammouda and Y. B. Yu, *Biopolymers*, 2012, **97**, 177–188.

105 D. Dasgupta, S. Srinivasan, C. Rochas, A. Ajayaghosh and J. M. Guenet, *Langmuir*, 2009, **25**, 8593–8598.

106 J. Wang, Z. Wang, J. Gao, L. Wang, Z. Yang, D. Kong and Z. Yang, *J. Mater. Chem.*, 2009, **19**, 7892–7896.

107 R. Huang, W. Qi, L. Feng, R. Su and Z. He, *Soft Matter*, 2011, **7**, 6222–6230.

108 J. Wang, H. Wang, Z. Song, D. Kong, X. Chen and Z. Yang, *Colloids Surf. B. Biointerfaces*, 2010, **80**, 155–160.

109 M. J. Meunier, *Ann. Chim. Phys.*, 1891, **22**, 412–432.

110 J. K. Wolfe, M. Hann and C. S. Hudson, *J. Am. Chem. Soc.*, 1942, **64**, 1493–1497.

111 S. J. Angyal and J. V Lawler, *J. Am. Chem. Soc.*, 1944, **66**, 837–838.

112 D. Brecknell, R. Carman, J. Kibby and L. Nichola, *Aust. J. Chem.*, 1976, **29**, 1859–1863.

113 S. Yamasaki, Y. Ohashi, H. Tsutsumi and K. Tsujii, *Bull. Chem. Soc. Jpn.*, 1995, **68**, 146–151.

114 F. Rongxiu, C. Lingong, H. Zhongke and S. Jian, *Trans. Tianjin Univ.*, 2007, **13**, 35–41.

115 R. Stan, C. Ott, N. Sulca, A. Lungu and H. Iovu, *Mater. Plast.*, 2009, **46**, 230–235.

116 G. Malle and T. Luukas, 2013, US Patent 20130039862.

117 H. Uchiyama, 1981, US Patent 4267110.

118 K. Murai, T. Kobayashi and K. Fujitani, 1984, US Patent 4429140.

119 G. Machell, 1985, US Patent 4562265.

120 J. M. Gardlik and R. V Burkes, 1992, US Patent 5106999.

121 T. Kobayashi, 1992, US Patent 5120863.

122 W. A. Scrivens and J. M. Salley, 1998, US Patent 5731474.

123 J. G. Lever, D. L. Dotson, J. D. Anderson, J. R. Jones and S. R. Sheppard, 2001, US Patent

6500964.

124   R. Stan, S. Roşca, C. Ott, S. Roşca, E. Perez, I. Rico-Lattes and A. Lattes, *Rev. Rou. Chem.*, 2006, **51**, 609–613.

125   R. Stan, N. Chira, C. Ott, C. Todasca and E. Perez, *Rev. Chemie*, 2008, **59**, 273–276.

126   A. Pavankumar and P. V Uppara, 2014, US Patent 8871954.

127   P. V Uppara, P. Aduri, M. Sakhalkar and U. Ratnaparkhi, 2014, US Patent 20130281716.

128   E. L. Roehl and H. B. Tan, 1979, US Patent 4154816.

129   E. L. Roehl, 1982, US Patent 4346079.

130   T. Schamper, M. Jablon, M. H. Randhawa, A. Senatore and J. D. Warren, *J. Soc. Cosmet. Chem.*, 1986, **37**, 225–231.

131   T. J. Schamper, M. M. Perl and J. D. Warren, 1988, US Patent 4720381.

132   R. B. Kasat, W. Lee, M. D. R and N. G. Telyan, 1996, US Patent 5490979.

133   J. P. Luebbe, P. R. Tanner and J. D. Melanson, 1989, US Patent 4816261.

134   M. H. Randhawa and T. J. Schamper, 1988, US Patent 4719102.

135   J. Mattai, C. Ortiz, E. Guenin and J. Afflitto, 2002, US Patent 6338841.

136   A. Esposito, T. Schamper and E. C. Henry, 2010, US Patent 7799318.

137   T. Ando and Y. Yamazaki, 1974, US Patent 3846363.

138   H. Fukuo and S. Tsujio, 2001, US Patent 6203910.

139   R. N. Vachon and H. R. R. Partin, 1981, US Patent 4257928.

140   K. Hamada and H. Uchiyama, 1977, US Patent 4016118.

141   Y. Kawai, K. Sasagawa, M. Maki, H. Ueda and M. Miyamoto, 1982, US Patent 4314039.

142   H. Uchiyama, 1984, US Patent 4483956.

143   J. W. Rekers, 1991, US Patent 5049605.

144   J. Xu, J. Li, B. W. Bolt, K. D. Lake, J. D. Sprinkle, B. M. Burkhart and K. A. Keller, 2011, US Patent 8022133.

145   T. D. Danielson, J. Rockwood and N. A. Mehl, 2014, US Patent 8653165.

146   J. Li, K. Fan, X. Guan, Y. Yu and J. Song, *Langmuir*, 2014, **30**, 13422–13429.

147   D. K. Smith, in *Supramolecular Chemistry; From Molecules to Nanomaterial*, eds. P. A.

Gale and J. W. Steed, Wiley-VCH, Weinheim, 2012.

148 Y. Zhang, H. Gu, Z. Yang and B. Xu, *J. Am. Chem. Soc.*, 2003, **125**, 13680–13681.

149 V. Jayawarna, M. Ali, T. A. Jowitt, A. F. Miller, A. Saiani, J. E. Gough and R. V Ulijn, *Adv. Mater.*, 2006, **18**, 611–614.

150 D. J. Adams, M. F. Butler, W. J. Frith, M. Kirkland, L. Mullen and P. Sanderson, *Soft Matter*, 2009, **5**, 1856–1862.

151 D. J. Adams, L. M. Mullen, M. Berta, L. Chen and W. J. Frith, *Soft Matter*, 2010, **6**, 1971–1980.

152 L. Chen, S. Revel, K. Morris, L. C Serpell and D. J. Adams, *Langmuir*, 2010, **26**, 13466–13471.

153 Y. Pocker and E. Green, *J. Am. Chem. Soc.*, 1972, **95**, 113–119.

154 S. R. Raghavan and B. H. Cipriano, in *Molecular Gels: Materials with Self-Assembled Fibrillar Networks*, eds. R. G. Weiss and P. Terech, Springer, Dordrecht, Netherlands, 2006.

155 V. J. Nebot and D. K. Smith, in *Functional Molecular Gels*, eds. B. Escuder and J. F. Miravet, Royal Society of Chemistry, Cambridge, UK, 2013.

156 J. Makarević, M. Jokić, B. Perić, V. Tomisić, B. Kojić-Prodić and M. Zinić, *Chem. Eur. J.*, 2001, **7**, 3328–3341.

157 B. Escuder, M. LLusar and J. F. Miravet, *J. Org. Chem.*, 2006, **71**, 7747–7752.

158 A. R. Hirst, I. A. Coates, T. R. Boucheteau, J. F. Miravet, B. Escuder, V. Castelletto, I. W. Hamley and D. K. Smith, *J. Am. Chem. Soc.*, 2008, **130**, 9113–9121.

159 Y. E. Shapiro, *Prog. Polym. Sci.*, 2011, **36**, 1184–1253.

160 M. Avrami, *J. Chem. Phys.*, 1939, **7**, 1103–1122.

161 M. Avrami, *J. Chem. Phys.*, 1940, **8**, 212–224.

162 M. Avrami, *J. Chem. Phys.*, 1941, **9**, 177–184.

163 X. Huang, P. Terech, S. R. Raghavan and R. G. Weiss, *J. Am. Chem. Soc.*, 2005, **127**, 4336–4344.

164 X. Huang, S. R. Raghavan, P. Terech and R. G. Weiss, *J. Am. Chem. Soc.*, 2006, **128**, 15341–15352.

165 N. Berova, K. Nakanishi and R. W. Woody, *Circular Dichroism: Principles and*

Applications, Wiley-VCH, Weinheim, 2nd edn., 1994.

166   M. A. Mateos-Timoneda, M. Crego-Calama and D. N. Reinhoudt, *Chem. Soc. Rev.*, 2004, **33**, 363–372.

167   J. R. Moffat and D. K. Smith, *Chem. Commun.*, 2008, 2248–2250.

168   J. Cui, A. Liu, Y. Guan, J. Zheng, Z. Shen and X. Wan, *Langmuir*, 2010, **26**, 3615–3622.

169   B. Roy, A. Saha, A. Esterrani and A. K. Nandi, *Soft Matter*, 2010, **6**, 3337–3345.

170   P. Echlin, *Handbook of Sample Preparation for Scannin Electron Microscopy*, Springer, New York, 2009.

171   C. Araki, *Bull. Chem. Soc. Jpn.*, 1956, **29**, 543–544.

172   E. R. Morris, D. A. Rees, D. Thom and E. J. Welsh, *J. Supramol. Struct.*, 1977, **6**, 259–274.

173   S. Arnott, A. Fulmer, W. E. Scott, I. C. Dea, R. Moorhouse and D. A. Rees, *J. Mol. Biol.*, 1974, **90**, 269–284.

174   P. Serwer, *Electrophoresis*, 1983, **4**, 375–382.

175   T. G. Mezger, *The Rheology Handbook*, Vincentz Network, Hanover, 3rd edn., 2011.

176   P. Sollich, in *Molecular Gels: Materials with Self-Assembled Fibrillar Networks*, eds. R. G. Weiss and P. Terech, Springer, Dordrecht, Netherlands, 2006.

177   H. F. Mark, *Encyclopedia of Polymer Science and Technology*, John Wiley & Sons, New York, 2004.

178   M.-O. M. Piepenbrock, G. O. Lloyd, N. Clarke and J. W. Steed, *Chem. Rev.*, 2010, **110**, 1960–2004.

179   N. M. Sangeetha, S. Bhat, U. Maitra and P. Terech, *J. Phys. Chem. B*, 2004, **108**, 16056–16063.

180   P. Terech, D. Pasquier, V. Bordas and C. Rossat, *Langmuir*, 2000, **16**, 4485–4494.

181   P. Li, X.-Q. Dou, C.-L. Feng and D. Zhang, *Soft Matter*, 2013, **9**, 3750–3757.

182   J. Wang, X. Miao, Q. Fengzhao, C. Ren, Z. Yang and L. Wang, *RSC Adv.*, 2013, **3**, 16739–16746.

183   J. Zhu, *Biomaterials*, 2010, **31**, 4639–4656.

184   F. E. Bailey and J. V Koleske, *Poly(Ethylene Oxide)*, Academic Press, New York, 1976.

185   J. H. Lee, H. B. Lee and J. D. Andrade, *Prog. Polym. Sci.*, 1995, **20**, 1043–1079.

186   N. A. Alcantar, E. S. Aydil and J. N. Israelachvili, *J. Biomed. Mater. Res.*, 2000, **51**, 343–351.

187   K. B. Keys, F. M. Andreopoulos and N. a. Peppas, *Macromolecules*, 1998, **31**, 8149–8156.

188   N. A. Peppas, K. B. Keys, M. Torres-Lugo and A. M. Lowman, *J. Control. Release*, 1999, **62**, 81–87.

189   C. Lin and K. S. Anseth, *Pharm. Res.*, 2009, **26**, 631–643.

190   M. Malkoch, R. Vestberg, N. Gupta, L. Mespouille, P. Dubois, A. F. Mason, J. L. Hedrick, Q. Liao, C. W. Frank, K. Kingsbury and C. J. Hawker, *Chem. Commun.*, 2006, 2774–2776.

191   B. D. Polizzotti, B. D. Fairbanks and K. S. Anseth, *Biomacromolecules*, 2008, **9**, 1084–1087.

192   T. J. Sanborn, P. B. Messersmith and A. E. Barron, *Biomaterials*, 2002, **23**, 2703–2710.

193   M. Ehrbar, S. C. Rizzi, R. Hlushchuk, V. Djonov, A. H. Zisch, J. A. Hubbell, F. E. Weber and M. P. Lutolf, *Biomaterials*, 2007, **28**, 3856–3866.

194   M. Ehrbar, S. C. Rizzi, R. G. Schoenmakers, B. San Miguel, J. A. Hubbell, F. E. Weber and M. P. Lutoff, *Biomacromolecules*, 2007, **8**, 3000–3007.

195   A. S. Sawhney, J. A. Pathak and J. A. Hubbell, *Macromolecules*, 1993, **26**, 581–587.

196   J. L. West and J. A. Hubbell, *React. Polym.*, 1995, **25**, 139–147.

197   S. Jo, P. S. Engel and A. G. Mikos, *Polymer*, 2000, **41**, 7595–7604.

198   J. D. Clapper, J. M. Skeie, R. F. Mullins and C. A. Guymon, *Polymer*, 2007, **48**, 6554–6564.

199   Z. Jiang, J. Hao, Y. You, Y. Liu, Z. Wang and X. Deng, *J. Biomed. Mater. Res. A*, 2008, **87**, 45–51.

200   S. Kaihara, S. Matsumura and J. P. Fisher, *Eur. J. Pharm. Biopharm.*, 2008, **68**, 67–73.

201   J. Zhang, A. Skardal and G. D. Prestwich, *Biomaterials*, 2008, **29**, 4521–4531.

202   S. Lin-Gibson, S. Bencherif, J. A. Cooper, S. J. Wetzel, J. M. Antonucci, B. M. Vogel, F. Horkay and N. R. Washburn, *Biomacromolecules*, 2004, **5**, 1280–1287.

203   S. J. Bryant and K. S. Anseth, *J. Biomed. Mater. Res.*, 2002, **59**, 63–72.

204   A. Revzin, R. J. Russell, V. K. Yadavalli, W.-G. Koh, C. Deister, D. D. Hile, M. B. Mellott and M. V. Pishko, *Langmuir*, 2001, **17**, 5440–5447.

205   A. Revzin, R. G. Tompkins and M. Toner, *Langmuir*, 2003, **19**, 9855–9862.

206   Y. Luo and M. S. Shoichet, *Nat. Mater.*, 2004, **3**, 249–253.

207   Y. Luo and M. S. Shoichet, *Biomacromolecules*, 2004, **5**, 2315–2323.

208   M. S. Hahn, J. S. Miller and J. L. West, *Adv. Mater.*, 2006, **18**, 2679–2684.

209   M. S. Hahn, L. J. Taite, J. J. Moon, M. C. Rowland, K. A. Ruffino and J. L. West, *Biomaterials*, 2006, **27**, 2519–2524.

210   S.-H. Lee, J. J. Moon and J. L. West, *Biomaterials*, 2008, **29**, 2962–2968.

211   J. H. Wosnick and M. S. Shoichet, *Chem. Mater.*, 2008, **20**, 55–60.

212   C. A. DeForest, B. D. Polizzotti and K. S. Anseth, *Nat. Mater.*, 2009, **8**, 659–664.

213   S. Khetan, J. S. Katz and J. A. Burdick, *Soft Matter*, 2009, **5**, 1601–1606.

214   A. M. Kloxin, A. M. Kasko, C. N. Salinas and K. S. Anseth, *Science*, 2009, **324**, 59–63.

215   H. Aubin, J. W. Nichol, C. B. Hutson, H. Bae, A. L. Sieminski, D. M. Cropek, P. Akhyari and A. Khademhosseini, *Biomaterials*, 2010, **31**, 6941–6951.

216   J. W. Nichol, S. T. Koshy, H. Bae, C. M. Hwang, S. Yamanlar and A. Khademhosseini, *Biomaterials*, 2010, **31**, 5536–5544.

217   A. Ovsianikov, M. Gruene, M. Pflaum, L. Koch, F. Maiorana, M. Wilhelmi, A. Haverich and B. Chichkov, *Biofabrication*, 2010, **2**, 014104.

218   A. Ovsianikov, M. Malinauskas, S. Schlie, B. Chichkov, S. Gittard, R. Narayan, M. Löbler, K. Sternberg, K.-P. Schmitz and A. Haverich, *Acta Biomater.*, 2011, **7**, 967–974.

219   A. Ovsianikov, A. Deiwick, S. Van Vlierberghe, P. Dubruel, L. Möller, G. Drager and B. Chichkov, *Biomacromolecules*, 2011, **12**, 851–858.

220   T. Weiß, R. Schade, T. Laube, A. Berg, G. Hildebrand, R. Wyrwa, M. Schnabelrauch and K. Liefeith, *Adv. Eng. Mater.*, 2011, **13**, B264–B273.

221   R. G. Wylie, S. Ahsan, Y. Aizawa, K. L. Maxwell, C. M. Morshead and M. S. Shoichet, *Nat. Mater.*, 2011, **10**, 799–806.

222   L. Cai, J. Lu, V. Sheen and S. Wang, *Biomacromolecules*, 2012, **13**, 1663–1674.

223   K. A. Mosiewicz, L. Kolb, A. J. van der Vlies, M. M. Martino, P. S. Lienemann, J. A. Hubbell, M. Ehrbar and M. P. Lutolf, *Nat. Mater.*, 2013, **12**, 1072–1078.

224   T. Vignaud, H. Ennoman, M. Thery and M. Piel, *Methods Cell Biol.*, 2014, **120**, 93–116.

225   F. Yanagawa, S. Sugiura, T. Takagi, K. Sumaru, G. Camci-Unal, A. Patel, A. Khademhosseini and T. Kanamori, *Adv. Healthc. Mater.*, 2014, **4**, 246–254.

226   K. M. C. Tsang, N. Annabi, F. Ercole, K. Zhou, D. J. Karst, F. Li, J. M. Haynes, R. A. Evans, H. Thissen, A. Khademhosseini and J. S. Forsythe, *Adv. Funct. Mater.*, 2015, **25**, 977–986.

227   F. Rodríguez-Llansola, B. Escuder, J. F. Miravet, D. Hermida-Merino, I. W. Hamley, C. J. Cardin and W. Hayes, *Chem. Commun.*, 2010, **46**, 7960–2.

228   D. M. Wood, B. W. Greenland, A. L. Acton, F. Rodríguez-Llansola, C. A. Murray, C. J. Cardin, J. F. Miravet, B. Escuder, I. W. Hamley and W. Hayes, *Chem. Eur. J.*, 2012, **18**, 2692–2699.

229   B. O. Okesola and D. K. Smith, *Chem. Commun.*, 2013, **49**, 11164–11166.

230   I. Tomatsu, K. Peng and A. Kros, *Adv. Drug Deliv. Rev.*, 2011, **63**, 1257–1266.

231   A. Ovsianikov, V. Mironov, J. Stampfl and R. Liska, *Expert Rev. Med. Devices*, 2012, **9**, 613–633.

232   J. Torgersen, X. H. Qin, Z. Li, A. Ovsianikov, R. Liska and J. Stampfl, *Adv. Funct. Mater.*, 2013, **23**, 4542–4554.

233   K. J. Skilling, F. Citossi, T. D. Bradshaw, M. Ashford, B. Kellam and M. Marlow, *Soft Matter*, 2014, **10**, 237–256.

234   H. Cui, M. J. Webber and S. I. Stupp, *Polym. Sci.*, 2009, **94**, 1–18.

235   J. B. Matson and S. I. Stupp, *Chem. Commun.*, 2012, **48**, 26–33.

236   M. Zhou, A. M. Smith, A. K. Das, N. W. Hodson, R. F. Collins, R. V Ulijn and J. E. Gough, *Biomaterials*, 2009, **30**, 2523–2530.

237   D. M. Ryan and B. L. Nilsson, *Polym. Chem.*, 2012, **3**, 18–33.

238   S. Zhang, T. C. Holmes, C. M. DiPersio, R. O. Hynes, X. Su and A. Rich, *Biomaterials*, 1995, **16**, 1385–1393.

239   T. C. Holmes, S. De Lacalle, X. Su, G. Liu, A. Rich and S. Zhang, *Proc. Natl. Acad. Sci.*, 2000, **97**, 6728–6733.

240   R. G. Ellis-Behnke, Y.-X. Liang, S.-W. You, D. K. C. Tay, S. Zhang, K.-F. So and G. E. Schneider, *Proc. Natl. Acad. Sci.*, 2006, **103**, 5054–5059.

241   G. A. Silva, C. Czeisler, K. L. Niece, E. Beniash, D. A. Harrington, J. A. Kessler and S. I. Stupp, *Science*, 2004, **303**, 1352–1355.

242   V. M. Tysseling-Mattiace, V. Sahni, K. L. Niece, D. Birch, C. Czeisler, M. G. Fehlings, S. I. Stupp and J. A. Kessler, *J. Neurosci.*, 2008, **28**, 3814–3823.

243   J. Kisiday, M. Jin, B. Kurz, H. Hung, C. Semino, S. Zhang and A. J. Grodzinsky, *Proc. Natl. Acad. Sci.*, 2002, **99**, 9996–10001.

244   M. E. Davis, J. P. M. Motion, D. A. Narmoneva, T. Takahashi, D. Hakuno, R. D. Kamm, S. Zhang and R. T. Lee, *Circulation*, 2005, **111**, 442–450.

245   K. Rajangam, H. A. Behanna, M. J. Hui, X. Han, J. F. Hulvat, J. W. Lomasney and S. I. Stupp, *Nano Lett.*, 2006, **6**, 2086–2090.

246   T. D. Sargeant, M. O. Guler, S. M. Oppenheimer, A. Mata, R. L. Satcher, D. C. Dunand and S. I. Stupp, *Biomaterials*, 2008, **29**, 161–171.

247   L. S. Birchall, S. Roy, V. Jayawarna, M. Hughes, E. Irvine, G. T. Okorogheye, N. Saudi, E. De Santis, T. Tuttle, A. A. Edwards and R. V. Ulijn, *Chem. Sci.*, 2011, **2**, 1349–1355.

248   S. Díaz-Oltra, C. Berdugo, J. F. Miravet and B. Escuder, *New J. Chem.*, 2015, **39**, 3785–3791.

249   J. Raeburn and D. J. Adams, *Chem. Commun.*, 2015, **51**, 5170–5180.

250   J. Raeburn, G. Pont, L. Chen, Y. Cesbron, R. Lévy and D. J. Adams, *Soft Matter*, 2012, **8**, 1168–1174.

251   F. Rodríguez-Llansola, B. Escuder and J. F. Miravet, *J. Am. Chem. Soc.*, 2009, **131**, 11478–11484.

252   C. Tang, A. M. Smith, R. F. Collins, R. V. Ulijn and A. Saiani, *Langmuir*, 2009, **25**, 9447–9453.

253   L. Chen, K. Morris, A. Laybourn, D. Elias, M. R. Hicks, A. Rodger, L. Serpell and D. J. Adams, *Langmuir*, 2010, **26**, 5232–5242.

254   A. Reddy, A. Sharma and A. Srivastava, *Chem. Eur. J.*, 2012, **18**, 7575–7581.

255   M. Wallace, J. A. Iggo and D. J. Adams, *Soft Matter*, 2015, **11**, 7739–7747.

256   A. Khademhosseini and R. Langer, *Biomaterials*, 2007, **28**, 5087–5092.

257   J. S. Katz and J. A. Burdick, *Macromol. Biosci.*, 2010, **10**, 339–48.

258   T. Billiet, M. Vandenhaute, J. Schelfhout, S. Van Vlierberghe and P. Dubruel, *Biomaterials*, 2012, **33**, 6020–6041.

259   A. M. Greiner, B. Richter and M. Bastmeyer, *Macromol. Biosci.*, 2012, **12**, 1301–1314.

260   Š. Selimović, J. Oh, H. Bae, M. Dokmeci and A. Khademhosseini, *Polymers*, 2012, **4**, 1554–1579.

261   P. Bajaj, R. M. Schweller, A. Khademhosseini, J. L. West and R. Bashir, *Annu. Rev. Biomed. Eng.*, 2014, **16**, 247–276.

262   L. Frkanec, M. Jokić, J. Makarević, K. Wolsperger and M. Žinić, *J. Am. Chem. Soc.*, 2002, **124**, 9716–9717.

263   S. Matsumoto, S. Yamaguchi, S. Ueno, H. Komatsu, M. Ikeda, K. Ishizuka, Y. Iko, K. V Tabata, H. Aoki, S. Ito, H. Noji and I. Hamachi, *Chem. Eur. J.*, 2008, **14**, 3977–86.

264   H. Komatsu, S. Matsumoto, S. I. Tamaru, K. Kaneko, M. Ikeda and I. Hamachi, *J. Am. Chem. Soc.*, 2009, **131**, 5580–5585.

265   M. He, J. Li, S. Tan, R. Wang and Y. Zhang, *J. Am. Chem. Soc.*, 2013, **135**, 18718–18721.

266   M. Ikeda, T. Tanida, T. Yoshii and I. Hamachi, *Adv. Mater.*, 2011, **23**, 2819–2822.

267   T. Yoshii, M. Ikeda and I. Hamachi, *Angew. Chem. Int. Ed.*, 2014, **53**, 7264–7267.

268   J. Raeburn, T. O. McDonald and D. J. Adams, *Chem. Commun.*, 2012, **48**, 9355–9357.

269   C. Maity, W. E. Hendriksen, J. H. Van Esch and R. Eelkema, *Angew. Chem. Int. Ed.*, 2015, **54**, 998–1001.

270   H.-J. Timpe and V. Schikowsky, *J. für Prakt. Chemie*, 1989, **331**, 447–460.

271   W. Behnck and J. Bargon, *Synth. Met.*, 1993, **54**, 223–228.

272   E. R. Draper, L. L. E. Mears, A. M. Castilla, S. M. King, T. O. McDonald, R. Akhtar and D. J. Adams, *RSC Adv.*, 2015, **5**, 95369–95378.

273   E. R. Draper, E. G. B. Eden, T. O. McDonald and D. J. Adams, *Nat. Chem.*, 2015, **7**, 848–852.

274   J. Raeburn, B. Alston, J. Kroeger, T. O. McDonald, J. R. Howse, P. J. Cameron and D. J. Adams, *Mater. Horiz.*, 2014, **1**, 241–246.

275   A. J. Engler, S. Sen, H. L. Sweeney and D. E. Discher, *Cell*, 2006, **126**, 677–689.

276   D. J. Cornwell, B. O. Okesola and D. K. Smith, *Soft Matter*, 2013, **9**, 8730–8736.

277   D. J. Cornwell, B. O. Okesola and D. K. Smith, *Angew. Chem. Int. Ed.*, 2014, **53**, 12461–12465.

278   E. J. Howe, B. O. Okesola and D. K. Smith, *Chem. Commun.*, 2015, **51**, 7451–7454.

279   V. M. P. Vieira, A. C. Lina, M. de Jong and D. K. Smith, *Unpublished results*.

280   D. J. Cornwell, O. J. Daubney and D. K. Smith, *J. Am. Chem. Soc.*, 2015, **137**, 15486–15492.